STUDY OF SOLITARY WAVES IN SPACE PLASMAS

A. A. Mamun

A Thesis Submitted for the Degree of PhD
at the
University of St Andrews

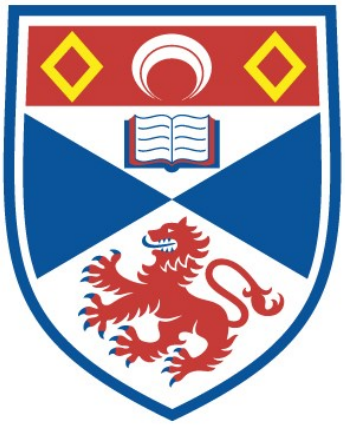

1997

STUDY OF SOLITARY WAVES IN SPACE PLASMAS

A. A. MAMUN

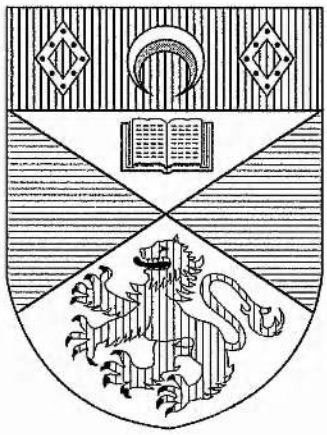

Thesis submitted for the degree of Doctor of Philosophy of the University of St. Andrews in June 1996

Tw C84

DEDICATED TO
MY PARENTS , BROTHERS & SISTERS

ABSTRACT

Theoretical investigations have been made of arbitrary amplitude electrostatic solitary waves in non-thermal plasmas, which may be of relevance to ionospheric and magnetospheric plasmas, and dusty plasmas, which are most common in earth's and cometary environments as well as in planetary rings, for understanding the nonlinear features of localised electrostatic disturbances in such space plasma systems. This thesis starts with an introductory chapter where a very brief historical review of solitary waves in plasmas has been presented.

The study of arbitrary amplitude electrostatic solitary waves in non-thermal plasma has considered a plasma system consisting of warm adiabatic ions and non-thermal electrons. It is found that a non-thermal electron distribution may change the nature of ion-acoustic solitary waves. If the ions are assumed to respond as a fluid to perturbations in the potential, with no significant trapping in a potential well, then a thermal plasma only supports solitary waves with a density peak. However, with a suitable distribution of non-thermal electrons, solitary waves with both density peaks and density depressions may exist. This study has also included a numerical analysis showing how these electrostatic solitary structures evolve with time.

The investigation has then been extended to magnetised plasmas to study the effects of magnetic field on obliquely propagating electrostatic solitary structures. This attempt first employed the reductive perturbation method and investigated the nonlinear properties of small but finite amplitude obliquely propagating solitary waves in this magnetised non-thermal plasma model. This study is then generalised to arbitrary amplitude solitary waves by the numerical solution of the full nonlinear system of equations. This numerical method has also been utilised to present a similar study in another popular plasma model, namely the two-electron-temperature plasma model.

The study of arbitrary amplitude solitary waves in a dusty plasma has considered another plasma system which consists of an inertial dust fluid and ions with Maxwellian distribution and has investigated the nonlinear properties of dust-acoustic solitary waves. A numerical study has also been made to show how these dust-acoustic solitary waves evolve with time. The effects of non-thermal and vortex-like ion distributions are then incorporated into this study.

The study of arbitrary amplitude electrostatic solitary waves in this thesis has finally been concluded with some brief discussion of our results and proposal for further studies, which are expected to generalise and develop our present work to some other extents, in this versatile area of research.

DECLARATION

I, A. A. Mamun, hereby certify that this thesis, which is approximately 25000 words in length, has been written by me, that it is the record of work carried out by me and that it has not been submitted in any previous application for a higher degree.

12/06/96
date

signature of candidate

POSTGRADUATE CAREER

I was admitted as a research student in October 1993 and as a candidate for the degree of Doctor of Philosophy in July 1994; the higher study for which this is a record was carried out in the University of St. Andrews between 1993 and 1996.

12/06/96
date

signature of candidate

CERTIFICATE

I hereby certify that the candidate has fulfilled the conditions of the Resolution and Regulations appropriate for the degree of Doctor of Philosophy in the University of St. Andrews and that the candidate is qualified to submit this thesis in application for that degree.

12/6/96

date signature of supervisor

COPYRIGHT

ACKNOWLEDGEMENTS

It is a matter of great pleasure for me to record my deepest sense of gratitude, indebtedness, honour and thankful acknowledgement to my esteemed supervisor Prof. R. A. Cairns for his indispensable guidance, constant encouragement, invaluable suggestions and unending patience through out the progress of this work.

I am very grateful to Dr. R. Bingham and Dr. P. K. Shukla for their stimulating influence and direct help in the progress of this work . Their enthusiasm for Plasma Physics has been a constant inspiration to me.

I desire to express my gratitude to Prof. J. J. Sanderson and Dr. D. McDonald for their invaluable suggestions during the course of this work. I also wish to offer my best thanks and compliments to Dr. P. Heggie, Dr. G. Inverarity, Dr. R. Jain and Dr. C. Parnell for their kind co-operation in some computational work.

My special thanks and appreciations must go to Cesar, Mike, Partha, Amro, Colin and my all other friends and colleagues for their helpful support. I would also like to thank Mr. and Mrs. Kitai for their love and constant encouragement through letters from Japan.

I am also very grateful to Prof. M. Salimullah, who first introduced me to Plasma Physics, and Dr. Ruhul Amin, who first inspired me to come to the nice environment of St. Andrews, for their constant encouragement during the period of this work.

I gratefully acknowledge the Commonwealth Scholarship Commission for their financial support, the British Council for their kind hospitality and the authority of Jahangirnagar University for extra-ordinary study leave during the course of this work.

Finally, I recognise the contributions of my wife and all my family members for their love, inspiration and sacrifice during the course of this work.

A. A. Mamun

Contents

Chapter 1

Solitary Waves in Plasmas

1.1 Introduction

Solitary waves, which are hump-shaped nonlinear waves of permanent profile, were first observed on the Edinburgh to Glasgow canal in 1834 by John Scott Russell. To introduce these solitary waves, we can quote his own striking description of that observation to the British Association in 1844 [1]:

"I believe I shall best introduce this phænomenon by describing the circumstances of my own first acquaintance with it. I was observing the motion of a boat which was rapidly drawn along a narrow channel by a pair of horses, when the boat suddenly stopped – not so the mass of water in the channel which it had put in motion; it accumulated round the prow of the vessel in a state of violent agitation, then suddenly leaving it behind, rolled forward with great velocity, assuming the form of a large solitary elevation, a rounded, smooth and well defined heap of water, which continued its course along the channel apparently without change of form or diminution of speed. I followed it on horseback, and overtook it still rolling on at a rate of some eight or nine miles an hour, preserving its original figure some thirty feet long and a foot to a foot and a half in height. Its height gradually diminished, and after a chase

of one or two miles I lost it in the windings of the channel. Such, in the month of August 1834, was my first chance interview with that singular and beautiful phænomenon which I have called the Wave of Translation, a name which it now generally bears; which I have since found to be an important element in almost every case of fluid resistance, and ascertained to be the type of that great moving elevation of the sea, which, with the regularity of a planet, ascends our rivers and rolls along our shores.

To study minutely this phænomenon with a view to determining accurately its nature and laws, I have adopted other more convenient modes of producing it than that which I just described, and have employed various methods of observation. A description of these will probably assist me in conveying just conceptions of the nature of this wave."

This striking description of Russell may serve to explain the interest in this same object that has been aroused in mathematicians and physicists some one hundred and fifty years later.

The inception of theoretical studies into the general topic of solitary waves had its origin in the 19th century when Korteweg and de Vries [2] established an equation to model the phenomenon of solitary waves observed by Russell. This equation, which is now known as the 'KdV equation', is the first of a fairly large class of nonlinear evolution equations which includes the nonlinear Schrödinger equation, the sine-Gordon equation, the Boussinesq equation and several others among its members [3]. These equations have received considerable attention among theoreticians in different branches of fluid dynamics, nonlinear electrodynamics and mathematical physics. New mathematical methods, such as the inverse scattering transform, have been developed and old techniques, such as Bäcklund transforms and Lie algebra, have been recalled to solve these equations. The details of these mathematical tools have been presented by a large number of authors during the last few decades, some of whom are Whitham [4], Toda [5], Miura [6], Lonngren and Scott [7], Lamb [8],

Ablowitz and Segur [9], Dodd *et al.* [10], Drazin [11], Infeld and Rowlands [12], Petviashvili and Pokhotelov [13].

Nowadays, the study of solitary waves or solitons (a soliton is a special solitary wave which preserves its shape and speed in a collision with another such solitary wave) promises to be a very rewarding and challenging topic of research for the next decade or so, not only for its vital role in fluid dynamics, nonlinear electrodynamics and mathematical physics but also from the view of its versatile applications in almost every branches of physics, viz. plasma physics, solid state physics, laser physics, elementary particle physics, bio-physics, etc. A large number of workers in different fields and different areas of research are actively engaging themselves in the study of solitons and trying to exploit their various attractive properties to their own area of research. As examples, elementary particle physicists are trying to use solitons in order to get better understanding of the internal structure of elementary particles, communication engineers are trying to exploit solitons in order to get signals (information) over long distances without being distorted and without suffering any significant loss in intensity[1], etc. In order to get a clear understanding of the nonlinear features of localised electrostatic disturbances in a plasma medium, we are interested in the study of solitary waves in this plasma medium and will, in this thesis, be mainly concerned with some questions arising from highly nonlinear properties of solitary waves in plasmas, particularly, in space plasmas.

The main motivation behind presenting this introductory chapter is to provide a brief historical review of solitary waves in plasmas and to introduce briefly some recent work which motivates us to study some nonlinear properties of solitary waves which are mainly relevant to space plasma phenomena.

[1]To define briefly this practical application of solitons, let us consider a pulse carrying a bit of information with it. If the pulse suffers heavy dissipation, it may not reach the destination with appreciable intensity. Similarly, if the pulse suffers a significant dispersion, the pulse, on reaching the destination, may be so spread out and blurred that the information may be totally unintelligible. However, if the pulse travels as a soliton, it can carry the information over long distances without being distorted and without suffering any significant loss in its intensity.

1.2 A Brief Historical Review

Solitary waves in plasmas, which are one of the main objects of nonlinear plasma physics, have been studied for about four decades. In 1966 Washimi and Taniuti [14] first studied the propagation of one dimensional solitary waves using the perturbation technique and showed that weakly nonlinear ion-acoustic wave disturbances could be described by the KdV equation. This paper led to the original ion-acoustic soliton experiment of Ikezi and Taylor [15] and had considerable impact in the plasma community. Karpman and Kadomtsev [16] showed that the exact balance between nonlinearity and dispersion is responsible for the growth of solitary waves. The other nonlinear evolution equation, which is important for describing soliton behaviour in plasmas, is the Nonlinear Schrödinger (NLS) equation. Taniuti and Washimi [17] also showed that hydromagnetic waves in a cold plasma could be described by the NLS equation. Karpman and Krushkal [18] studied, in general, the propagation of modulated waves in a nonlinear dispersive media. This study led to the derivation of a coupled set of nonlinear equations which are now known as the Zakharov equations. This was also noted by Hasegawa [19] who derived this set and the NLS equation for modulated electrons and ion cyclotron waves. The coupled set of nonlinear partial differential equations was derived and applied to the study of Langmuir turbulence by Zakharov [20]. The details of these two nonlinear evolution equations, the KdV and the NLS equations, have been presented by a number of authors, e.g. Hasegawa [21], Whitham [4], Makhankov [22], Infeld and Rowlands [12], Petviashvili and Pokhotelov [13]. The KdV and NLS equations have also been used by different authors for the study of other plasma modes, viz. Trivelpiece-Gould [23], upper-hybrid [24], Alfvén [25], whistler [26] and lower-hybrid [27]. At the same time of Washimi and Taniuti [14], Sagdeev [28] investigated fully nonlinear ion-acoustic solitary waves in an unmagnetised plasma where the exact nonlinear equations governing the plasma waves are used to derive the energy integral and to study the characteristics of solitary waves without using the perturbation method. The study of solitary waves in plasmas, starting from the works of Washimi and

Taniuti [14] and Sagdeev [28], has been extensively developed and reported in many books and journals of plasma physics in the last two decades. These developments are now being used as tools in laboratory experiments, computational study and space research.

In recent years, the study of electrostatic solitary waves in plasmas, which plays a vital role in understanding the nonlinear features of localised electrostatic disturbances in laboratory plasmas [29-31] as well as in space plasmas [32-34], has attracted the attention of many workers. The nonlinear properties of electrostatic solitary waves, under different physical situations, in cold or warm unmagnetised or magnetised plasmas with electrons at two different temperatures [35-37], with trapped electrons [38,39], with negative ions [40,41], with drifting ions [42,43], with electron beam [44,45], etc. have been studied in past few couple of years.

The study of solitary waves has not been limited only to theoretical analyses. A number of solitary wave experiments [46-54], with different arrangements and different machines, e.g. Double-Plasma (D-P) machine [46], multi-dipole type plasma device [47] and Q-machine [48], have been performed in order to find various nonlinear properties of solitary waves of different modes, such as ion-acoustic solitons [49,50], Langmuir solitons [51,52] and Trivelpiece-Gould solitons [53,54], in last ten years or so.

The first experimental observation of ion-acoustic solitons was by Ikezi and Taylor [49] in a D-P type machine. This experiment, along with one of its subsequent developments [50], has verified the relation between the KdV and NLS equations, that has been found by the inverse scattering method, and confirmed some fundamental properties of each individual soliton, e.g. velocity is amplitude-dependent and soliton amplitude multiplied by the square of soliton width is constant. The predicted velocity, which was obtained from this experiment for cold ion limit, was somewhat less than the measured value. A better agreement was found if the previously assumed value for ion temperature (T_i) was made more realistic [55], i.e. $T_i/T_e \sim 0.05 - 0.1$, where T_e is the electron temperature. This was later clarified in

the experiment of Pierre *et al.* [56]. Further experimental studies on ion-acoustic solitons were also made, using different machines with different techniques, by a number of experimentalists, e.g. Nakamura *et al.* [30,31] and Cooney *et al.* [57].

An experimental observation of Langmuir solitons in an unmagnetised plasma, where electron plasma waves would be trapped in the troughs of the ion-acoustic wave [58], was made by Ikezi [51]. A series of experiments, where Langmuir solitons are excited and studied in magnetised plasmas, were also performed by Antipov *et al.* [52,59,60]. These have been reviewed in more details by Antipov *et al.* [61]. The experiments on Langmuir solitons are less complete than those on ion-acoustic solitons. It should be mentioned here that the excitation of Langmuir solitons is thought to occur naturally in space, e.g. at the earth's bow shock [62], around the bow shock of Jupiter [63] and in some pulsars [64].

The experiments on Trivelpiece-Gould solitons, usually performed in Q-machines, are less extensive than those on ion-acoustic solitons or Langmuir solitons. A novel technique to excite these solitons, by injecting a velocity modulated electron beam into the plasma column, was developed by Fedorchenko *et al.* [53]. The authors examined the effects of changing the beam and plasma parameters and geometrical dimensions on the soliton formation. There are some other experiments on Trivelpiece-Gould solitons performed by different research workers, such as Karpman *et al.* [54,65], Lynov *et al.* [66] and Saeki *et al.* [67].

1.3 Solitary Waves in Space Plasmas

Solitary waves in space plasmas have been studied both by passive observation and by active experimentation. This has not only given us a dramatically different concept of nonlinear plasma dynamics in space; it also provides us with a new source of empirical knowledge that can help us to understand the physics of our universe. As we will, in this thesis, mainly be concerned with the nonlinear properties of solitary waves in non-thermal and dusty plasmas (which may be of relevance to the nonlinear dynamics of charged particles in earth's and cometary environments as

well as in planetary rings), in this section we will confine ourselves to a very brief review of some satellite observations of solitary structures and some recent works which motivate us to work in this area of space research.

Solitary waves were first observed in the magnetosphere by the American S3-3 satellite in 1976 [68]. One of the most interesting features of these solitary waves was that they all possessed weak double layers. The S3-3 results were subsequently confirmed and substantially extended by the experiments with the Swedish Viking satellite [69-71]. The double layer-structures [71] were observed in the auroral region (a region, in between the upper part of the ionosphere[2] and the lower part of the magnetosphere[3], which is illuminated by the aurora[4]). These structures, which have scale lengths of about 100m and where the plasma density is reduced by up to 50%, are negatively charged and have net potential drops of up to a few volts directed upwards in the same direction as the electric currents along the geomagnetic field lines, i.e. the structures are dissipative elements of the magnetospheric electric circuit. Figure 1.3 shows some of these observational results by the Viking satellite

[2]A region around the earth which extends from about 60 km to about 600 km and contains sufficient free electrons and ions produced by the ionising action of solar radiation.

[3]The magnetosphere, shown in figure 1.1, is a comet-shaped region which is above the ionosphere and extends out to about ten earth radii in the sunward direction and to several hundred earth radii in the anti-sunward direction and where ionised gases and magnetic fields play key roles. The edge of the magnetosphere, called the magneto-pause, represents a perfect boundary between the planetary field and plasma, and the interplanetary field and solar wind plasma. There is a thin layer, called the mantle, just inside the magneto-pause. The magnetic field lines from the day-side of the magnetosphere are drawn over the poles and into the night side to form the long stretched tail and the northern and southern lobes which are separated from each other by an interesting region called the plasma sheet (shown in the upper diagram of figure 1.1).

[4]The aurora is caused by high energy particles, namely electrons with energies typically of the order of kilovolts, which bombard the atmosphere from above and excite atmospheric oxygen and hydrogen atoms and molecules. The de-excitation of these atoms and molecules results in the spectral lights called the aurora. The maximum luminosity is usually located at about 110 km above the ground level. The upper diagram of figure 1.2 shows a view of aurora from the earth. It should be mentioned here that this, together with diagrams in figure 1.1, is collected from the home pages of Rice University.

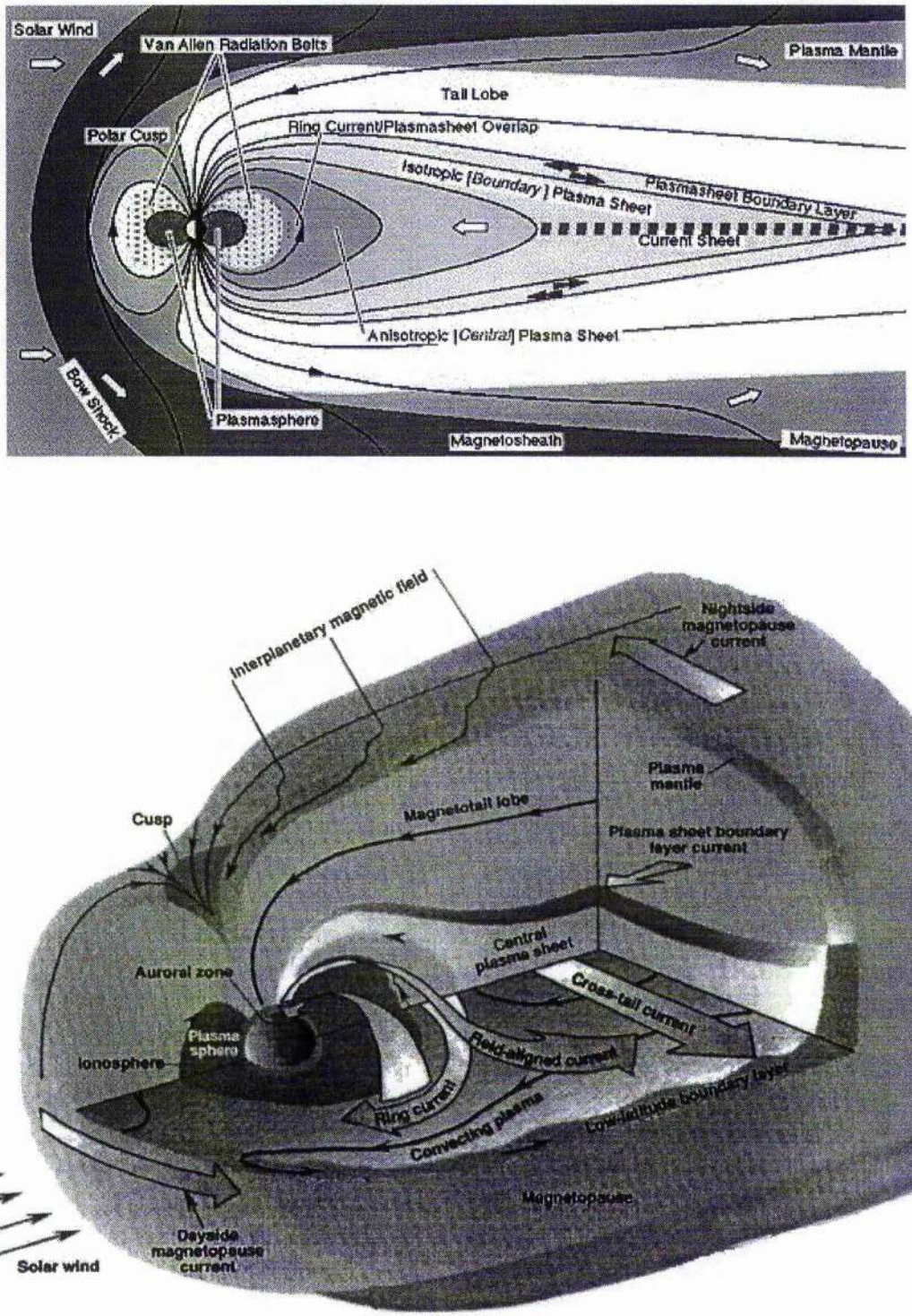

Figure 1.1: 2D sketch (upper view) and 3D sketch (lower view) of the magnetosphere showing the main particle region and some important features.

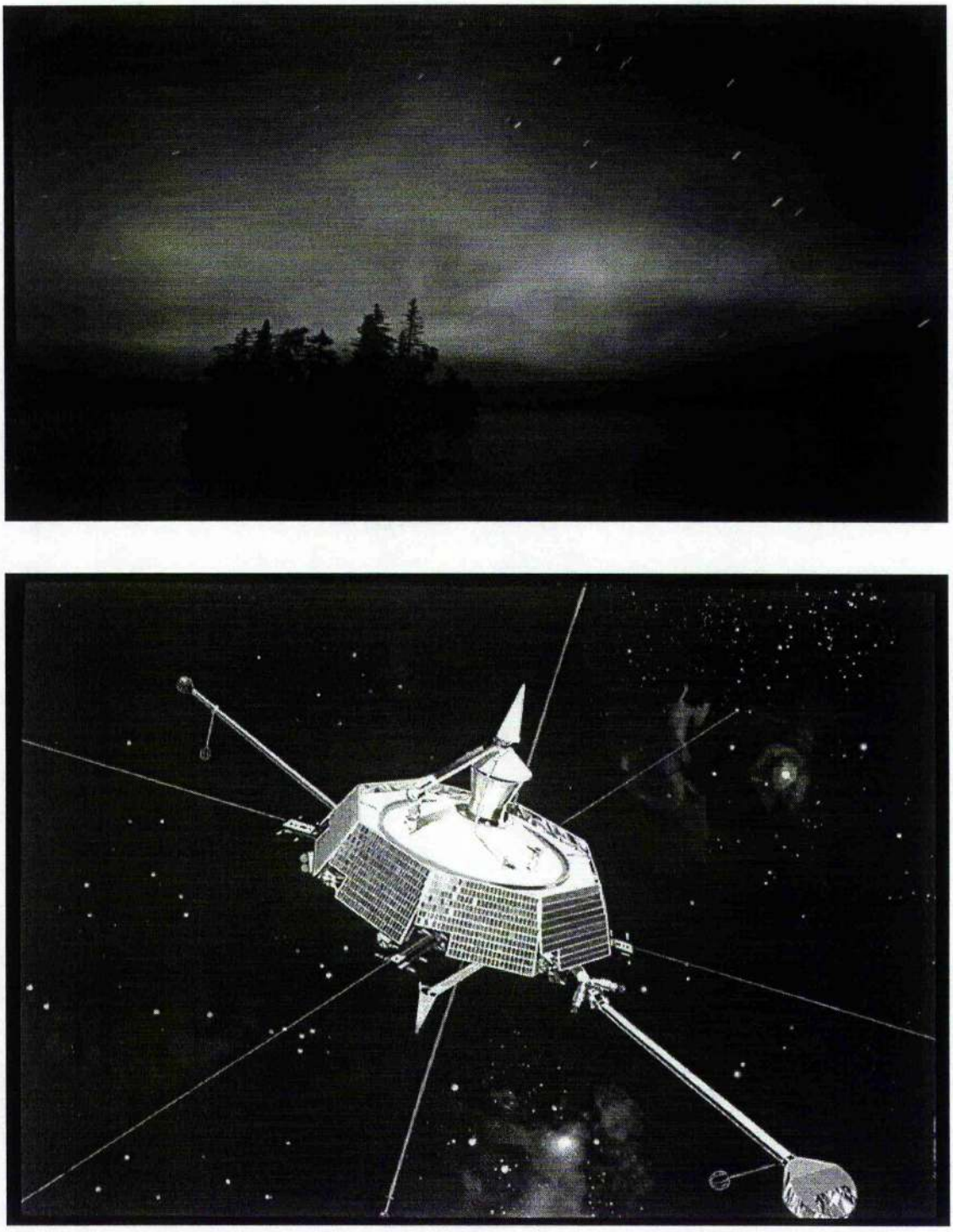

Figure 1.2: The upper diagram shows a view of the aurora from earth and the lower diagram shows an image of the Viking spacecraft.

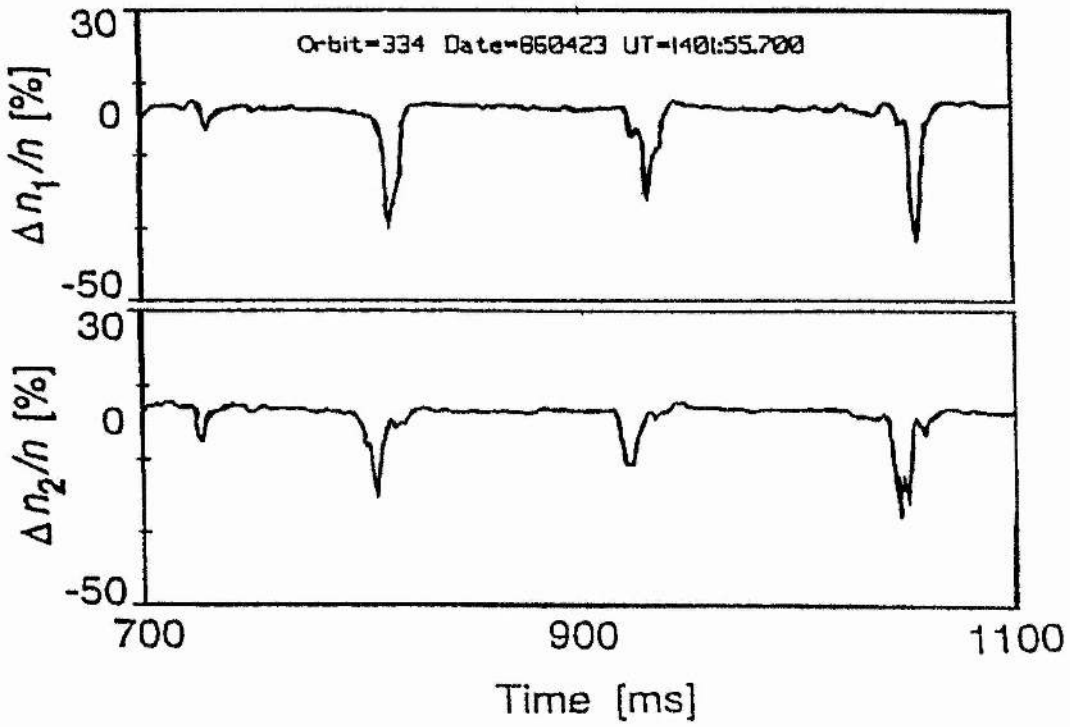

Figure 1.3: Density and lower hybrid cavities observed by the Viking satellite [71]

[71]. In Viking experiments the use of two points measurements, separated by 80 m, of the associated density fluctuation made it possible to infer their propagation characteristics. These double layer structures [71] were observed in the auroral acceleration region, with a maximum abundance at altitudes around 8000 km [72]. As no magnetic field measurements at sufficiently high sampling frequency were available, only indirect evidence (velocity estimates) of their electrostatic nature was available. Recently, Dovner *et al.* [73] in their wave experiment (F4) on the Freja satellite, has overcome the limitations of the Viking measurements by using higher time resolution and a three component search coil magnetometer and sampling six signals simultaneously. Figure 1.4 shows an image of the Freja satellite along with its launching view. These images of the Freja and Viking satellites are collected from the home pages of Swedish Institute of Space Physics. The Freja satellite scans altitudes of 600 km (the upper part of the ionosphere) to 1750 km (the lower part of the magnetosphere) in an orbit with an inclination of 63°. The Freja satellite F4

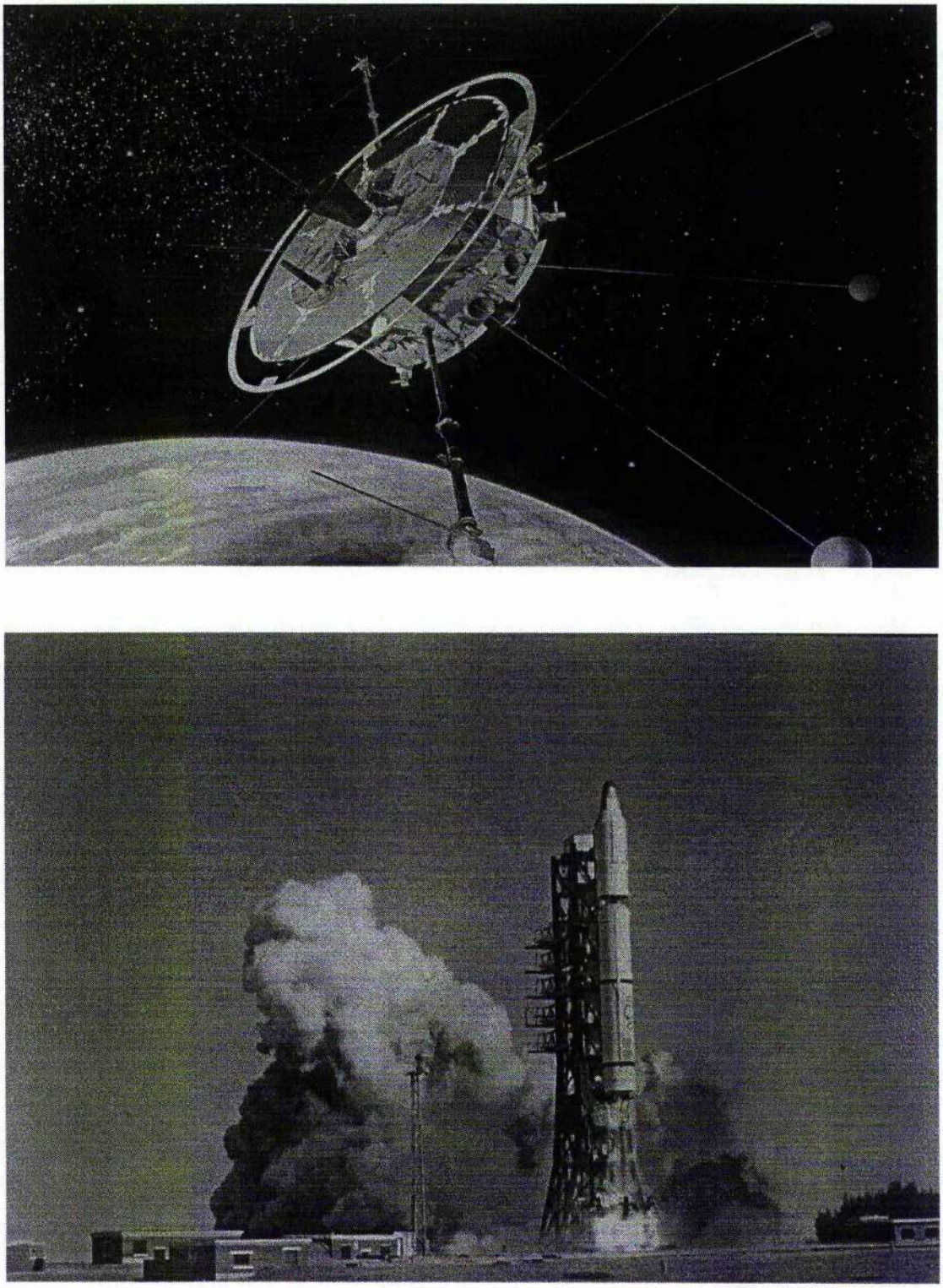

Figure 1.4: The upper diagram shows an image of the Freja satellite and the lower diagram shows its launching view.

experiment [73] has detected various types of electrostatic solitary structures, some of which are qualitatively similar to the electrostatic solitary wave pulses observed by the S3-3 and Viking satellites [68-71]. Some are lower hybrid cavities, which are characterised by the ambient electron density depletion associated with a lower hybrid wave packet inside, and some are related to lower hybrid cavities, but inside the density depletion there are solitary electrostatic structures as well as lower hybrid waves. Figure 1.5 shows some (density and lower hybrid cavities) of these results

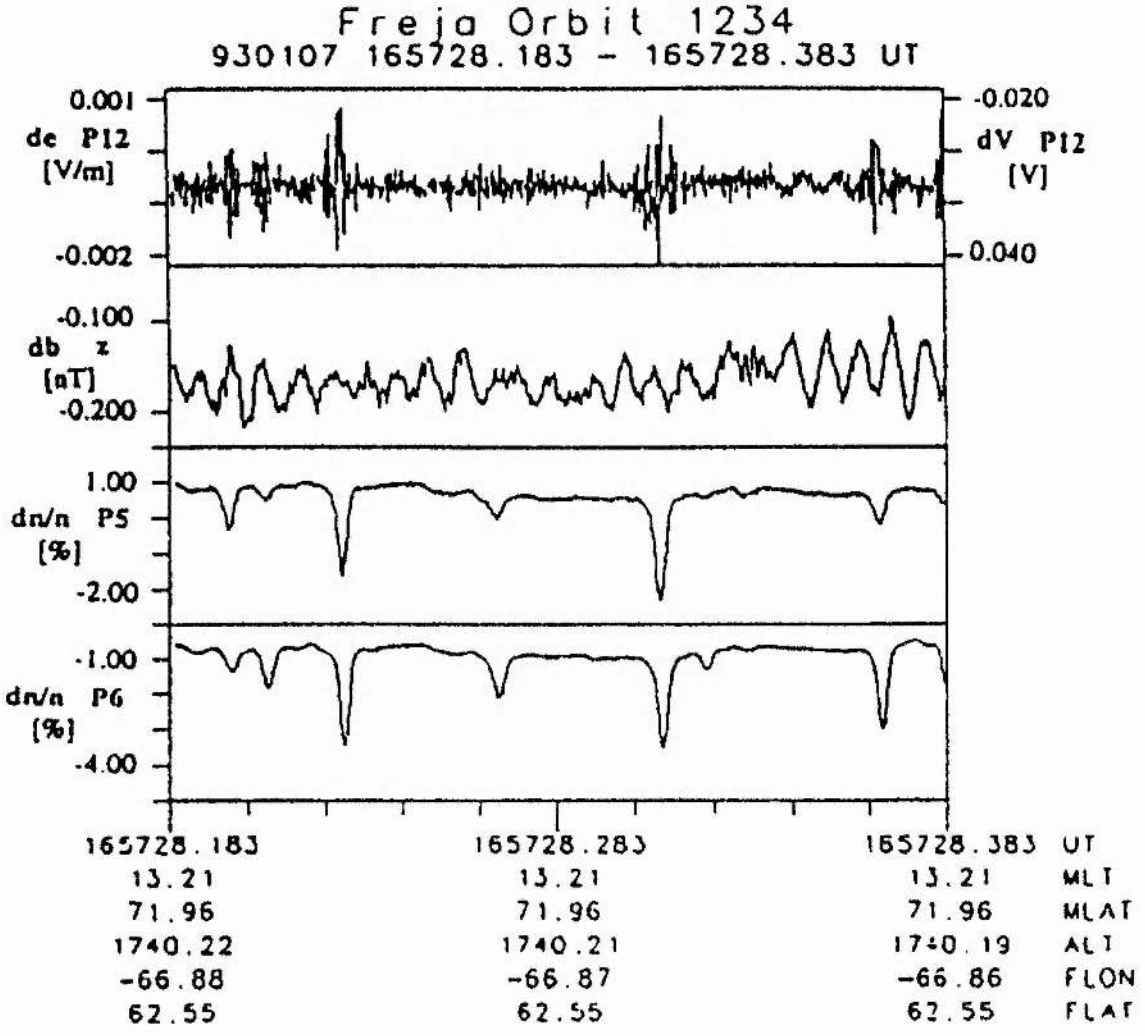

Figure 1.5: Density and lower hybrid cavities observed by the Freja satellite [73].

from the Freja satellite F4 experiment [73]. It is clear that the Freja and Viking satellites [71,73] have shown solitary structures with density depressions, some times associated with an enhanced level of lower hybrid turbulence, in which case they may be explained as cavities produced by the ponderomotive force of lower hybrid waves. However, in some cases the density depressions seem to exist without any associated turbulence. The latter class of events has motivated our study of solitary waves in non-thermal plasmas (chapters 2 and 3).

Recently, in the study of the nonlinear properties of solitary waves in space plasmas, there have arisen some interesting questions concerning dusty plasmas which are very common in space (viz. in cometary environments, planetary rings, around proto-stars and supernova remnants) and in the earth's environment (especially in the earth's ionosphere as result of rocket exhaust) as well as in the laboratory. The dusty plasma is characterised by a low-temperature ionised gas whose constituents are electrons, ions and extremely massive micron-sized dust particulates which are usually highly negatively charged due to the attachment of the back-ground plasma electrons to their surfaces. The research of dusty plasmas has not advanced much and it is still at a preliminary stage. The physics of dusty plasmas has recently been investigated by a number of authors [74-76] and some possible applications to space plasmas have also been discussed [77-79].

A number of attempts [80-89] have been made on the linear and nonlinear properties of waves in dusty plasmas. De Angelis *et al.* [75, 80] and Forlani *et al.* [81] found some changes in the dispersion relation of small-amplitude waves in dusty plasmas, in which a spatial inhomogeneity is created by the distribution of immobile dust grains. Shukla and Silin [82] found that the presence of static charged dust grains modifies the existing plasma wave spectra. Recently, it is found that the presence of charged dust grains not only modifies the properties of plasma wave modes (such as the ion-acoustic or electrostatic ion cyclotron) but also gives rise to some new modes that are more specifically dust modes, in the sense that they involve in an essential manner the dust dynamics. The dust-acoustic mode was first

considered theoretically by Rao *et al.* [90] and subsequently by several other authors [91-95]. This dust acoustic mode has also been studied experimentally by Barkan *et al.* [96] last year. The nonlinear properties of this new dust-acoustic mode has motivated our present study of solitary waves in dusty plasmas (chapter 4).

To conclude it may be added that the study of solitary waves in space plasma seems to be a wide field, which promises new and interesting results, and a fruitful approach not only in the near-future but perhaps also for a long period of time to come.

1.4 Outline of Thesis

The main aim of this thesis is to study the nonlinear properties of arbitrary amplitude ion-acoustic solitary waves in non-thermal plasmas, which may be of relevance to magnetospheric or ionospheric plasmas, and dust-acoustic solitary waves in dusty plasmas which are most common in earth's and cometary environments as well as in planetary rings. The thesis is organised as follows:

Chapter 1: This is the introductory chapter where a brief historical review of solitary waves in plasmas has been presented. The motivation behind of this introductory chapter is to provide a comprehensive source of basic ideas on solitary waves in plasmas.

Chapter 2: This is our first attempt, which has been motivated by the observations of Viking spacecraft [71] and Freja satellite [73], to study the nonlinear properties of arbitrary amplitude electrostatic solitary waves in unmagnetised non-thermal plasmas. The effects of non-thermal electrons as well as ion temperature on these solitary waves in one and three dimensional structures are studied in detail. The time evolution of these structures is also investigated.

Chapter 3: The study of arbitrary amplitude solitary waves (presented in chapter 2) has been extended to magnetised non-thermal plasmas and the effects of the

magnetic field and the angle between the directions of magnetic field and wave propagation on these solitary structures are investigated. A similar study has been made by considering another popular plasma model, namely the two-electron-temperature plasma model. This chapter also presents an analysis of the stability of obliquely propagating small but finite amplitude solitary waves in the magnetised non-thermal plasmas.

Chapter 4: This chapter, which has been motivated by recent theoretical and experimental results [90,96], has considered a two-component dusty plasma with extremely massive, micron-sized, negatively charged inertial dust grains and Maxwellian distributed ions, and has studied the nonlinear properties of large amplitude dust-acoustic solitary waves in such a dusty plasma model. A numerical analysis of how these dust-acoustic solitary waves evolve with time has then presented. The effects of non-thermal and trapped ion distributions on these solitary waves are also incorporated.

Chapter 5: This is the concluding chapter where we have added a brief summary of the results of this thesis and, for further research, we have proposed some closely related problems which are beyond the scope of this thesis.

Chapter 2

Electrostatic Solitary Waves in Non-thermal Plasmas

2.1 Introduction

The study of electrostatic solitary waves in plasmas has received considerable attention because of its vital role in understanding the nonlinear features of localised electrostatic disturbances in laboratory plasmas [29-31] as well as in space plasmas [32-34] and has been extensively studied in the past few years [35-45]. It is found theoretically and confirmed experimentally that if the ions are assumed to respond as a fluid to perturbations in the potential, with no significant trapping in a potential well, a thermal plasma supports only compressive solitary waves (solitary structures with density compression) but not rarefactive ones (solitary structures with density depletion). Recent observations [73] made by the Freja satellite, which scans altitudes of 600 to 1750 km (the upper part of the ionosphere to the lower part of the magnetosphere), have detected solitary structures with density depletions of the order of 10%, see figure 1.5. These are associated with electric fields which suggest that they are most likely to be electrostatic in nature. Similar structures, shown in figure 1.3, have been observed previously in the magnetosphere by the Viking satellite [71]. There are basically two types of density structures observed by these satellites [71,73]. The first kind of structures (observed by only the Freja satellite

[73]) are associated with small scale lower hybrid turbulence and can be explained as cavities generated by the ponderomotive force of the lower hybrid waves. These density cavities, known as lower-hybrid cavitons [97], in the auroral zone were first reported by Vago *et al.* [98]. The other type of structures, observed by the Freja and Viking satellites [71,73], are density depletions in the absence of lower hybrid waves. The latter class of events has motivated our present study.

A number of theories have been advanced to explain these density depletions (in the absence of lower hybrid waves). The theory of wave-collapse of the lower-hybrid mode was developed by Shapiro *et al.* [99,100]. These collapsing of lower hybrid cavitons are also responsible for accelerating the ions perpendicular to the magnetic field. Mälkki *et al.* [101] put forward a BGK (Bernstein-Greene-Kruskal) mode model for the pure density depletions. Other theories have assumed them to be associated with weak double layers while others have considered the possibility of producing ion-acoustic potential structures by plasma currents [102] and have associated them with solitary wave structures. The aim of this chapter is to develop a possible theoretical explanation of these structures, which we take to be large amplitude ion-acoustic waves. We show that a non-thermal electron distribution may change the nature of ion-acoustic solitary waves and that it is possible to obtain solitary waves with density depletions and dimensions roughly in agreement with those observed. The structures, we find, involve only a simple fluid response of the ions and so differ fundamentally from those found in some previous works on ion holes [38,39] which involve a BGK type of equilibrium, in which trapped ions play an essential role while electrons are assumed to be Maxwellian.

This chapter is organised as follows. The basic equations are given in Sec. 2.2. The one dimensional solitary structures with ion temperature effects have been studied by the pseudopotential approach in Sec. 2.3. This study has then been extended to three dimensional structures in Sec. 2.4. To study the time evolution of these electrostatic solitary structures, a numerical analysis is presented in Sec. 2.5. Finally, a brief discussion is given in Sec. 2.6.

2.2 Basic Equations

We consider a plasma system consisting of warm adiabatic ions and non-thermally distributed electrons. The basic system of equations governing the ion dynamics in this plasma system is given by [4]

$$\frac{\partial n}{\partial t} + \nabla \cdot (n\mathbf{u}) = 0, \tag{2.1}$$

$$\frac{\partial \mathbf{u}}{\partial t} + (\mathbf{u} \cdot \nabla)\mathbf{u} = -\nabla\varphi - \frac{\sigma}{n}\nabla P, \tag{2.2}$$

$$\frac{\partial P}{\partial t} + \mathbf{u} \cdot \nabla P + \gamma P \nabla \cdot \mathbf{u} = 0, \tag{2.3}$$

$$\nabla^2\varphi = n_e - n, \tag{2.4}$$

where n (n_e) is the ion (electron) density normalised to the unperturbed ion density n_0; $\sigma = T_i/T_e$, with T_i (T_e) being ion (electron) temperature; u is the ion fluid velocity normalised to the ion-acoustic speed $C_s = (K_B T_e/m)^{1/2}$, with K_B and m being the Boltzmann constant and ion mass, respectively; P is the ion pressure normalised to $(n_0 K_B T_i)$; $\gamma = (2+N)/N$, N being the number of degrees of freedom (which has value 1 for the one dimensional case and 3 for the three dimensional case); φ is the electrostatic potential normalised to $K_B T_e/e$, with e being the electronic charge; the space variable is normalised to the Debye length $\lambda_D = (K_B T_e/4\pi n_0 e^2)^{1/2}$ and the time variable is normalised to the ion plasma period $\omega_p^{-1} = (m/4\pi n_0 e^2)^{1/2}$.

To model an electron distribution with a population of fast particles, we can choose the distribution function as

$$f(v) = \frac{1}{(1+3\alpha)\sqrt{2\pi}}(1+\alpha v^4)e^{-\frac{1}{2}v^2}, \tag{2.5}$$

where v is normalised to the electron thermal velocity. This distribution of electrons is shown in figure 2.1 for different values of α, viz. $\alpha = 0.15$ (solid curve), $\alpha = 0.20$ (dotted curve) and $\alpha = 0.25$ (dashed curve). The electron distribution, shown in figure 2.1, is of a shape which might be expected if particles were being accelerated by quasi-linear diffusion as a result of a spectrum of waves with phase velocities in the region where the distribution has shoulders.

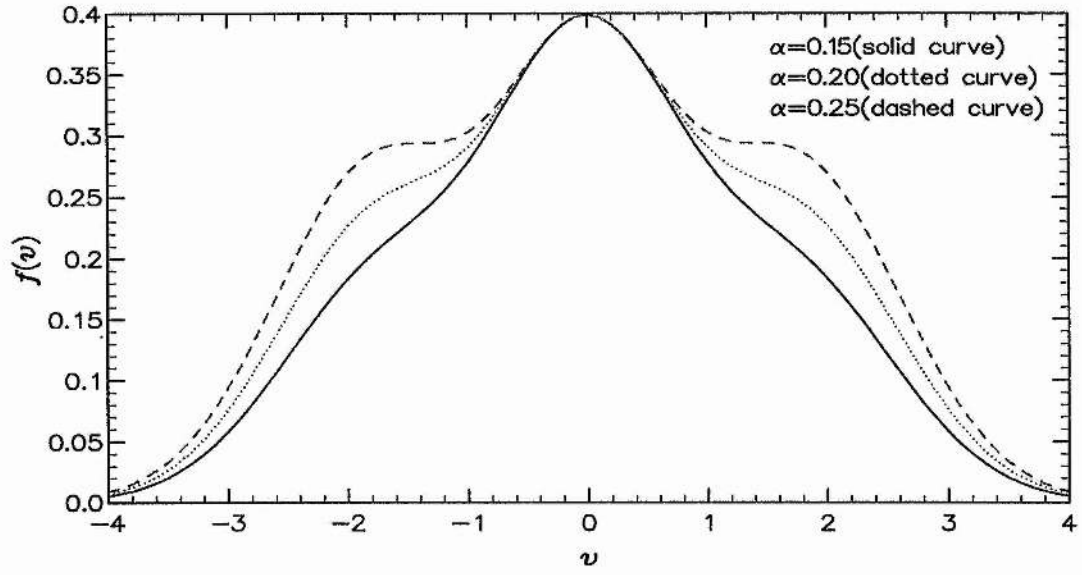

Figure 2.1: The electron distribution function for $\alpha = 0.15$ (solid curve), $\alpha = 0.20$ (dotted curve) and $\alpha = 0.25$ (dashed curve).

We now assume that the velocity of the solitary wave is small compared to the electron thermal velocity and the electrons take up an equilibrium distribution which is a function of their energy and is given simply by replacing v^2 in Eq. (2.5) with $(v^2 - 2\varphi)$. Integrating this equilibrium electron distribution function over velocity, we can write the electron density n_e as

$$\begin{aligned} n_e &= \frac{1 + 3\alpha - 4\alpha\varphi + 4\alpha\varphi^2}{1 + 3\alpha} e^{\varphi} \\ &= (1 - \beta\varphi + \beta\varphi^2) e^{\varphi}, \end{aligned} \tag{2.6}$$

where

$$\beta = \frac{4\alpha}{1 + 3\alpha}. \tag{2.7}$$

2.3 One Dimensional Structures

We will confine ourself, in this section, to a study of solitary waves in our non-thermal plasma model for one dimensional structures. The basic equations, in the one dimensional case where $\gamma = 3$, can be expressed as

$$\frac{\partial n}{\partial t} + \frac{\partial}{\partial x}(nu) = 0, \tag{2.8}$$

$$\frac{\partial u}{\partial t} + u\frac{\partial u}{\partial x} = -\frac{\partial \varphi}{\partial x} - \frac{\sigma}{n}\frac{\partial P}{\partial x}, \tag{2.9}$$

$$\frac{\partial P}{\partial t} + u\frac{\partial P}{\partial x} + 3P\frac{\partial u}{\partial x} = 0, \tag{2.10}$$

$$\frac{\partial^2 \varphi}{\partial x^2} = (1 - \beta\varphi + \beta\varphi^2)e^{\varphi} - n. \tag{2.11}$$

To obtain a solitary wave solution, we make all the dependent variables depend on a single independent variable $\xi = x - Mt$, where M is the Mach number (the velocity of the solitary wave normalised to the ion-acoustic speed C_s). Considering the steady state condition, i.e. $\frac{\partial}{\partial t} = 0$, we can write our basic set of equations as

$$M\frac{\partial n}{\partial \xi} - \frac{\partial}{\partial \xi}(nu) = 0, \tag{2.12}$$

$$M\frac{\partial u}{\partial \xi} - u\frac{\partial u}{\partial \xi} - \frac{\sigma}{n}\frac{\partial P}{\partial \xi} = \frac{\partial \varphi}{\partial \xi}, \tag{2.13}$$

$$M\frac{\partial P}{\partial \xi} - u\frac{\partial P}{\partial \xi} - 3P\frac{\partial u}{\partial \xi} = 0, \tag{2.14}$$

$$\frac{\partial^2 \varphi}{\partial \xi^2} = (1 - \beta\varphi + \beta\varphi^2)e^{\varphi} - n. \tag{2.15}$$

Now, under the appropriate boundary conditions, viz. $\varphi \to 0$, $u \to 0$, $P \to 1$ and $n \to 1$ at $\xi \to \pm\infty$, Eqs. (2.12) and (2.14) can be integrated to give

$$n = \frac{1}{1 - u/M}, \tag{2.16}$$

$$P = n^3. \tag{2.17}$$

If we substitute Eq. (2.16) into Eq. (2.13) and then multiply this by 2, we obtain

$$2M\frac{\partial u}{\partial \xi} - 2u\frac{\partial u}{\partial \xi} - 2\sigma\frac{\partial P}{\partial \xi} + 2\frac{\sigma}{M}u\frac{\partial P}{\partial \xi} = 2\frac{\partial \varphi}{\partial \xi}. \tag{2.18}$$

Again, multiplying Eq. (2.14) by σ/M one can write

$$\sigma\frac{\partial P}{\partial \xi} - \frac{\sigma}{M}u\frac{\partial P}{\partial \xi} - 3P\frac{\sigma}{M}\frac{\partial u}{\partial \xi} = 0. \tag{2.19}$$

Now, subtracting Eq. (2.18) from Eq. (2.19), one can get a differential equation which has the form

$$3\sigma\frac{\partial P}{\partial \xi} - 3\frac{\sigma}{M}\frac{\partial}{\partial \xi}(Pu) - 2M\frac{\partial u}{\partial \xi} + 2u\frac{\partial u}{\partial \xi} + 2\frac{\partial \varphi}{\partial \xi} = 0. \tag{2.20}$$

The integration of this equation yields

$$3\frac{\sigma}{M}Pu - 3\sigma(P-1) + 2Mu - u^2 - 2\varphi = 0, \tag{2.21}$$

where we have used the same boundary conditions, viz. $\varphi \to 0$, $u \to 0$, $P \to 1$ and $n \to 1$ at $\xi \to \pm\infty$. Substituting u and P, obtained from Eqs. (2.16) and (2.17), respectively, into this equation one can obtain a quadratic equation for n^2 as

$$(3\sigma)n^4 - (3\sigma + M^2 - 2\varphi)n^2 + M^2 = 0. \tag{2.22}$$

Therefore, the solution of this equation for n is given by

$$n = \frac{\sigma_1}{\sqrt{2}\sigma_0}[1 - \frac{2\varphi}{M^2\sigma_1^2} - \sqrt{(1 - \frac{2\varphi}{M^2\sigma_1^2})^2 - 4\frac{\sigma_0^2}{\sigma_1^4}}]^{1/2}, \tag{2.23}$$

where

$$\left.\begin{aligned}\sigma_0 &= \sqrt{3\sigma/M^2},\\ \sigma_1 &= \sqrt{1+\sigma_0^2}.\end{aligned}\right\} \tag{2.24}$$

The substitution of this expression for n into Eq. (2.15) gives

$$\begin{aligned}\frac{d^2\varphi}{d\xi^2} &= (1 - \beta\varphi + \beta\varphi^2)e^{\varphi}\\ &- \frac{\sigma_1}{\sqrt{2}\sigma_0}[1 - \frac{2\varphi}{M^2\sigma_1^2} - \sqrt{(1 - \frac{2\varphi}{M^2\sigma_1^2})^2 - 4\frac{\sigma_0^2}{\sigma_1^4}}]^{1/2}.\end{aligned} \tag{2.25}$$

The qualitative nature of the solutions of this equation is most easily seen by introducing the Sagdeev potential [28]. Therefore, Eq. (2.25) takes the form

$$\frac{d^2\varphi}{d\xi^2} = -\frac{dV(\varphi)}{d\varphi}, \tag{2.26}$$

where the Sagdeev potential $V(\varphi)$ is given by

$$V(\varphi) = -[1+3\beta(1-\varphi)+\beta\varphi^2]e^{\varphi} - M^2\sqrt{\sigma_0}[e^{\theta/2}+\frac{1}{3}e^{-3\theta/2}] + C_1, \quad (2.27)$$

$$\theta = \cosh^{-1}[\frac{\sigma_1^2}{2\sigma_0}(1-\frac{2\varphi}{M^2\sigma_1^2})], \quad (2.28)$$

and C_1 is the integration constant which we will choose in such a manner that $V(\varphi)=0$ at $\varphi=0$. It is important to note here that we cannot consider the limit $\sigma \to 0$ in the Sagdeev potential $V(\varphi)$ in its present form. To consider this limit $\sigma \to 0$, we express θ as

$$\theta = \ln[\frac{\sigma_1^2}{2\sigma_0}(1-\frac{2\varphi}{M^2\sigma_1^2}) + \sqrt{\frac{\sigma_1^4}{4\sigma_0^2}(1-\frac{2\varphi}{M^2\sigma_1^2})^2-1}]. \quad (2.29)$$

It is also important to mention that in our study the condition for ion density to be real, $|1-2\frac{\varphi}{M^2\sigma_1^2}| \geq 2\sigma_0/\sigma_1^2$, must always be satisfied. Using Eq. (2.29) we can express the Sagdeev potential $V(\varphi)$ as

$$\begin{aligned} V(\varphi) = & -[1+3\beta(1-\varphi)+\beta\varphi^2]e^{\varphi} \\ & - \frac{M^2\sigma_1}{\sqrt{2}}[1-\frac{2\varphi}{M^2\sigma_1^2}+\sqrt{(1-\frac{2\varphi}{M^2\sigma_1^2})^2-4\frac{\sigma_0^2}{\sigma_1^4}}]^{1/2} \\ & - \frac{2\sqrt{2}\sigma}{\sigma_1^3}[1-\frac{2\varphi}{M^2\sigma_1^2}+\sqrt{(1-\frac{2\varphi}{M^2\sigma_1^2})^2-4\frac{\sigma_0^2}{\sigma_1^4}}]^{1/2} + C_1. \end{aligned} \quad (2.30)$$

Now, we are again going back to our general equation, Eq. (2.26), which can be regarded as an "energy law" of an oscillating particle of unit mass with velocity $d\varphi/d\xi$ and position φ in a potential $V(\varphi)$. The solitary wave solutions of Eq. (2.26) exist if (i) $(d^2V/d\varphi^2)_{\varphi=0} < 0$, so that the fixed point at the origin is unstable, (ii) there exists a non-zero φ_m, the maximum or minimum value of φ at which $V(\varphi_m) = 0$, and (iii) $V(\varphi) < 0$ when φ lies between 0 and φ_m. Some more general results can be obtained as follows. The nature of these solitary waves, whose amplitude tends to zero as the Mach number M tends to its critical value, can be found by expanding the Sagdeev potential to third order in a Taylor series in φ. The critical Mach number is that which corresponds to the vanishing of the quadratic term. At

the same time, if the cubic term is negative, there is a potential well on the negative side and if the cubic term is positive, there is a potential well on the positive side.

Therefore, by expanding the Sagdeev potential $V(\varphi)$, given by Eq. (2.30), around the origin the critical Mach number, at which the second derivative changes sign, can be found as

$$M_c = \sqrt{\frac{1}{2(1-\beta)}[1+\sqrt{1+12\sigma(1-\beta)}]} \tag{2.31}$$

and at this critical value of M the third derivative is negative, i.e. rarefactive solitary waves exist, if

$$\left.\begin{aligned} &S_\alpha < 0, \\ &S_\alpha = \tfrac{1}{2S_o^2}(1+19\tfrac{\sigma}{S_o}) - \tfrac{1}{6}, \\ &S_o = \tfrac{1}{2(1-\beta)}[1+\sqrt{1+12\sigma(1-\beta)}]. \end{aligned}\right\} \tag{2.32}$$

This gives us a very simple criterion for analysing the range of different parameters, viz. α and σ, for which the compressive and rarefactive types of solitary waves exist. We, from this point, will first study arbitrary amplitude solitary waves for the cold ion limit ($\sigma = 0$) and later show the ion temperature effects on these solitary waves.

2.3.1 Cold Ion Limit ($\sigma = 0$)

The cold ion limit, i.e. $\sigma = 0$, allows us to write our working equations, such as Eq. (2.30) (the expression for the Sagdeev potential in the energy integral), Eq. (2.31) (the expression for the critical Mach number) and Eq. (2.32) (criterion for the coexistence of compressive and rarefactive solitary waves), in the simplified form

$$\begin{aligned} V(\varphi) = &- [1+3\beta(1-\varphi)+\beta\varphi^2]e^{\varphi} \\ &- M^2\sqrt{1-2\varphi/M^2} + 1 + 3\beta + M^2, \end{aligned} \tag{2.33}$$

$$M_c = \frac{1}{\sqrt{1-\beta}}, \tag{2.34}$$

$$\alpha > \frac{\sqrt{3}-1}{3+\sqrt{3}} \simeq 0.155. \tag{2.35}$$

We first consider the behaviour of the Sagdeev potential $V(\varphi)$ with $\alpha = 0$, i.e. Maxwellian electrons. Our analytical calculations show that for $\alpha = 0$ the critical Mach number M_c becomes 1. Figure 2.2 shows the behaviour of $V(\varphi)$ near the origin as the Mach number goes through 1. It is clear that, for values below 1, there is a potential well and solutions oscillate around the origin. This means that if $\alpha = 0$, the origin is a stable fixed point for Mach number less than 1. As the Mach number M approaches 1, the potential well gets shallower and the wavelength longer. This is just the standard linear behaviour of the ion sound wave. The origin becomes an unstable point for $M > 1$. Now, looking at the potential for M around 1 on a larger scale, we get figure 2.3. This shows that there is a potential well on the positive side and we can obtain a solitary wave corresponding to a point starting from the saddle as $\xi \to -\infty$ and returning to it as $\xi \to +\infty$. There is never a well on the negative side for a Maxwellian electron distribution (i.e. $\alpha = 0$).

Now, we consider the case $\alpha = 0.2$. The critical Mach number M_c is then $\sqrt{2}$ and as we go through this value, we get the behaviour shown in figure 2.4. We see a potential well forming on the negative side, resulting in the existence of solitary waves with negative potentials and negative densities. To see what happens on the positive side, we plot curves for the same value of α and for the same set of Mach numbers on a larger scale. These are clearly shown in figure 2.5. It is seen that as we go through the critical Mach number, there is a well on the negative potential side (figure 2.4), allowing a small amplitude negative solitary wave solution with a negative potential and a negative density perturbation. The larger scale view of the potential in figure 2.5 shows that there is also a well on the positive side, which is much larger and deeper, allowing a large amplitude positive solitary wave solution with a positive potential and a positive density perturbation.

Thus, Poisson's equation, Eq. (2.26), with the Sagdeev potential $V(\varphi)$ given by Eq. (2.33), allows solitary wave solutions with both the positive and negative potentials. It is seen that as the Mach number M increases, the amplitude of the solitary waves (the amplitude of the solitary wave, if it exists, would be the value

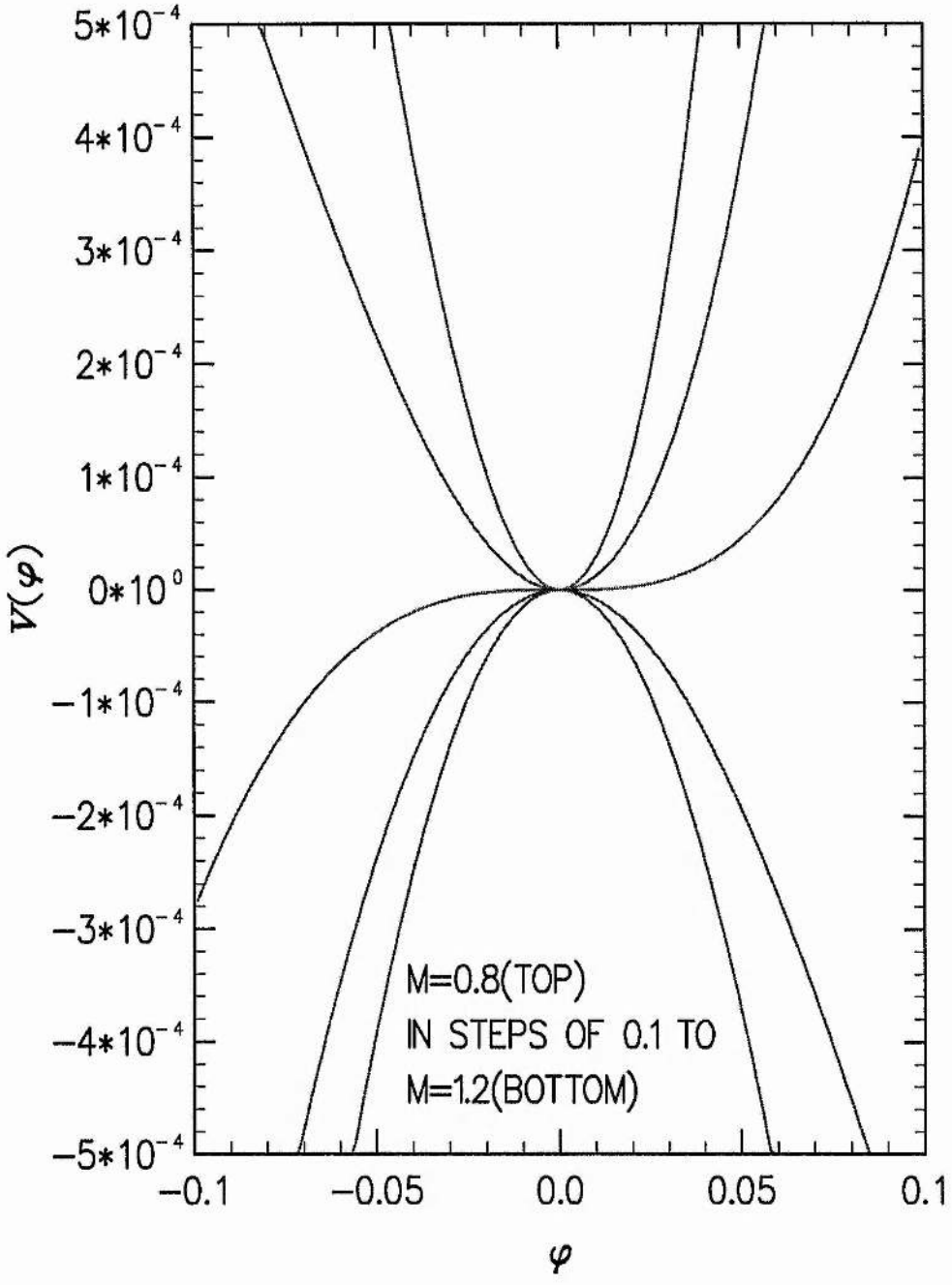

Figure 2.2: The behaviour of the Sagdeev potential $V(\varphi)$ near the origin for $\alpha = 0$ and for a series of Mach numbers, 0.8 (top) in steps of 0.1 to 1.2 (bottom).

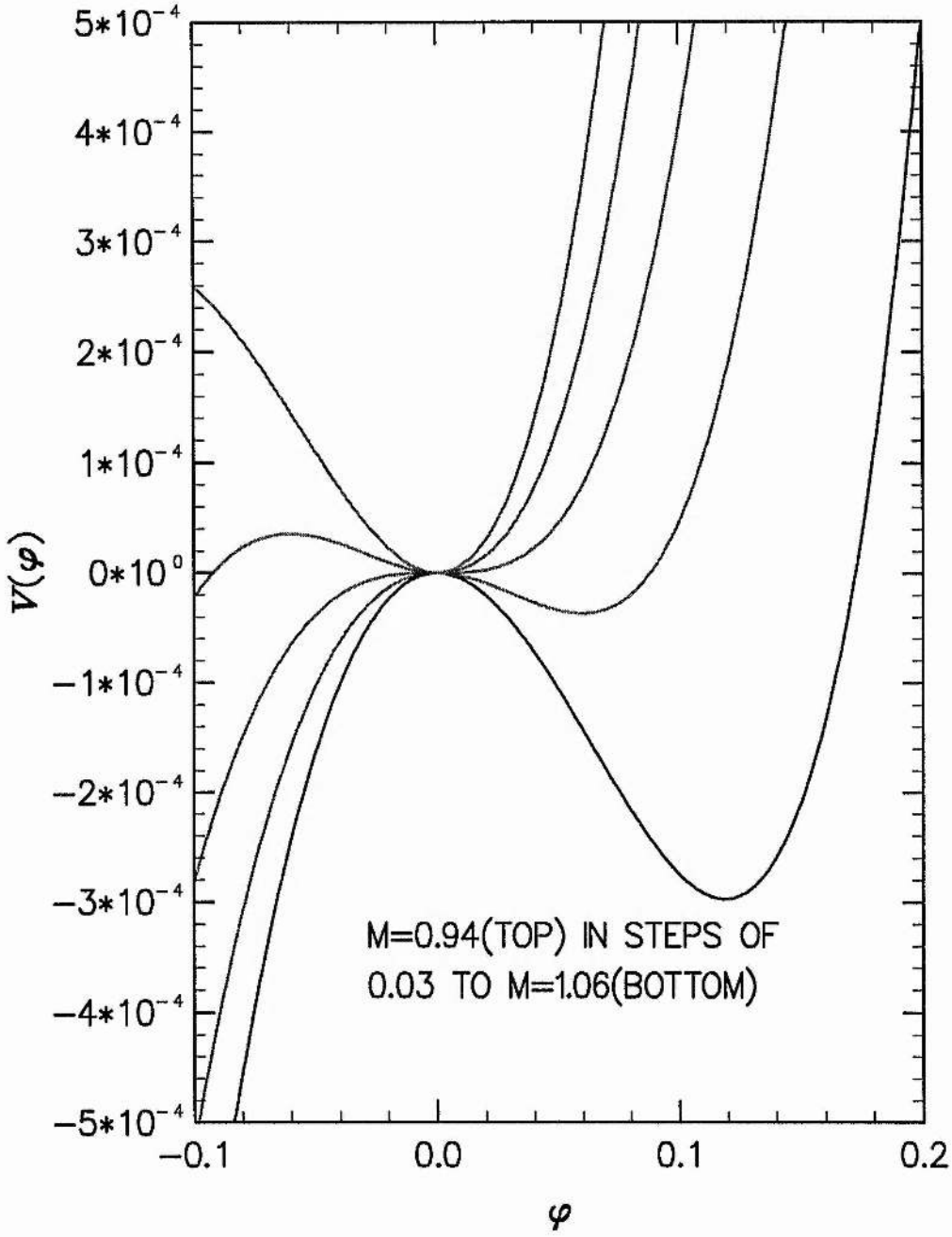

Figure 2.3: The behaviour of the Sagdeev potential $V(\varphi)$ on a larger scale for $\alpha = 0$ and for a series of Mach numbers, 0.94 (top) in steps of 0.03 to 1.06 (bottom).

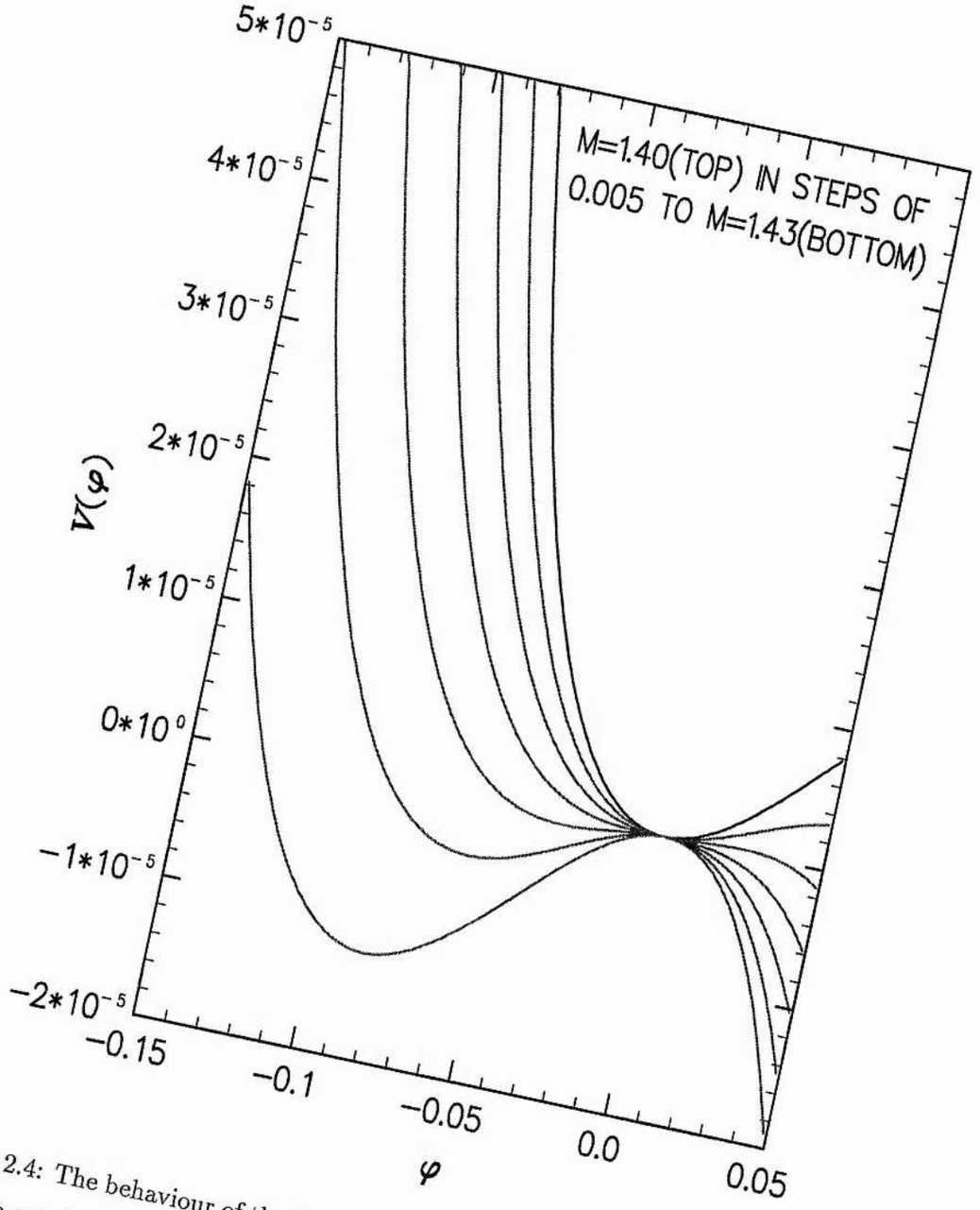

Figure 2.4: The behaviour of the Sagdeev potential $V(\varphi)$ for $\alpha = 0.2$ and for a series of Mach numbers, 1.40 (top) in steps of 0.005 to 1.43 (bottom).

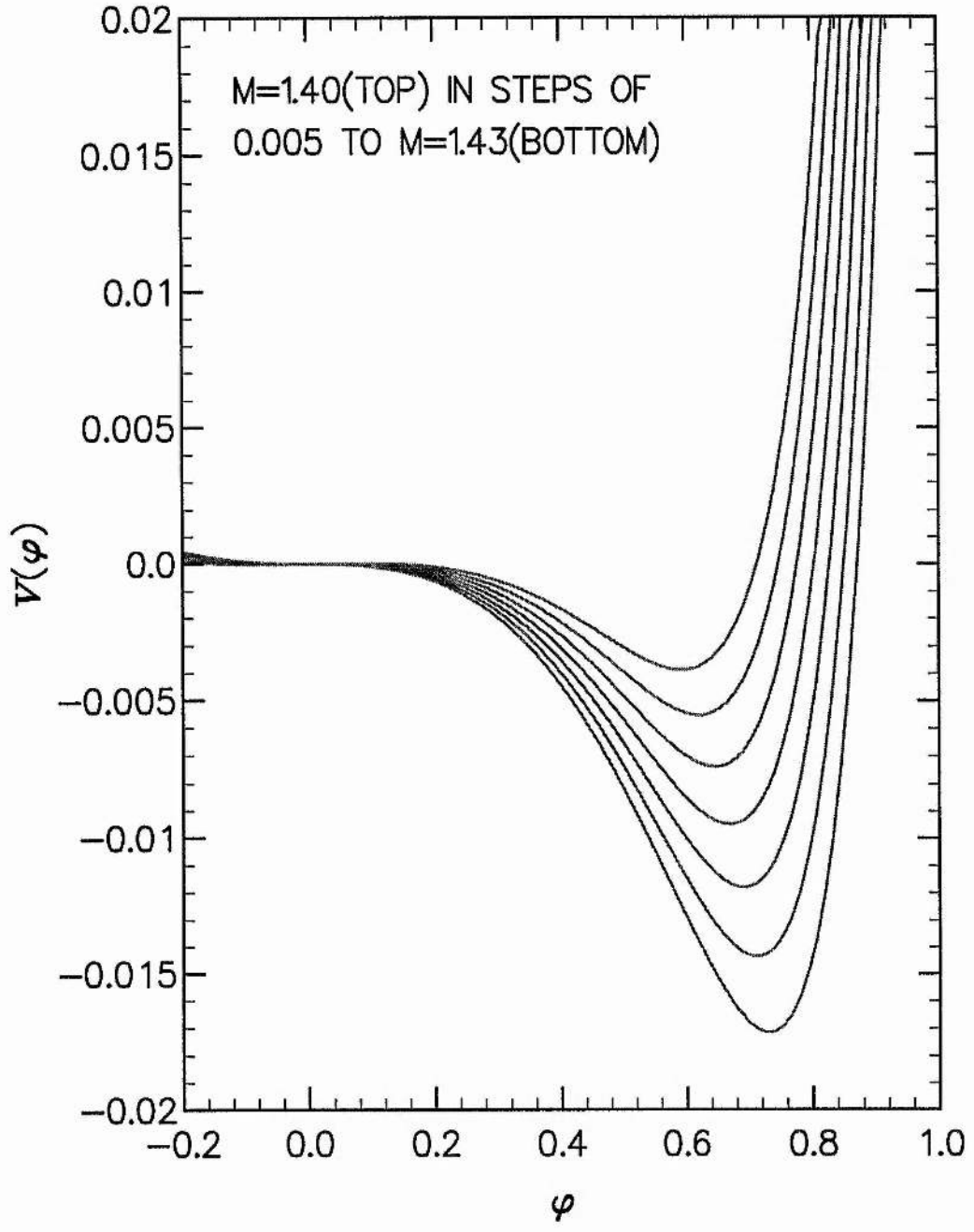

Figure 2.5: The behaviour of the Sagdeev potential $V(\varphi)$ on a larger scale for $\alpha = 0.2$ and for a series of Mach numbers, 1.40 (top) in steps of 0.005 to 1.43 (bottom).

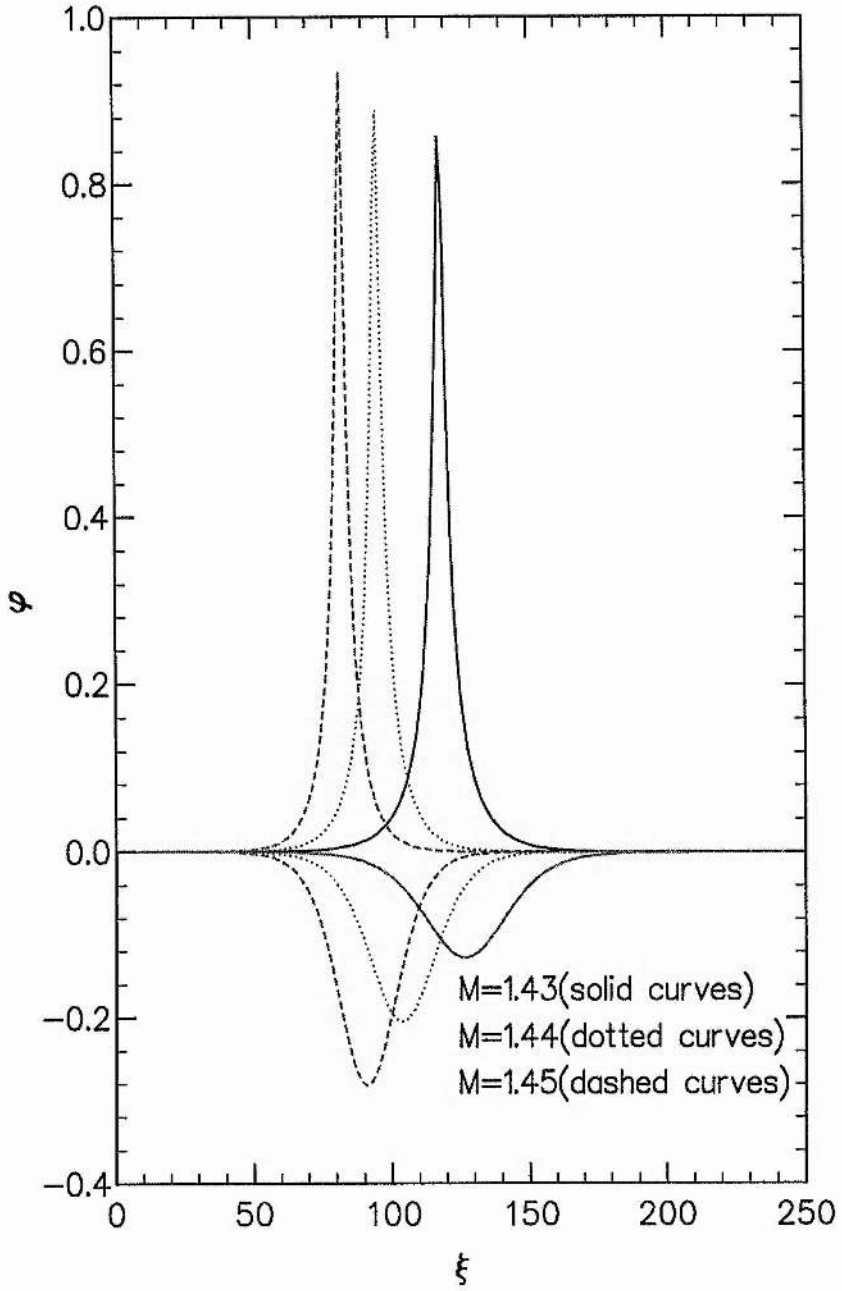

Figure 2.6: Potential profiles for $\alpha = 0.2$ and for $M = 1.43$ (solid curve), $M = 1.44$ (dotted curve) and $M = 1.45$ (dashed curve).

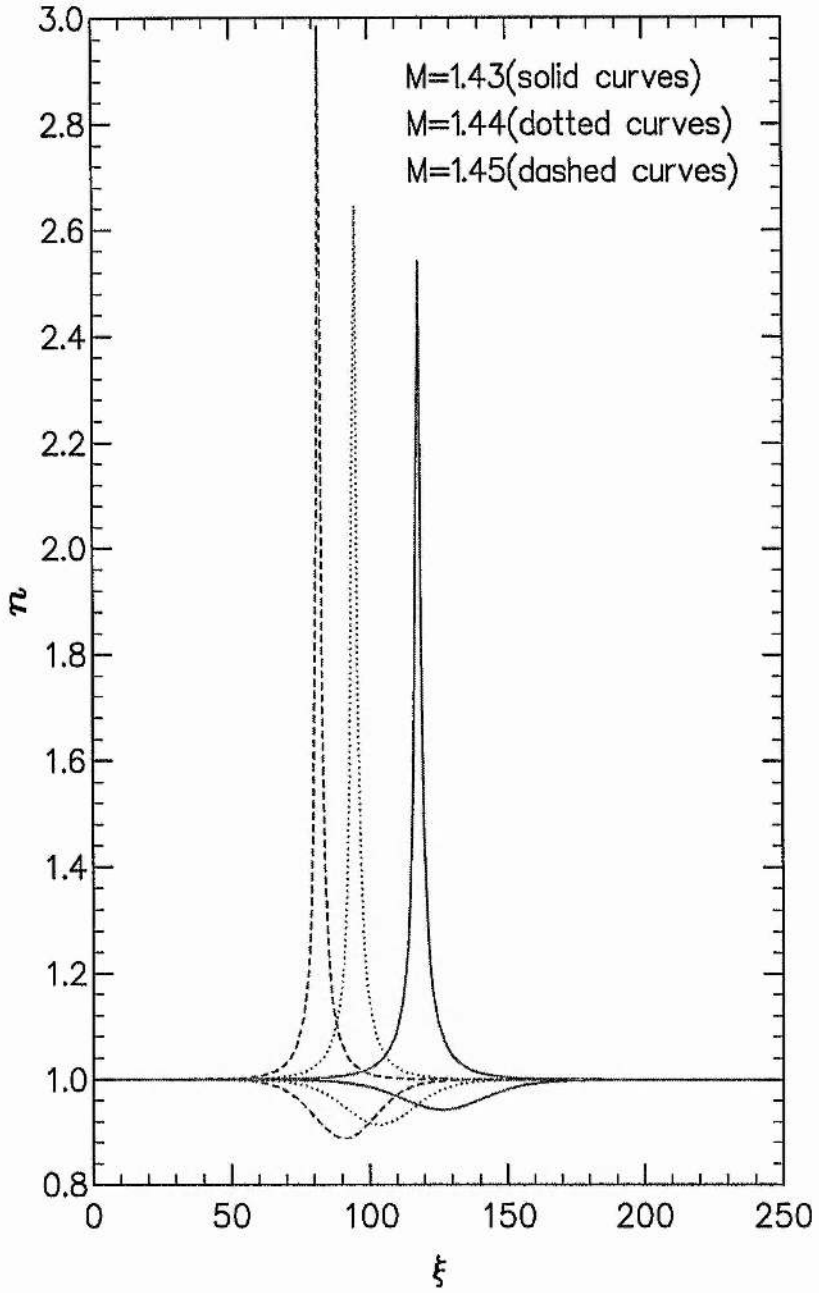

Figure 2.7: Density profiles corresponding to potentials shown in figure 2.6, i.e. for $\alpha = 0.2$ and for $M = 1.43$ (solid curve), $M = 1.44$ (dotted curve) and $M = 1.45$ (dashed curve).

of φ at which $V(\varphi)$ crosses the φ-axis from the below.) increases. Figure 2.6 shows potential profiles for two solitary wave solutions, found by solving Poisson's equation with exactly the same parameters, but different initial conditions. Figure 2.7 shows density profiles corresponding to the potential shown in figure 2.6 for two solitary wave solutions. This shows the possibility of a density hump as well as a density hole. It can be seen that the structure with a density depletion is a fairly shallow wave, with a density depletion of the order of that which is observed [71,73], and also a length scale, of the order of 50 Debye lengths, which is of the order of observed length scales. The positive structure, on the other hand, is highly nonlinear and would, presumably, require a very large initial perturbation to produce it. This may be why only density depletions have been observed [71,73]. The changed properties of the solitary waves arise from the change in the way that the electron density depends on potential.

2.3.2 Ion Temperature Effect ($\sigma \neq 0$)

We now study the effects of ion temperature on the solitary waves discussed in the previous section. It is clear from Eqs. (2.30) – (2.32) that the Sagdeev potential $V(\varphi)$, the critical Mach number M_c (which we can now define as that minimum value of M above which compressive as well as rarefactive solitary waves exist) and S_α (which determines the criterion for the coexistence of compressive and rarefactive solitary waves) nonlinearly depend on σ, i.e. on ion temperature. Figure 2.8 shows how the minimum value of α, for which compressive and rarefactive solitary waves coexist, changes with σ, i.e. with ion temperature. This shows that as the ion temperature increases, we need more non-thermal electrons in order for rarefactive solitary waves to exist. We have already showed that for $\alpha = 0.2$ the critical Mach number is $\sqrt{2}$, but due to the effect of the ion temperature this value changes. The plot in figure 2.9 shows how the critical Mach number changes with α and σ. It is clear that as the ion temperature increases, the critical Mach number (M_c) increases. It is observed that, for cold ions, i.e. $\sigma = 0$, and for $\alpha = 0.2$ (a value which we shall

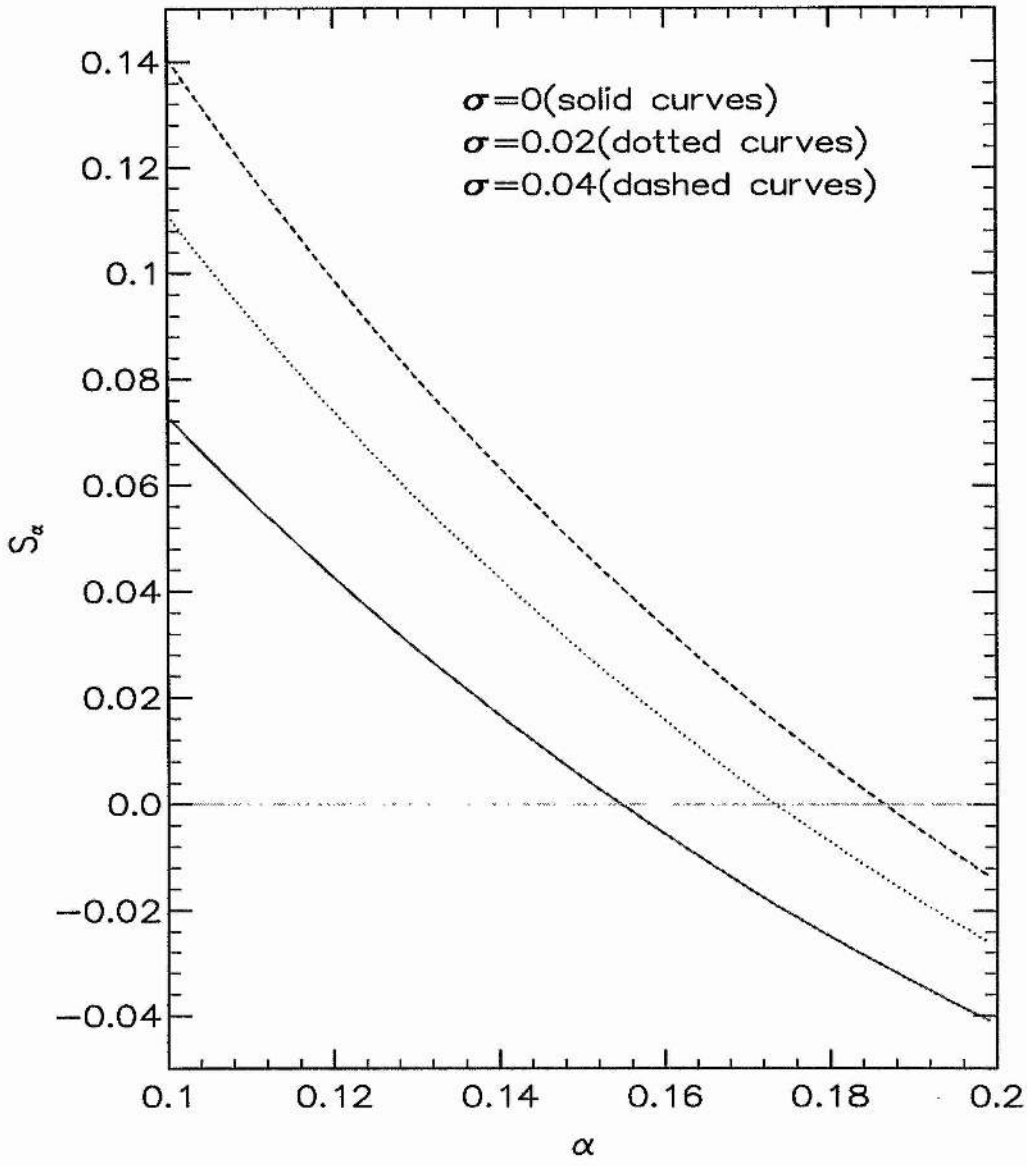

Figure 2.8: Effect of ion temperature on the minimum value of α for which compressive and rarefactive solitary waves coexist.

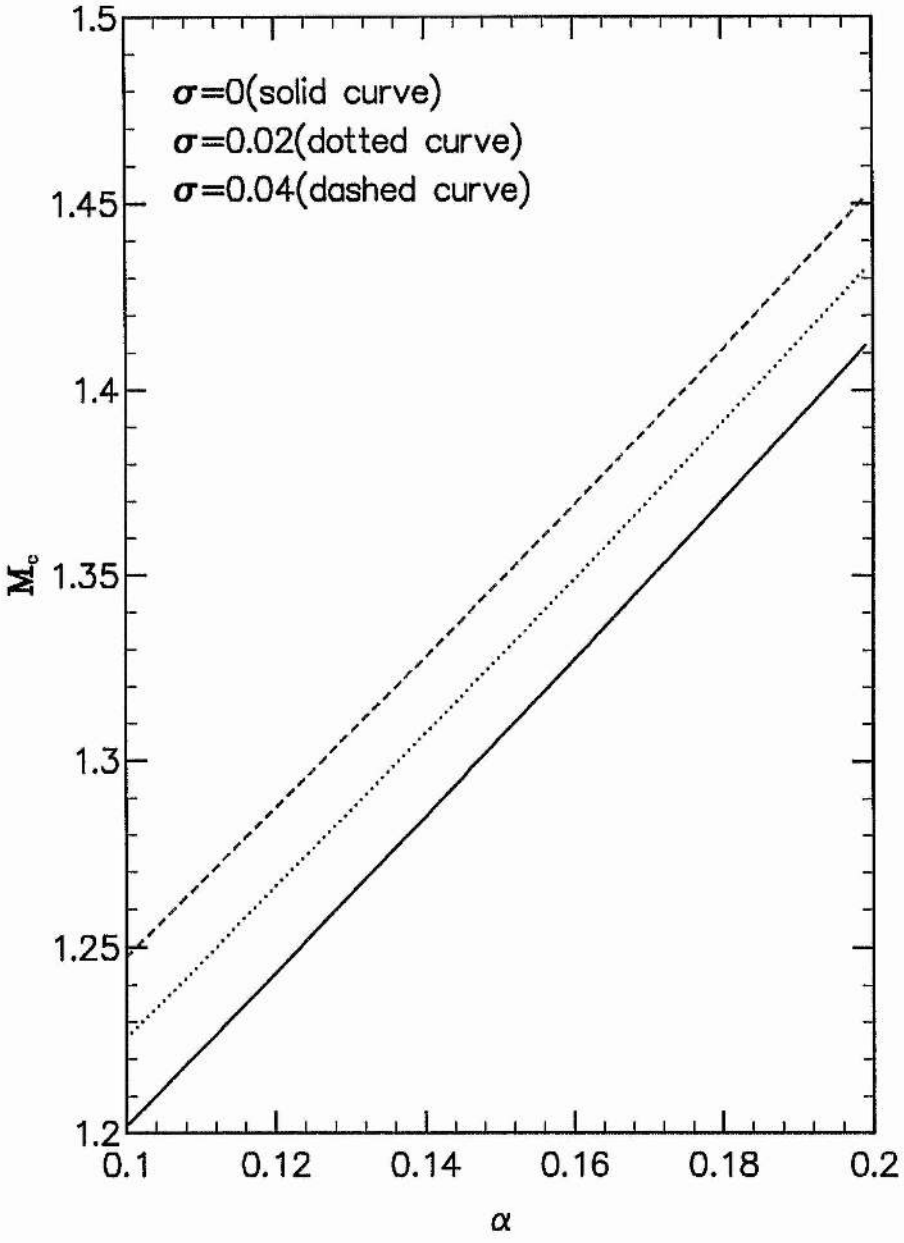

Figure 2.9: Effect of ion temperature on variation of critical Mach number with α.

continue to use in most of our numerical illustrations, if any different value of α is used, it will be mentioned), the compressive and rarefactive solitary waves are found to coexist when the Mach number passes the value $\sqrt{2} \simeq 1.414$, but for $\sigma = 0.02$, the rarefactive solitary waves do not exist until the Mach number exceeds the value 1.435. Figure 2.10 shows the behaviour of the Sagdeev potential $V(\varphi)$ when the Mach number passes from 1.43 to 1.45. This shows that when the Mach number exceeds the value 1.435, a potential well forms on the negative φ-axis, resulting in the existence of rarefactive solitary waves. To find what happens on the positive side, we plot curves for the same set of parameters on a larger scale. This is shown in figure 2.11 where it is seen that the compressive solitary waves also exist.

Now, to see what happens when the ion temperature is further increased, we numerically study the behaviour of the Sagdeev potential $V(\varphi)$ and find the parameters for which compressive and rarefactive solitary waves may coexist. These are displayed in figures 2.12 and 2.13. It is seen from figure 2.12 that when $\sigma = 0.04$, rarefactive solitary waves no longer exist for $M = 1.45$ (we have already found that, for the value less than this, rarefactive solitary waves exist when $\sigma = 0.02$), but when it exceeds this value, the rarefactive solitary waves start to exist. Figure 2.13, where the behaviour of the Sagdeev potential is shown for the same set of parameters on a larger scale, shows what happens on the positive φ-axis. It is shown that as we increase the ion temperature, we need a higher Mach number in order to obtain the coexistence of compressive and rarefactive solitary waves. Figure 2.14 shows the effects of the ion temperature on potential profiles for two (compressive and rarefactive) solitary wave solutions found by solving Poisson's equation with exactly the same parameters, but different initial conditions. It is found that as the ion temperature increases, the amplitude of both the compressive and rarefactive solitary waves decreases, whereas their width increases.

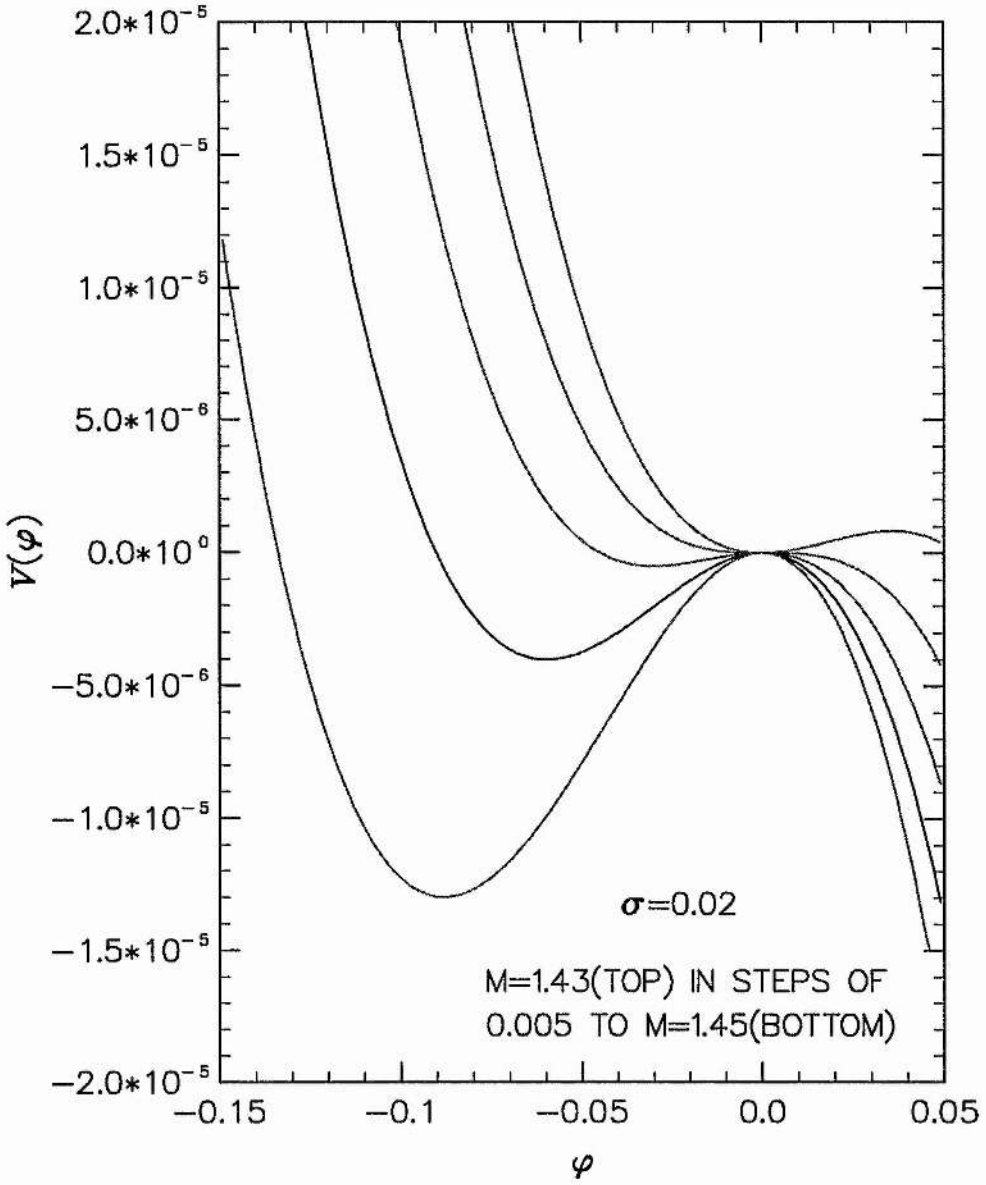

Figure 2.10: The behaviour of the Sagdeev potential $V(\varphi)$ for $\alpha = 0.2$, $\sigma = 0.02$ and a series of Mach numbers, 1.43 (top) in steps of 0.005 to 1.45 (bottom).

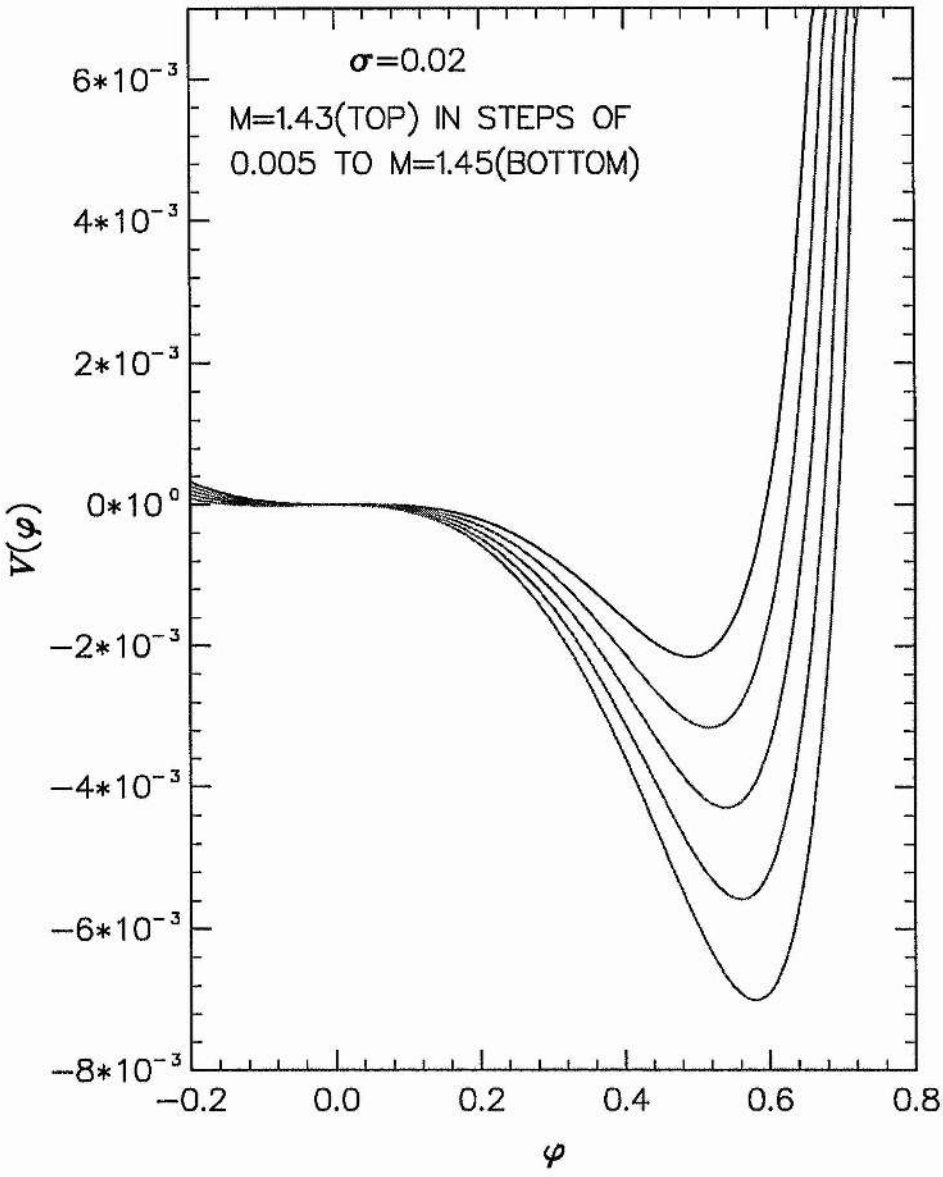

Figure 2.11: The behaviour of the Sagdeev potential $V(\varphi)$ on a larger scale for $\alpha = 0.2$, $\sigma = 0.02$ and a series of Mach numbers, 1.43 (top) in steps of 0.005 to 1.45 (bottom).

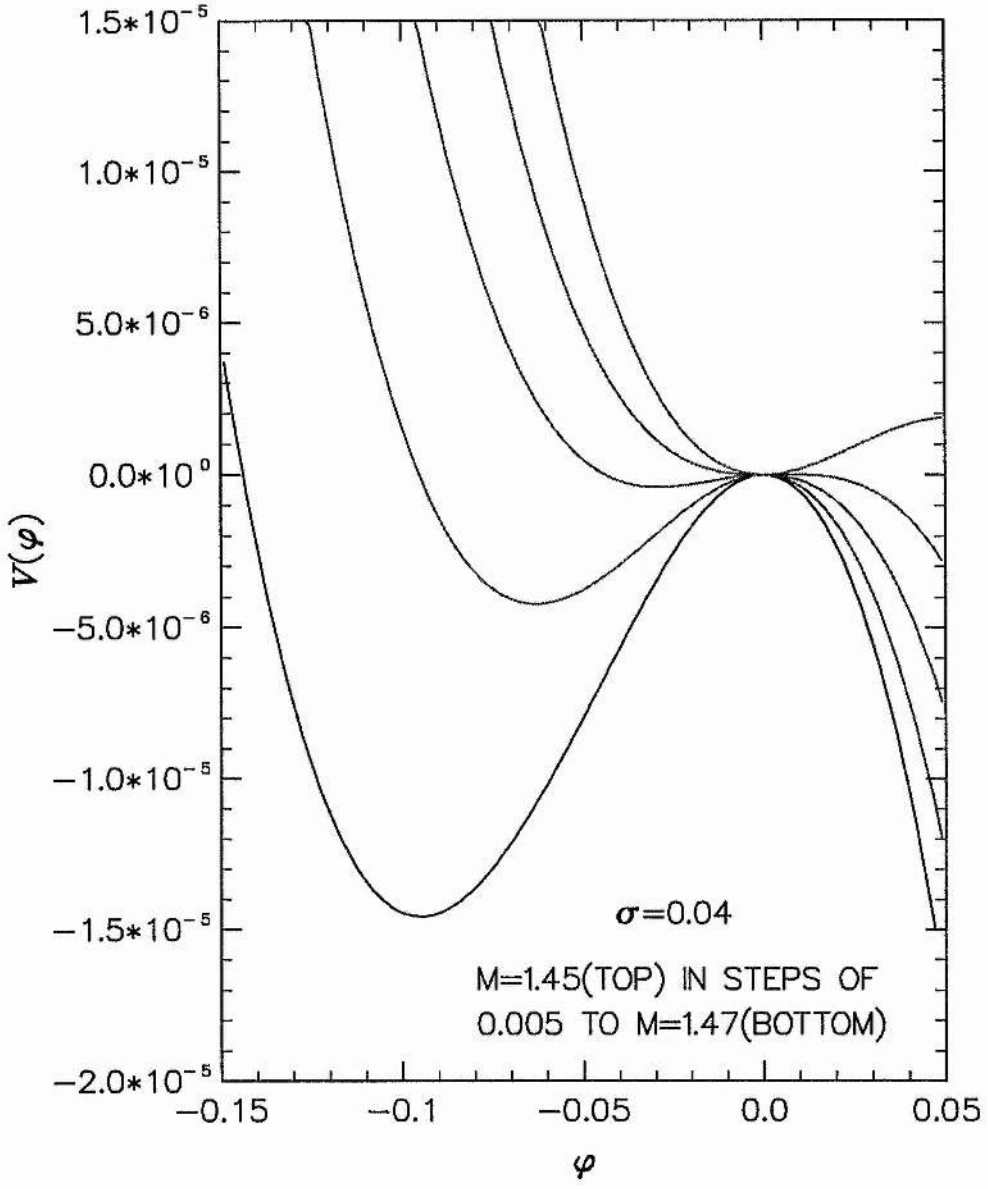

Figure 2.12: The behaviour of the Sagdeev potential $V(\varphi)$ for $\alpha = 0.2$, $\sigma = 0.04$ and a series of Mach numbers, 1.45 (top) in steps of 0.005 to 1.47 (bottom).

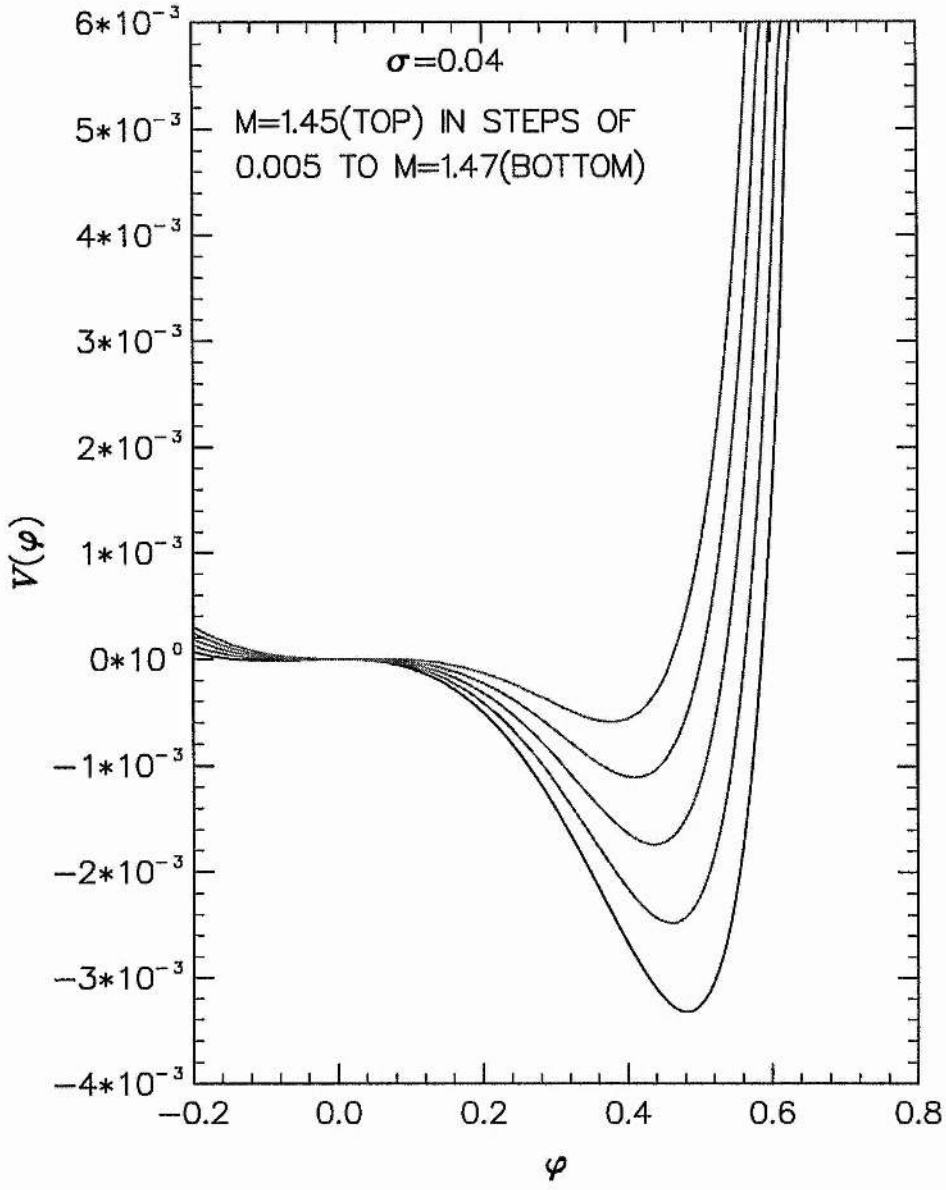

Figure 2.13: The behaviour of the Sagdeev potential $V(\varphi)$ on a larger scale for $\alpha = 0.2$, $\sigma = 0.04$ and a series of Mach numbers, 1.45 (top) in steps of 0.005 to 1.47 (bottom).

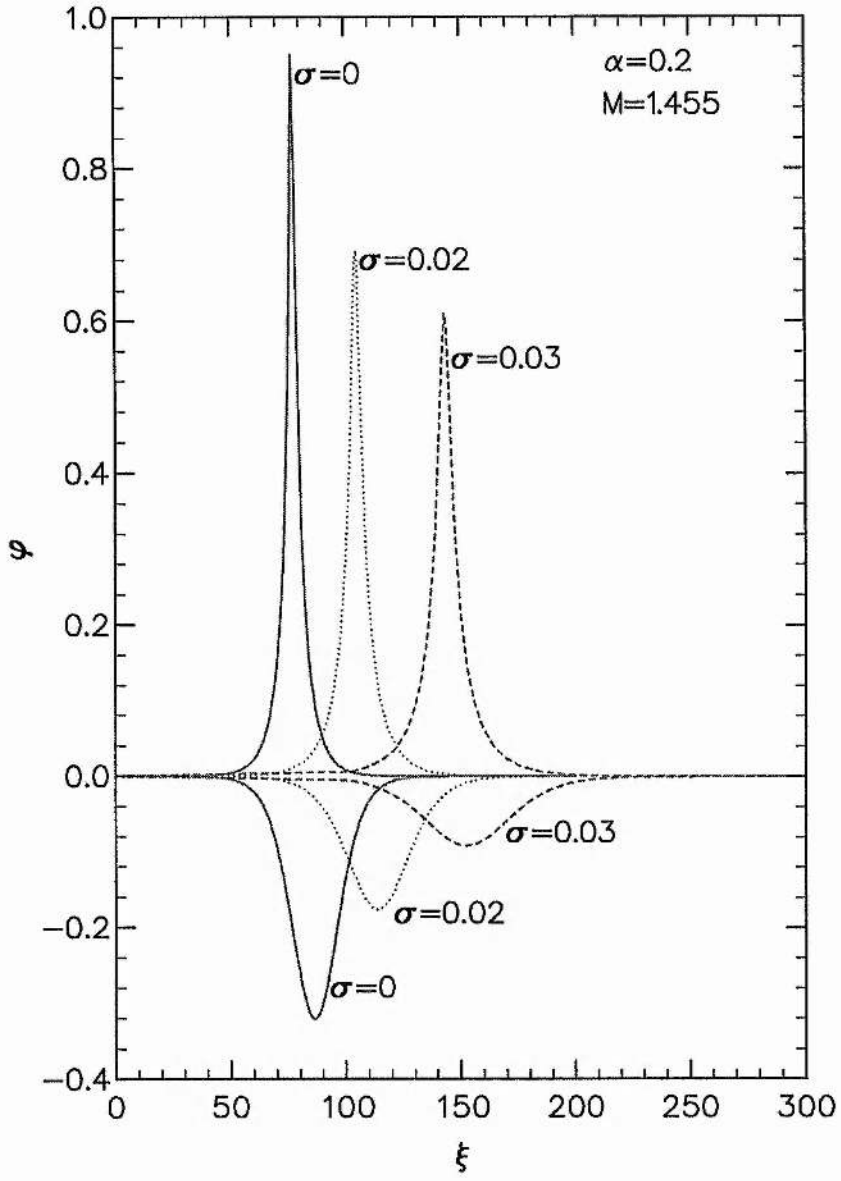

Figure 2.14: Potential profiles for $\alpha = 0.2$, $M = 1.455$ and $\sigma = 0$ (solid curve), $\sigma = 0.02$ (dotted curve) and $\sigma = 0.03$ (dashed curve).

2.4 Three Dimensional Structures

The solitary structures, discussed up to now, are one dimensional. In the present section, we will switch our attention to three dimensional solitary structures, since the structures observed in space are certainly not infinite in two directions. A very simple three dimensional analogue of the structures, discussed in the previous section, can be constructed by assuming that they are moving parallel to a strong magnetic field. If the ion Larmor radius is small compared to this size of the structure, we can just consider the ions to be a beam flowing along the field lines (in the rest frame of the structure). The ion density n then just depends on the potential, as before, and is given by Eq. (2.23). We also assume that the electrons have the same kind of adiabatic response and that the one dimensional distribution, considered up to now, is obtained by integrating over the parallel degrees of freedom. Thus, the electron density n_e is also the same and is directly given by Eq. (2.6). Therefore, under these assumptions, Poisson's equation, Eq. (2.4), can be expressed in the spherically symmetric case as

$$\begin{aligned} \frac{d^2\varphi}{dr^2} + \frac{2}{r}\frac{d\varphi}{dr} &= (1 - \beta\varphi + \beta\varphi^2)e^{\varphi} \\ &- \frac{\sigma_1}{\sqrt{2}\sigma_0}[1 - \frac{2\varphi}{M^2\sigma_1^2} - \sqrt{(1 - \frac{2\varphi}{M^2\sigma_1^2})^2 - 4\frac{\sigma_0^2}{\sigma_1^4}}]^{1/2}, \end{aligned} \tag{2.36}$$

where the space variable r is normalised to the Debye length λ_D. We will now numerically solve this equation and find spherically symmetric structures that exist as solutions of this equation. It is important to note here that, in our numerical solutions of this equation, the condition for ion density to be real, $|1 - 2\frac{\varphi}{M^2\sigma_1^2}| \geq 2\sigma_0/\sigma_1^2$, must always be valid. The potential and density profiles in a spherically symmetric solution of this equation are illustrated in figures 2.15 and 2.16. These plots also show the effects of ion temperature on these radial profiles. The most obvious change, found by comparing these radial profiles with one dimensional structures (discussed in the previous section), is that there is a larger dip in the potential as well as in the density for the same parameters. It is also seen that as we increase the ion temperature, this dip in the potential or density decreases.

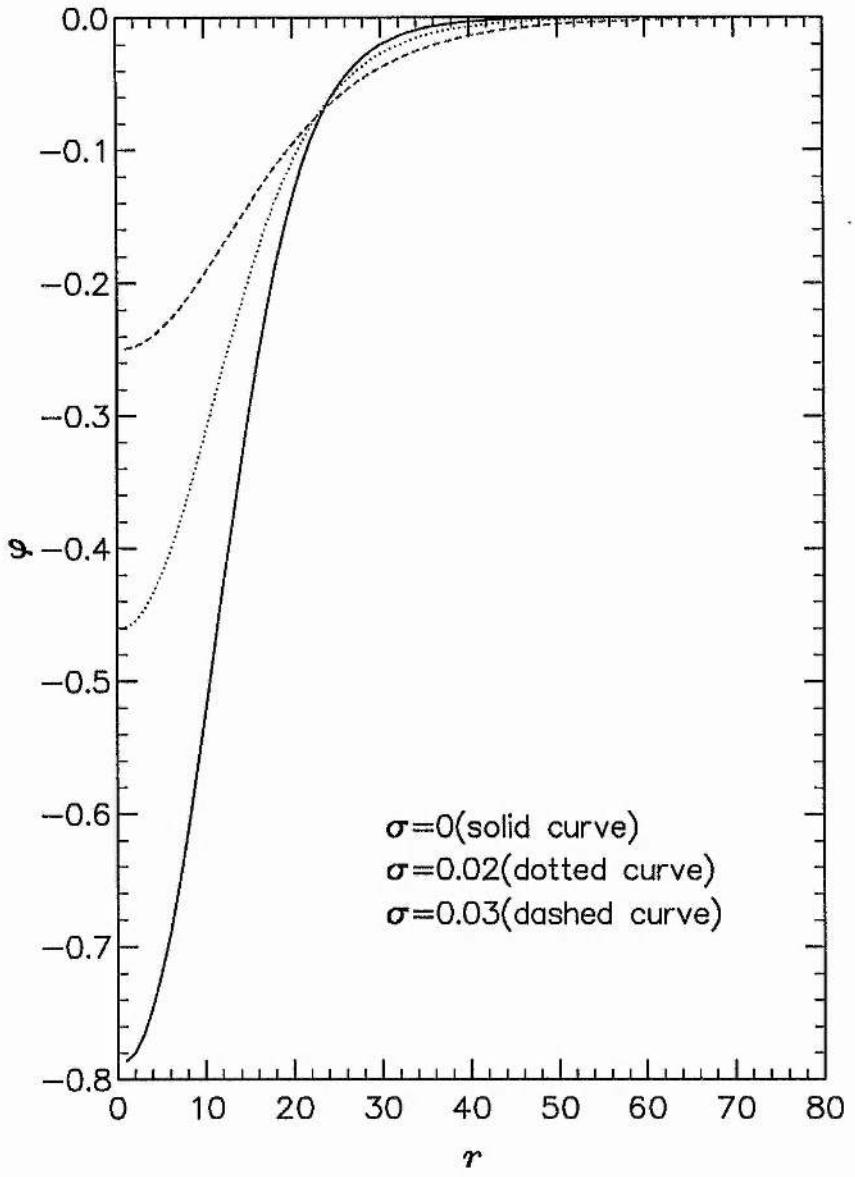

Figure 2.15: The radial potential profiles for spherically symmetrical solitary structures and for the same parameters used in figure 2.14, viz. $\alpha = 0.2$, $M = 1.455$ and $\sigma = 0$ (solid curve), $\sigma = 0.02$ (dotted curve) and $\sigma = 0.03$ (dashed curve).

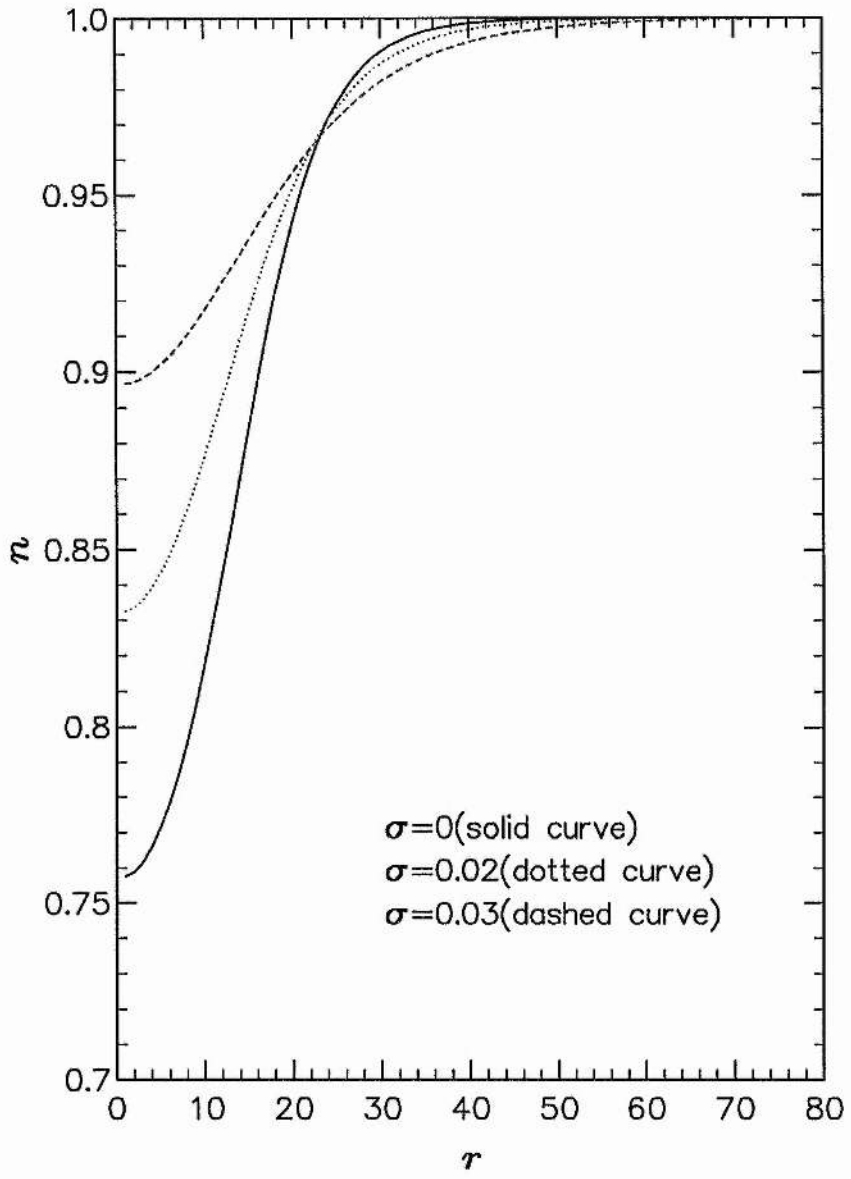

Figure 2.16: The radial density profiles corresponding to potentials shown in figure 2.15, i.e for $\alpha = 0.2$, $M = 1.455$, $\sigma = 0$ (solid curve), $\sigma = 0.02$ (dotted curve) and $\sigma = 0.03$ (dashed curve).

2.5 Time Dependent Solitary Structures

In this section, we investigate the propagation of an initial perturbation by integrating numerically the original fluid equations which can be written from our basic system of equations as

$$\frac{\partial n}{\partial t} + \frac{\partial}{\partial x}(nu) = 0, \tag{2.37}$$

$$\frac{\partial u}{\partial t} + \frac{\partial}{\partial x}(\frac{1}{2}u^2 + \varphi) = 0, \tag{2.38}$$

$$\frac{\partial^2 \varphi}{\partial x^2} = (1 - \beta\varphi + \beta\varphi^2)e^{\varphi} - n. \tag{2.39}$$

It may be mentioned here that, for the sake of simplicity, ion pressure is neglected when we are trying to see how one dimensional solitary structures evolve with time. The propagation of a single pulse of two different forms is simulated by the numerical solution of these equations using the Lax-Wendroff difference scheme. The time difference Δt and space difference Δx are 0.05 and 0.1, respectively. The two different initial pulses, which are used in this numerical simulation, are of the form

$$\varphi(x,0) = \begin{cases} \pm 0.025\ \mathrm{sech}^2(x - 20), \\ \pm 0.025 \exp[-(\frac{x}{2} - 10)^2]. \end{cases} \tag{2.40}$$

Though these initial pulses are not stationary solutions, we use the following stationary solutions for the other initial quantities:

$$u(x,0) = V_0[1 - (1 - 2\varphi/V_0^2)^{1/2}], \tag{2.41}$$

$$n(x,0) = (1 - 2\varphi/V_0^2)^{-1/2}, \tag{2.42}$$

where V_0 is the velocity of the initial pulse. The value of V_0 is chosen to be 0.773 for $\alpha = 0$ (which is nearly equal to the velocity of the solitary wave of amplitude 0.025 for $\alpha = 0$) and 0.975 for $\alpha = 0.2$ (which is close to the velocity of the solitary wave of amplitude 0.025 for $\alpha = 0.2$). We now study the time evolution of solitary structures by the numerical simulation of the original equations, Eqs. (2.37) – (2.39), with the two different initial pulses given by Eqs. (2.40), for Maxwellian ($\alpha = 0$) and non-thermal ($\alpha = 0.2$) distribution of electrons. The numerical results are

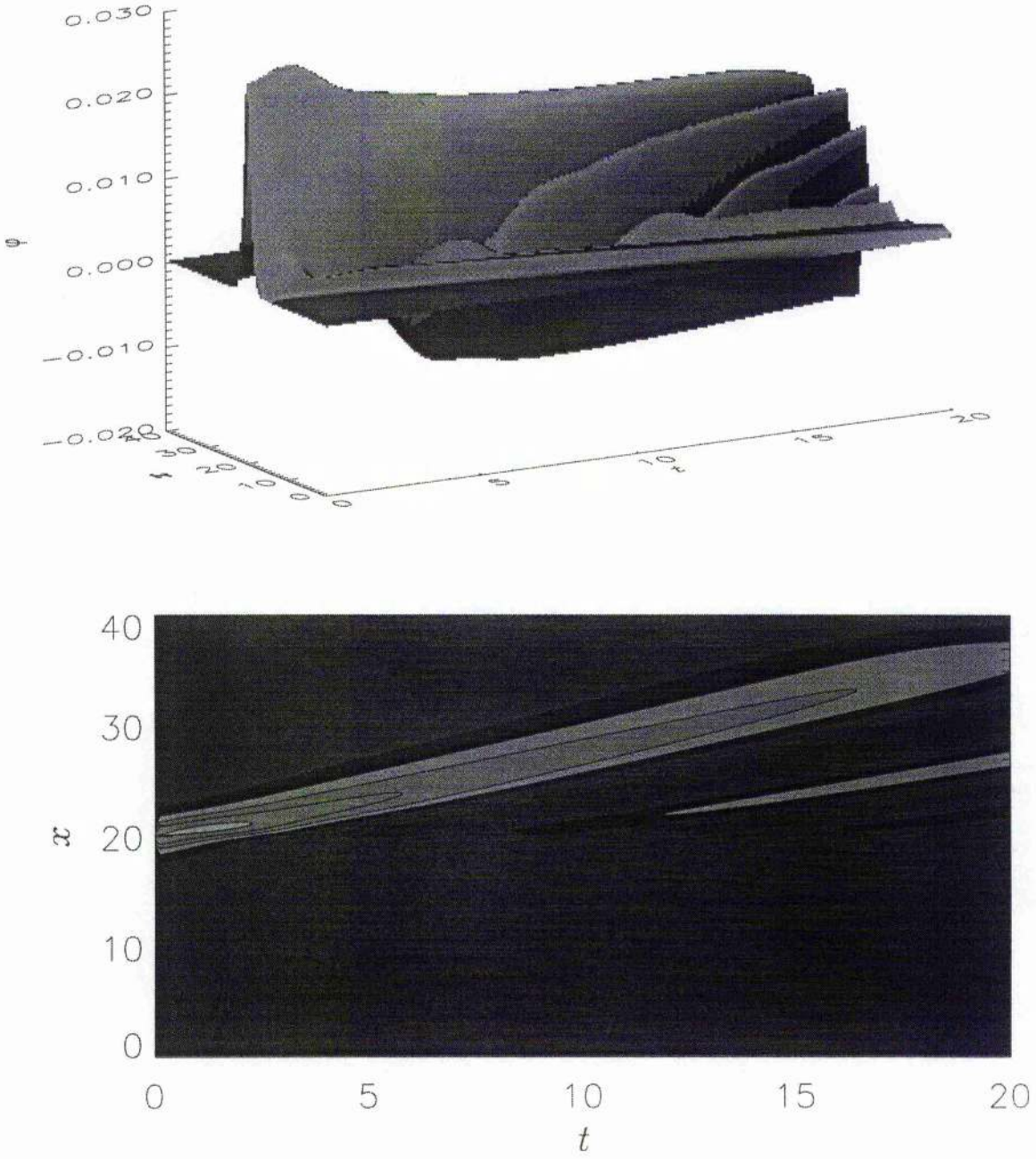

Figure 2.17: Time evolution of the initial perturbation, $0.025\ \mathrm{sech}^2(x-20)$, for $\alpha = 0$ and $V_0 = 0.773$. The lower view is the contour map of the upper plot.

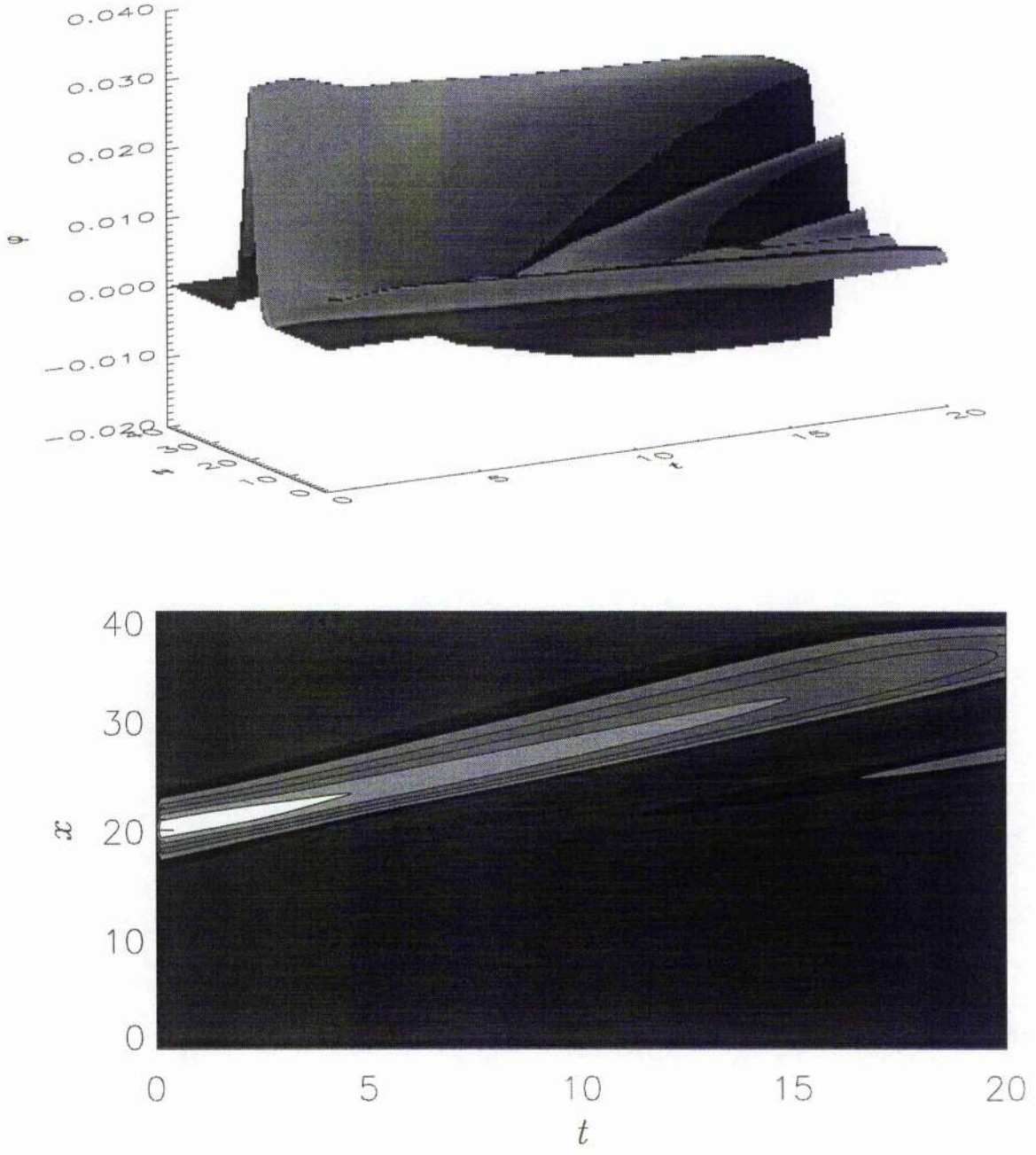

Figure 2.18: Time evolution of the initial perturbation, $0.025\exp[-(\frac{x}{2}-10)^2]$, for $\alpha = 0$ and $V_0 = 0.773$. The lower view is the contour map of the upper plot.

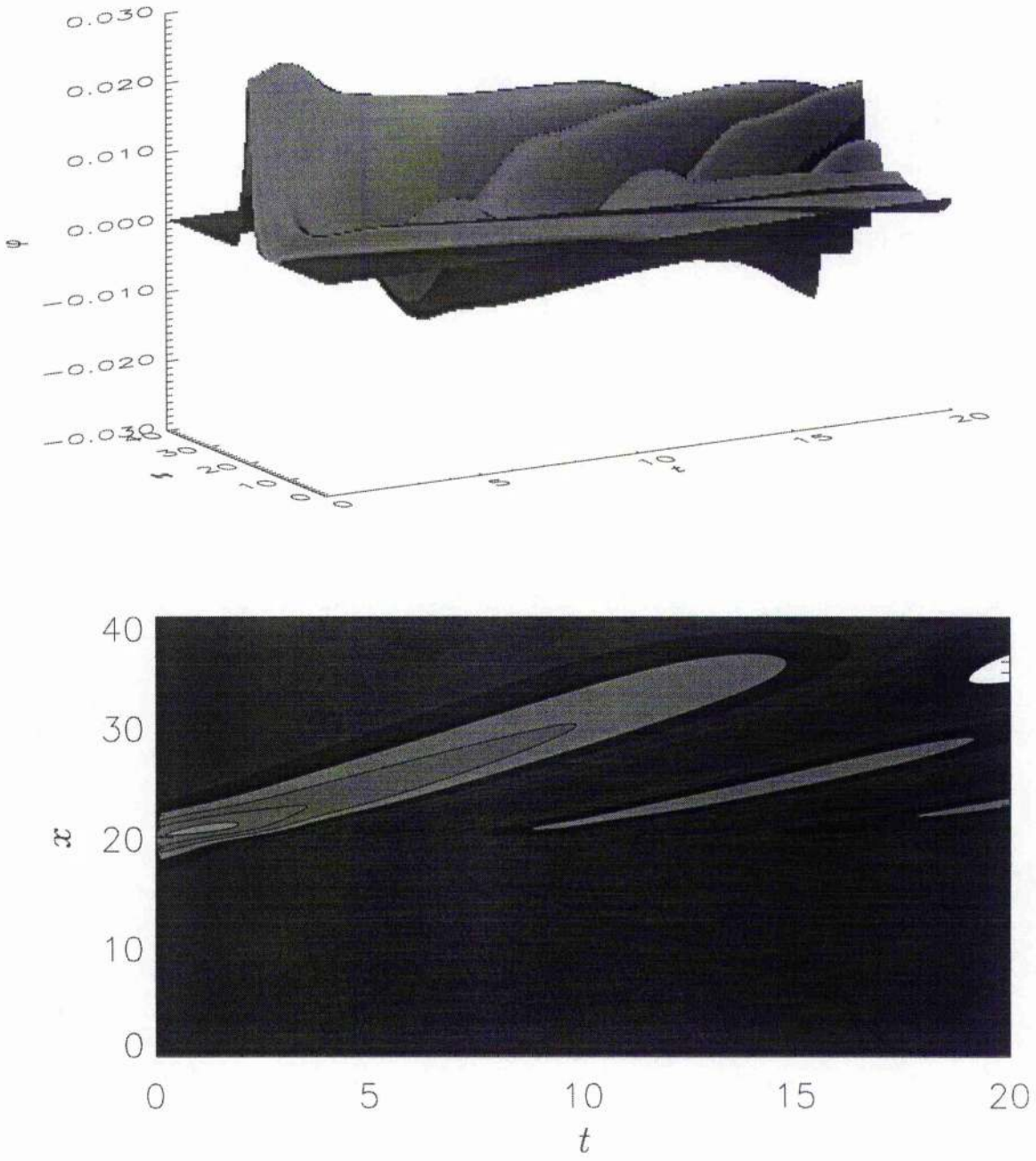

Figure 2.19: Time evolution of the initial perturbation, $0.025\ \mathrm{sech}^2(x-20)$, for $\alpha = 0.2$ and $V_0 = 0.975$. The lower view is the contour map of the upper plot.

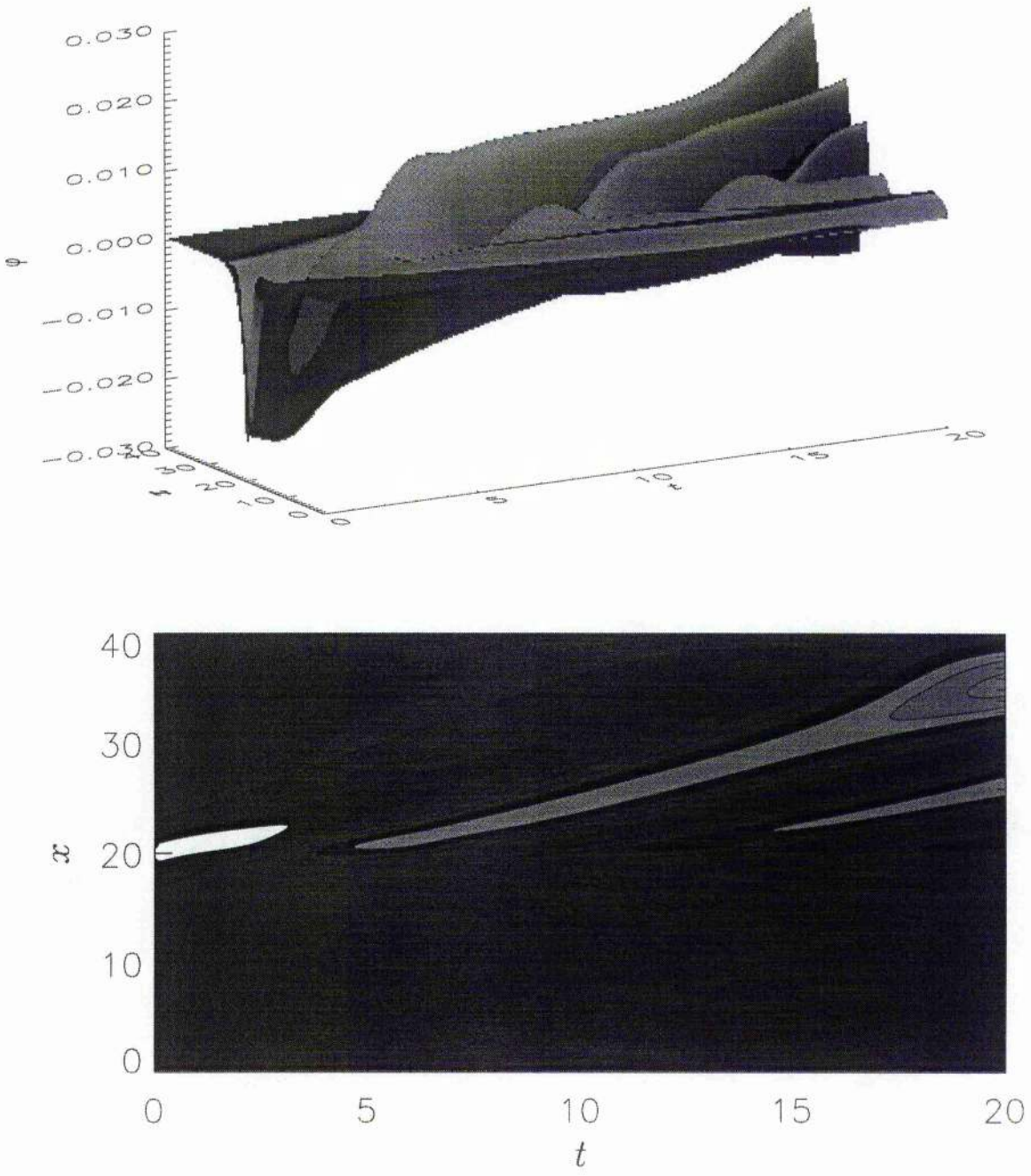

Figure 2.20: Time evolution of the initial perturbation, $-0.025\ \mathrm{sech}^2(x-20)$, for $\alpha = 0.2$ and $V_0 = 0.975$. The lower view is the contour map of the upper plot.

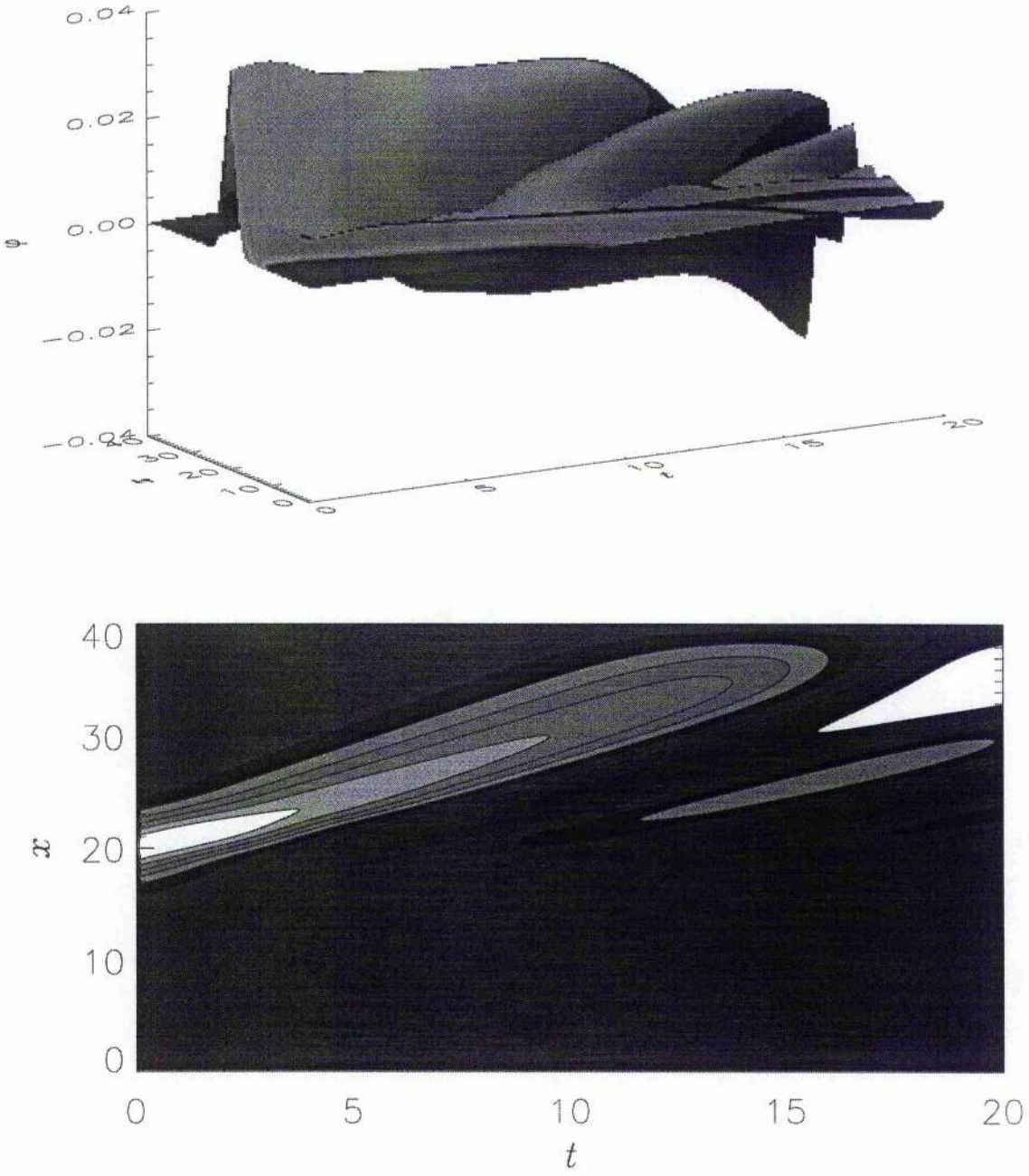

Figure 2.21: Time evolution of the initial perturbation, $0.025\exp[-(\frac{1}{2}x-10)^2]$, for $\alpha = 0.2$ and $V_0 = 0.975$. The lower view is the contour map of the upper plot.

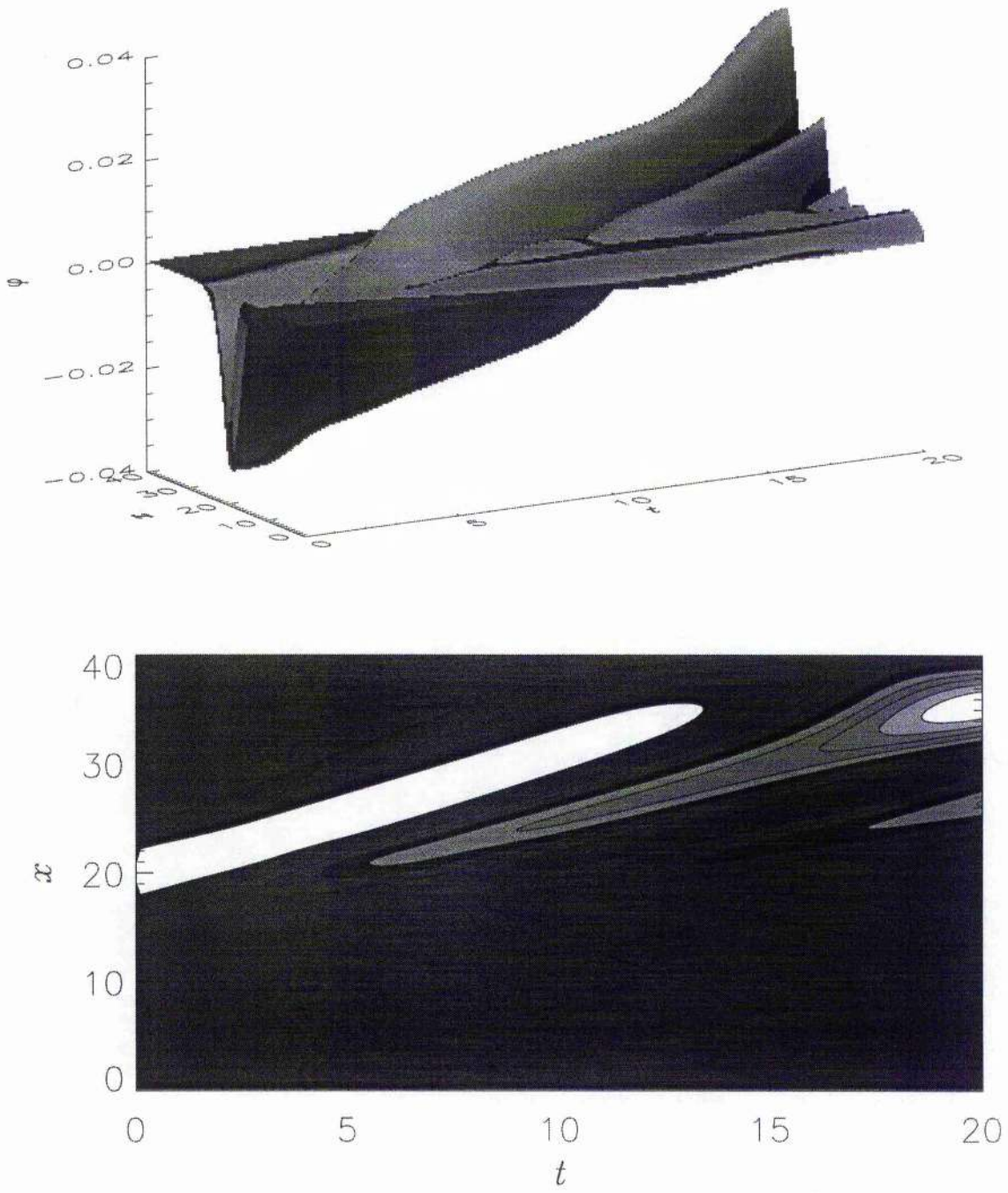

Figure 2.22: Time evolution of the initial perturbation, $-0.025\exp[-(\frac{x}{2}-10)^2]$, for $\alpha = 0.2$ and $V_0 = 0.975$. The lower view is the contour map of the upper plot.

displayed in the adjoining plots (figures 2.17 – 2.22). The numerical simulation in figures 2.17 and 2.18 considers the Maxwellian electron distribution ($\alpha = 0$) and shows how two different types of initial perturbation, viz. $0.025\text{sech}^2(x - 10)$ and $0.025\exp[-(\frac{x}{2} - 10)^2]$, evolve with time, whereas the numerical analyses in figures 2.19–2.22 assume the non-thermal electron distribution ($\alpha = 0.2$) and illustrate how these two types of initial pulse, with their positive and negative forms, evolve with time. The behaviour in figures 2.17 – 2.19 and 2.21 seems typical of the compressive solitary waves. The initial disturbance breaks up into a series of solitons with the largest in front. The behaviour of the rarefactive solitary waves shown in figures 2.20 and 2.22 is quite different. These waves appear to be unstable and to produce compressive waves at a later time. This behaviour, of course, rather casts doubt on our suggestion that such waves are observed, though it is possible that three dimensional structures could be more stable. This is a question which we have not examined.

2.6 Discussion

Motivated by the observations of solitary structures, with density depletions, made by the Viking and Freja satellites [71,73], we have shown that the presence of a population of energetic electrons changes the properties of ion-acoustic solitary waves. If a simple fluid response of the ions is taken, so we do not allow trapped ion distributions, then the only solitary wave structures in a thermal plasma have an enhanced density. However, with a non-thermal electron population, we have shown that solitary waves with both positive (compressive) and negative (rarefactive) density perturbations can exist. The weakly nonlinear solution, which might be expected to be set up in response to a moderate perturbation of the plasma, is that with a density depletion. The structure with a density enhancement, which can exist under the same conditions, is highly nonlinear and would be expected to require a large initial perturbation to set it up. In a magnetic field, the one dimensional

structures would have to propagate along the magnetic field. However, we have also demonstrated that three dimensional structures can exist.

We can compare our results obtained from this non-thermal plasma model with those obtained from another popular model, the two-electron-temperature plasma (two Maxwellian plasma) model, which is very common in various applications and has been considered previously by other workers [35], just by replacing our electron distribution function by

$$f(v) = \frac{\alpha}{\sqrt{2\pi}} e^{-v^2/2} + \frac{1-\alpha}{\sqrt{2\pi\mu_0}} e^{-v^2/2\mu_0},$$

where v is normalised to the thermal velocity of the first component (i.e. component with temperature T_{e1}), $\alpha = 1/(1+\alpha_0)$, with α_0 being the ratio of equilibrium electron density at temperature T_{e2} to that at temperature T_{e1}, and $\mu_0 = T_{e2}/T_{e1}$. The normalised electron density, with the normalised potential, is given by

$$n_e = \alpha e^{\varphi} + (1-\alpha) e^{\varphi/\mu_0}.$$

The same method, used for our non-thermal plasma model, implies that the quadratic term becomes negative if

$$M^2 > \frac{\mu_0}{1-\alpha+\alpha\mu_0}$$

and the third order coefficient is negative at this critical Mach number if

$$\frac{\mu_0 - 5 - \sqrt{\mu_0^2 - 10\mu_0 + 1}}{6(\mu_0 - 1)} < \alpha < \frac{\mu_0 - 5 + \sqrt{\mu_0^2 - 10\mu_0 + 1}}{6(\mu_0 - 1)}.$$

This only makes sense if the quantity under the square root is positive, which imposes the restriction that μ_0 be between 0 and 0.101 or greater than 9.899. The two ranges reflect an obvious symmetry in the problem, where replacing μ_0 with its inverse and α with $(1-\alpha)$ gives the same form of distribution function. In the regime, where small amplitude negative solitary waves exist, examination of the Sagdeev potential

shows that larger amplitude positive solitary waves may also exist, as in our non-thermal plasma model.

It is found, in our study of ion temperature effects on these solitary waves, that as we increase the ion temperature we need more non-thermal electrons in order to make rarefactive solitary waves exist. It has also been shown that as the ion temperature rises, the amplitude of both the compressive and rarefactive solitary waves decreases, whereas the width of these solitary waves increases.

A numerical study has also been made of the time evolution of the solitary waves found to exist in our non-thermal plasma model. We use two different types of initial perturbation and see how they evolve with time in the cases of Maxwellian ($\alpha = 0$) and non-thermal ($\alpha = 0.2$) distribution of electrons. These results are clearly shown in figures 2.17 – 2.22. Figures 2.17 – 2.19 and 2.21 represent the usual temporal behaviour of the compressive solitary waves. The initial disturbance breaks up into a series of solitary waves at the rear of the largest one. Figures 2.20 and 2.22 show the time evolution of rarefactive solitary waves. The behaviour of these rarefactive solitary waves is quite different. It seems that rarefactive solitary waves go unstable and give rise to compressive solitary waves at later time.

This analysis may be of relevance to observations in the magnetosphere of density depressions. A possible scenario is that lower hybrid turbulence produces, through modulational instability, cavities which collapse until the lower hybrid wave amplitude is sufficient to trap and accelerate a substantial number of electrons [100,103]. The damping of the turbulence could then leave a cavity and also create just the kind of energetic electron population necessary for it to live on as an ion-acoustic solitary structure no longer supported by the ponderomotive pressure of the high frequency turbulence. However, the type of electron distribution we have looked at is common to many space and laboratory plasmas in which wave damping produces an electron tail, so the theory may be of more general interest.

Chapter 3

Electrostatic Solitary Waves in Magnetised Non-thermal Plasmas

3.1 Introduction

The detailed study of electrostatic solitary waves in unmagnetised non-thermal plasmas has been presented in the previous chapter which is based on our recent work [104,105]. It is found by several authors [32,106,107] that the presence of an external magnetic field drastically modifies the properties of the electrostatic solitary waves. Thus, in this chapter, we have switched our attention to the effect of an external magnetic field on these solitary waves by studying obliquely propagating electrostatic solitary structures in a magnetised plasma with non-thermal electrons. We have neglected here the effect of ion-pressure (which has been studied in detail in chapter 2) for the scope of simplicity.

This chapter is designed as follows. The basic equations are given in Sec. 3.2. We have then, in Sec. 3.3, studied the small but finite amplitude solitary waves by the reductive perturbation method. In Sec. 3.4 we return to the study of the full nonlinear system of equations and investigate the properties of arbitrary amplitude solitary waves, first by the pseudopotential approach and later by solving the full nonlinear system of equations. In the latter case, we show that the problem of finding

stationary solutions reduces to a set of four coupled first order ordinary differential equations. The standard approach, when the equations reduce to a second order set, is to exploit the analogy with particle motion in an effective potential, the Sagdeev potential. In our problem, working in a higher dimensional phase space, we search for solitary waves directly. Such solutions arise when the equilibrium is unstable and there is a phase space orbit which approaches the equilibrium as $x \to \pm\infty$ (a homoclinic orbit). By linearising about the origin we identify the unstable manifold (i.e. the orbit which approaches the origin as $x \to -\infty$) in the vicinity of the origin. This then gives us the initial conditions in order to search for a homoclinic orbit. Some results of this procedure are presented. We then apply this technique to a study of obliquely propagating ion-acoustic solitary waves in another popular plasma model, namely two-electron-temperature plasma model, in Sec. 3.5. Finally, Sec. 3.6 provides a brief discussion.

3.2 Basic equations

We consider a fully ionised collisionless plasma consisting of cold ions and non-thermal electrons in the presence of an external static magnetic field $\mathbf{B_0} = B_0\hat{z}$. We assume that the particle pressure is much smaller than the magnetic pressure. The nonlinear behaviour of ion-acoustic waves in this plasma system may be described by the following set of fluid equations:

$$\frac{\partial n}{\partial t} + \nabla \cdot (n\mathbf{u}) = 0, \tag{3.1}$$

$$\frac{\partial \mathbf{u}}{\partial t} + (\mathbf{u} \cdot \nabla)\mathbf{u} = -\nabla\varphi + \omega_c(\mathbf{u} \times \hat{z}), \tag{3.2}$$

$$\nabla^2\varphi = n_e - n, \tag{3.3}$$

where all the variables except the new term ω_c, which is the ion cyclotron frequency normalised to ion plasma frequency ($\omega_p = \sqrt{4\pi n_0 e^2/m}$), are the same as in the previous chapter (chapter 2).

To model an electron distribution with a population of fast particles, we can also choose the distribution function as before. Thus, n_e, as before, takes the form

$$n_e = (1 - \beta\varphi + \beta\varphi^2)e^{\varphi}, \tag{3.4}$$

where

$$\beta = \frac{4\alpha}{1+3\alpha}. \tag{3.5}$$

3.3 Small Amplitude Solitary Waves

In this section, we confine ourself to the study of obliquely propagating ion-acoustic solitary waves in a magnetised non-thermal plasma by the reductive perturbation method [14] which is valid for small but finite amplitude waves. We first derive the Zakharov-Kuznetsov (ZK) equation and study the compressive and rarefactive solitary waves as steady state solutions of this equation. We then extend this study to a stability analysis of these solitary waves.

3.3.1 Zakharov-Kuznetsov Equation

We now construct a weakly nonlinear theory of the obliquely propagating arbitrary amplitude ion-acoustic solitary waves with small but finite-amplitude which leads to a scaling of the independent variables through the stretched coordinates[1] [36,37,108]

$$\left.\begin{aligned} x' &= \epsilon^{1/2}x, \quad y' = \epsilon^{1/2}y, \\ z' &= \epsilon^{1/2}(z - v_0 t), \quad t' = \epsilon^{3/2}t, \end{aligned}\right\} \tag{3.6}$$

where ϵ is a small parameter measuring the weakness of the dispersion and v_0 is the unknown wave phase velocity (to be determined later). It should be noted here that x', y', z' are all normalised to the Debye length (λ_D), t' is normalised to the ion time period (ω_p^{-1}) and v_0 is normalised to the ion-acoustic speed (C_s). We can

[1]The stretched coordinates are introduced in **Appendix A.1**

now expand the perturbed quantities about their equilibrium values in powers of ϵ as

$$\begin{aligned} n &= 1 + \epsilon n^{(1)} + \epsilon^2 n^{(2)} + \epsilon^3 n^{(3)} + \cdots, \\ \varphi &= 0 + \epsilon\varphi^{(1)} + \epsilon^2\varphi^{(2)} + \epsilon^3\varphi^{(3)} + \cdots, \\ u_z &= 0 + \epsilon u_z^{(1)} + \epsilon^2 u_z^{(2)} + \epsilon^3 u_z^{(3)} + \cdots, \\ u_x &= 0 + \epsilon^{3/2} u_x^{(1)} + \epsilon^2 u_x^{(2)} + \epsilon^{5/2} u_x^{(3)} + \cdots, \\ u_y &= 0 + \epsilon^{3/2} u_y^{(1)} + \epsilon^2 u_y^{(2)} + \epsilon^{5/2} u_y^{(3)} + \cdots. \end{aligned} \tag{3.7}$$

We now use Eqs. (3.4) – (3.7) in Eqs. (3.1) – (3.3) and develop equations in various powers of ϵ. To lowest order in ϵ, i.e. equating the coefficient of ϵ, one can obtain the first order continuity equation, x- and y-components of momentum equation and Poisson's equation which in turn give

$$\left.\begin{aligned} &n^{(1)} = (1-\beta)\varphi^{(1)} = \tfrac{1}{v_0} u_z^{(1)}, \\ &u_x^{(1)} = -\tfrac{1}{\omega_c}\tfrac{\partial\varphi^{(1)}}{\partial y'}, \quad u_y^{(1)} = \tfrac{1}{\omega_c}\tfrac{\partial\varphi^{(1)}}{\partial x'}. \end{aligned}\right\} \tag{3.8}$$

Here, the first one, together with the z-component of momentum equation, $u_z = \varphi^{(1)}/v_0$, gives the linear dispersion relation $v_0 = 1/\sqrt{1-\beta}$ and the last two, respectively, represent the x- and y- components of $\mathbf{E} \times \mathbf{B}_0$ drift. These last two equations are also satisfied by the next higher (second) order continuity equation. Similarly, to next higher order in ϵ we obtain the second order x- and y- components of momentum equation and Poisson's equation as

$$\left.\begin{aligned} &u_x^{(2)} = \tfrac{v_0}{\omega_c^2}\tfrac{\partial^2\varphi^{(1)}}{\partial z'\partial x'}, \quad u_y^{(2)} = \tfrac{v_0}{\omega_c^2}\tfrac{\partial^2\varphi^{(1)}}{\partial z'\partial y'}, \\ &(\tfrac{\partial^2}{\partial x'^2} + \tfrac{\partial^2}{\partial y'^2} + \tfrac{\partial^2}{\partial z'^2})\varphi^{(1)} = \tfrac{1}{2}[\varphi^{(1)}]^2 + (1-\beta)\varphi^{(2)} - n^{(2)}. \end{aligned}\right\} \tag{3.9}$$

The first two denote the x- and y- components of the ion polarisation drift, respectively. Again, following the same procedure one can obtain the next higher order continuity equation and z-component of the momentum equation as

$$\left.\begin{aligned} &\tfrac{\partial n^{(1)}}{\partial t'} - v_0\tfrac{\partial n^{(2)}}{\partial z'} + \tfrac{\partial u_x^{(2)}}{\partial x'} + \tfrac{\partial u_y^{(2)}}{\partial y'} + \tfrac{\partial}{\partial z'}(u_z^{(2)} + n^{(1)}u_z^{(1)}) = 0, \\ &\tfrac{\partial u_z^{(1)}}{\partial t'} - v_0\tfrac{\partial u_z^{(2)}}{\partial z'} + u_z^{(1)}\tfrac{\partial u_z^{(1)}}{\partial z'} + \tfrac{\partial\varphi^{(2)}}{\partial z'} = 0. \end{aligned}\right\} \tag{3.10}$$

Now, using Eqs. (3.8) - (3.10) we can readily obtain

$$\frac{\partial\varphi^{(1)}}{\partial t'} + AB\varphi^{(1)}\frac{\partial\varphi^{(1)}}{\partial z'} + \frac{1}{2}A\frac{\partial}{\partial z'}[\frac{\partial^2}{\partial z'^2} + D(\frac{\partial^2}{\partial x'^2} + \frac{\partial^2}{\partial y'^2})]\varphi^{(1)} = 0, \tag{3.11}$$

where

$$\begin{aligned} A &= (1-\beta)^{-3/2}, \\ B &= \frac{1}{2}[3(1-\beta)^2 - 1], \\ D &= (1 + \frac{1}{\omega_c^2}). \end{aligned} \tag{3.12}$$

This equation (3.11) is known as the Zakharov-Kuznetsov (ZK) equation or the Korteweg-de Vries equation in three dimensions.

3.3.2 Solitary Wave Solution

To study the solitary waves propagating in a direction making an angle δ with the z'-axis, i.e. with the external magnetic field, and lying in the (x', z') plane, we first rotate the co-ordinate axes x', z' through an angle δ, keeping the y'-axis fixed. Thus, we transform our independent variables to

$$\left.\begin{aligned} \zeta &= x'\cos\delta - z'\sin\delta, \quad \eta = y', \\ \xi &= x'\sin\delta + z'\cos\delta, \quad \tau = t.' \end{aligned}\right\} \tag{3.13}$$

This transformation of the independent variables allows us to write the ZK equation of the form

$$\begin{aligned} &\frac{\partial\varphi^{(1)}}{\partial\tau} + \delta_1\varphi^{(1)}\frac{\partial\varphi^{(1)}}{\partial\xi} + \delta_2\frac{\partial^3\varphi^{(1)}}{\partial\xi^3} + \delta_3\varphi^{(1)}\frac{\partial\varphi^{(1)}}{\partial\zeta} + \delta_4\frac{\partial^3\varphi^{(1)}}{\partial\zeta^3} \\ &\quad + \delta_5\frac{\partial^3\varphi^{(1)}}{\partial\xi^2\partial\zeta} + \delta_6\frac{\partial^3\varphi^{(1)}}{\partial\xi\partial\zeta^2} + \delta_7\frac{\partial^3\varphi^{(1)}}{\partial\xi\partial\eta^2} + \delta_8\frac{\partial^3\varphi^{(1)}}{\partial\zeta\partial\eta^2} = 0, \end{aligned} \tag{3.14}$$

where

$$\begin{aligned} \delta_1 &= AB\cos\delta, \\ \delta_2 &= \frac{1}{2}A(\frac{1}{2}\cos^3\delta + D\sin^2\delta\cos\delta), \\ \delta_3 &= -AB\sin\delta, \end{aligned}$$

$$\begin{aligned}
\delta_4 &= -\frac{1}{2}A(\sin^3\delta + D\cos^2\delta\sin\delta),\\
\delta_5 &= A[D(\sin\delta\cos^2\delta - \frac{1}{2}\sin^3\delta) - \frac{3}{2}\cos^2\delta\sin\delta],\\
\delta_6 &= -A[D(\sin^2\delta\cos\delta - \frac{1}{2}\sin^3\delta) - \frac{3}{2}\cos\delta\sin^2\delta],\\
\delta_7 &= \frac{1}{2}AD\cos\delta,\\
\delta_8 &= -\frac{1}{2}AD\sin\delta.
\end{aligned} \tag{3.15}$$

We now look for the steady state solution of the ZK equation in the form

$$\varphi^{(1)} = \varphi_0(Z),$$

where

$$Z = \xi - u_0\tau, \tag{3.16}$$

in which u_0 is a constant velocity normalised to the ion-acoustic speed (C_s). Using this transformation we can write the ZK equation in steady state form as

$$-u_0\frac{d\varphi_0}{dZ} + \delta_1\varphi_0\frac{d\varphi_0}{dZ} + \delta_2\frac{d^3\varphi_0}{dZ^3} = 0. \tag{3.17}$$

Now, using the appropriate boundary conditions, viz. $\varphi^{(1)} \to 0$, $\frac{d\varphi^{(1)}}{dZ} \to 0$, $\frac{d^2\varphi^{(1)}}{dZ2} \to 0$ at $Z \to \pm\infty$, the solution of this equation is given by[2]

$$\varphi_0(Z) = \varphi_m \mathrm{sech}^2\mu Z, \tag{3.18}$$

where $\varphi_m = 3u_0/\delta_1$ is the amplitude and $\mu = \sqrt{u_0/4\delta_2}$ is the inverse of the width of the solitary waves. It is clear that as β is always less than 1, i.e. $A > 0$, depending on whether B is positive or negative, the solitary waves will be either compressive ($\varphi_m > 0$) or rarefactive ($\varphi_m < 0$). Therefore, there exist compressive solitary waves when $B > 0$, i.e. $\alpha < (\sqrt{3}-1)/(\sqrt{3}+3) \simeq 0.155$ and rarefactive solitary waves when $B < 0$ i.e. $\alpha > (\sqrt{3}-1)/(\sqrt{3}+3) \simeq 0.155$. It is also seen from Eqs. (3.15) and (3.18) that the amplitude of compressive as well as rarefactive solitary waves increases with δ for its lower range. The magnitude of the external magnetic field has no effect on the amplitude of these solitary waves. However, it does have an

[2]The derivation is given in **Appendix A2**.

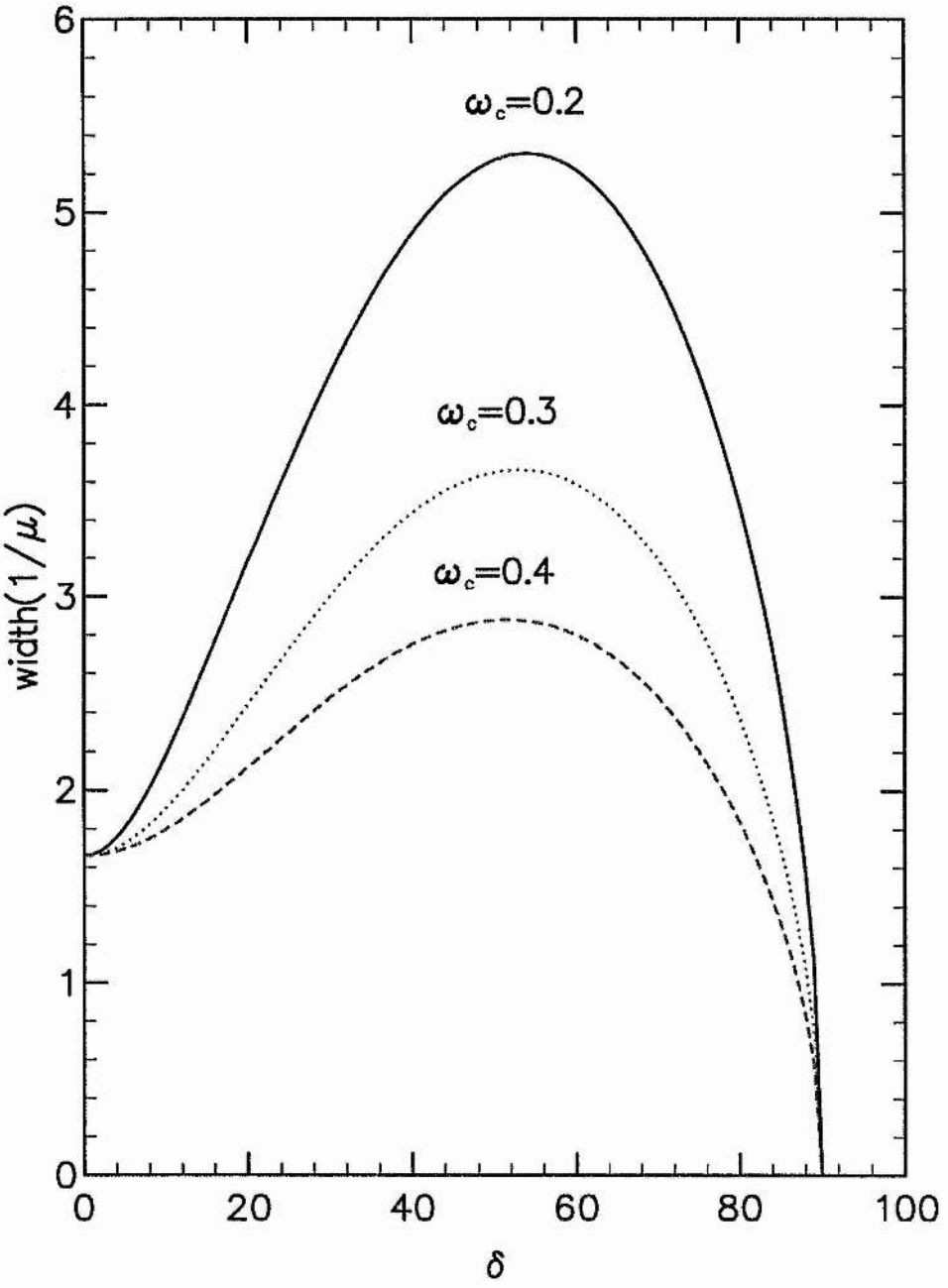

Figure 3.1: Variation of width of the solitary waves for $\alpha = 0.2$, $u_0 = 1.45$, $\omega_c = 0.2$ (solid curve), $\omega_c = 0.3$ (dotted curve) and $\omega_c = 0.4$ (dashed curve).

effect on the width of these solitary waves. Figure 3.1 shows how the width $(1/\mu)$ of these solitary waves changes with δ and ω_c. We see that the width of the solitary waves increases with δ for its lower range, but decreases for its higher range. It is obvious that for large angles the width tends to 0 and the amplitude tends to ∞. It is likely that for large angles the assumption that the waves are electrostatic is no longer a valid one, and we should look for fully electromagnetic structures.

3.3.3 Stability Analysis

We now study the stability of the obliquely propagating solitary waves, discussed in the previous section, by the small-k perturbation expansion method [108-111]. We first assume that

$$\varphi^{(1)} = \varphi_0(Z) + \varphi(Z, \zeta, \eta, \tau), \tag{3.19}$$

where φ_0 is defined by Eq. (3.18) and φ, for a long-wavelength plane wave perturbation in a direction with direction cosines $(l_\zeta,\ l_\eta,\ l_\xi)$, is given by

$$\varphi = \psi(Z) e^{i[k(l_\zeta \zeta + l_\eta \eta + l_\xi Z) - \omega\tau]}, \tag{3.20}$$

in which $l_\zeta^2 + l_\eta^2 + l_\xi^2 = 1$ and $\psi(Z)$ and ω, for small k, can be expanded as [107-111]

$$\left.\begin{aligned} \psi(Z) &= \psi_0(Z) + k\psi_1(Z) + k^2\psi_2(Z) + \cdots, \\ \omega &= 0 + k\omega_1 + k^2\omega_2 + \cdots. \end{aligned}\right\} \tag{3.21}$$

Now, substituting Eq. (3.19) into Eq. (3.14) and linearising with respect to φ, we can express the linearised ZK equation in the form

$$\begin{aligned} \frac{\partial\varphi}{\partial\tau} - u_0\frac{\partial\varphi}{\partial Z} + \delta_1\varphi_0\frac{\partial\varphi}{\partial Z} + \delta_1\varphi\frac{\partial\varphi_0}{\partial Z} + \delta_2\frac{\partial^3\varphi}{\partial Z^3} + \delta_3\varphi_0\frac{\partial\varphi}{\partial\zeta} + \delta_4\frac{\partial^3\varphi}{\partial\zeta^3} \\ + \delta_5\frac{\partial^3\varphi}{\partial Z^2\partial\zeta} + \delta_6\frac{\partial^3\varphi}{\partial Z\partial\zeta^2} + \delta_7\frac{\partial^3\varphi}{\partial Z\partial\eta^2} + \delta_8\frac{\partial^3\varphi}{\partial\zeta\partial\eta^2} = 0. \end{aligned} \tag{3.22}$$

Our main object is now to find ω_1 by solving the zeroth-, first- and second-order equations obtained from these last three equations.

The zeroth-order equation obtained from Eqs. (3.20) – (3.22) can be written, after integration, as

$$(-u_0 + \delta_1\varphi_0)\psi_0 + \delta_2\frac{d^2\psi_0}{dZ^2} = C, \tag{3.23}$$

where C is the integration constant. It is clear from Eq. (3.17) that the homogeneous part of this equation has two linearly independent solutions, namely

$$f = \frac{d\varphi_0}{dZ}, \tag{3.24}$$

$$g = f\int^Z \frac{dZ}{f^2}. \tag{3.25}$$

Therefore, the general solution of this zeroth order equation can be written as

$$\psi_0 = C_1 f + C_2 g - Cf\int^Z \frac{g}{W}dZ + Cg\int^Z \frac{f}{W}dZ, \tag{3.26}$$

where C_1 and C_2 are two constants and W is the Wronskian defined by $W = f\frac{dg}{dZ} - g\frac{df}{dZ}$. Now, evaluating all the integrals, the general solution of this zeroth-order equation, for ψ_0 not tending to $\pm\infty$ as $Z \to \pm\infty$, can finally be simplified to

$$\psi_0 = C_1 f. \tag{3.27}$$

The first-order equation, i.e. the equation with terms linear in k, obtained from Eqs. (3.20) – (3.22) and (3.27), can be expressed, after integration, as

$$(-u_0 + \delta_1\varphi_0)\psi_1 + \delta_2\frac{d^2\psi_1}{dZ^2} = iC_1(\alpha_1 + \beta_1\tan^2\mu Z)\varphi_0 + K, \tag{3.28}$$

where K is the integration constant and α_1 and β_1 are given by

$$\left.\begin{aligned} \alpha_1 &= (\omega_1 + l_\xi u_0) - \tfrac{1}{2}\varphi_m\mu_1 + 2\mu^2\mu_2, \\ \beta_1 &= \tfrac{1}{2}\varphi_m\mu_1 - 6\mu^2\mu_2, \\ \mu_1 &= \delta_1 l_\xi + \delta_3 l_\zeta, \\ \mu_2 &= 3\delta_2 l_\xi + \delta_5 l_\zeta. \end{aligned}\right\} \tag{3.29}$$

Now, following the same procedure, the general solution of this first-order equation, for ψ_1 not tending to $\pm\infty$ as $Z \to \pm\infty$, can be expressed as

$$\psi_1 = K_1 f + \frac{iC_1}{8\delta_2\mu^2}[(\alpha_1 + \beta_1)Zf + \frac{2}{3}(3\alpha_1 + \beta_1)\varphi_0]. \tag{3.30}$$

The second-order equation, i.e. equation with terms involving k^2, obtained from Eq. (3.22), after substituting Eqs. (3.20) and (3.21), can be written as

$$[-u_0\frac{d}{dZ}+\delta_1\frac{d}{dZ}\varphi_0+\delta_2\frac{d^3}{dZ^3}]\psi_2 = i\omega_2\psi_0+i(\omega_1+l_\xi u_0)\psi_1-i\mu_1\varphi_0\psi_1 \\ +\mu_3\frac{d\psi_0}{dZ}-i\mu_2\frac{d^2\psi_1}{dZ^2}, \qquad (3.31)$$

where

$$\mu_3 = 3\delta_2 l_\xi^2+2\delta_5 l_\varsigma l_\xi+\delta_6 l_\varsigma^2+\delta_7 l_\eta^2. \qquad (3.32)$$

The solution of this second-order equation exists if the right-hand side is orthogonal to a kernel of the operator adjoint to the operator

$$-u_0\frac{d}{dZ}+\delta_1\frac{d}{dZ}\varphi_0+\delta_2\frac{d^3}{dZ^3}. \qquad (3.33)$$

This kernel, which must tend to zero as $Z\to\pm\infty$, is $\varphi_0/\varphi_m = \mathrm{sech}^2\mu Z$. Thus, we can write the following equation determining ω_1:

$$\int_{-\infty}^{\infty}\varphi_0[i\omega_2\psi_0+i(\omega_1+l_\xi u_0)\psi_1-i\mu_1\varphi_0\psi_1+\mu_3\frac{d\psi_0}{dZ}-i\mu_2\frac{d^2\psi_1}{dZ^2}]dZ = 0. \qquad (3.34)$$

Now, substituting the expressions for ψ_0 and ψ_1, Eqs. (3.27) and (3.30), into this equation and then performing the integration we arrive at the following dispersion relation:

$$\omega_1 = \Omega-l_\xi u_0+\sqrt{\Omega^2-\Upsilon}, \qquad (3.35)$$

where

$$\left.\begin{aligned}\Omega &= \tfrac{2}{3}(\varphi_m\mu_1-2\mu_2\mu^2),\\ \Upsilon &= \tfrac{16}{45}(\varphi_m^2\mu_1^2-3\varphi_m\mu_1\mu_2\mu^2-3\mu_2^2\mu^4+12\mu_3\mu^4).\end{aligned}\right\} \qquad (3.36)$$

It is clear from our dispersion relation, Eq. (3.35), that there is always instability if $\Upsilon-\Omega^2>0$. Thus, using Eqs. (3.12), (3.15), (3.29), (3.32) and (3.36) we can express this instability criterion as

$$\left.\begin{aligned}&S_i>0,\\ &S_i = l_\varsigma^2[\omega_c^2-\tfrac{5}{3}(1+\omega_c^2)\tan^2\delta]+l_\eta^2(\omega_c^2+\sin^2\delta).\end{aligned}\right\} \qquad (3.37)$$

We have numerically analysed the ω_c-value ranges for different values of δ and the

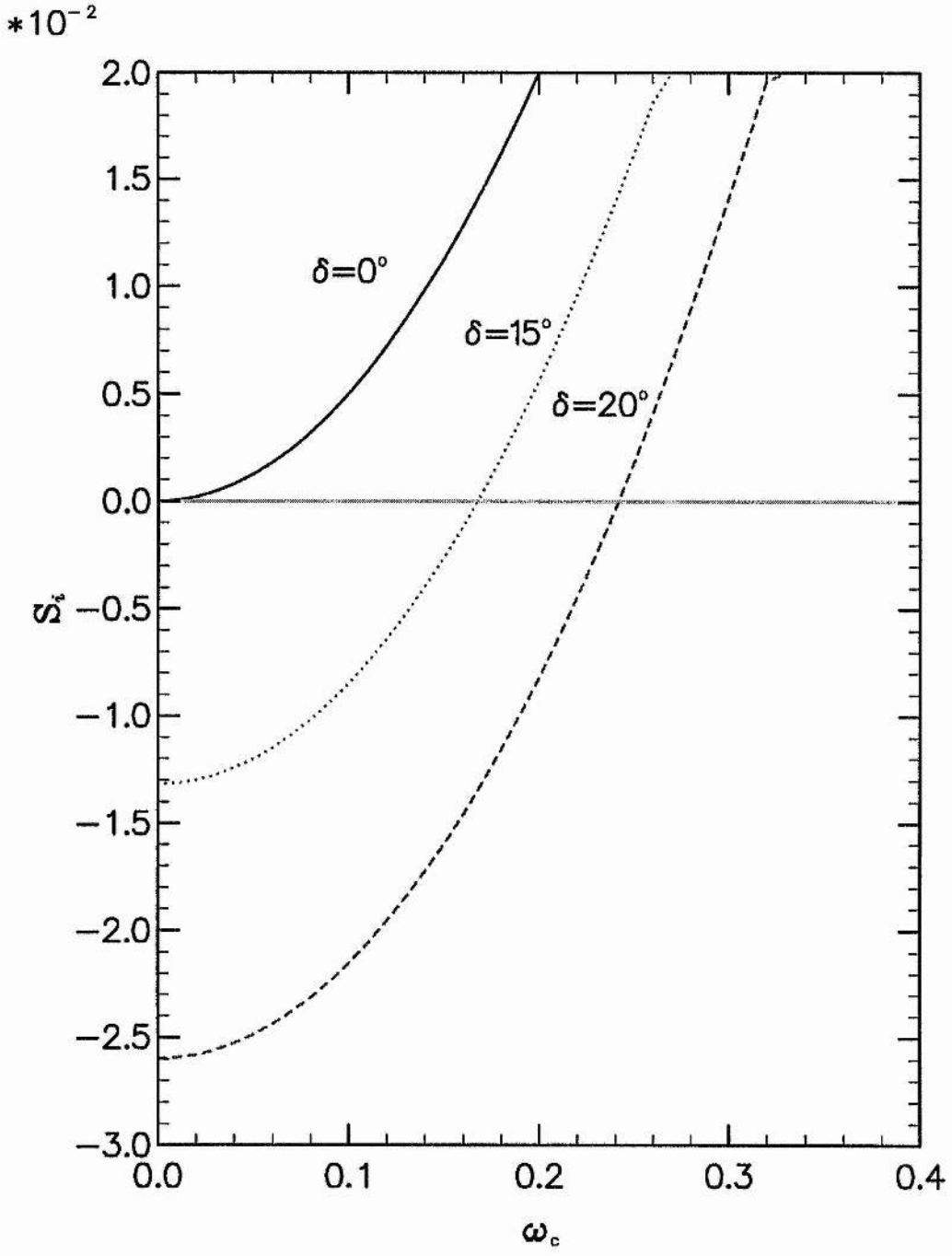

Figure 3.2: Variation of S_i with ω_c for $l_\eta = 0.5$, $l_\zeta = 0.5$, $\delta = 0°$ (solid curve), $\delta = 15°$ (dotted curve) and $\delta = 20°$ (dashed curve)

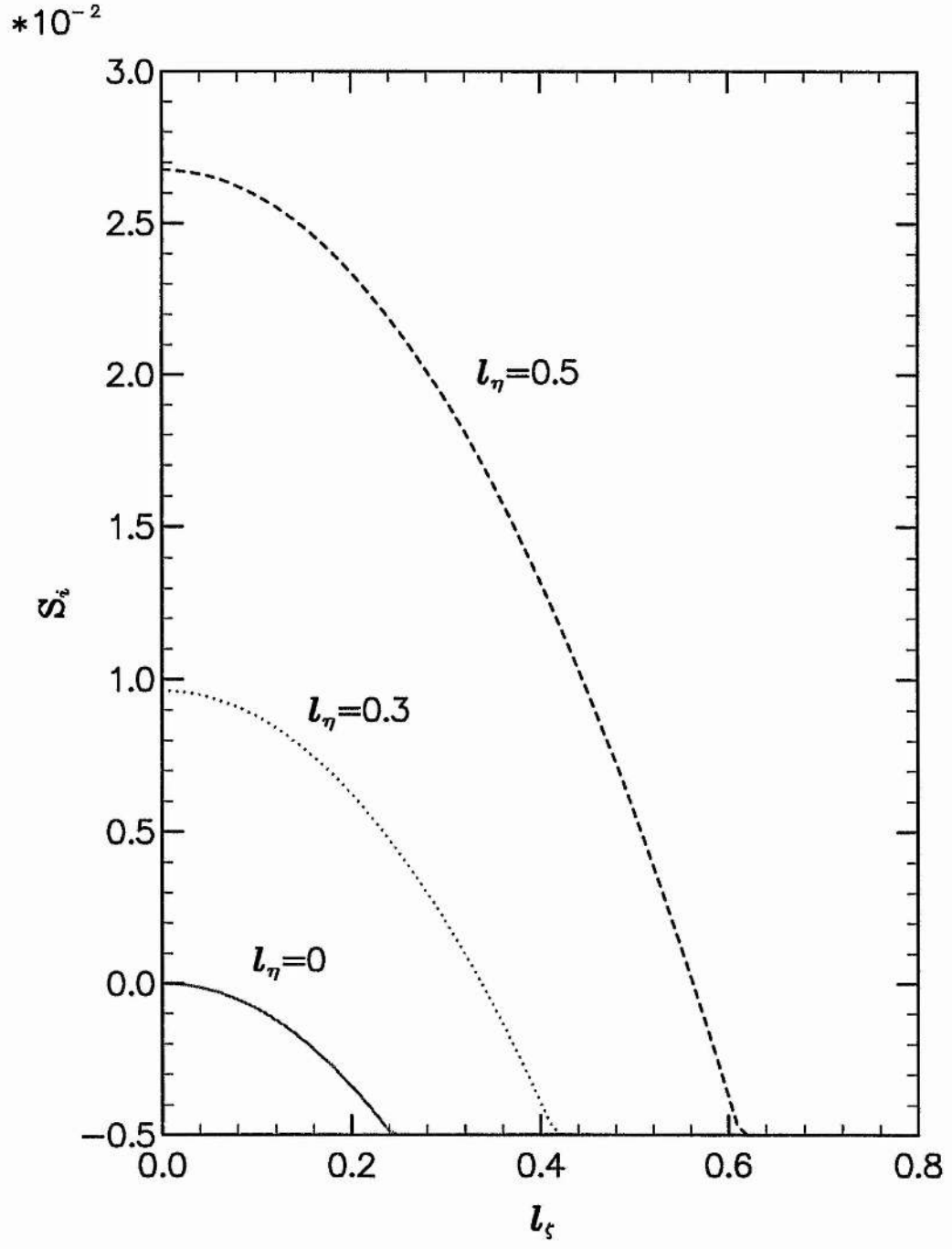

Figure 3.3: Variation of S_i with l_ζ for $\omega_c = 0.2$, $\delta = 15°$, $l_\eta = 0$ (solid curve), $l_\eta = 0.3$ (dotted curve) and $l_\eta = 0.5$ (dashed curve).

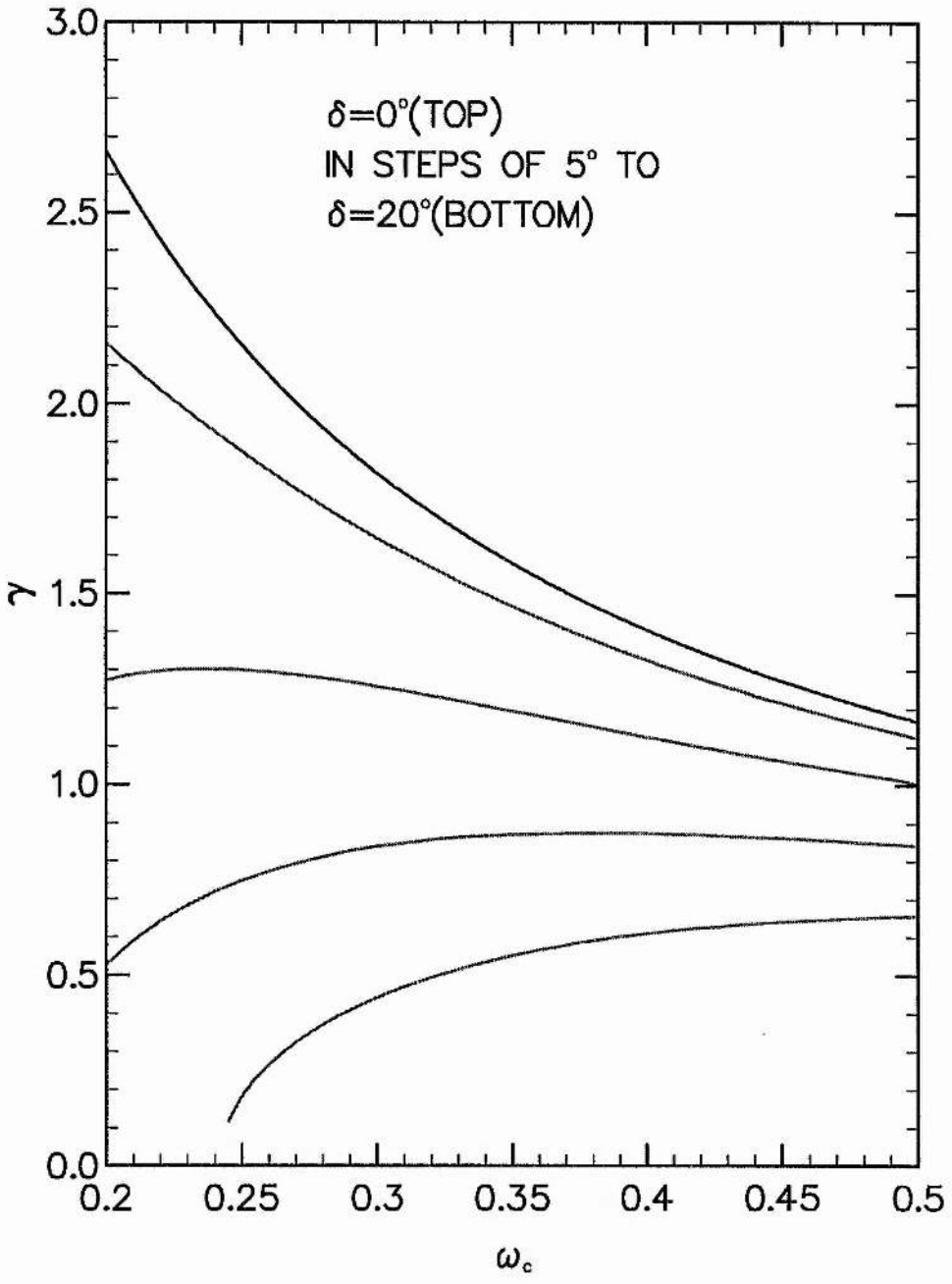

Figure 3.4: Variation of γ with ω_c for $u_0 = 1.43$, $l_\zeta = 0.5$, $l_\eta = 0.5$ and different values of δ, $\delta = 0°$ (top) in steps of 5° to $\delta = 20°$ (bottom).

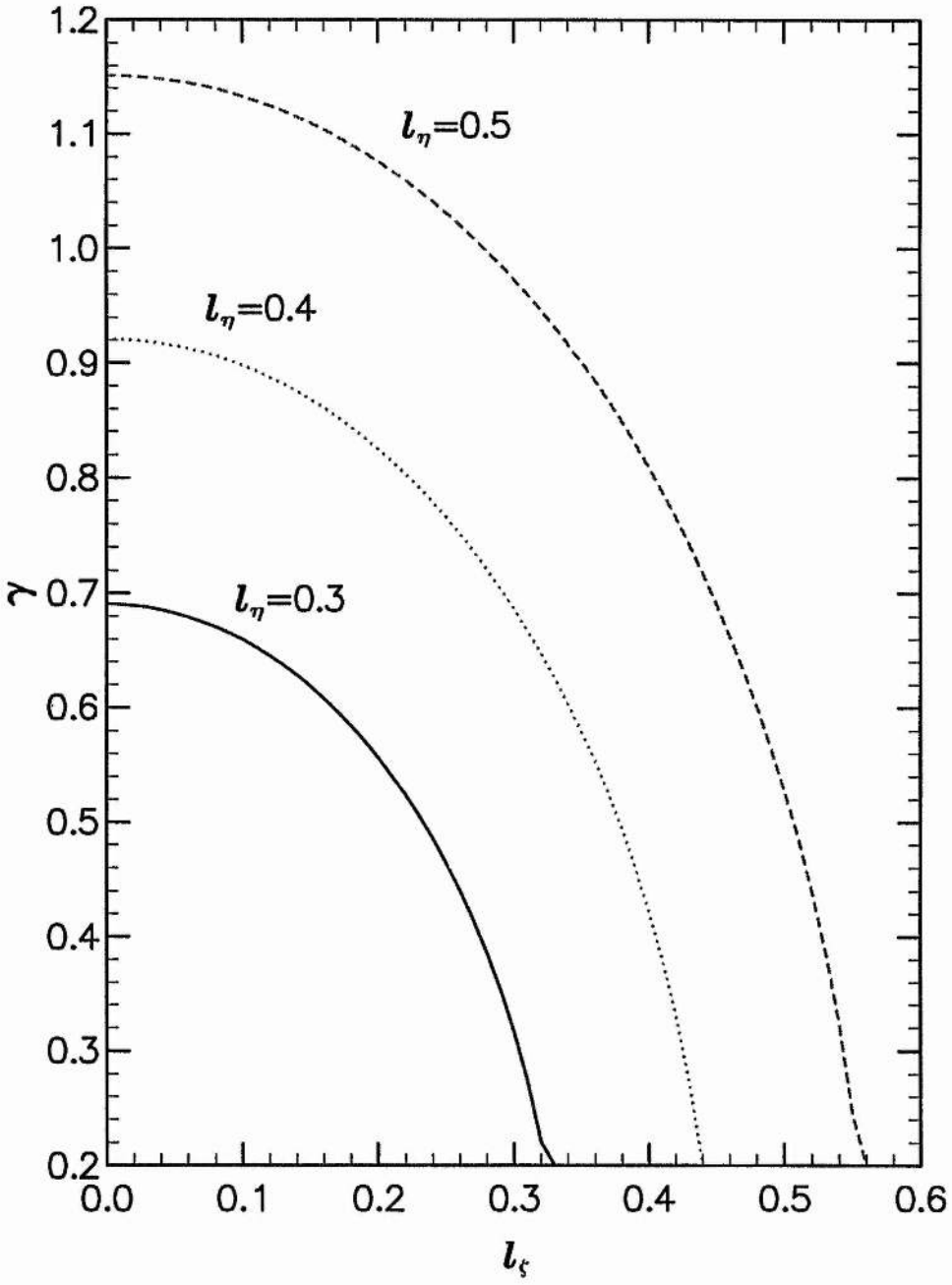

Figure 3.5: Variation of γ with l_ζ for $u_0 = 1.43$, $\omega_c = 0.2$, $\delta = 15°$, $l_\eta = 0.3$ (solid curve), $l_\eta = 0.4$ (dotted curve) and $l_\eta = 0.5$ (dashed curve).

l_ζ-value ranges for different values of l_η for which the solitary waves become stable and unstable. These numerical results are displayed in figures 3.2 and 3.3. If this instability criterion $S_i > 0$ is satisfied, the growth rate $\gamma = \sqrt{\Upsilon - \Omega^2}$ of the unstable perturbation of these solitary waves is given by

$$\gamma = \frac{2}{\sqrt{15}} \frac{u_0 \sqrt{S_i(1+\omega_c^2)}}{\sin^2\delta + \omega_c^2}. \tag{3.38}$$

This equation clearly indicates that growth rate γ is a linear function of u_0 (γ increases linearly with u_0) but a nonlinear function of ω_c, δ, l_ζ and l_η. The nonlinear variations of γ with ω_c, δ, l_ζ and l_η are shown in figures 3.4 and 3.5.

3.4 Arbitrary Amplitude Solitary Waves

We now study obliquely propagating arbitrary amplitude solitary waves in the magnetised plasma under consideration. We first use the pseudopotential approach and try to find the ranges of different parameters for which compressive and rarefactive solitary waves may coexist. We then reduce our basic equations, Eqs. (3.1) – (3.3), to a set of coupled 1st order ordinary differential equations and solve this set of equations numerically to see the effects of obliqueness and magnetic field strength on these solitary wave structures.

3.4.1 Pseudopotential Approach

To find the stationary solution of the full nonlinear system of equations, we first make all dependent variables depend on a single independent variable defined by $\xi = \hat{l} \cdot \mathbf{r} - Mt$, with M being the Mach number and $\hat{l}$ being the unit vector in the propagation direction of the solitary waves, and write Eqs. (3.1) – (3.3) as

$$\frac{d}{d\xi}[n(M - \hat{l} \cdot \mathbf{u})] = 0, \tag{3.39}$$

$$(M - \hat{l} \cdot \mathbf{u})\frac{d\mathbf{u}}{d\xi} = \hat{l}\frac{d\varphi}{d\xi} - \omega_c(\mathbf{u} \times \hat{z}), \tag{3.40}$$

$$\frac{d^2\varphi}{d\xi^2} = (1 - \beta\varphi + \beta\varphi^2)e^{\varphi} - n. \tag{3.41}$$

Now, integrating Eq. (3.39), under the appropriate boundary conditions, namely $n \to 1$ and $u_{z,\perp} \to 0$ at $\xi \to \pm\infty$, and multiplying Eq. (3.40) by n and Eq. (3.41) by $\frac{d\varphi}{d\xi}$ one can write

$$n(M - \hat{l} \cdot \mathbf{u}) = M, \tag{3.42}$$

$$M\frac{d\mathbf{u}}{d\xi} = \hat{l}n\frac{d\varphi}{d\xi} - n\omega_c(\mathbf{u} \times \hat{z}), \tag{3.43}$$

$$\frac{d}{d\xi}[\frac{1}{2}(\frac{d\varphi}{d\xi})^2 + 1 + 3\beta - (1 + 3\beta - 3\beta\varphi + \beta\varphi^2)e^{\varphi}] + n\frac{d\varphi}{d\xi} = 0. \tag{3.44}$$

Taking dot product of Eq. (3.43) with $\hat{z}$, we can express the last term of Eq. (3.44), $n\frac{d\varphi}{d\xi}$, as

$$n\frac{d\varphi}{d\xi} = \frac{M}{l_z}\frac{d}{d\xi}(u_z). \tag{3.45}$$

Again, taking dot product of Eq. (3.43) with $\mathbf{u}$ and using Eq. (3.42), we obtain

$$n\frac{d\varphi}{d\xi} = \frac{d}{d\xi}[\varphi + \frac{1}{2}(u_\perp^2 + u_z^2)].$$

Substituting Eq. (3.45) into this last equation and integrating this new equation, under the appropriate boundary conditions, viz. $\varphi \to 0$ and $u_{z,\perp} \to 0$ at $\xi \to \pm\infty$, we can express u_z as

$$u_z = \frac{M}{l_z}[1 - \sqrt{1 - \frac{l_z^2}{M^2}(2\varphi + u_\perp^2)}]. \tag{3.46}$$

Now, using Eqs. (3.45) and (3.46) in Eq. (3.44) and integrating this new equation, under the same boundary conditions, viz. $\varphi \to 0$, $u_{z,\perp} \to 0$ and $n \to 1$ at $\xi \to \pm\infty$, we can finally express our Poisson's equation, Eq. (3.41), as

$$\frac{1}{2}(\frac{d\varphi}{d\xi})^2 + V(\varphi, u_\perp) = 0, \tag{3.47}$$

where $V(\varphi, u_\perp)$ is given by

$$V(\varphi, u_\perp) = 1 + 3\beta - (1 + 3\beta - 3\beta\varphi + \beta\varphi^2)e^{\varphi} + \frac{M^2}{l_z^2}[1 - \sqrt{1 - \frac{l_z^2}{M^2}(2\varphi + u_\perp^2)}]. \tag{3.48}$$

The function $V(\varphi, u_\perp)$ contains two variables and so we have not succeeded in reducing the problem to something analogous to particle motion in a one dimensional potential. Nevertheless, Eq. (3.47) does provide some useful information in that solutions must be confined to regions in which $V(\varphi, u_\perp) \leq 0$. Thus, it may be possible to show that the solution is confined to a bounded region in the $(\varphi, u_\perp)$ plane, though it is not possible to determine from Eq. (3.47) alone just what path the solution follow in the bounded region. It may be noted here that if we consider parallel propagation, i.e $l_z = 1$ and $u_\perp = 0$, this reduces to the one dimensional problem which has been studied in chapter 2.

We can now numerically examine the behaviour of the function $V(\varphi, u_\perp)$ and find the effects of various parameters (namely M, α and l_z) on the possibility of existence of the compressive and rarefactive solitary waves. The numerical results are displayed in figures 3.6 – 3.14. We have found in figures 3.6 – 3.8 that for $\alpha \leq 0.155$ there is a potential well only in the positive φ-axis, i.e. compressive solitary waves may exist, but for $\alpha \geq 0.156$ there are potential wells in both the positive and negative φ-axis, resulting in the possibility of coexistence of the compressive and rarefactive solitary waves for $l_z = 0.8$ and $M = 1.057$. Figures 3.9 – 3.11 show how the behaviour of the function $V(\varphi, u_\perp)$ changes with M for $\alpha = 0.2$ and $l_z = 0.8$. It is seen that as we increase M, the amplitude of the wave (if it exists) increases. It is also found that as M reaches the value of 1.214, the rarefactive solitary wave disappears, but the compressive one still exists. Figures 3.12 – 3.14 represent the similar behaviour with a different value of l_z, viz. $l_z = 0.7$.

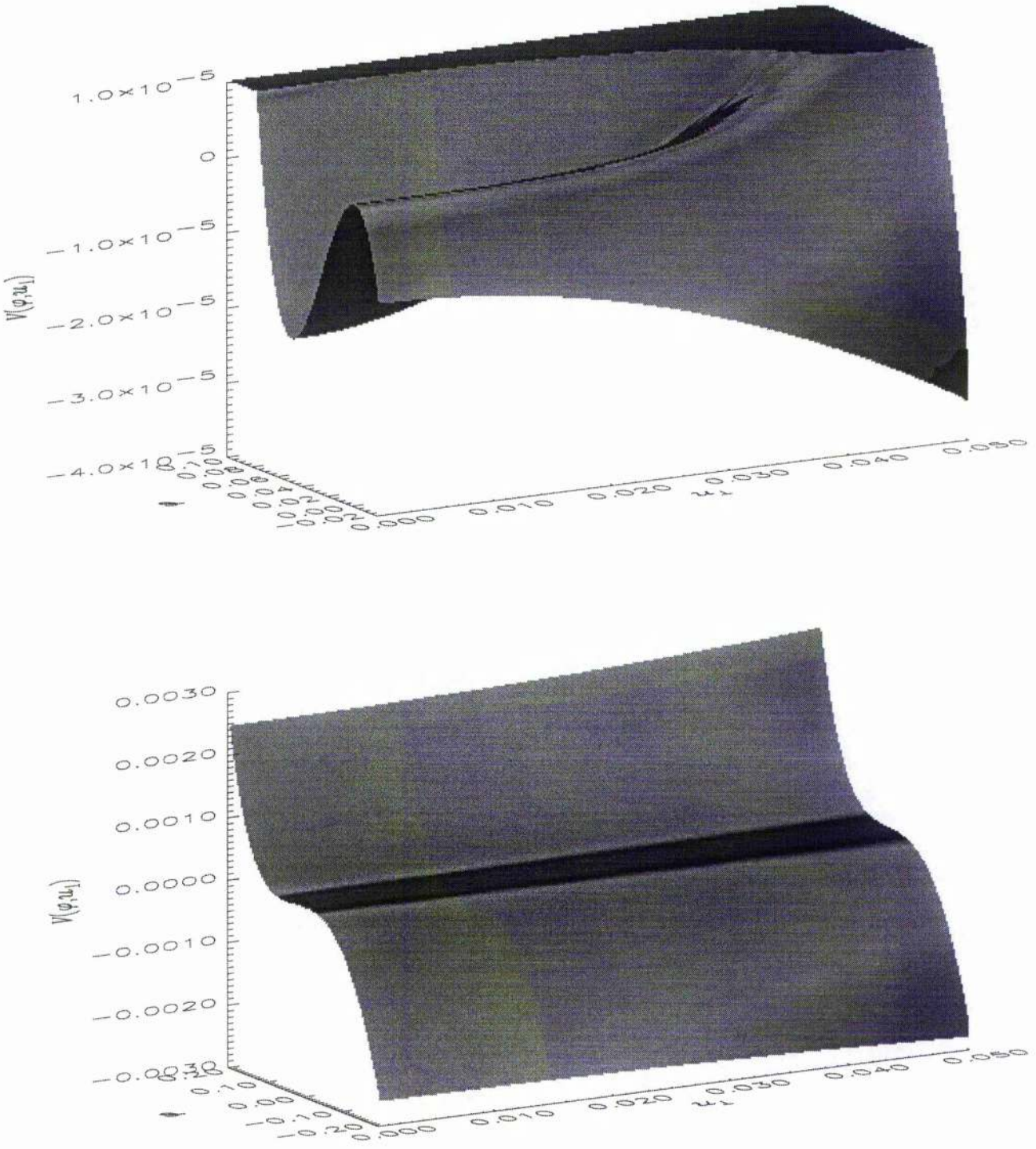

Figure 3.6: Showing the existence of compressive solitary waves (upper plot) and the non-existence of rarefactive one (lower plot) for $\alpha = 0$, $l_z = 0.8$ and $M = 0.82$.

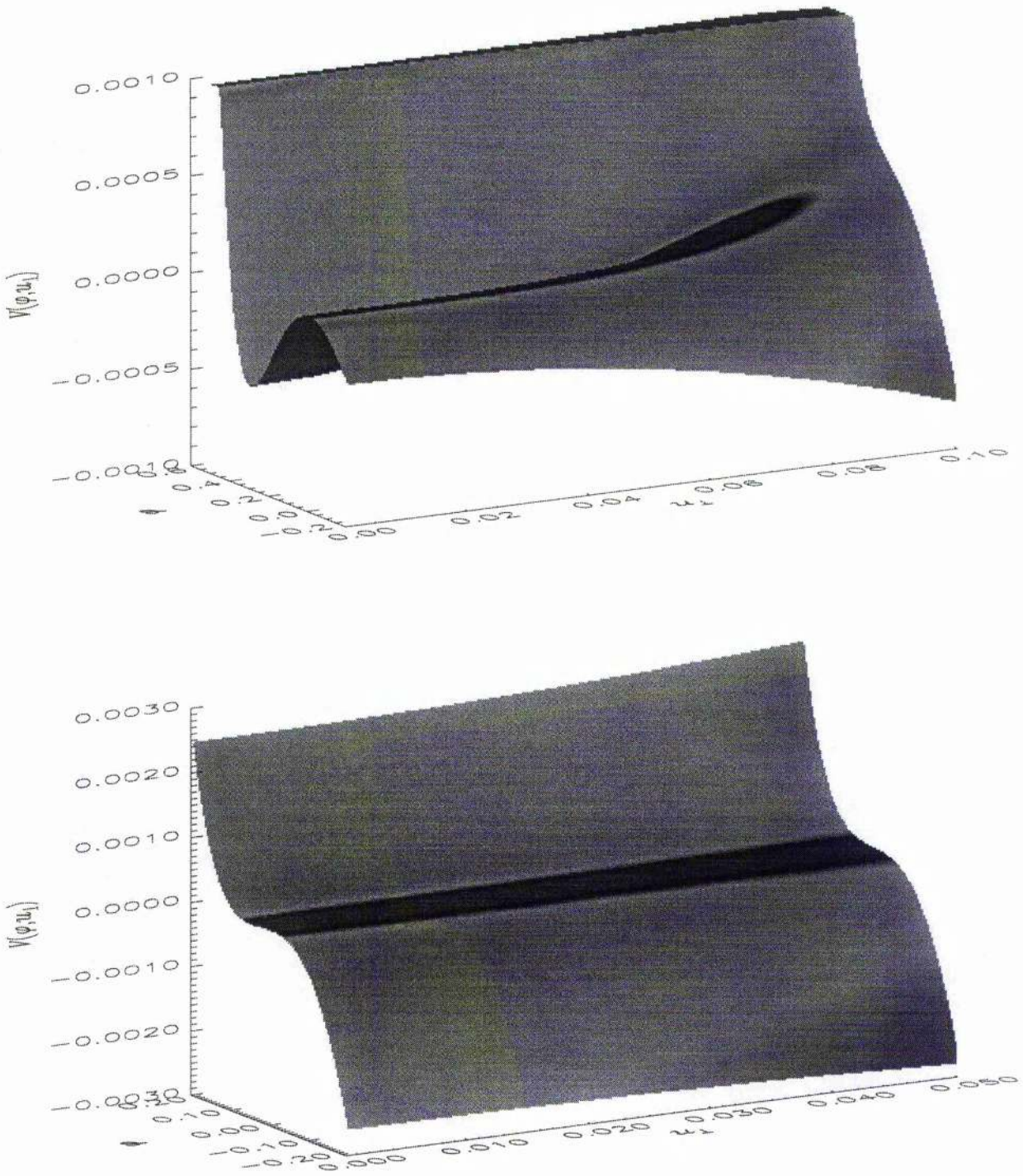

Figure 3.7: Showing the existence of compressive solitary waves (upper plot) but non-existence of rarefactive one (lower plot) for $l_z = 0.8$ and $M = 1.06$ although α is increased to 0.15.

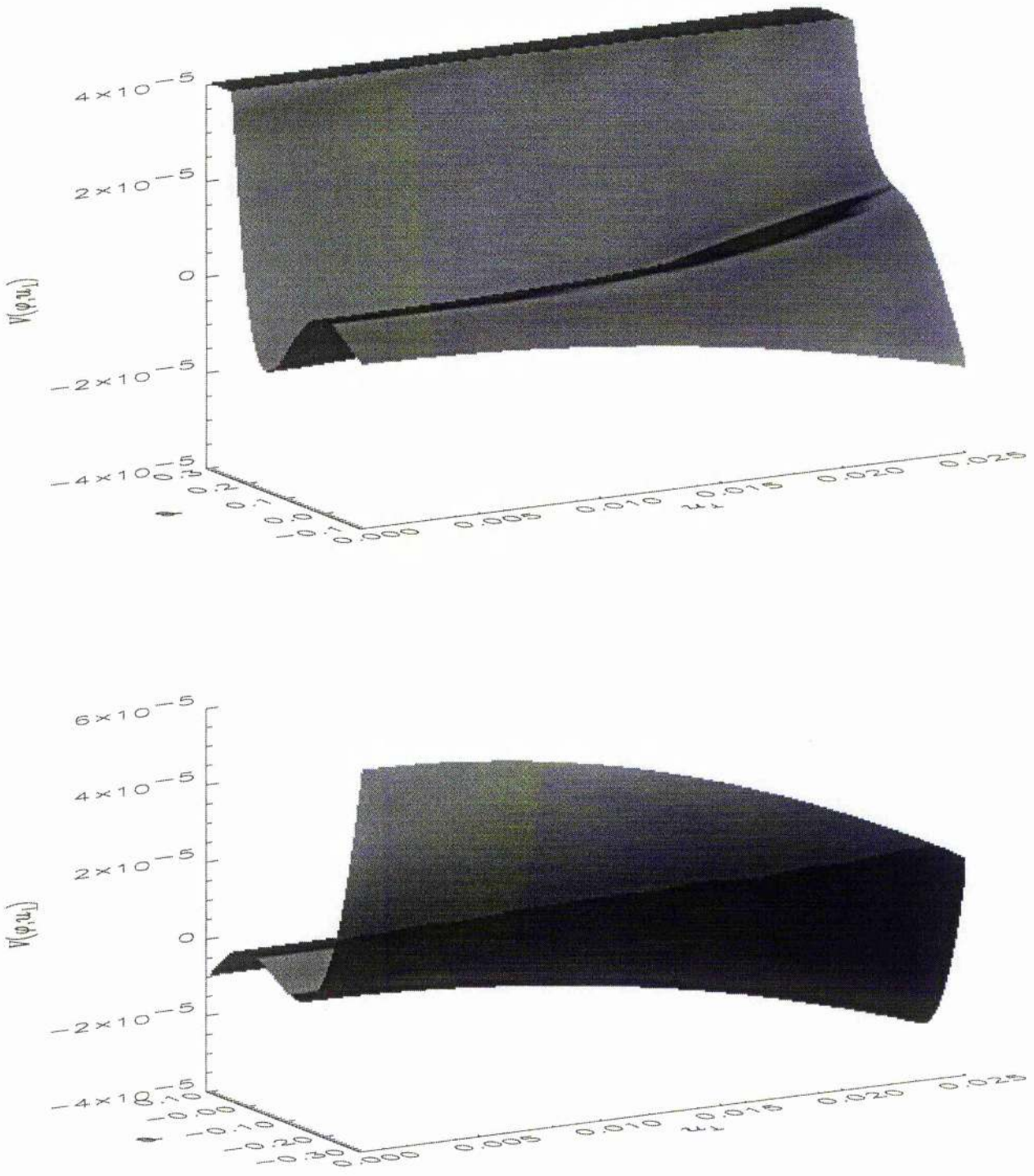

Figure 3.8: Showing the coexistence of compressive (upper plot) and rarefactive (lower plot) solitary waves for $l_z = 0.8$ and $M = 1.057$ when α passes the value 0.156.

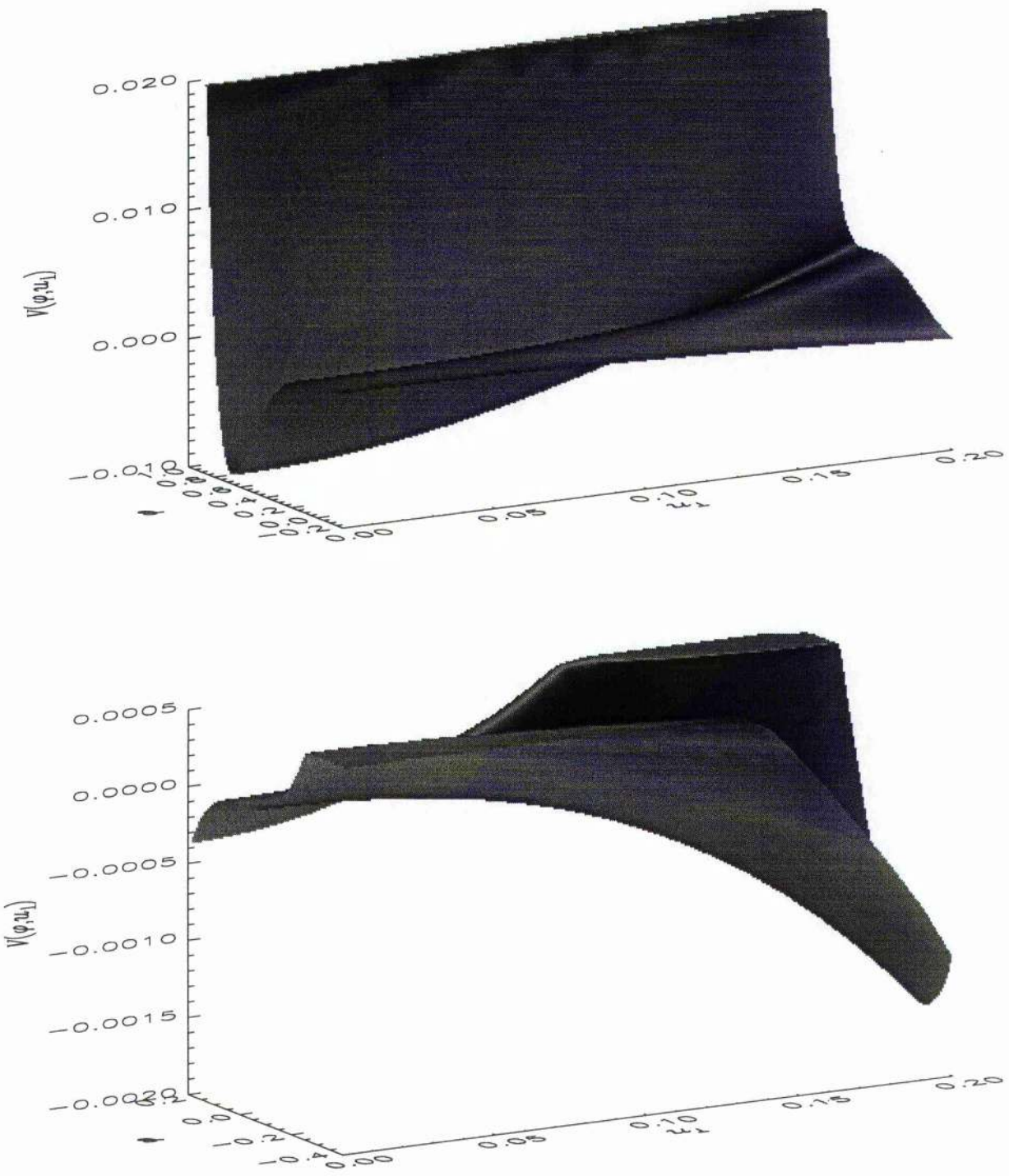

Figure 3.9: Showing the possibility of the existence of compressive (upper one) and rarefactive (lower one) solitary waves for $\alpha = 0.2$ and $l_z = 0.8$ when M passes the value 1.132.

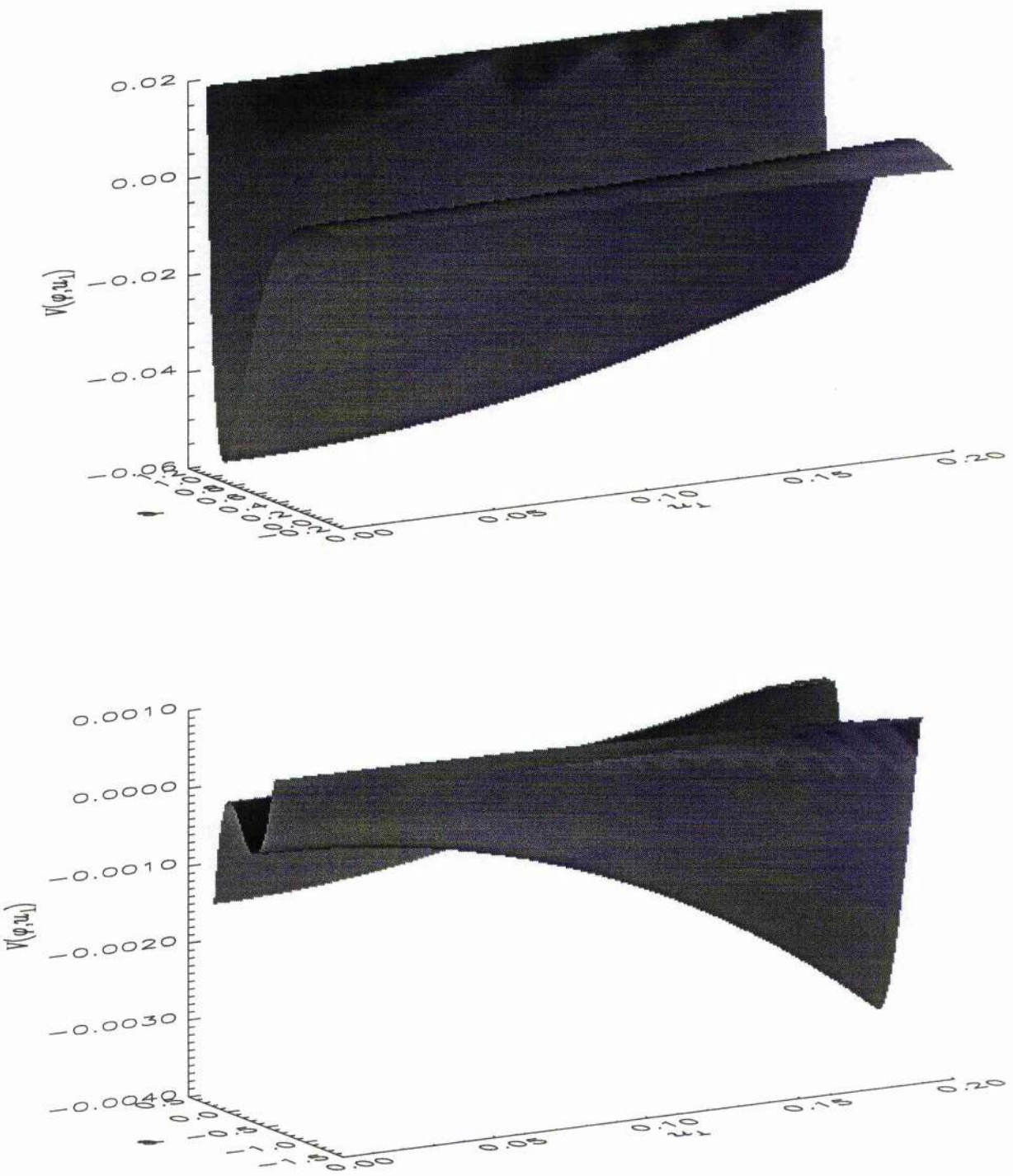

Figure 3.10: Showing how the potential well on both the positive φ-axis (upper plot) and negative φ-axis (lower plot) shown in figure 3.9 changes when the Mach number is increased by 0.05, i.e. $M = 1.182$.

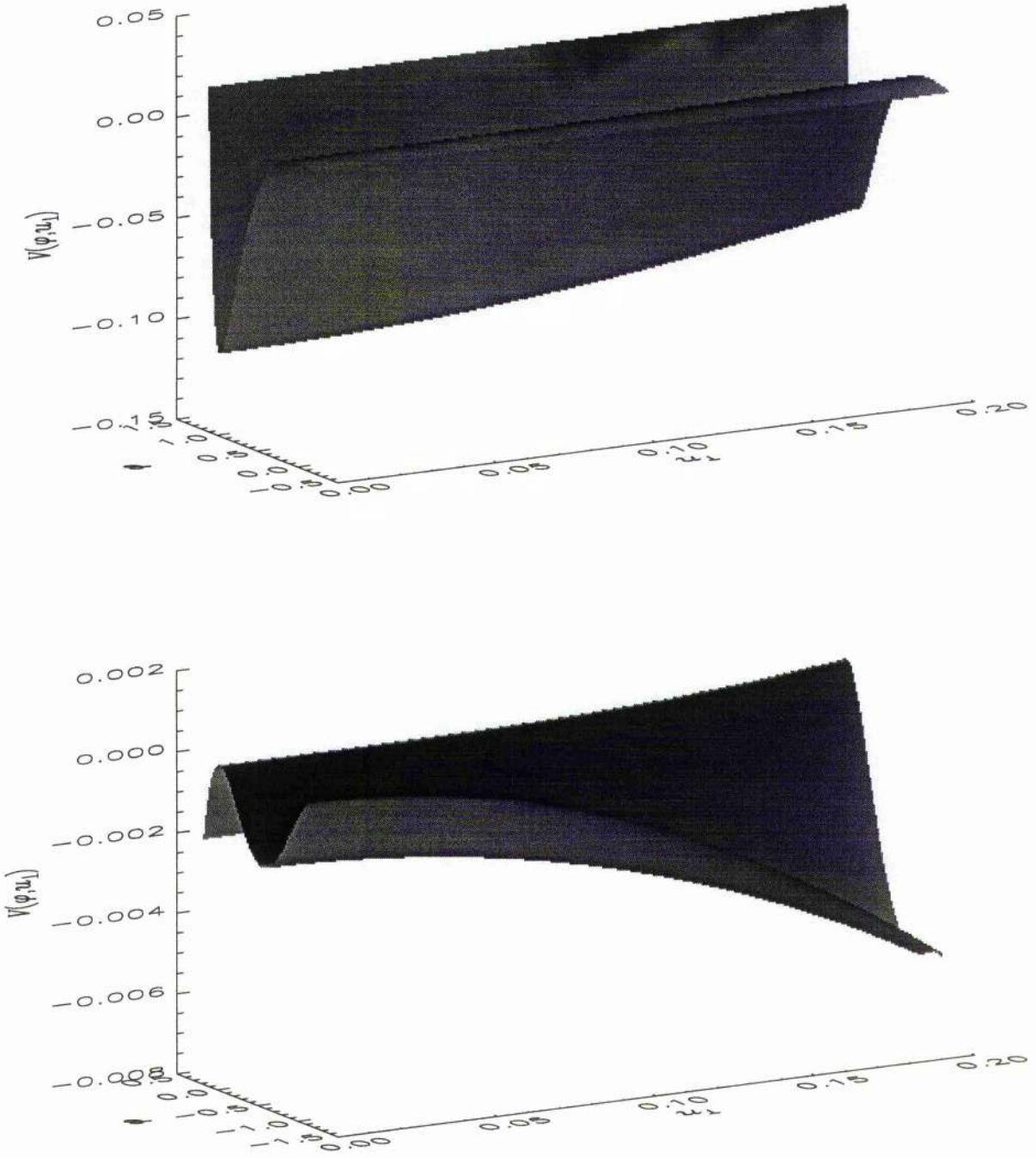

Figure 3.11: Showing the existence of compressive solitary waves (upper plot) and non-existence of rarefactive one (lower plot) for $\alpha = 0.2$ and $l_z = 0.8$ when M passes the value 1.214.

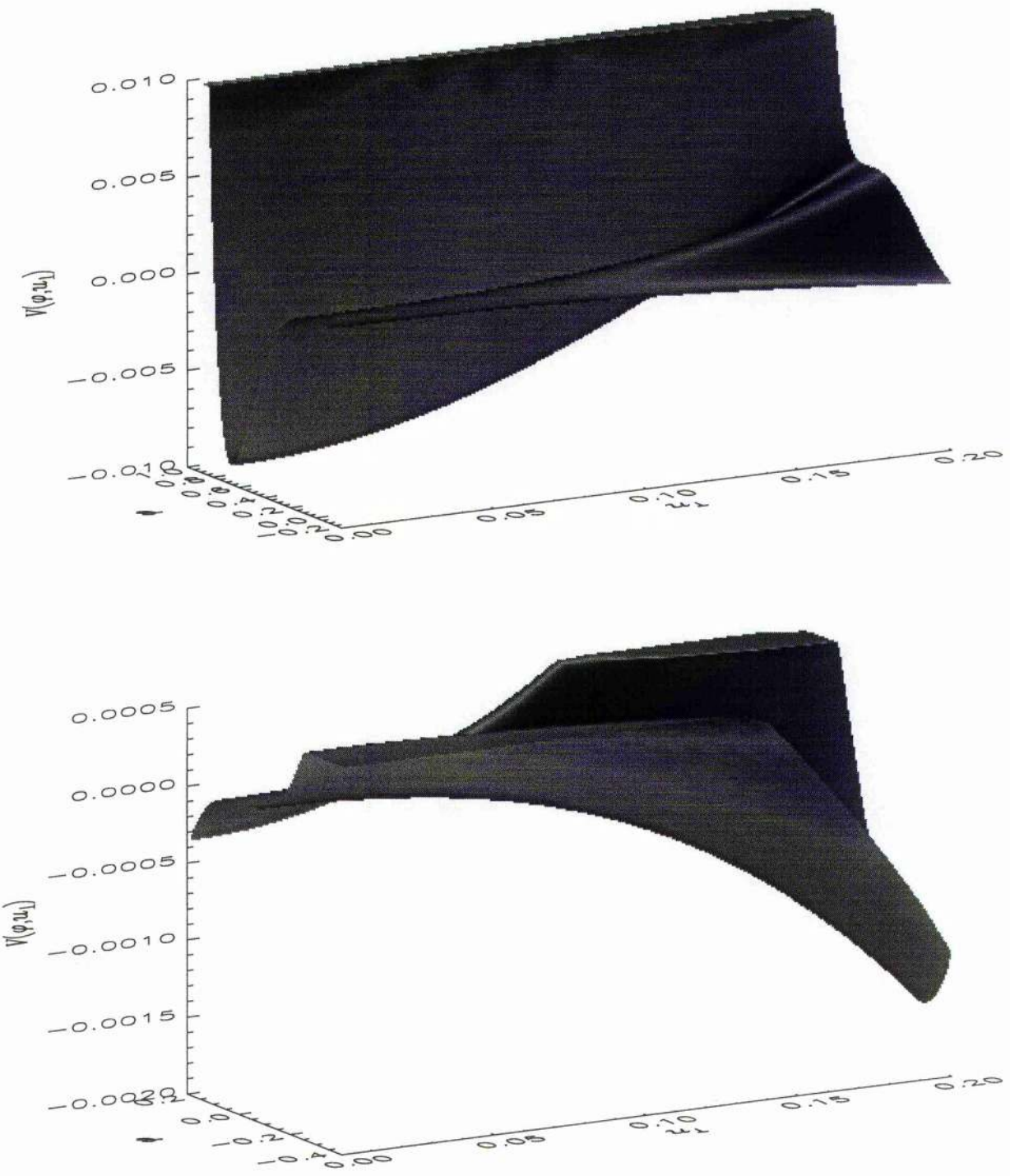

Figure 3.12: Showing the possibility of the existence of compressive (upper plot) and rarefactive (lower plot) solitary waves for $\alpha = 0.2$ and $l_z = 0.7$ when M passes the value 0.99.

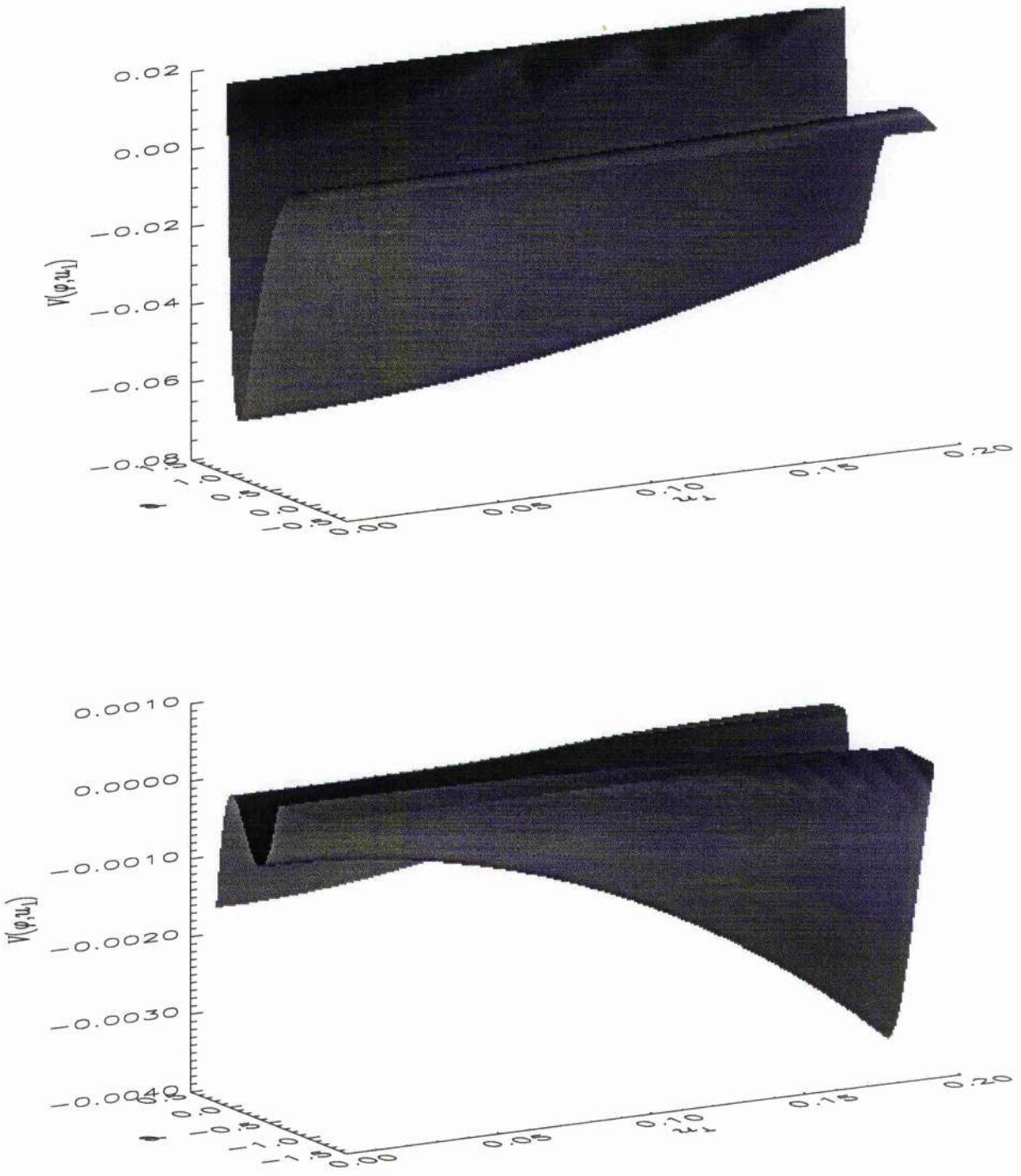

Figure 3.13: Showing how the potential well on both the positive φ-axis (upper plot) and negative φ-axis (lower plot) shown in figure 3.12 changes when the Mach number is increased by 0.05, i.e. $M = 1.04$.

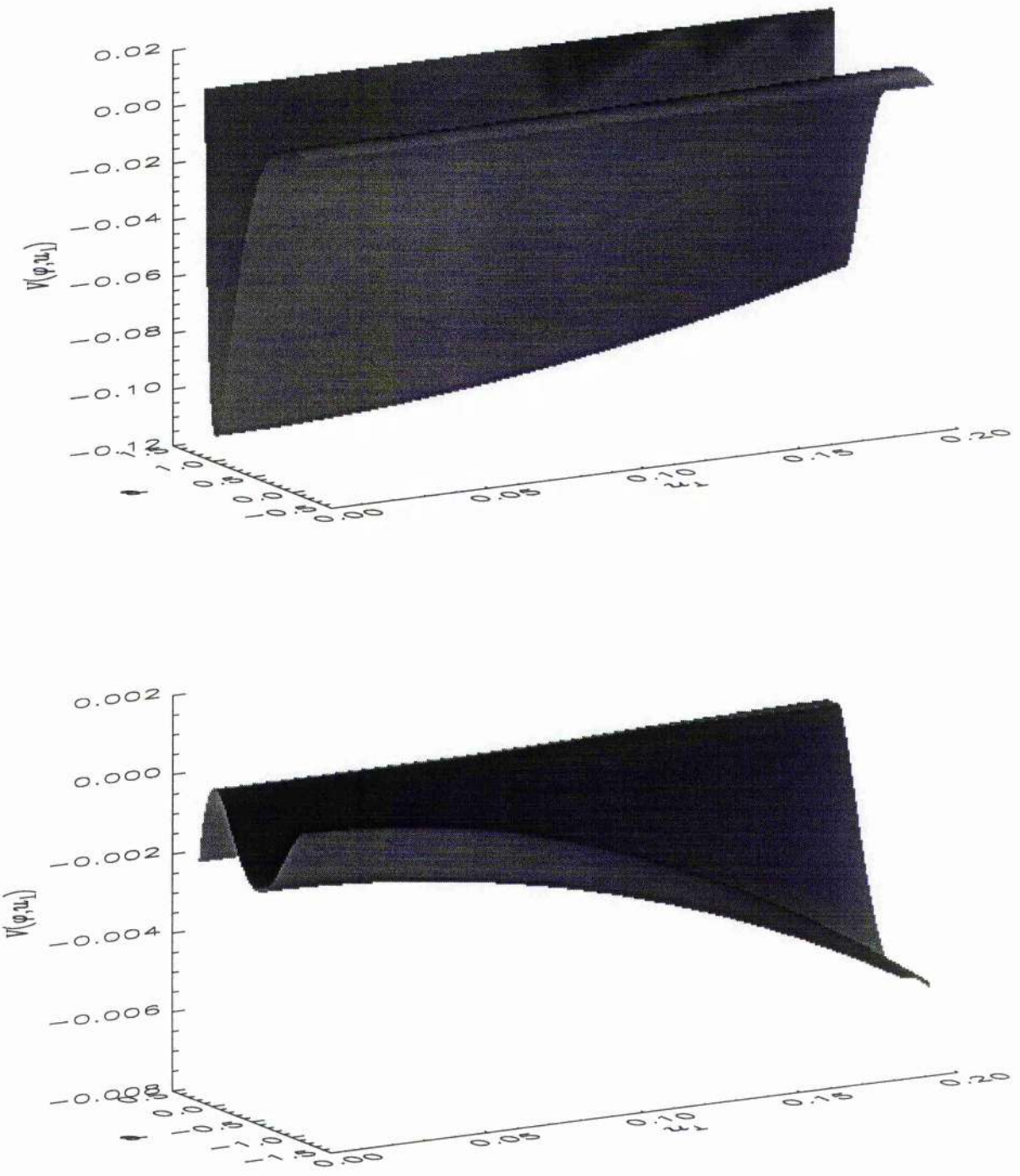

Figure 3.14: Showing the existence of compressive solitary waves (upper plot) and the non-existence of rarefactive one (lower plot) for $\alpha = 0.2$ and $l_z = 0.7$ when M passes the value 1.063.

3.4.2 Numerical Simulation

In this section, we numerically solve the full set of equations and study the nonlinear properties of obliquely propagating electrostatic solitary waves in a magnetised non-thermal plasma. We first assume that the solitary waves propagate in the $(x,\ z)$ plane, i.e. $\hat{l} = \hat{x}l_x + \hat{z}l_z$. Therefore, we can write our full set of equations as

$$\frac{d(nU)}{d\xi} = 0, \tag{3.49}$$

$$U\frac{du_x}{d\xi} = l_x\frac{d\varphi}{d\xi} - \omega_c u_y, \tag{3.50}$$

$$U\frac{du_y}{d\xi} = \omega_c u_x, \tag{3.51}$$

$$U\frac{du_z}{d\xi} = l_z\frac{d\varphi}{d\xi}, \tag{3.52}$$

$$\frac{d^2\varphi}{d\xi^2} = (1 - \beta\varphi + \beta\varphi^2)e^{\varphi} - n, \tag{3.53}$$

where

$$U = M - l_x u_x - l_z u_z. \tag{3.54}$$

Now, under the appropriate boundary conditions, namely $u_x \to 0$, $u_y \to 0$, $\varphi \to 0$, $n \to 1$ at $\xi \to \pm\infty$, Eq. (3.49) can be integrated to give

$$n = \frac{M}{U}. \tag{3.55}$$

To eliminate u_z, we first write Eqs. (3.50) – (3.52) in the form

$$U\frac{d}{d\xi}(u_x - l_x M) = l_x\frac{d\varphi}{d\xi} - \omega_c u_y, \tag{3.56}$$

$$U\frac{du_y}{d\xi} = \omega_c u_x, \tag{3.57}$$

$$U\frac{d}{d\xi}(u_z - l_z M) = l_z\frac{d\varphi}{d\xi}. \tag{3.58}$$

Now, multiplying these three equations by $(u_x - l_x M)$, u_y and $(u_z - l_z M)$, respectively, and adding these new three equations we obtain

$$\frac{1}{2}U\frac{d}{d\xi}[(u_x - l_x M)^2 + u_y^2 + (u_z - l_z M)^2 + 2\varphi] - M l_x \omega_c u_y = 0. \tag{3.59}$$

Again, adding Eq. (3.50)$\times l_z$ and Eq. (3.52)$\times(-l_x)$ and multiplying this new equation by Ml_x/l_z we can express the last term of Eq. (3.59) as

$$-Ml_x\omega_c u_y = UM\frac{d}{d\xi}(l_x u_x - \frac{l_x^2}{l_z}u_z). \tag{3.60}$$

Now, substituting this equation into Eq. (3.59) and integrating this new one, under the appropriate boundary conditions, namely $u_x \to 0$, $u_y \to 0$, $\varphi \to 0$, $n \to 1$ at $\xi \to \pm\infty$, we obtain a quadratic equation for $(u_z - l_z M)$ in the form

$$\begin{aligned}(u_z - l_z M)^2 - 2\frac{l_x^2}{l_z}M(u_z - l_z M) - M^2(1 + 2l_x^2) + u_y^2 \\ +2\varphi + 2Ml_x u_x + (u_x - l_x M)^2 = 0.\end{aligned} \tag{3.61}$$

Therefore, solving this equation for $(u_z - l_z M)$ one can find u_z as

$$u_z = \frac{M}{l_z}[1 - \sqrt{1 - \frac{l_z^2}{M^2}(u_x^2 + u_y^2 + 2\varphi)}] \tag{3.62}$$

and substituting this u_z into Eq. (3.54) one can also express U in terms of u_x, u_y, and φ as

$$U = M\sqrt{1 - \frac{l_z^2}{M^2}(u_x^2 + u_y^2 + 2\varphi)} - l_x u_x. \tag{3.63}$$

Therefore, our problem of finding stationary solutions of the basic nonlinear set of equations finally reduces to a set of four coupled 1st order ordinary differential equations in the form

$$\frac{du_x}{d\xi} = \frac{1}{U}(l_x\psi - \omega_c u_y), \tag{3.64}$$

$$\frac{du_y}{d\xi} = \frac{1}{U}\omega_c u_x, \tag{3.65}$$

$$\frac{d\varphi}{d\xi} = \psi, \tag{3.66}$$

$$\frac{d\psi}{d\xi} = (1 - \beta\varphi + \beta\varphi^2)e^{\varphi} - \frac{M}{U}. \tag{3.67}$$

Now, working in this higher dimensional phase space, we search for solitary waves directly. Such solutions arise when the equilibrium is unstable and there is a phase space orbit which approaches the equilibrium as $\xi \to \pm\infty$ (a homoclinic orbit). By

linearising about the origin we identify the unstable manifold (i.e. the orbit which approaches the origin as $\xi \to -\infty$) in the vicinity of the origin. This then gives us the initial conditions in order to search for a homoclinic orbit. Some results of this procedure are displayed in figures 3.15 – 3.26. In figure 3.15 we have considered $\alpha = 0$, i.e. Maxwellian electrons, and shown that rarefactive solitary waves do not exist and that for $l_z = 0.8$ and $\omega_c = 0.1$ compressive ones start to exist when M passes the value 0.810. We have found in figures 3.16 and 3.17 that only compressive solitary waves exist for $\alpha < 0.155$, but compressive and rarefactive solitary waves coexist when $\alpha \geq 0.156$. Figure 3.18 shows the variation of φ with ξ for $l_z = 0.8$, $\omega_c = 0.1$, $\alpha = 0.2$, $M = 1.132$ (solid curves) and $M = 1.137$ (dotted curves). It shows that as M passes the value 1.132, a small amplitude rarefactive solitary wave appears together with a large amplitude compressive one and that their amplitude increases as M increases. Figure 3.19 shows what happens at higher values of M. As M reaches the value of 1.214, the rarefactive solitary wave disappears, but the compressive one still exists. Figures 3.20 and 3.21 show similar behaviour with $l_z = 0.7$, $\omega_c = 0.1$, $\alpha = 0.2$, i.e. propagation at a larger angle to the field. The transitions occur at lower Mach number in this case. In figures 3.22 and 3.23 the magnetic field is increased, so that $\omega_c = 0.3$. The rarefactive solitary wave behaves in a similar fashion to before. However, above a certain Mach number, the compressive solitary wave seems to go over to a structure which is almost, but not completely periodic. To see the precise nature of this type of structures, we have shown this compressive solitary wave structures for $M = 1.15$, $M = 1.18$ and 1.195 in figure 3.24 and $M = 1.21$ in figures 3.25 and 3.26. Figure 3.25 shows the potential structures plotted in both the positive and negative directions of ξ, whereas figure 3.26 compares the potential structures with structures of the y- and x-components of the velocity $\mathbf{u}$. These plots suggest us that the magnetic field changes the compressive solitary wave structure with higher velocity to the form shown in figures 3.23 and 3.26. The more precise nature of this requires further investigation.

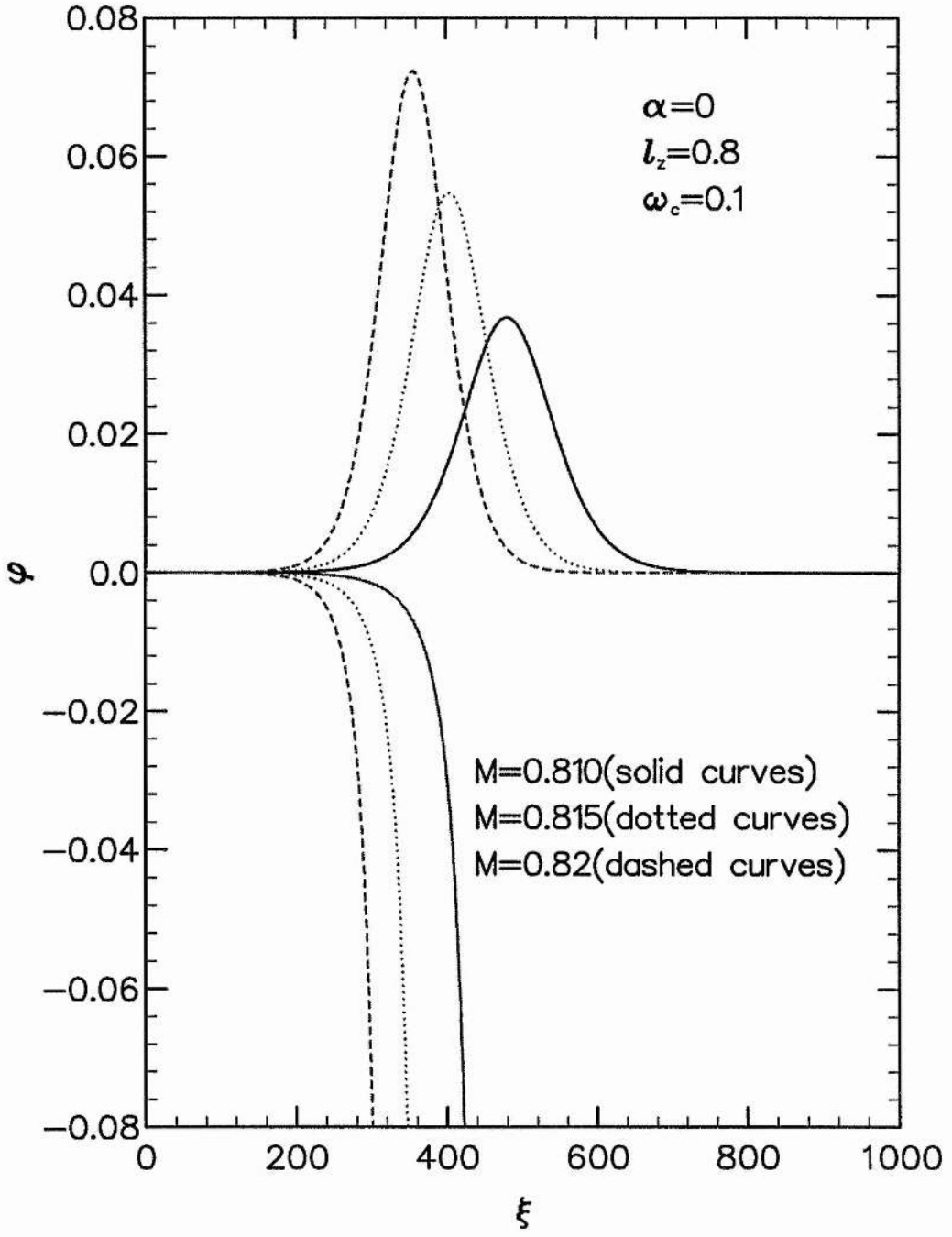

Figure 3.15: φ is plotted against ξ for $\alpha = 0$, $l_z = 0.8$, $\omega_c = 0.1$ and $M = 0.810$ (solid curves), $M = 0.815$ (dotted curves) and $M = 0.82$ (dashed curves).

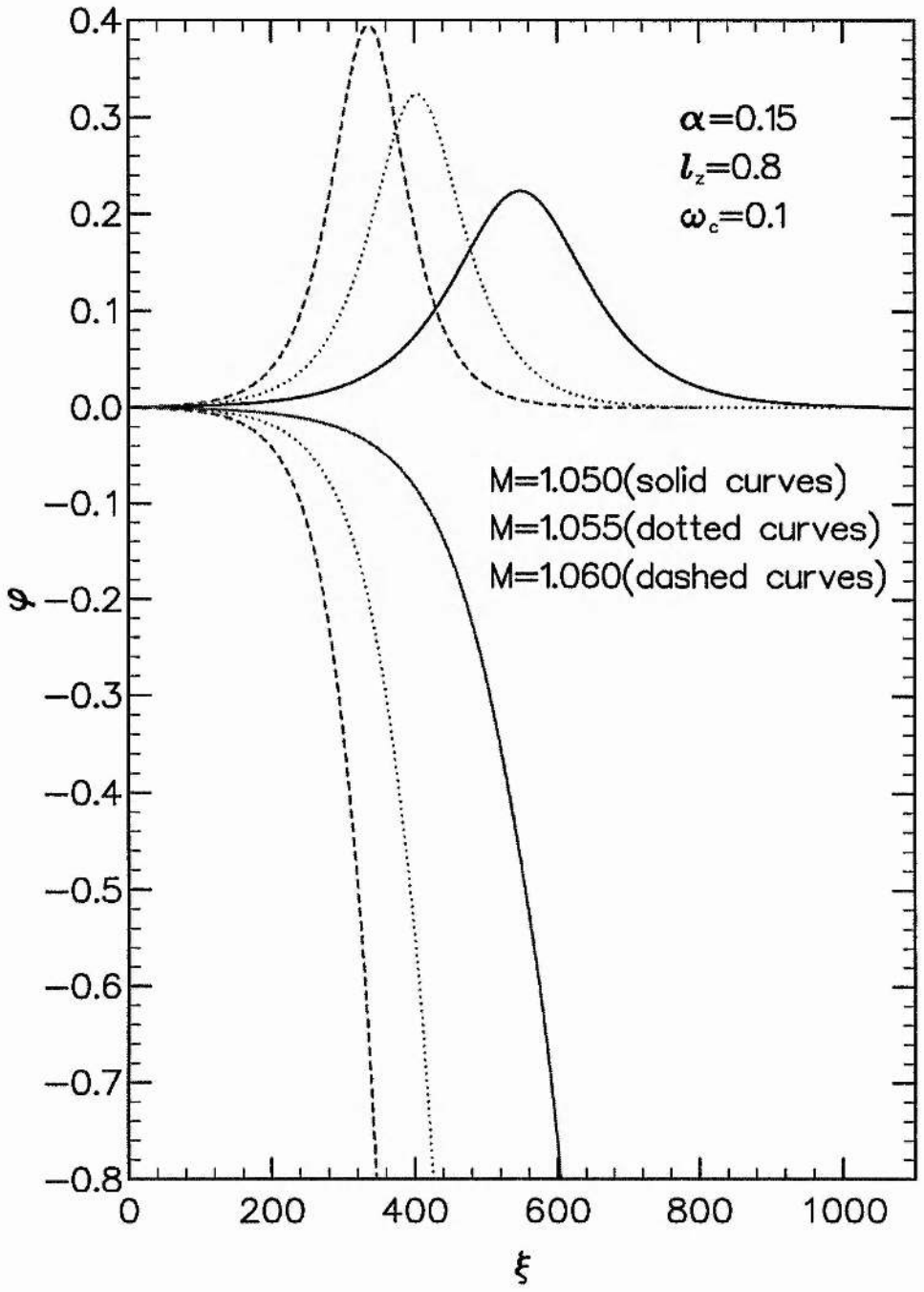

Figure 3.16: φ is plotted against ξ for $\alpha = 0.15$, $l_z = 0.8$, $\omega_c = 0.1$ and $M = 1.050$ (solid curves), $M = 1.055$ (dotted curves) and $M = 1.060$ (dashed curves).

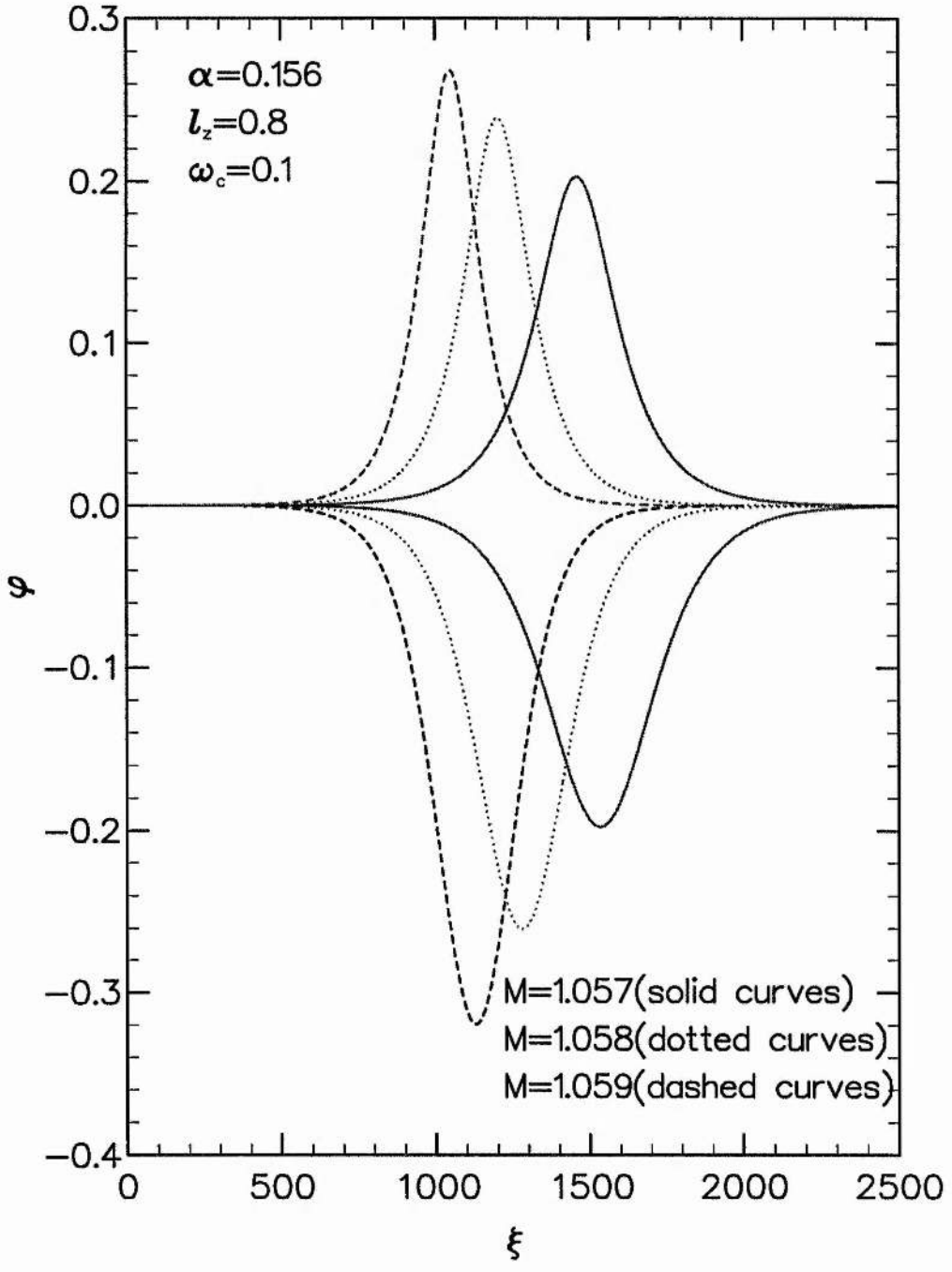

Figure 3.17: φ is plotted against ξ for $\alpha = 0.156$, $l_z = 0.8$, $\omega_c = 0.1$ and $M = 1.057$ (solid curves), $M = 1.058$ (dotted curves) and $M = 1.059$ (dashed curves).

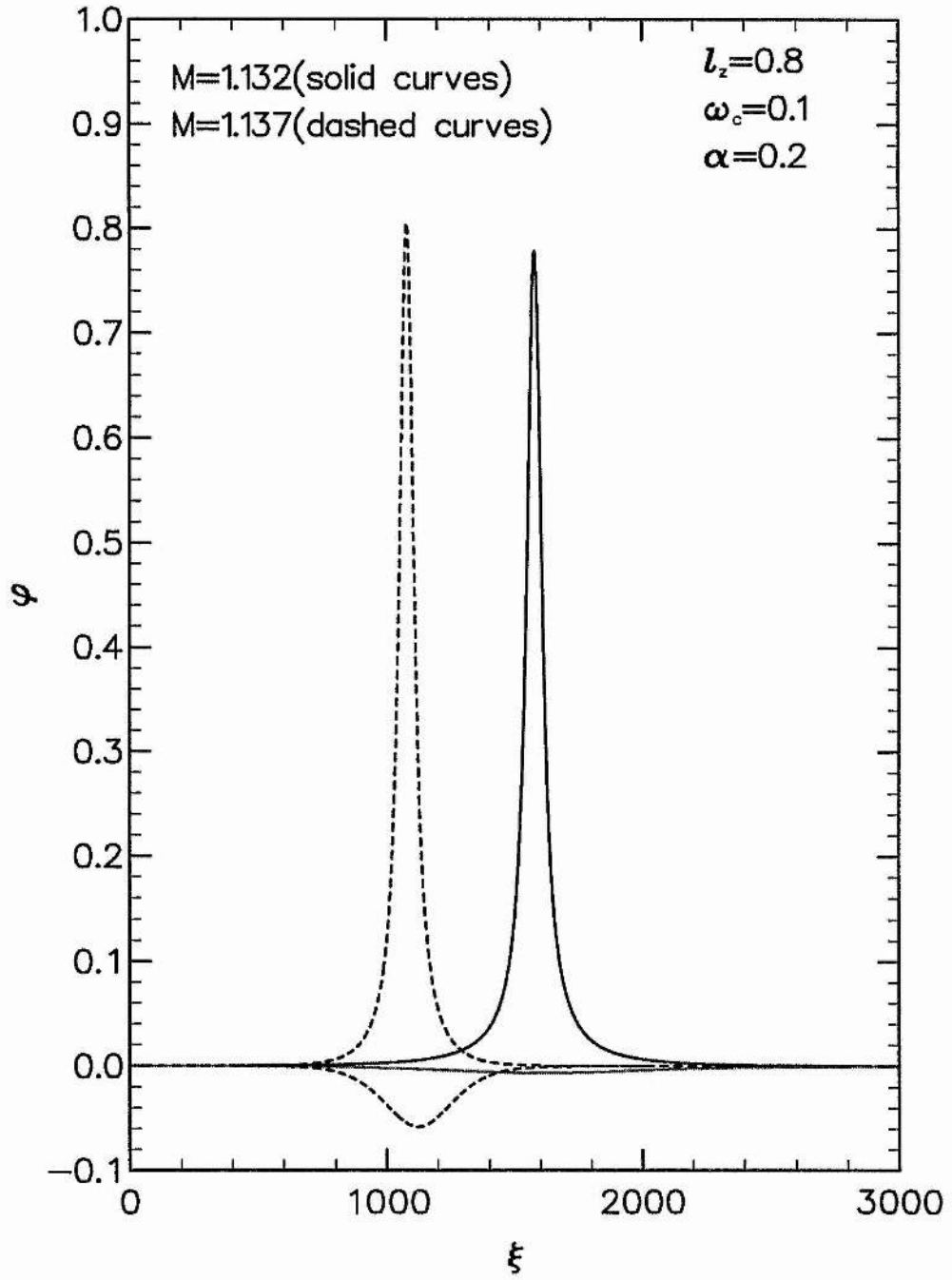

Figure 3.18: φ is plotted against ξ for $\alpha = 0.2$, $l_z = 0.8$, $\omega_c = 0.1$, $M = 1.132$ (solid curves) and $M = 1.137$ (dashed curves).

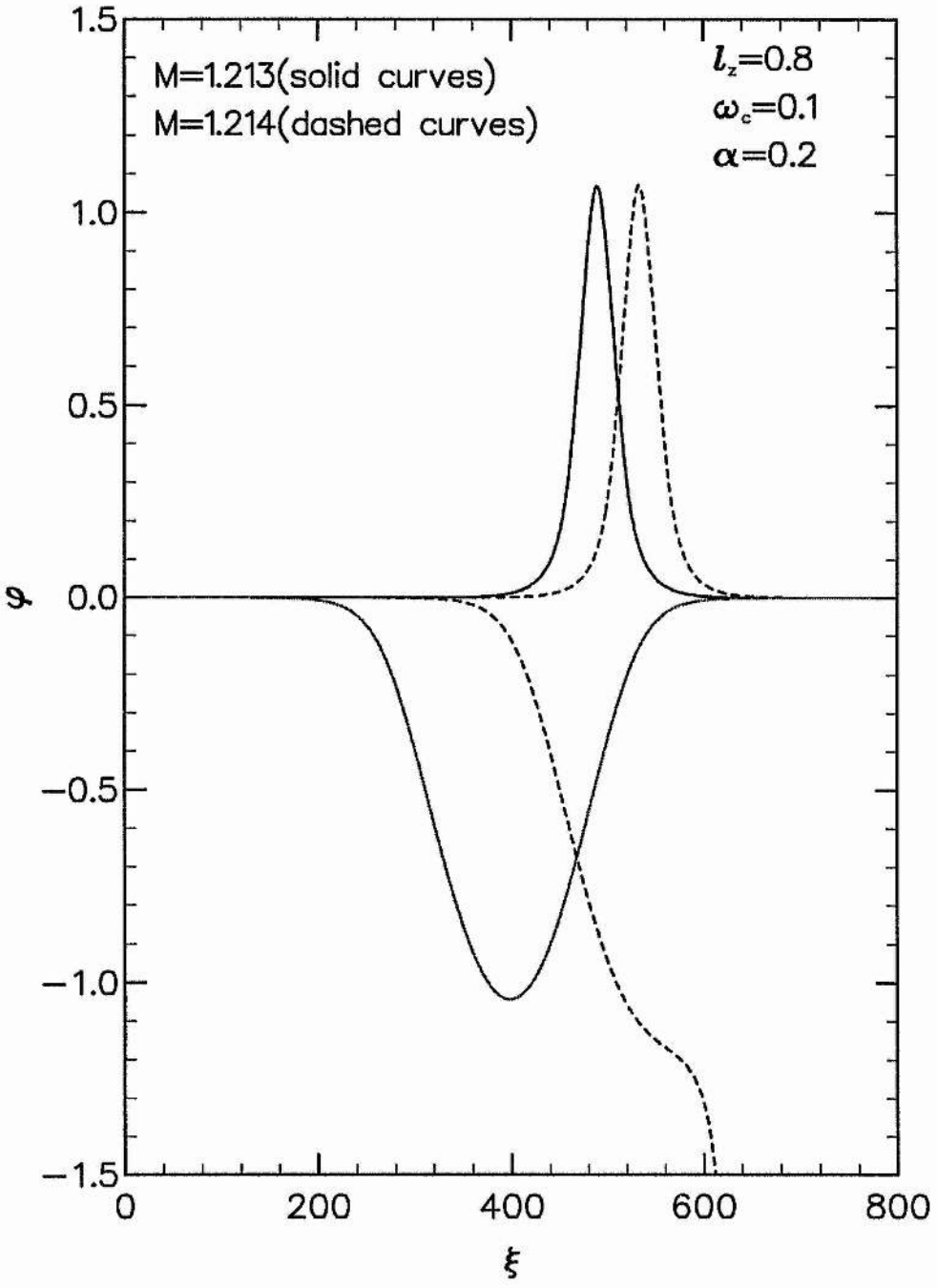

Figure 3.19: φ is plotted against ξ for $\alpha = 0.2$, $l_z = 0.8$, $\omega_c = 0.1$, $M = 1.213$ (solid curves) and $M = 1.214$ (dashed curves).

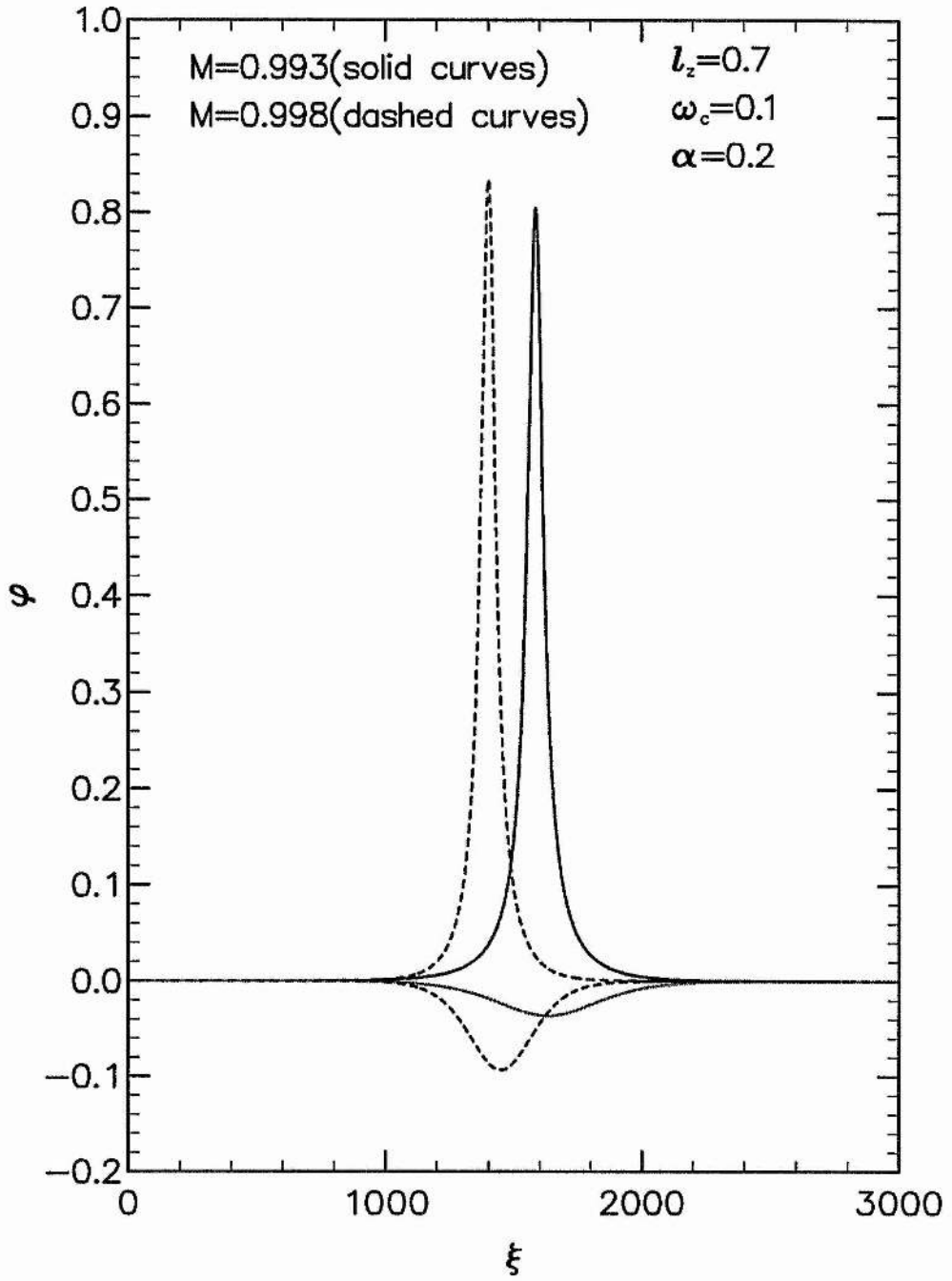

Figure 3.20: φ is plotted against ξ for $\alpha = 0.2$, $l_z = 0.7$, $\omega_c = 0.1$, $M = 0.993$ (solid curves) and $M = 0.998$ (dashed curves).

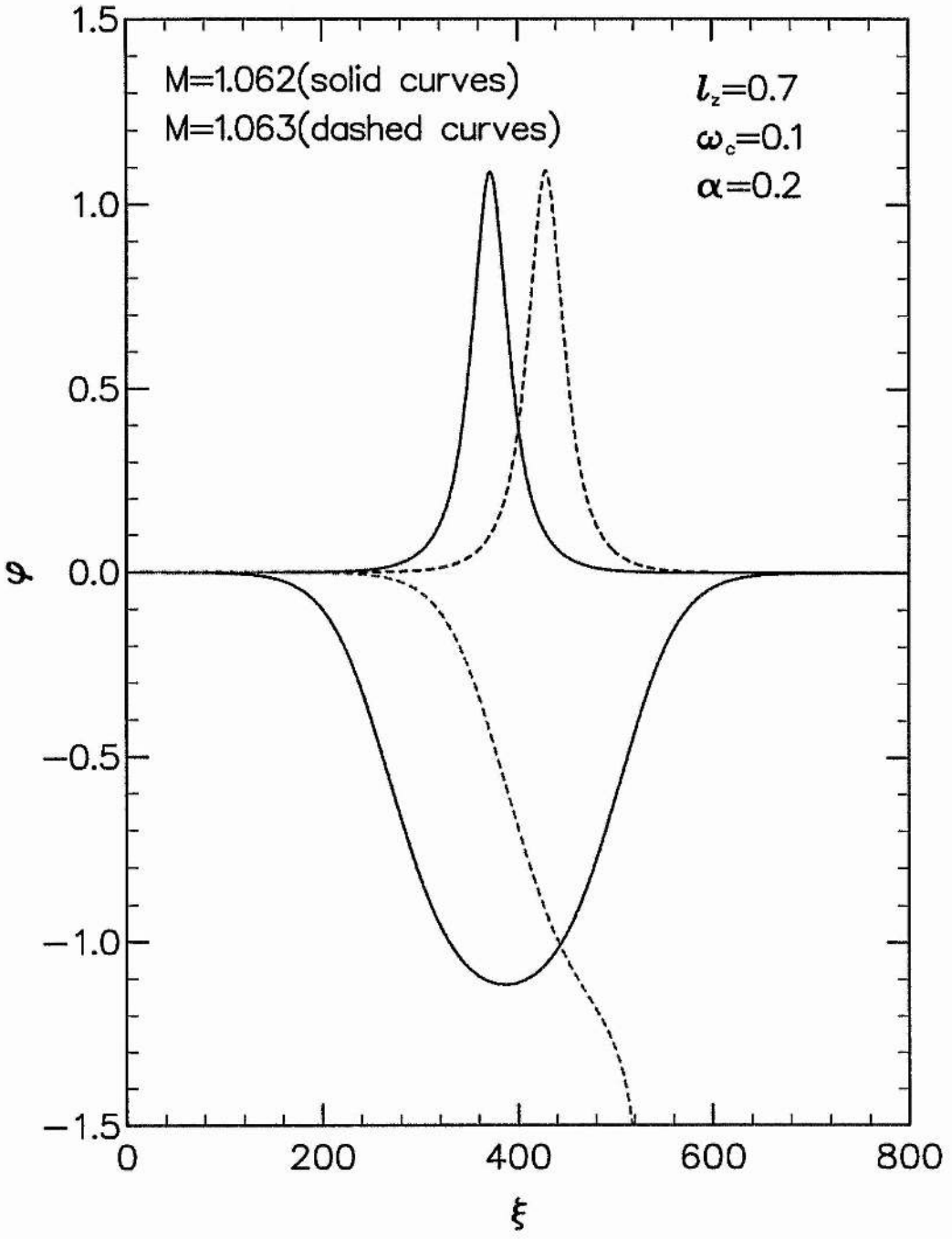

Figure 3.21: φ is plotted against ξ for $\alpha = 0.2$, $l_z = 0.7$, $\omega_c = 0.1$, $M = 1.062$ (solid curves) and $M = 1.063$ (dashed curves).

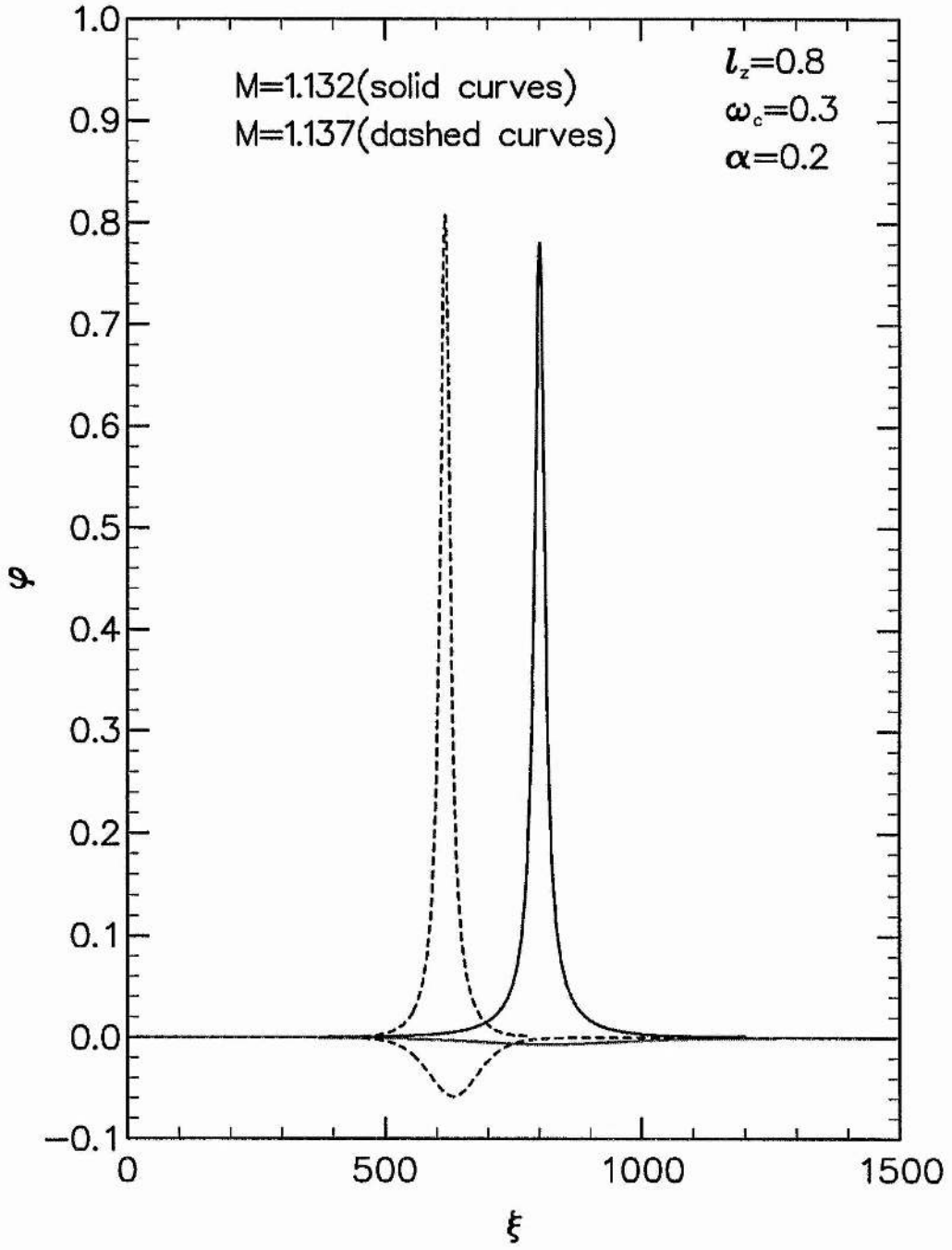

Figure 3.22: φ is plotted against ξ for $\alpha = 0.2$, $l_z = 0.8$, $\omega_c = 0.3$, $M = 1.132$ (solid curves) and $M = 1.137$ (dashed curves).

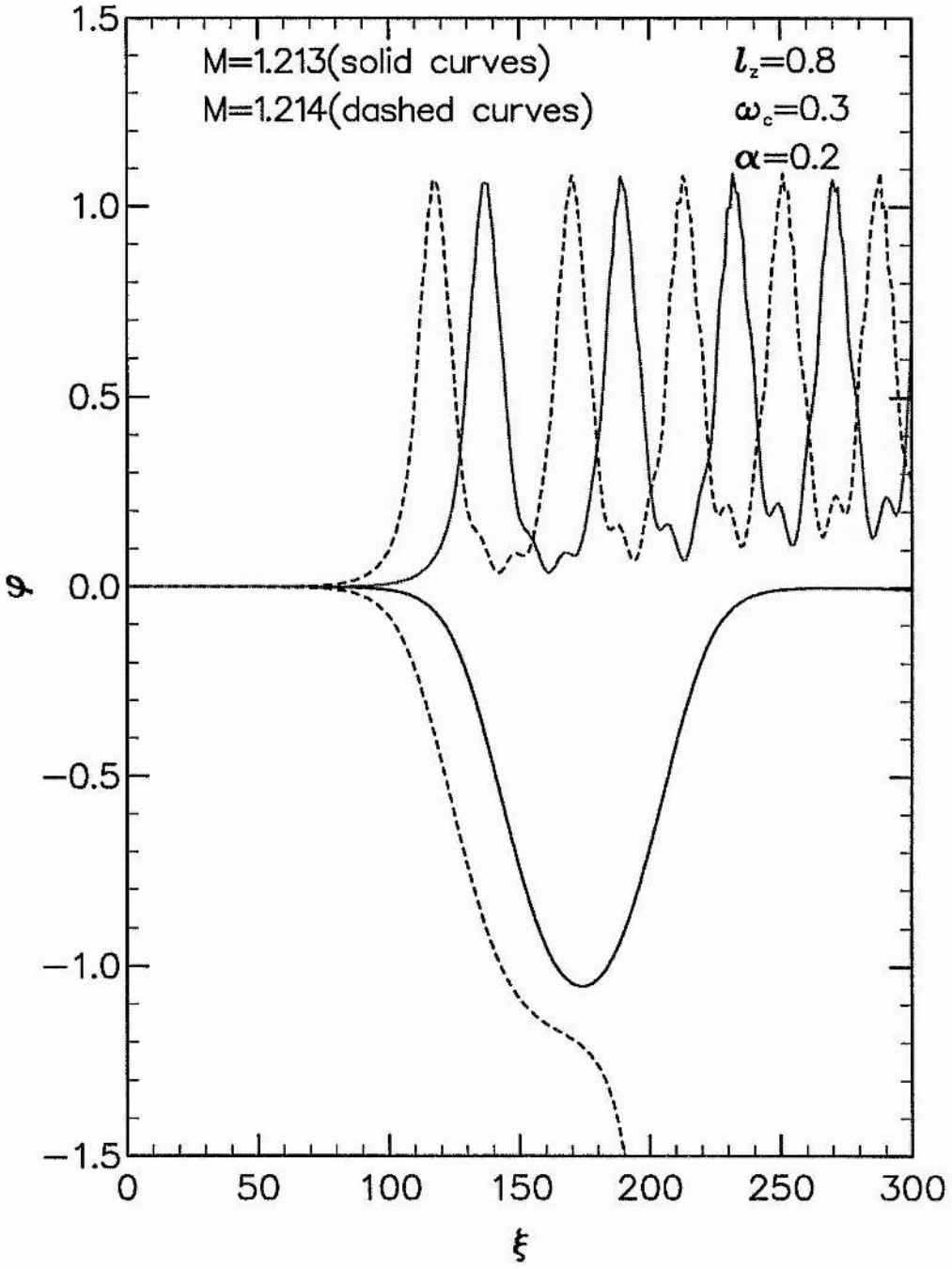

Figure 3.23: φ is plotted against ξ for $\alpha = 0.2$, $l_z = 0.8$, $\omega_c = 0.3$, $M = 1.213$ (solid curves) and $M = 1.214$ (dashed curves).

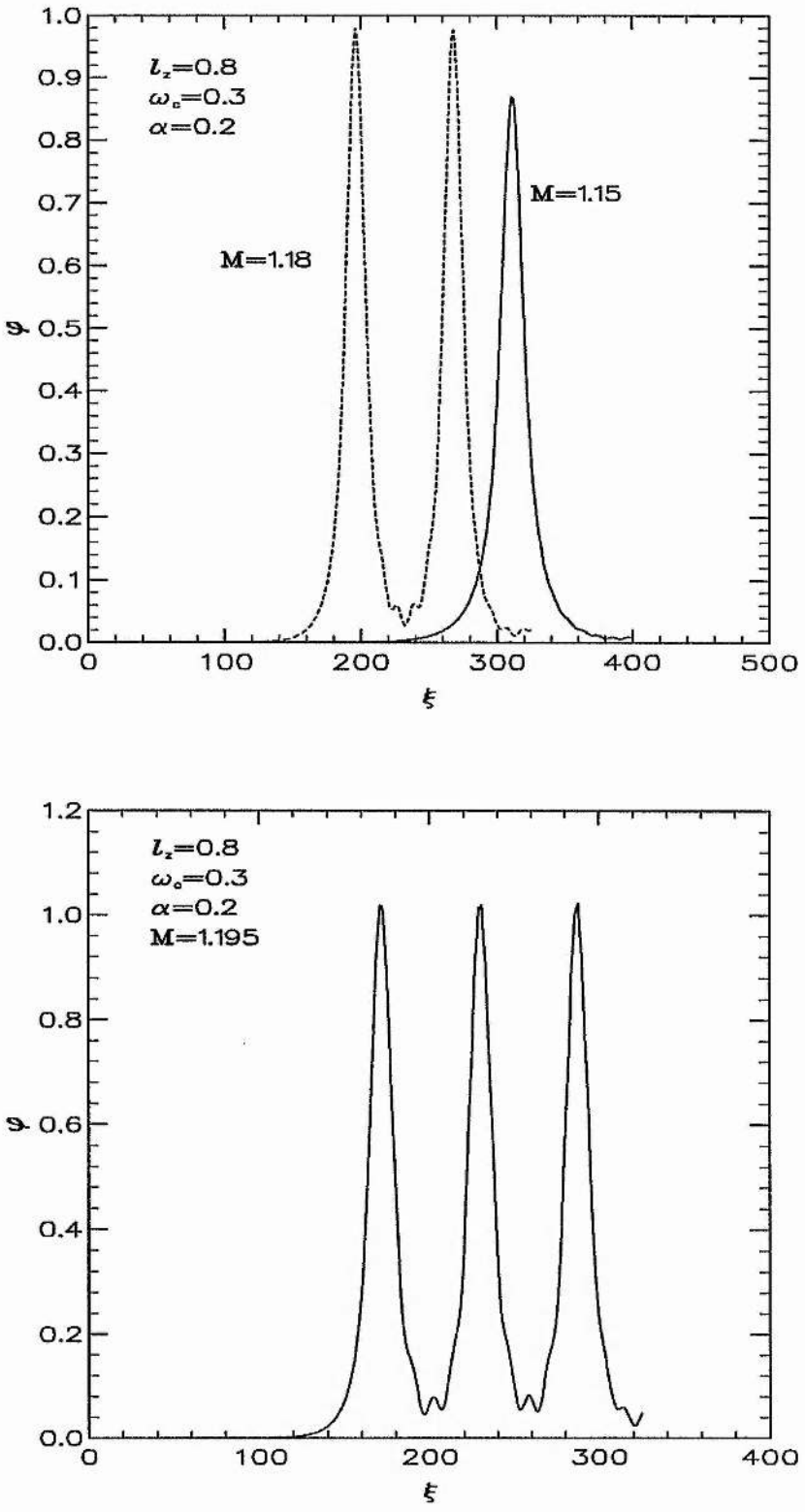

Figure 3.24: φ is plotted against ξ for $\alpha = 0.2$, $l_z = 0.8$, $\omega_c = 0.3$, $M = 1.15$ (solid curve) and $M = 1.18$ (dashed curve) in upper plot and M=1.195 in lower plot.

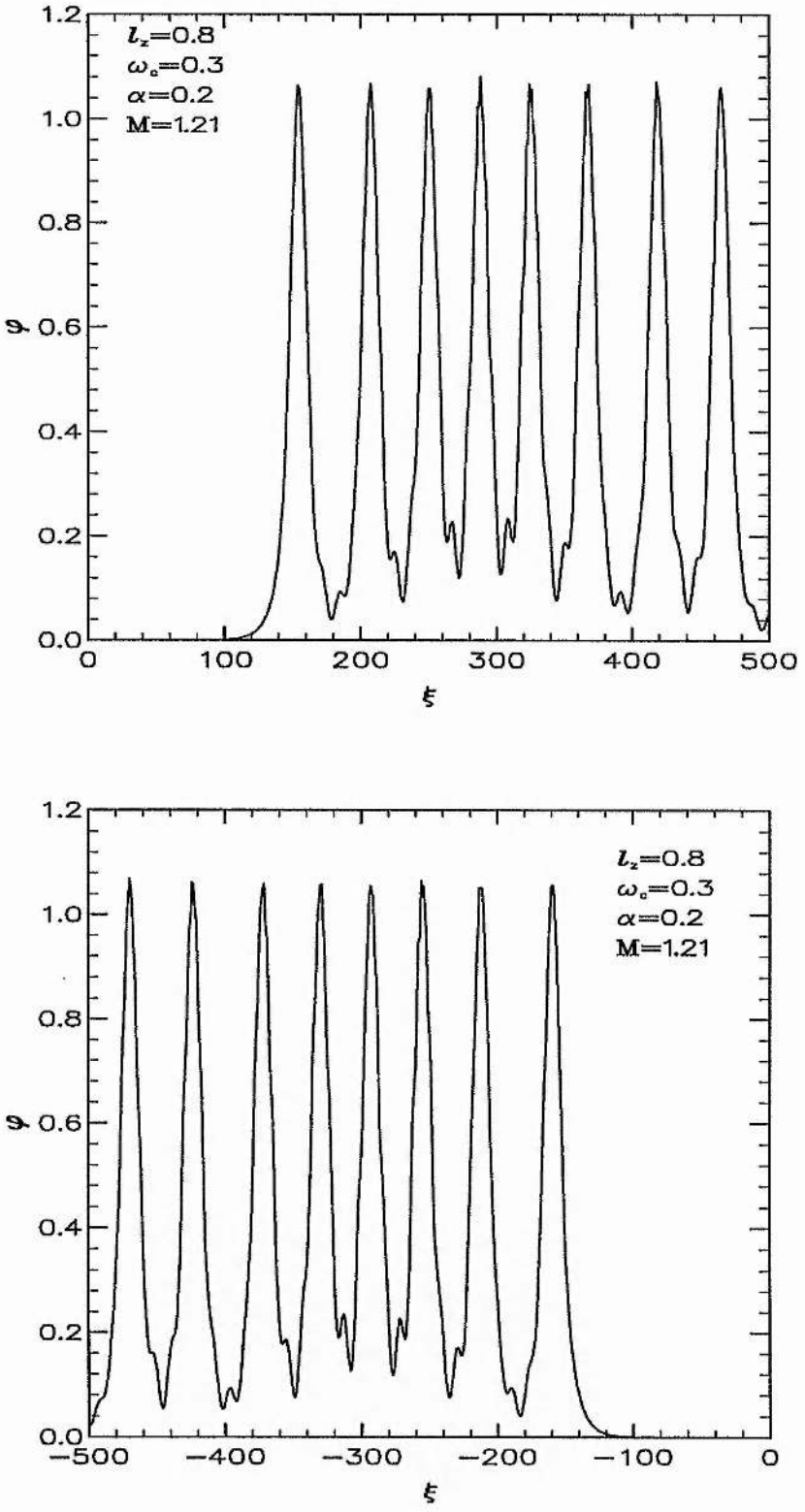

Figure 3.25: φ is plotted against ξ for $\alpha = 0.2$, $l_z = 0.8$, $\omega_c = 0.3$ and M=1.21 in positive direction (upper plot) and in negative direction (lower plot).

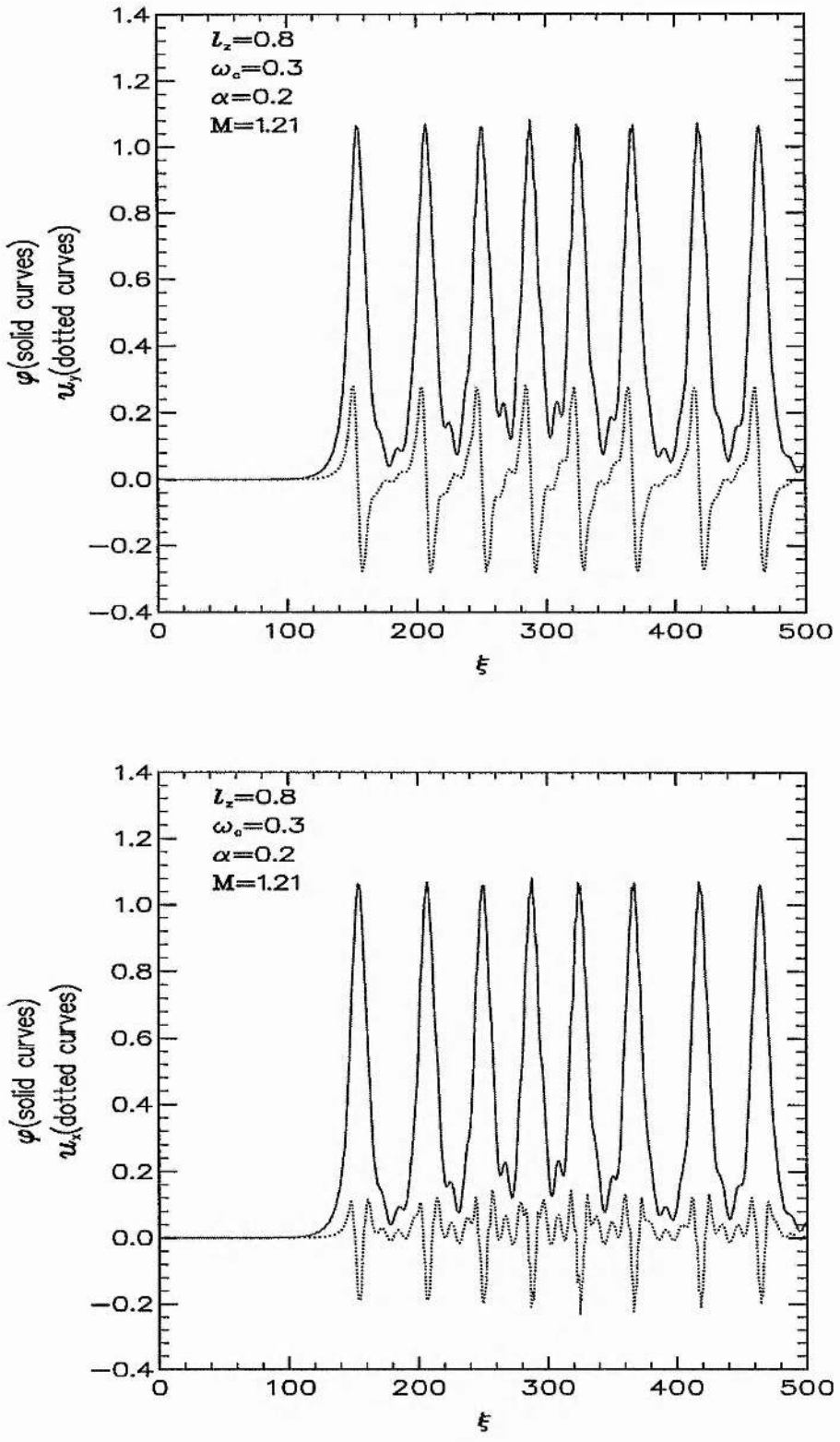

Figure 3.26: φ(solid curves), u_y(dotted curves in upper plot) and u_x(dotted curves in lower plot) are plotted against ξ for $\alpha = 0.2$, $l_z = 0.8$, $\omega_c = 0.3$ and $M = 1.21$.

3.5 Two-Electron-Temperature Plasma

We have briefly explained the two-electron-temperature plasma model, which is very common in laser-produced plasmas [112], laboratory plasmas [113] and space plasmas [68] and has attracted the attention of many workers because of its vital role in space research [68,69] and basic laboratory experiments [113,114], and compared it with our non-thermal plasma model in the discussion of chapter 2. A number of theoretical investigations [35-37] have been made of solitary waves in this two-electron-temperature plasma model. Some [35] of them are in unmagnetised and one-dimensional geometry, some [36,37] are in magnetised plasma by the reductive perturbation method, which is not valid for large amplitude limit, and some [32,107] have assumed the quasi-neutrality condition which is also not valid when the ratio of the electron Debye-length to the ion gyro-radius is comparable to the sine of the angle between directions of the wave propagation and the magnetic field. In this section, we will exploit our method, which has used neither the reductive perturbation method nor the quasi-neutrality condition, to a study of arbitrary amplitude electrostatic solitary waves in a magnetised two-electron-temperature plasma. We can consider here the ion dynamics as before. The only change is to replace the electron density n_e in Poisson's equation by

$$n_e = \alpha e^{\varphi} + (1-\alpha)e^{\varphi/\mu_0}, \tag{3.68}$$

where $\alpha = 1/(1+\alpha_0)$, with α_0 being the ratio of the unperturbed electron density (n_{e02}) with temperature T_{e2} to that (n_{e01}) with temperature T_{e1}, $\mu_0 = T_{e2}/T_{e1}$, φ is normalised to $K_B T_{e1}/e$ and n_e is normalised to $n_0 = n_{e01} + n_{e02}$. Now, following the same procedure as applied in the previous section, we can study the arbitrary amplitude ion-acoustic solitary waves in this magnetised two-electron-temperature plasma model. As before, we make this investigation first by the pseudopotential approach and later by solving the full nonlinear system of equations.

3.5.1 Pseudopotential Approach

The use of this new expression for normalised electron density n_e in two-electron-temperature plasma model, given by Eq. (3.68), and the method, applied in Sec. 3.4.1, allow us to write Poisson's equation in the form

$$\frac{1}{2}(\frac{d\varphi}{d\xi})^2 + V(\varphi, u_\perp) = 0, \tag{3.69}$$

where $V(\varphi, u_\perp)$ is given by

$$\begin{aligned} V(\varphi, u_\perp) = \alpha \; &+ \; (1-\alpha)\mu_0 - [\alpha e^{\varphi} + (1-\alpha)\mu_0 e^{\varphi/\mu_0}] \\ &+ \; \frac{M^2}{l_z^2}[1 - \sqrt{1 - \frac{l_z^2}{M^2}(2\varphi + u_\perp^2)}]. \end{aligned} \tag{3.70}$$

It is important to note here that $u_\perp$ and M both are normalised to $\sqrt{K_B T_{e1}/m}$, with m being the ion mass, and ξ is normalised to $\sqrt{K_B T_{e1}/4\pi n_0 e^2}$. As before, we can now numerically examine the function $V(\varphi, u_\perp)$ and find the ranges of various parameters, viz. α, μ_0, l_z and M, for which compressive and rarefactive solitary waves may exist. As we are interested in the study of the effects of obliqueness and magnetic field on large amplitude solitary waves in a two-electron-temperature plasma previously studied by other workers [35], in our numerical study we will choose the same parameters as were chosen in the previous work [35] where $n_{e01}/n_{e02} = 3.5$ and $T_{e1}/T_{e2} = 20$. Therefore, we can take our parameters $\alpha = 3.5/4.5$ and $\mu_0 = 0.05$ which we will use in all of our numerical calculations. A very brief summary of our numerical results showing the effects of obliqueness on the coexistence of compressive and rarefactive solitary waves are displayed in figures 3.27 – 3.29. Figure 3.27 shows that there coexist compressive and rarefactive solitary waves for $\alpha = 3.5/4.5$, $\mu_0 = 0.05$ and $l_z = 1$ when M passes the value 0.434. Figures 3.28 and 3.29 show what happens when we decrease l_z to the values $\sqrt{3}/2$ and $1/2$. We see that, for same values of α $(= 3.5/4.5)$ and μ_0 $(= 0.05)$, as we decrease l_z, i.e. increase the angle between the directions of solitary wave propagation and the magnetic field, the minimum value of M, for which compressive and rarefactive solitary waves coexist, decreases.

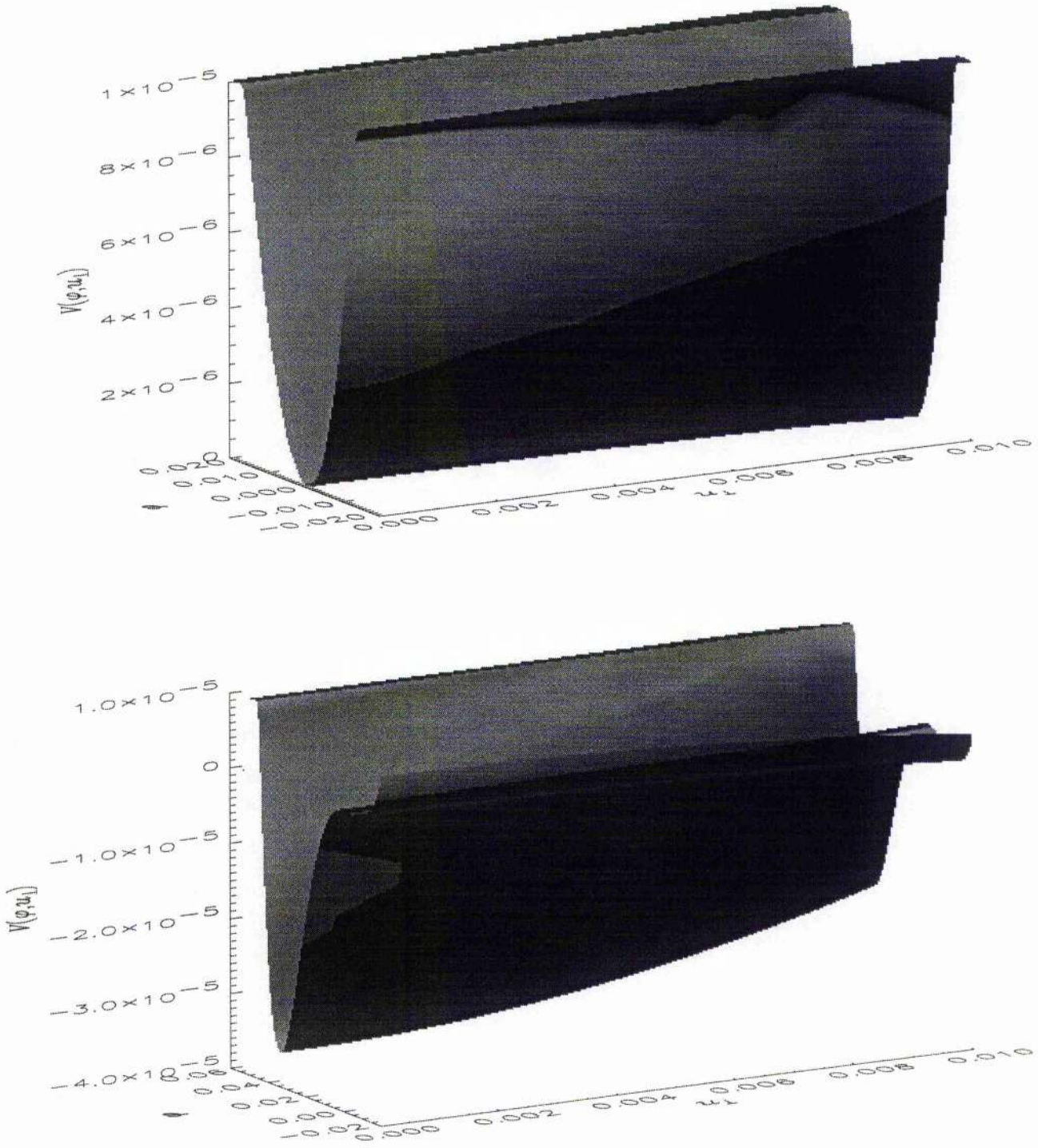

Figure 3.27: Showing the possibility of existence of compressive and rarefactive solitary waves for $l_z = 1$ when M passes the value 0.434. The upper plot is for $M = 0.434$ and the lower plot is for $M = 0.439$.

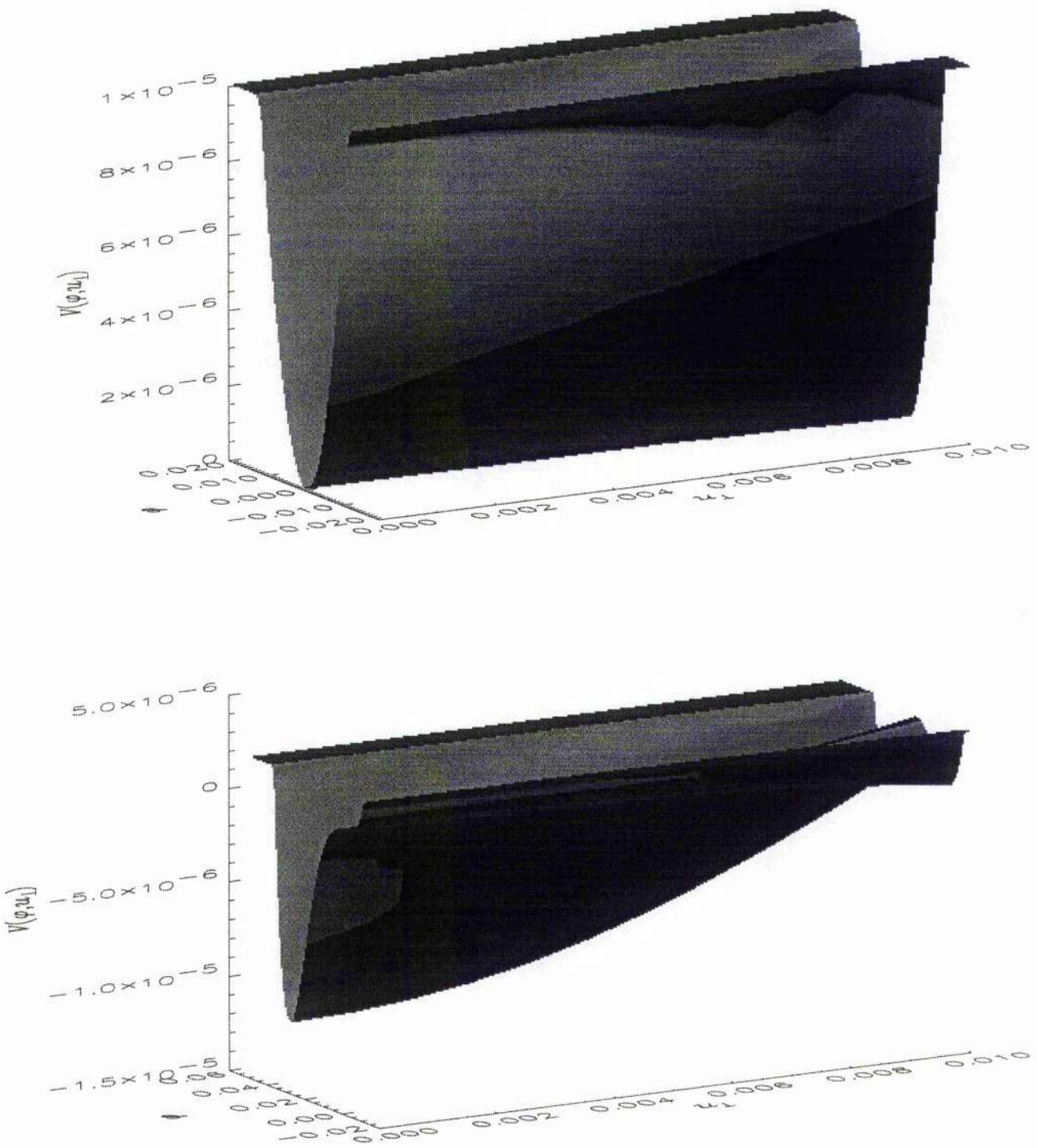

Figure 3.28: Showing the possibility of existence of compressive and rarefactive solitary waves for $l_z = \sqrt{3}/2$ when M passes the value 0.374. The upper plot is for $M = 0.374$ and the lower plot is for $M = 0.379$.

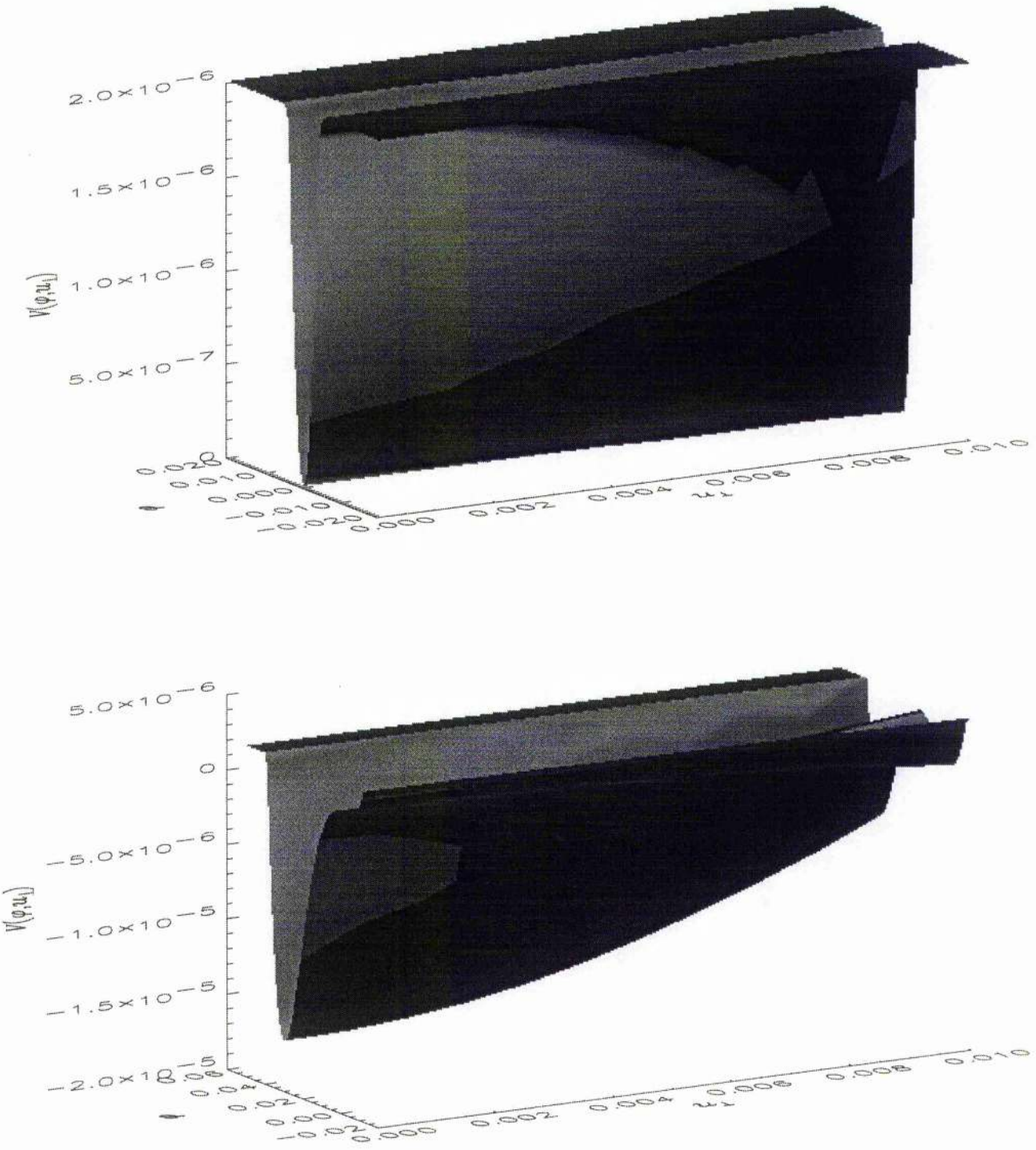

Figure 3.29: Showing the possibility of existence of compressive and rarefactive solitary waves for $l_z = 1/2$ when M passes the value 0.214. The upper plot is for $M = 0.214$ and the lower plot is for $M = 0.219$.

3.5.2 Numerical Simulation

To find stationary solutions of the basic nonlinear set of equations with normalised electron density given by Eq. (3.68), one can use exactly the same method as applied in Sec. 3.4.2 and can thus reduce this set of equations to a set of four coupled 1st order ordinary differential equations of the form

$$\frac{du_x}{d\xi} = \frac{1}{U}(l_x\psi - \omega_c u_y), \tag{3.71}$$

$$\frac{du_y}{d\xi} = \frac{1}{U}\omega_c u_x, \tag{3.72}$$

$$\frac{d\varphi}{d\xi} = \psi, \tag{3.73}$$

$$\frac{d\psi}{d\xi} = \alpha e^{\varphi} + (1-\alpha)e^{\varphi/\mu_0} - \frac{M}{U}, \tag{3.74}$$

where U is given by Eq. (3.63). Now, working in this higher dimensional phase space, we search for solitary waves directly in the same way as before. Some results of this procedure are displayed in figures 3.30 – 3.34 which show the effects of obliqueness (i.e. the angle between the directions of the wave propagation and the external magnetic field) and the magnitude of the magnetic field on the coexistence of compressive and rarefactive solitary waves and their structures. Figures 3.30–3.32 show how the critical Mach number (the minimum value of M above which compressive and rarefactive solitary waves coexist) changes when we increase the the angle between the directions of wave propagation and the external magnetic field. Figures 3.33 and 3.34 show the effects of obliqueness (l_z) and the magnitude of the magnetic field on these compressive and rarefactive solitary wave structures. It is seen from figure 3.33 that as we decrease l_z, the amplitude of the solitary waves increases, whereas their width decreases. It is obvious from figure 3.34 that ω_c has no any effect on the amplitude of the solitary waves, but it does have an effect on the width of the solitary waves, namely as ω_c increases, their width decreases. It should be mentioned here that in all these plots we keep α and μ_0 constant, viz. $\alpha = 3.5/4.5$ and $\mu_0 = 0.05$.

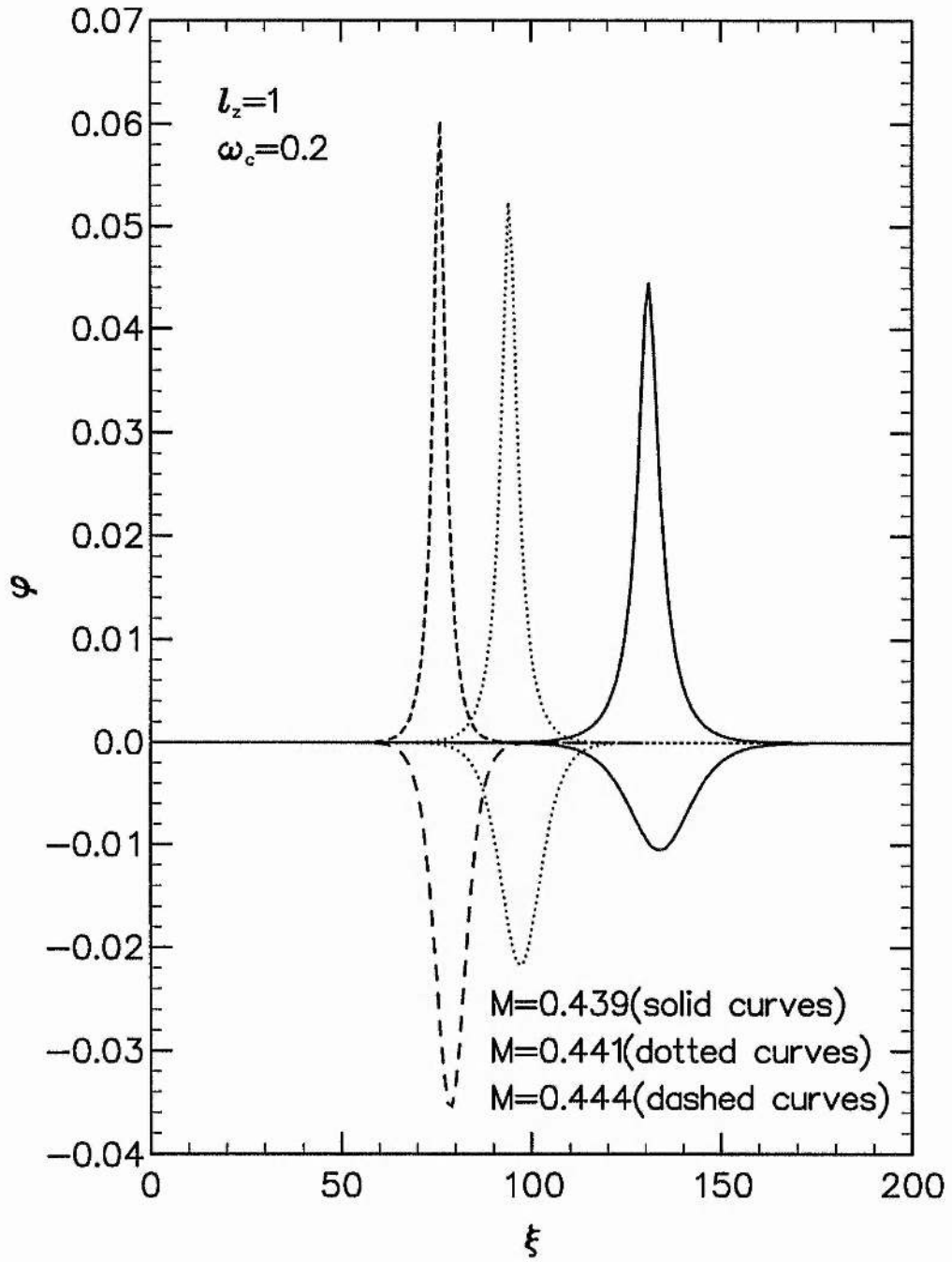

Figure 3.30: φ is plotted against ξ for $l_z = 1$, $\omega_c = 0.2$, $M = 0.439$ (solid curves), $M = 0.441$ (dotted curves) and $M = 0.444$ (dashed curves).

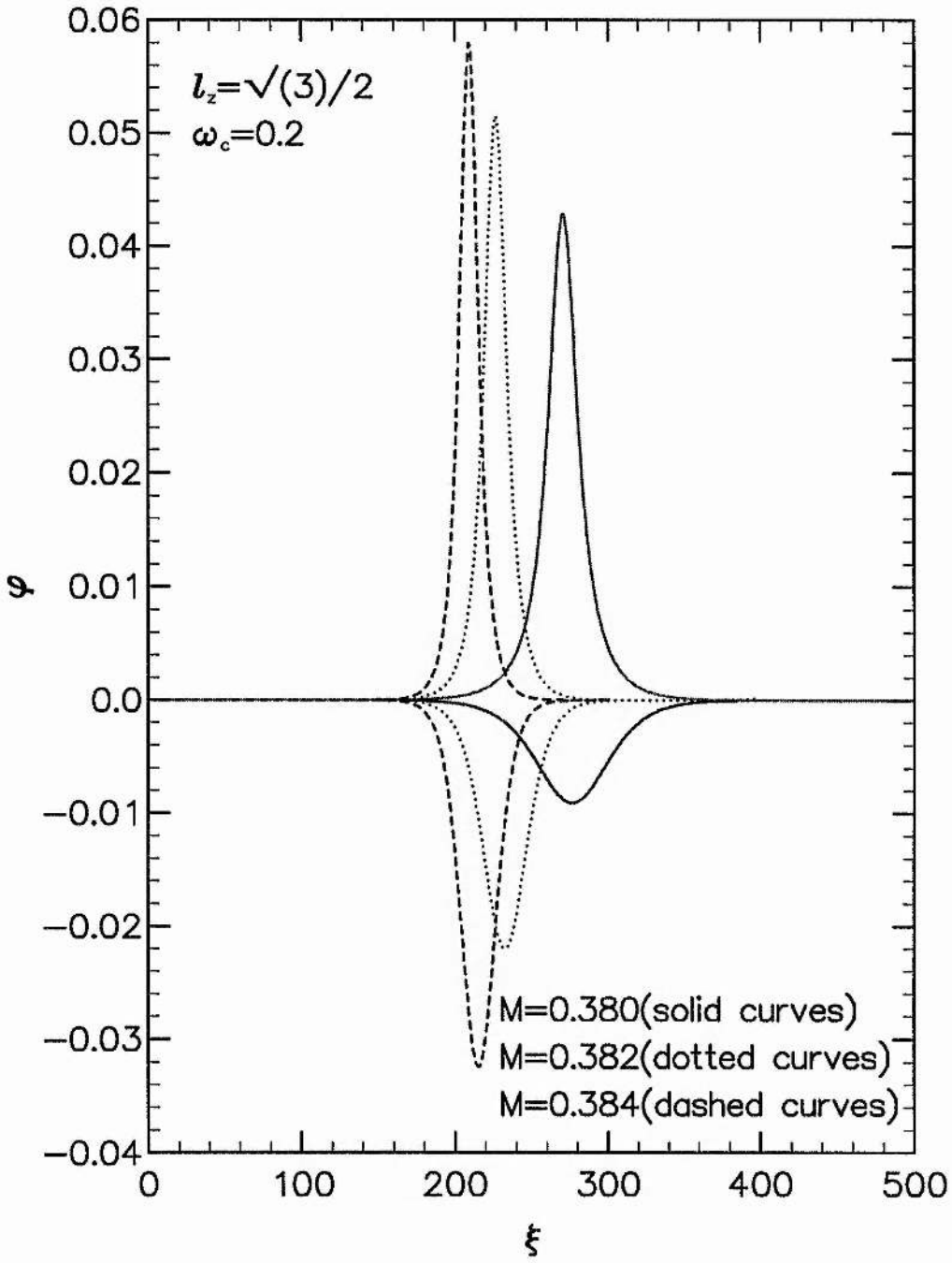

Figure 3.31: φ is plotted against ξ for $l_z = \sqrt{3}/2$, $\omega_c = 0.2$, $M = 0.380$ (solid curves), $M = 0.382$ (dotted curves) and $M = 0.384$ (dashed curves).

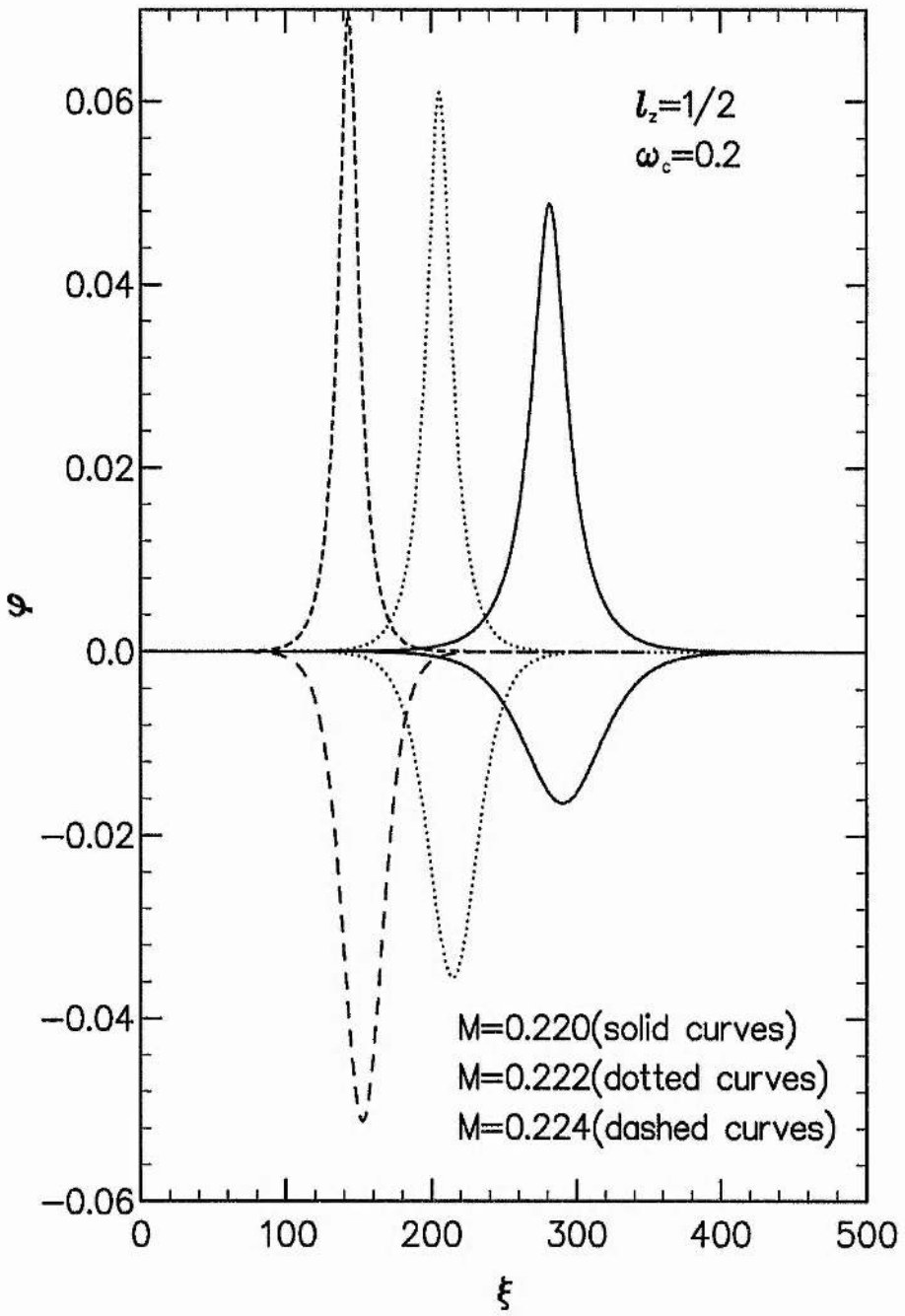

Figure 3.32: φ is plotted against ξ for $l_z = 1/2$, $\omega_c = 0.2$, $M = 0.220$ (solid curves), $M = 0.222$ (dotted curves) and $M = 0.224$ (dashed curves).

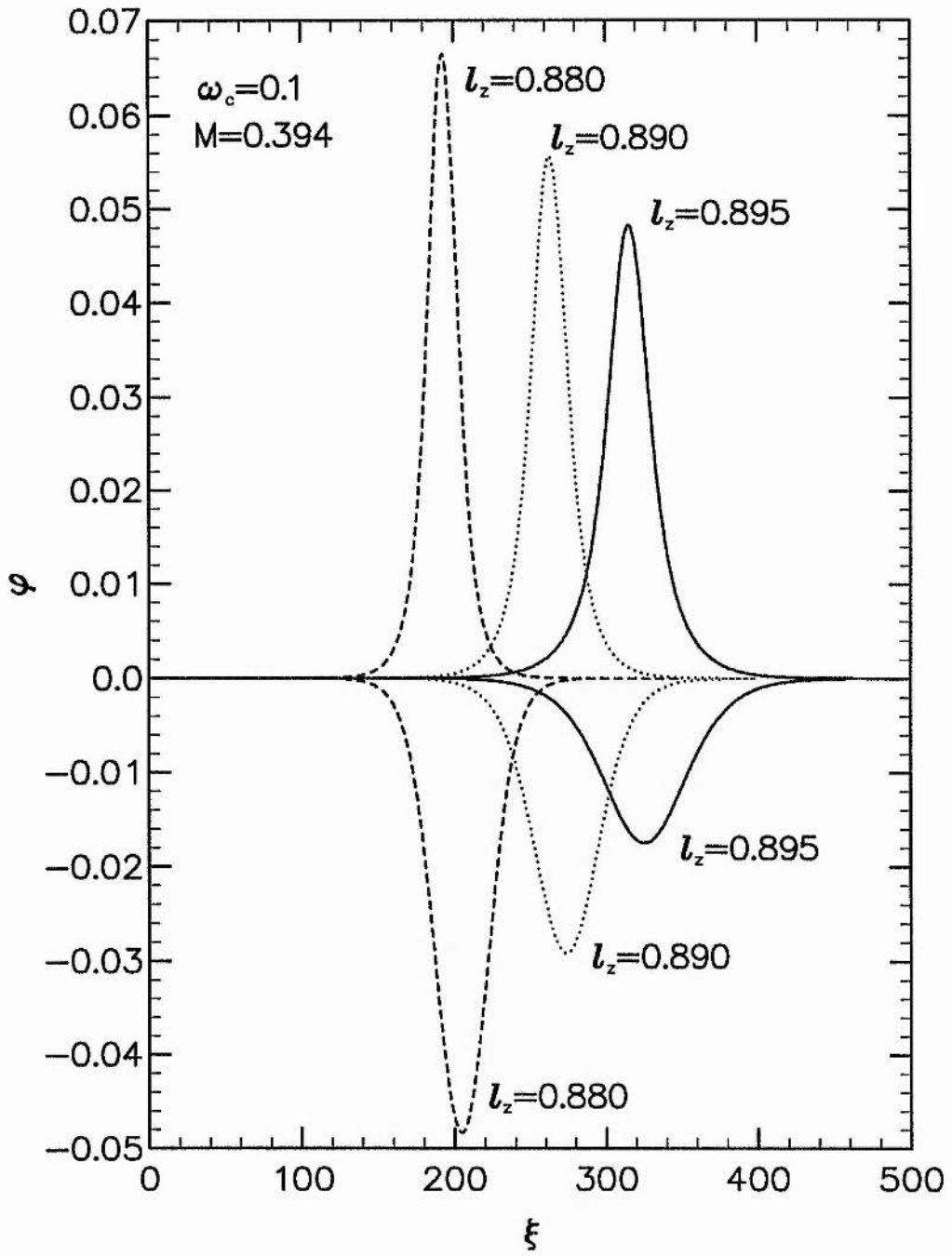

Figure 3.33: φ is plotted against ξ for $M = 0.394$, $\omega_c = 0.1$, $l_z = 0.895$ (solid curves), $l_z = 0.890$ (dotted curves) and $l_z = 0.880$ (dashed curves).

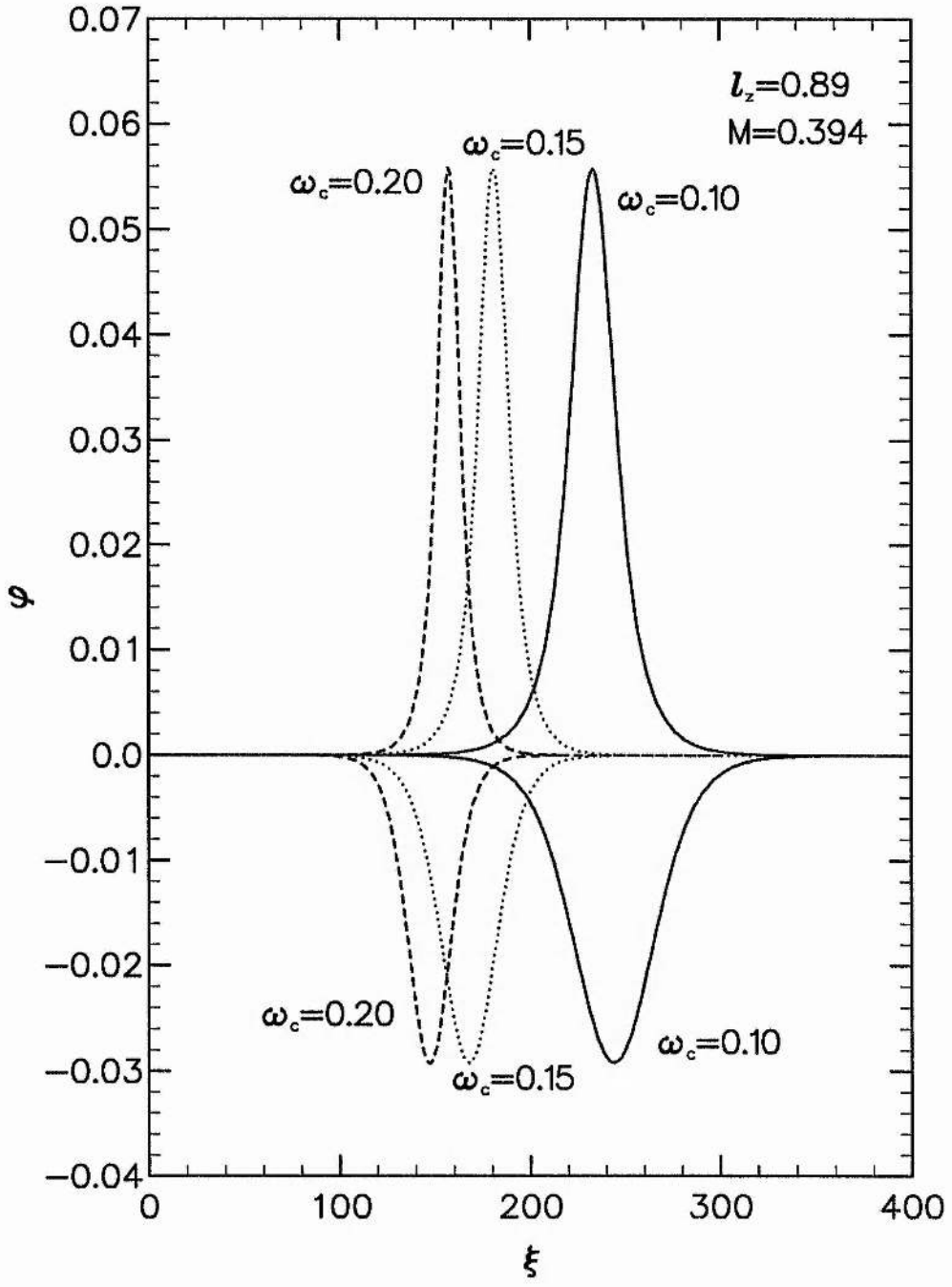

Figure 3.34: φ is plotted against ξ for $l_z = 0.89$, $M = 0.394$, $\omega_c = 0.10$ (solid curves), $\omega_c = 0.15$ (dotted curves) and $\omega_c = 0.20$ (dashed curves).

It may be noted that φ, ξ and M are normalised to $K_B T_{e1}/e$, $\sqrt{K_B T_{e1}/4\pi n_0 e^2}$ and $\sqrt{K_B T_{e1}/m}$, respectively. To compare our results with some other earlier works [36,37], which are valid for small amplitude limit, in these normalisations one must use $T_{ef} = T_{e1}T_{e2}/[(n_{e02}/n_0)T_{e1} + (n_{e01}/n_0)T_{e2}]$ instead of T_{e1}. In other words, one can find φ normalised to $K_B T_{ef}/e$ and M normalised to $\sqrt{K_B T_{ef}/m}$ just by multiplying our φ by T_{e1}/T_{ef} and M by $\sqrt{T_{e1}/T_{ef}}$, respectively. It is obvious that, for $\alpha = 3.5/4.5$ and $\mu_0 = 0.05$, the value of T_{e1}/T_{ef} becomes 23.5/4.5.

3.6 Discussion

In this chapter we have extended the theory of chapter 2 to propagation oblique to an external magnetic field. The results can be summarised as follows:

i) We have first studied small but finite amplitude solitary waves in non-thermal plasmas by introducing the Zakharov-Kuznetsov equation or the Korteweg-de Vries equation in three dimensions and then analysed the stability of these solitary waves by the small-k perturbation expansion method. It is found that, depending on the value of α, the solitary waves may change from compressive to rarefactive and that there exists only compressive solitary waves when $\alpha < 0.155$ and only rarefactive solitary waves when $\alpha > 0.155$.

It is also found that as the angle δ (that the solitary wave propagation direction makes with the magnetic field) increases, the amplitude of both the compressive and rarefactive solitary waves increases and their width increases for its lower range, i.e from 0° to $\sim$ 45°, but decreases for its higher range i.e. from $\sim$ 45° to 90°. When $\delta \to 90°$, the width tends to 0 and the amplitude tends to ∞. It is likely that for large angles the assumption that the waves are electrostatic is no longer a valid one, and we should look for fully electromagnetic structures. The magnitude of the magnetic field ($\mathbf{B}_0$) has no direct effect on the amplitude of the solitary waves. However, it does have a direct effect on the width of these solitary waves and it is found that as

its magnitude increases, the width of both the compressive and rarefactive solitary waves decreases, i.e. the magnetic field makes the solitary structures more spiky.

It is shown that the α-value has no any effect on whether the solitary waves will be stable or unstable, stability strongly depends on the external magnetic field and on the propagation directions of both the nonlinear wave and its perturbation mode. It is found that for an obliquely propagating perturbation mode with constant direction cosines, the solitary waves become unstable for lower values of δ and for higher values of the magnetic field. It is seen that as δ increases, the magnetic field, for which the solitary waves become unstable, increases. It is also found that, for constant ω_c and δ, as l_η increases, the range of l_ζ for which the solitary waves become unstable increases. It is found that as the magnitude of the magnetic field increases, the growth rate γ of the unstable perturbation mode decreases for the lower range of δ (from 0° to $\sim$ 10°) and increases for the higher range of δ. It is also shown that, with other parameters being constant, the growth rate γ increases with l_η, but decreases with l_ζ.

ii) We have then studied the effects of an external static magnetic field ($\mathbf{B}_0$) and the angle δ (that the propagation direction of the solitary waves makes with the magnetic field) on these solitary structures. It is found that as this angle δ increases the amplitude of both the compressive and rarefactive solitary waves increases in both the small and large amplitude limits. It is also important to note from the analysis in the large amplitude limit that as the obliqueness increases, the minimum value of the Mach number (M), above which the compressive and rarefactive solitary waves coexist, decreases (viz. for $l_z = 1$, $l_z = 0.8$ and $l_z = 0.7$ this M is 1.415, 1.132 and 0.99, respectively). As the Mach number increases from these values, the amplitude of both the compressive and rarefactive solitary waves increases and their width decreases, but after a certain value of this Mach number (namely 1.514 for $l_z = 1$, 1.213 for $l_z = 0.8$ and 1.062 for $l_z = 0.7$) the rarefactive one no longer exists.

The magnitude of the magnetic field ($\mathbf{B}_0$) also has no direct effect on the amplitude of these large amplitude solitary waves and the critical Mach number (the Mach number above which compressive and rarefactive solitary waves coexist). However, it has a direct effect on the width of these solitary waves and it is found that as its magnitude increases, the width of both the compressive and rarefactive solitary waves decreases, i.e. the magnetic field makes the solitary structures more spiky.

To compare the results obtained from the analysis in the small amplitude limit with those in arbitrary amplitude, it is important to note that in the small amplitude limit either compressive or rarefactive solitary waves are found to exist, whereas in the more complete theory they may exist together. In the small amplitude limit, both of these analyses give the same results.

iii) We have found, in our study of arbitrary amplitude solitary waves in two-electron-temperature plasma model, that as the angle δ increases, the amplitude of both the compressive and rarefactive solitary waves increases, but their width decreases. It is also found that as this angle δ increases, the minimum value of the Mach number for which the compressive and rarefactive solitary waves coexist decreases (viz. for $l_z = 1$, $l_z = \sqrt{3}/2$ and $l_z = 1/2$ this Mach number is 0.439, 0.379 and 0.219, respectively). It may be noted here that M is normalised to $\sqrt{T_{e1}/m}$. If M is normalised to $\sqrt{T_{ef}/m}$, the corresponding values become 1.005, 0.867 and 0.872, respectively. As the Mach number increases from this critical value, the amplitude of both the compressive and rarefactive solitary waves increases and their width decreases.

The magnitude of the magnetic field ($\mathbf{B}_0$) has no direct effect on the amplitude of the solitary waves and the minimum value of the Mach number M for which compressive and rarefactive solitary waves coexist. However, it does have a direct effect on the width of these solitary waves, as we found in our non-thermal plasma model, and it is found that as its magnitude increases, the width of both the compressive and rarefactive solitary waves decreases, i.e. the magnetic field makes the solitary structures more spiky. It may be added here that our present results are valid for

solitary waves of arbitrary amplitude and agree with the existing published results [35] for $\theta = 0$ and [36,37] for small amplitude limit. In the small amplitude limit [35,36] the solitary waves may change from compressive to rarefactive, while our study of the full nonlinear equations may allow rarefactive and compressive solitary waves to coexist.

In conclusion, we stress that the results of our investigation should be useful in understanding the nonlinear features of localised electrostatic disturbances in both the space and laboratory plasmas where ions, which can be assumed to respond as a fluid to perturbations in the potential, and non-thermal or two Maxwellian electrons are the major plasma species.

Chapter 4

Dust-acoustic Solitary Waves in Dusty Plasmas

4.1 Introduction

Recently, there has been a great deal of interest in understanding different types of collective processes in dusty plasmas which are very common in laboratory and astrophysical environments. It has been found that the presence of static charged dust grains modifies the existing plasma wave spectra, whereas the dust charge dynamics introduces new eigenmodes in dusty plasmas. Rao *et al.* [90], for example, were the first to report theoretically the existence of extremely low phase velocity (in comparison with the electron and ion thermal velocities) dust-acoustic waves in an unmagnetised dusty plasma whose constituents are an inertial charged dust fluid and Boltzmann distributed electrons and ions. Thus, in the dust-acoustic waves the dust particle mass provides the inertia, whereas the restoring force comes from the pressures of inertialess electrons and ions. A recent laboratory experiment [96] has conclusively verified the theoretical prediction of Rao *et al.* [90] and has reported the nonlinear features of the dust-acoustic waves. The laboratory observations [96] of low phase velocity dust-acoustic waves, which are associated with significant depletion of the electron number density, suggest that the wave dynamics is governed by the inertia of the dust fluid and the pressure of inertialess ions only. In this chapter,

we confine ourself to the study of dust acoustic solitary waves in such a two fluid model of dusty plasma, where the wave phase velocity is much smaller than the ion thermal velocity and the electron number density is sufficiently depleted during the charging of the dust grains, on account of the attachment of the background plasma electrons to the surface of the dust grains, and investigate the nonlinear properties of these dust-acoustic solitary waves, first by considering a Boltzmann ion distribution and later by incorporating the effects of non-isothermal ion distributions which are taken to be either non-thermal [104,105] or vortex-like [38,39].

The objectives of this chapter are as follows. In Sec 4.2 we have presented the relevant equations governing the dynamics of nonlinear dust-acoustic waves. We then, in Sec. 4.3, have studied the nonlinear properties of stationary dust-acoustic solitary waves in a dusty plasma with three different types of ion distribution functions, namely Boltzmann, non-thermal [104,105] and vortex-like [38,39]. In Sec. 4.4 we have studied the time evolution of these solitary structures by a numerical solution of the full set of nonlinear equations. Finally, a brief summary of our findings have been presented in Sec. 4.5.

4.2 Governing Equations

We consider a two component dusty plasma with extremely massive, micron-sized, negatively charged inertial dust grains and arbitrarily (by arbitrary we mean ion distribution may be Boltzmann or non-thermal or vortex-like) distributed ions. Thus, at equilibrium, we have $n_{i0} = Z_d n_{d0}$, where n_{i0} and n_{d0} are the unperturbed ion and dust number densities, respectively, and Z_d is the number of charges residing on the dust grains. The dynamics of low phase velocity (lying between the ion and dust

thermal velocities, viz. $v_{td} << v_p << v_{ti}$) dust-acoustic oscillations is governed by

$$\frac{\partial n_d}{\partial t} + \frac{\partial}{\partial x}(n_d u_d) = 0, \tag{4.1}$$

$$\frac{\partial u_d}{\partial t} + u_d \frac{\partial u_d}{\partial x} = \frac{\partial \varphi}{\partial x}, \tag{4.2}$$

$$\frac{\partial^2 \varphi}{\partial x^2} = n_d - n_i(\varphi), \tag{4.3}$$

where n_d is the dust particle density normalised to n_{d0}, $n_i(\varphi)$ is the ion density normalised to n_{i0}, u_d is the dust fluid velocity normalised to the dust-acoustic velocity $C_d = (Z_d T_i/m_d)^{1/2}$ and φ is the electrostatic wave potential normalised to T_i/e, where T_i is the ion temperature in units of the Boltzmann constant (K_B) and e is the magnitude of an electron charge. The time and space variables are in units of the dust plasma period ${\omega_{pd}}^{-1} = (m_d/4\pi n_{d0} Z_d^2 e^2)^{1/2}$ and the Debye length $\lambda_{Dd} = (T_i/4\pi Z_d n_{d0} e^2)^{1/2}$, respectively.

4.3 Stationary Solitary Waves

To study the nonlinear properties of arbitrary amplitude solitary waves in a stationary frame, we first assume that all the dependent variables in Eqs. (4.1) – (4.3) depend only on a single variable $\xi = x - Mt$, where again ξ is normalised to λ_{Dd} and M is the Mach number (solitary wave velocity/C_d). In a stationary frame ($\partial/\partial t \to 0$) we can express our basic equations, Eqs. (4.1) – (4.3), in terms of this new independent single variable ξ as

$$-M\frac{dn_d}{d\xi} + \frac{d}{d\xi}(n_d u_d) = 0, \tag{4.4}$$

$$-M\frac{du_d}{d\xi} + u_d \frac{du_d}{d\xi} = \frac{d\varphi}{d\xi}, \tag{4.5}$$

$$\frac{d^2\varphi}{d\xi^2} = n_d - n_i(\varphi). \tag{4.6}$$

Now, Eqs (4.4) and (4.5) can be integrated to give

$$n_d = \frac{1}{1 - u_d/M}, \tag{4.7}$$

$$u_d = M[1 \pm \sqrt{1 + 2\varphi/M^2}], \tag{4.8}$$

where we have imposed the appropriate boundary conditions for localised disturbances, viz. $\varphi \to 0$, $u_d \to 0$ and $n \to 1$ at $\xi \to \pm\infty$. The combination of these last two equations gives

$$n_d = \frac{1}{\sqrt{1 + 2\varphi/M^2}}. \tag{4.9}$$

Now, choosing the appropriate ion distribution for $n_i(\varphi)$ and using these n_i and n_d in Poisson's equation, Eq. (4.6), one can study arbitrary amplitude solitary waves by the pseudopotential approach. In the following, for $n_i(\varphi)$, we will choose three different ion distribution functions, viz. Boltzmann, non-thermal and vortex-like, and study the effects of these distribution functions on the properties of dust-acoustic solitary waves.

4.3.1 Solitary Waves for Boltzmann Ion Distribution

We first study the dust acoustic waves in our two fluid dusty plasma model with a Boltzmann ion distribution function. The choice of this distribution function allows us to write the normalised ion density $n_i(\varphi)$ as

$$n_i(\varphi) = e^{-\varphi}. \tag{4.10}$$

Now, substituting n_d and n_i, obtained from Eqs. (4.9) and (4.10), respectively, into Poisson's equation, Eq. (4.6), and multiplying both sides of the resulting equation by $d\varphi/d\xi$, integrating once, and imposing the appropriate boundary conditions for localised solutions, namely $\varphi \to 0$ and $d\varphi/d\xi \to 0$ at $\xi \to \pm\infty$, we obtain

$$\frac{1}{2}(\frac{d\varphi}{d\xi})^2 + V(\varphi) = 0, \tag{4.11}$$

where the Sagdeev potential $V(\varphi)$, for our purposes, reads

$$V(\varphi) = 1 + M^2 - M^2\sqrt{1 + 2\varphi/M^2} - e^{-\varphi}. \tag{4.12}$$

Eq. (4.11) can be regarded as an "energy law" of an oscillating particle of unit mass with velocity $d\varphi/d\xi$ and position φ in a potential $V(\varphi)$. It is clear from Eq.

(4.12) that $V(\varphi) = 0$ and $dV(\varphi)/d\varphi = 0$ at $\varphi = 0$. Solitary wave solutions of Eq. (4.11) exist if (i) $(d^2V/d\varphi^2)_{\varphi=0} < 0$, so that the fixed point at the origin is unstable, (ii) there exists a non-zero φ_m, the maximum or minimum value of φ at which $V(\varphi_m) = 0$ and (iii) $V(\varphi) < 0$ when φ lies between 0 and φ_m. If we expand the Sagdeev potential $V(\varphi)$ around the origin, we can write the condition for the existence of solitary waves as $M > 1$. We have numerically analysed Eq. (4.12) for different values of M. The numerical results are displayed in figures 4.1 and 4.2. It is seen that the Sagdeev potential is never zero for any positive value of φ and $M > 1$, thereby ruling out the possibility of dust-acoustic solitary waves with positive potential ($\varphi_m > 0$). It is, however, clear that solitary waves with negative potential ($\varphi_m < 0$) exist. It is of interest to find out whether or not there exists an upper limit of M for which solitary waves exist. This upper limit of M can be found by the condition $V(\varphi_c) \geq 0$, where $\varphi_c = -M^2/2$ is the minimum value of φ for which the dust density n_d is real. Thus, we have $1 + M^2 - \exp(M^2/2) > 0$; the latter holds for $M < 1.58$. Clearly, finite amplitude dust-acoustic solitary waves exist for $1 < M < 1.58$, as indicated in figures 4.1 and 4.2. We also numerically solve Eq. (4.11) to see the structures of these solitary waves with negative potential. It is shown that the amplitude of these solitary waves increases with the rise of the Mach number M. Figure 4.3 depicts the potential profiles of the dust-acoustic solitary pulses for different values of the Mach number M. It is clear that since dust-acoustic solitary pulses always have negative potentials, both the dust and ion densities are enhanced.

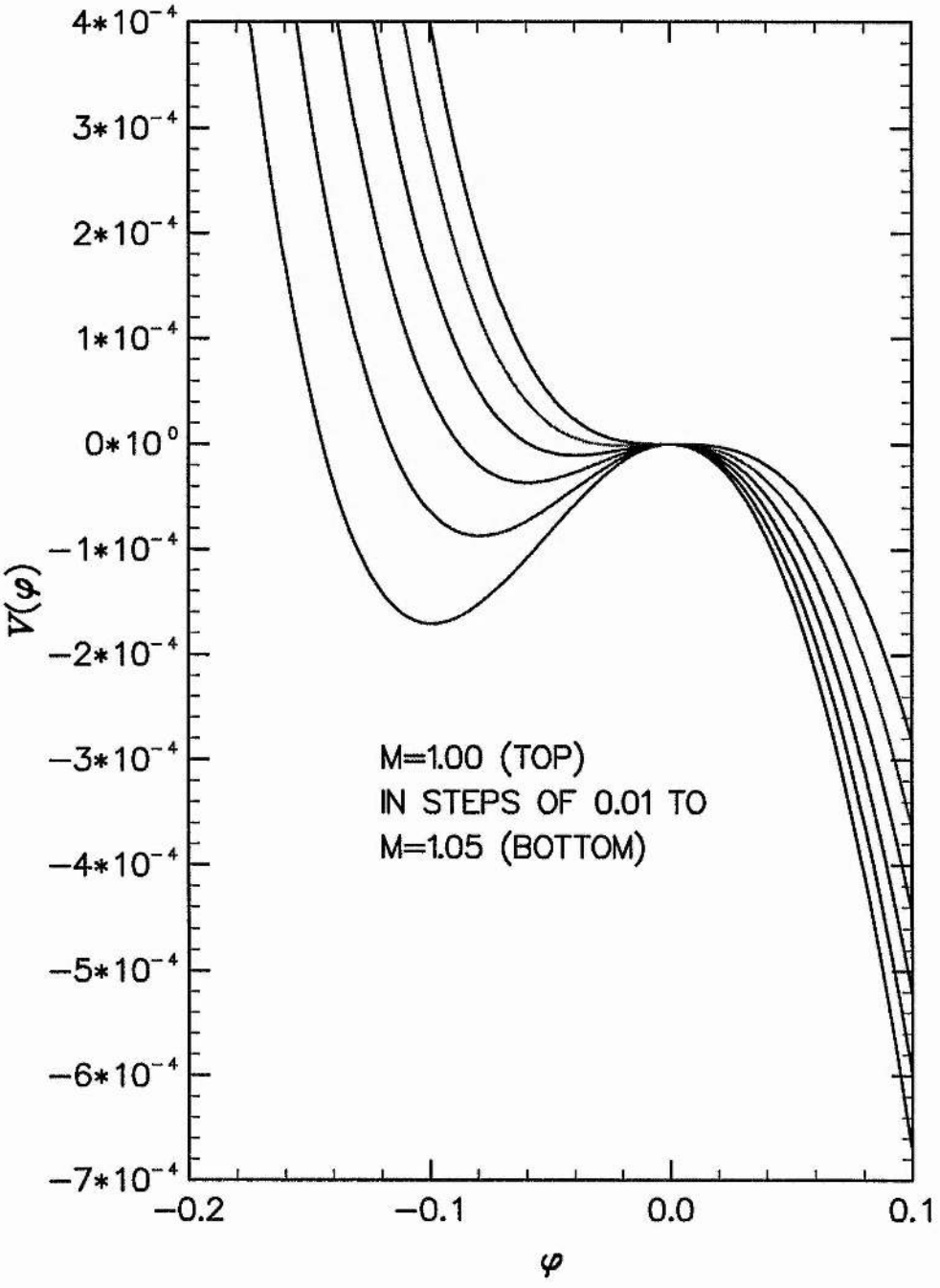

Figure 4.1: Behaviour of the Sagdeev potential $V(\varphi)$ for a series of Mach numbers, 1.00 (top) in steps of 0.01 to 1.05 (bottom).

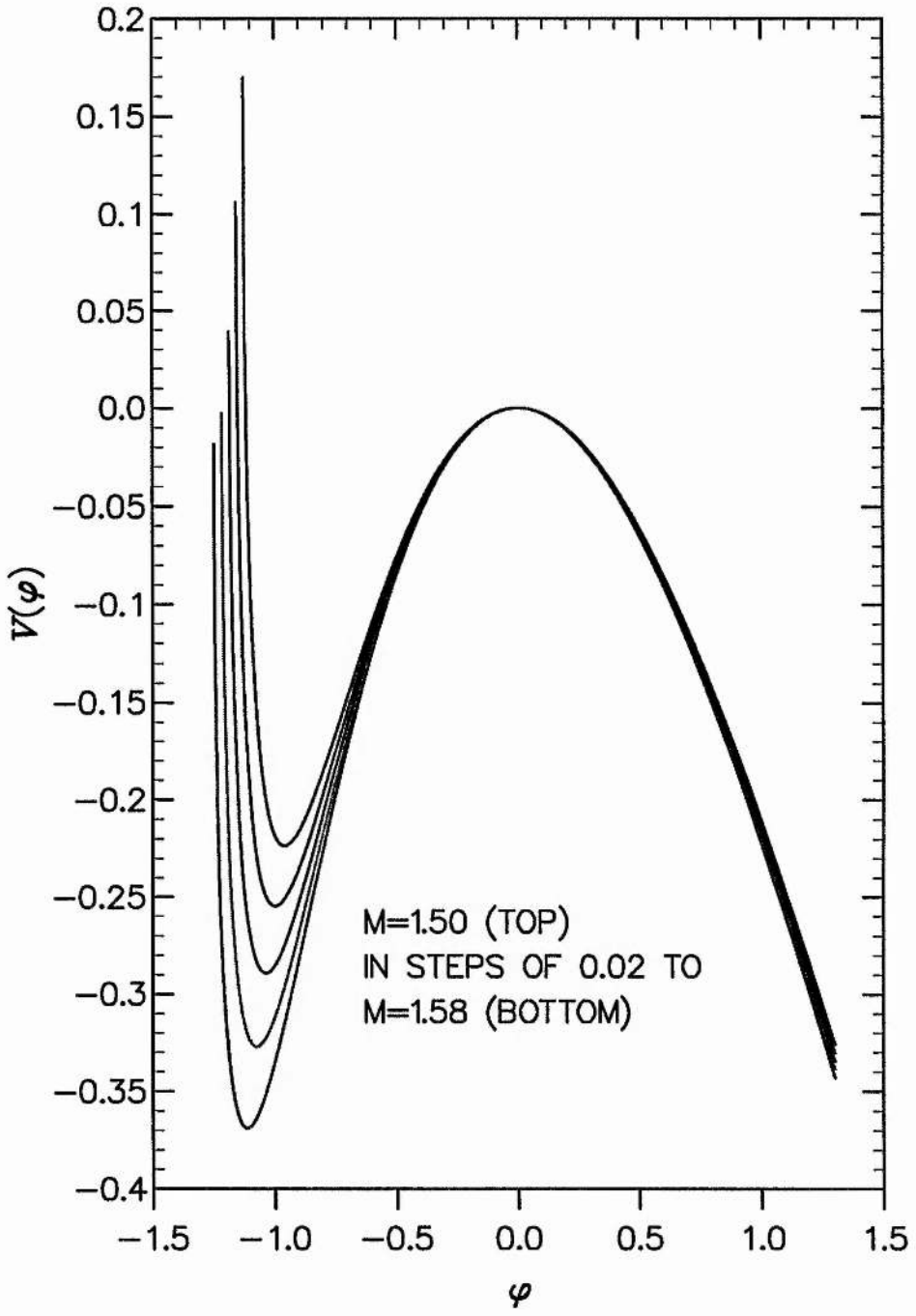

Figure 4.2: Behaviour of the Sagdeev potential $V(\varphi)$ for a series of Mach numbers, 1.50 (top) in steps of 0.02 to 1.58 (bottom).

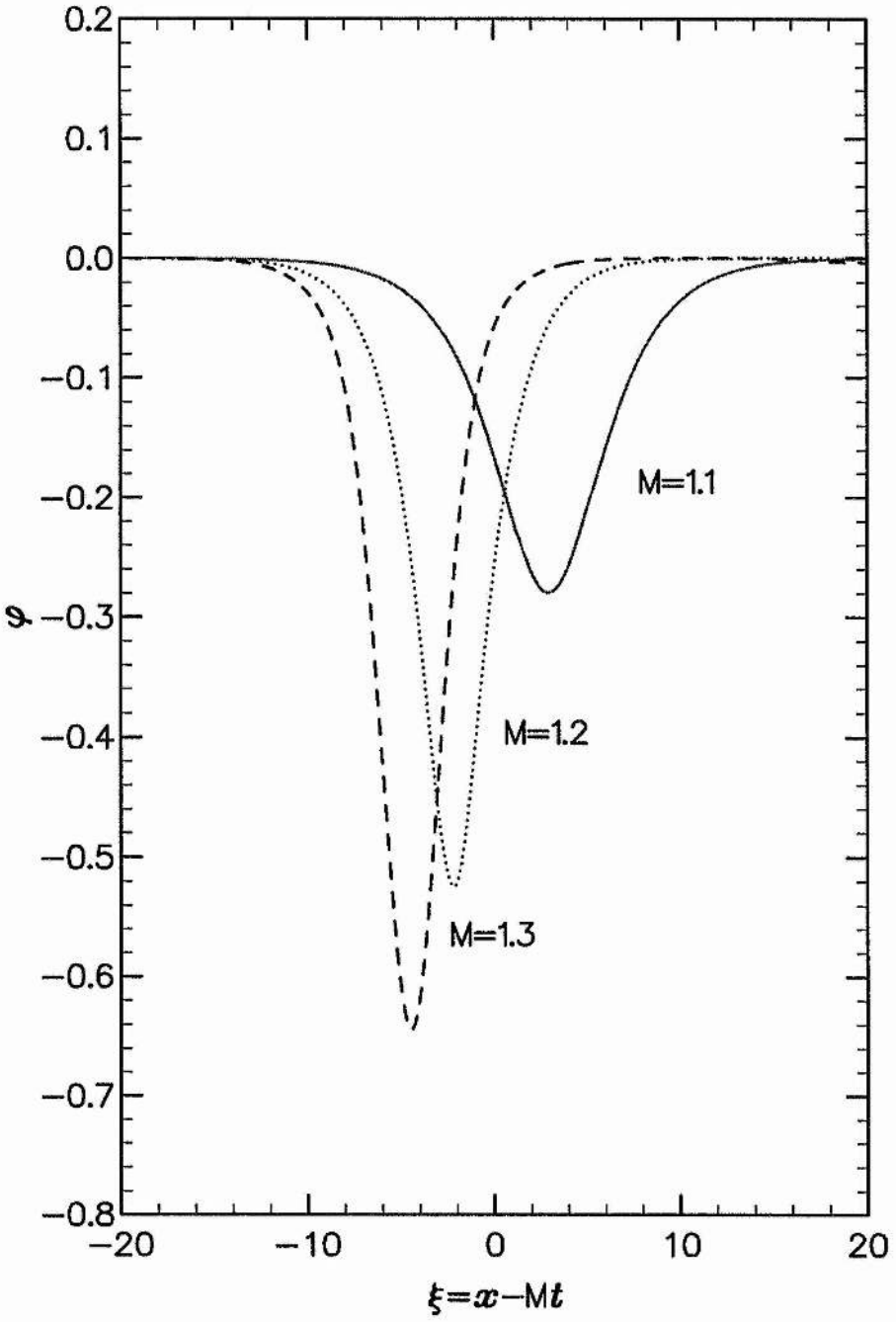

Figure 4.3: φ is plotted against $\xi = x - Mt$ for $M = 1.1$ (solid curve), $M = 1.2$ (dotted curve) and $M = 1.3$ (dashed curve).

To study the dynamics of small amplitude ($|\varphi| << 2M^2$) dust-acoustic solitary waves, we derive the Korteweg-de Vries (KdV) equation from Eqs. (4.1) – (4.3) by employing the reductive perturbation technique [17] and the stretched coordinates

$$\left.\begin{aligned}\zeta &= \epsilon^{1/2}(x - v_0 t),\\ \tau &= \epsilon^{3/2} t,\end{aligned}\right\} \tag{4.13}$$

where ϵ is a smallness parameter measuring the weakness of the amplitude or dispersion and v_0 is the unknown solitary wave velocity (normalised to C_d), to be determined later. We can then expand the variables n_d, u_d and φ about the unperturbed states in power series of ϵ as

$$\left.\begin{aligned}n_d &= 1 + \epsilon n_d^{(1)} + \epsilon^2 n_d^{(2)} + \cdots,\\ u_d &= 0 + \epsilon u_d^{(1)} + \epsilon^2 u_d^{(2)} + \cdots,\\ \varphi &= 0 + \epsilon\varphi^{(1)} + \epsilon^2\varphi^{(2)} + \cdots.\end{aligned}\right\} \tag{4.14}$$

Now, using Eqs. (4.13) and (4.14) in Eqs. (4.1) – (4.3) and Eq. (4.10) one can develop equations in various powers of ϵ. To lowest order in ϵ, Eqs. (4.1) – (4.3) and Eq. (4.10) give

$$\left.\begin{aligned}n_d^{(1)} &= -\varphi^{(1)}/v_0^2,\\ u_d^{(1)} &= -\varphi^{(1)}/v_0,\\ v_0 &= 1.\end{aligned}\right\} \tag{4.15}$$

To next higher order in ϵ, we have a set of equations which read

$$\frac{\partial n_d^{(1)}}{\partial \tau} - v_0\frac{\partial n_d^{(2)}}{\partial \zeta} + \frac{\partial u_d^{(2)}}{\partial \zeta} + \frac{\partial}{\partial \zeta}(n_d^{(1)} u_d^{(1)}) = 0, \tag{4.16}$$

$$\frac{\partial u_d^{(1)}}{\partial \tau} - v_0\frac{\partial u_d^{(2)}}{\partial \zeta} - \frac{\partial \varphi^{(2)}}{\partial \zeta} + u_d^{(1)}\frac{\partial u_d^{(1)}}{\partial \zeta} = 0, \tag{4.17}$$

$$\frac{\partial^2 \varphi^{(1)}}{\partial \zeta^2} - \varphi^{(2)} - n^{(2)} + \frac{1}{2}[\varphi^{(1)}]^2 = 0. \tag{4.18}$$

Now, using these last three equations we readily obtain

$$\frac{\partial \varphi^{(1)}}{\partial \tau} + a\varphi^{(1)}\frac{\partial \varphi^{(1)}}{\partial \zeta} + b\frac{\partial^3 \varphi^{(1)}}{\partial \zeta^3} = 0, \tag{4.19}$$

which is the KdV equation with $a = -1$ and $b = 1/2$. The stationary localised solution of this KdV equation is given by[1]

$$\varphi = \varphi_m \, \mathrm{sech}^2[(\zeta - u_0 t)\mu], \tag{4.20}$$

where $\varphi_m = -3u_0$ is the amplitude of the solitary waves and $\mu = \sqrt{u_0/2}$ is the inverse of the width of the solitary waves. As $u_0 > 0$, Eq. (4.20) clearly indicates that there exist only solitary waves (with negative potential) of amplitude $3u_0$ and width $\sqrt{2/u_0}$. It is found that as u_0 increases, the amplitude φ_m increases while the width decreases.

4.3.2 Solitary Waves for Non-thermal Ion Distribution

We have rigourously studied the effects of non-thermal electron distribution on ion-acoustic solitary waves in last two chapters. In the present section, we are interested in the study of the effect of a non-thermal ion distribution function [104], which might result owing to the quasi-linear modification introduced by the dust-acoustic fluctuations themselves, on the dust-acoustic solitary waves discussed in the previous section. To determine the ion number density $n_i(\varphi)$ associated with non-thermal ion distributions, as before (Sec. 2.2), we can model the ion distribution function which includes the population of a fast component. Thus, we take [104]

$$f_i(v) = \frac{1}{(1+3\alpha)\sqrt{2\pi}}(1 + \alpha v^4)e^{-\frac{1}{2}v^2}, \tag{4.21}$$

where the velocity v is normalised to the ion thermal velocity v_{ti}. The effect of electrostatic disturbances on the equilibrium ion distributions can easily be incorporated by replacing v^2 with $v^2 + 2\varphi$ in Eq. (4.21). The resulting distribution function is then integrated over the velocity space, yielding

$$\left.\begin{aligned} n_i &= (1 + \beta\varphi + \beta\varphi^2)e^{-\varphi}, \\ \beta &= \tfrac{4\alpha}{1+3\alpha}. \end{aligned}\right\} \tag{4.22}$$

[1]The derivation is shown in **Appendix A.2**

Now, substituting n_d and n_i, obtained from Eqs. (4.9) and (4.22), respectively, into Poisson's equation, Eq. (4.3), and multiplying both sides of the resulting equation by $d\varphi/d\xi$, integrating once, and imposing the appropriate boundary conditions for localised solutions, namely $\varphi \to 0$ and $d\varphi/d\xi \to 0$ at $\xi \to \pm\infty$, we obtain

$$\frac{1}{2}(\frac{d\varphi}{d\xi})^2 + V(\varphi) = 0, \tag{4.23}$$

where the Sagdeev potential, for this case of non-thermal ion distribution, reads

$$\begin{aligned} V(\varphi) &= 1 + 3\beta + M^2 - M^2\sqrt{1 + 2\varphi/M^2} \\ &- (1 + 3\beta + 3\beta\varphi + \beta\varphi^2)e^{-\varphi}. \end{aligned} \tag{4.24}$$

As before, Eq. (4.23) can be regarded as an "energy law" for an oscillating particle of unit mass with velocity $d\varphi/d\xi$ and position φ in a potential $V(\varphi)$. It is clear from Eq. (4.24) that $V(\varphi) = 0$ and $dV(\varphi)/d\varphi = 0$ at $\varphi = 0$. Solitary wave solutions of Eq. (2.23) exist if (i) $(d^2V/d\varphi^2)_{\varphi=0} < 0$, so that the fixed point at the origin is unstable, (ii) there exists a non-zero φ_m, the maximum or minimum value of φ at which $V(\varphi_m) = 0$ and (iii) $V(\varphi) < 0$ when φ lies between 0 and φ_m. Now, following the same procedure as explained in Sec. 2.3, the the critical Mach number (the minimum value of M above which solitary waves exist) and the criterion for the coexistence of rarefactive and compressive solitary waves are readily given by

$$\left.\begin{aligned} &M_c = \sqrt{\tfrac{1+3\alpha}{1-\alpha}}, \\ &\alpha > \tfrac{\sqrt{3}-1}{3+\sqrt{3}}. \end{aligned}\right\} \tag{4.25}$$

If we consider $\alpha = 0$, i.e. a Boltzmann ion distribution, we get exactly the same results as discussed in the previous section (Sec. 4.3.1). It is clear from Eq. (4.25) that the rarefactive and compressive solitary waves will coexist if $\alpha > 0.155$. We now consider $\alpha = 0.2$ for which the critical Mach number defined by Eq. (4.25) becomes $\sqrt{2}$. It is of interest to examine whether or not there exists an upper limit of M for which rarefactive solitary waves exist. This upper limit of M can be found by the condition $V(\varphi_c) \geq 0$, where $\varphi_c = -M^2/2$ is the minimum value of φ for which the dust density n_d is real. Thus, on using Eq. (4.24) this upper limit of

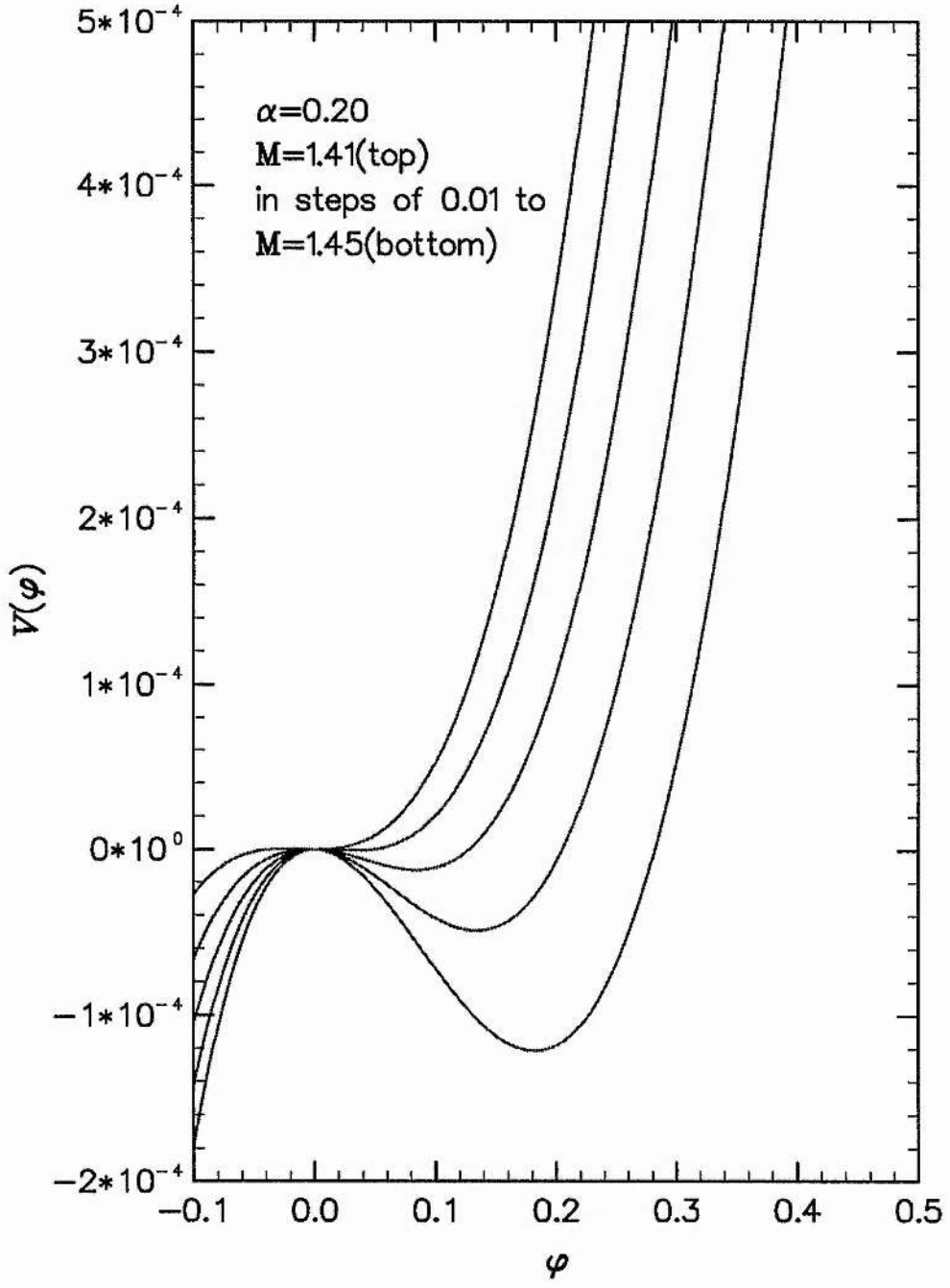

Figure 4.4: Behaviour of the Sagdeev potential $V(\varphi)$ for $\alpha = 0.2$ which shows a possibility of existence of solitary waves with positive potential when the Mach number M passes the value 1.414.

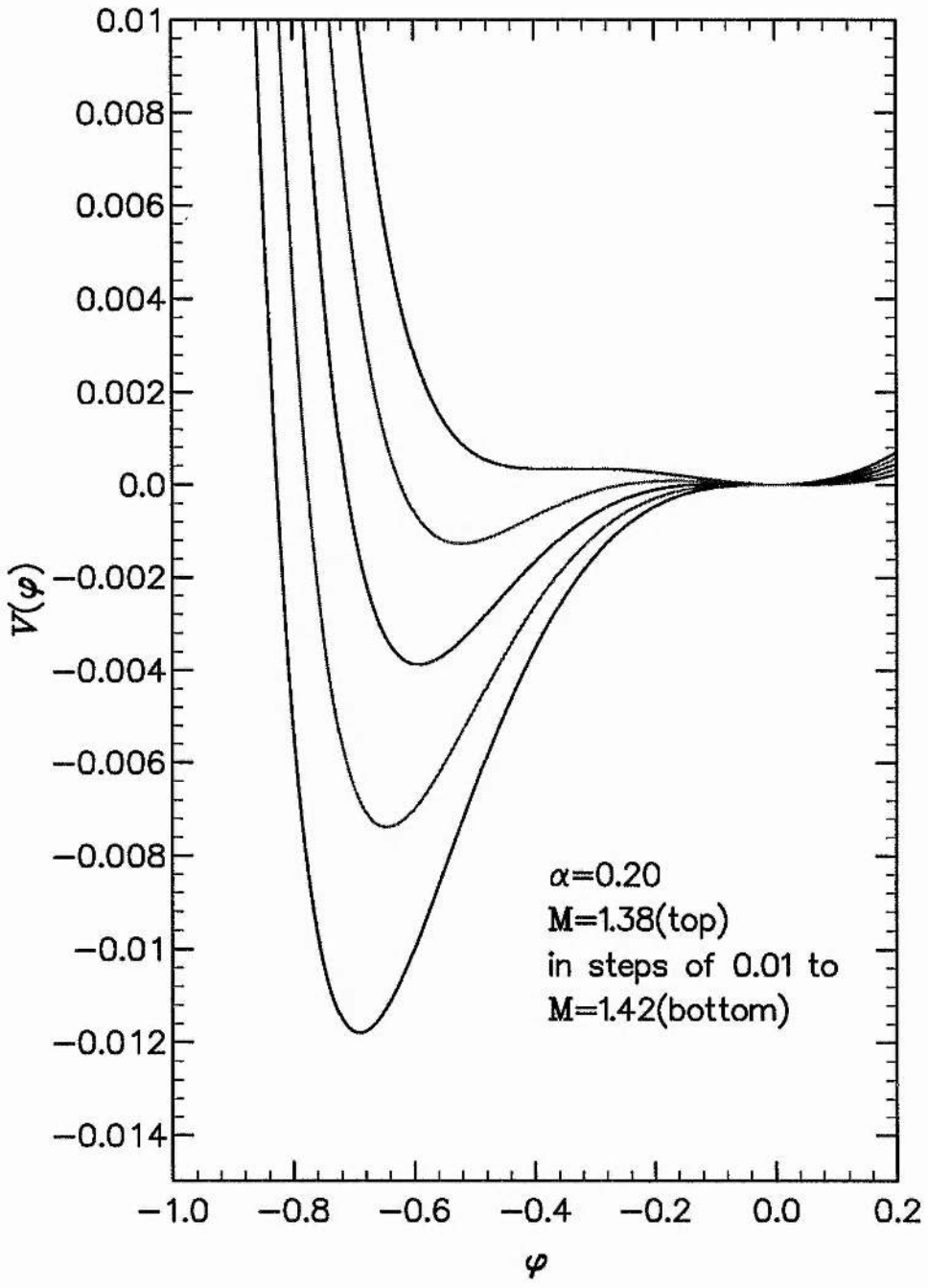

Figure 4.5: Behaviour of the Sagdeev potential $V(\varphi)$ for $\alpha = 0.2$ which shows a possibility of existence of solitary waves with negative potential when the Mach number M passes the value 1.414.

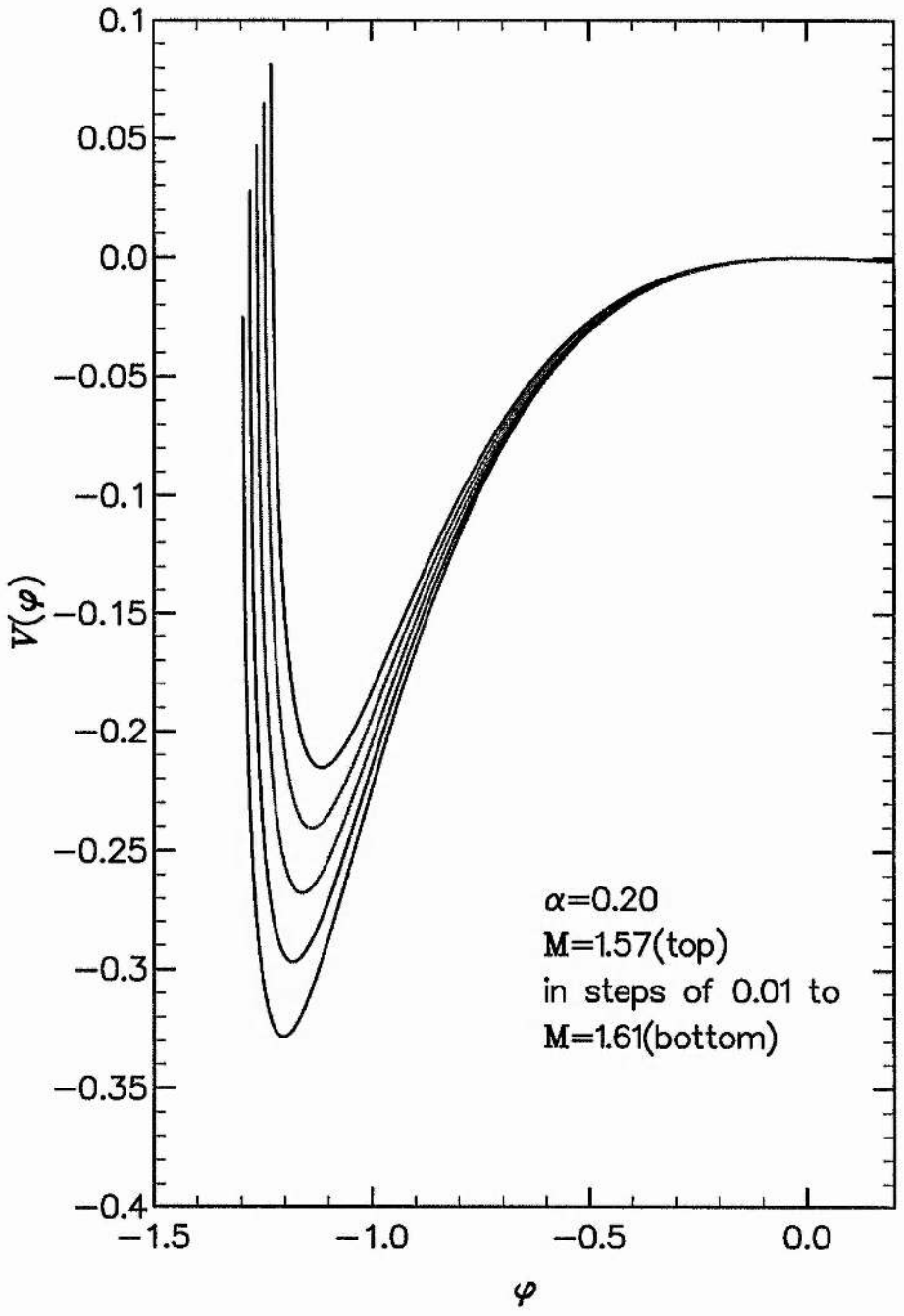

Figure 4.6: Behaviour of the Sagdeev potential $V(\varphi)$ for $\alpha = 0.2$ which shows that solitary wave with negative potential no longer exists when the Mach number M exceeds the value 1.60.

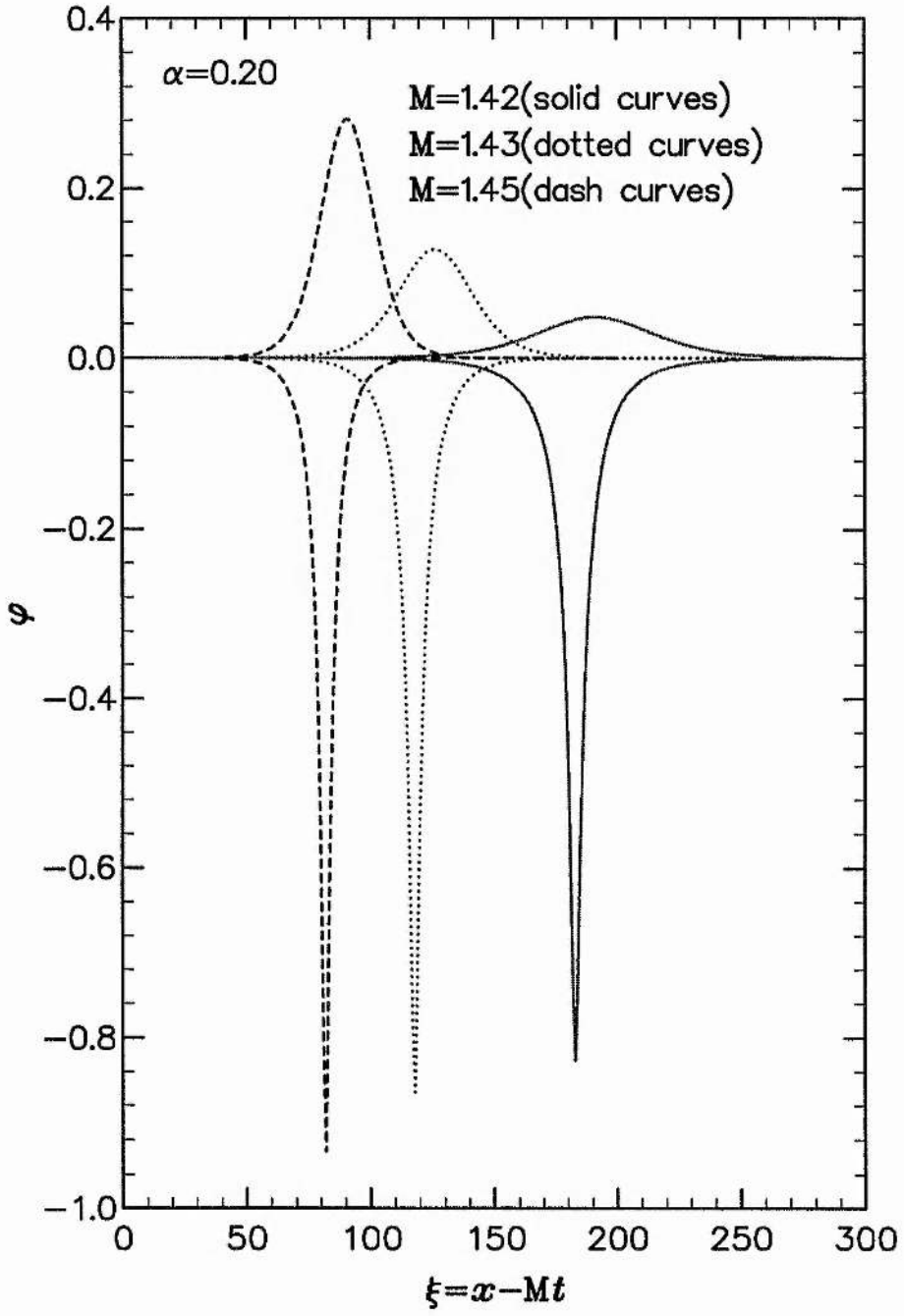

Figure 4.7: φ is plotted against $\xi = x - Mt$ for $\alpha = 0.2$, $M = 1.42$ (solid curves), $M = 1.43$ (dotted curves) and $M = 1.45$ (dashed curves).

M, for $\alpha = 0.2$, can be found as 1.6. We numerically analyse the behaviour of the Sagdeev potential $V(\varphi)$ given by Eq. (4.24) for different values of M and find the range of M for which compressive and rarefactive solitary wave solutions of Eq. (4.23) exist. The numerical results are displayed in figures 4.4 – 4.7. It is clear from figure 4.4 that for $M > 1.41$ there is a potential well on the positive φ-axis, resulting in the existence of dust-acoustic solitary waves with positive potential ($\varphi_m > 0$). It is also seen from figures 4.5 and 4.6 that for $1.38 < M \leq 1.60$ there are potential wells on the negative φ-axis, resulting in the existence of the dust-acoustic solitary waves with negative potential ($\varphi_m < 0$). Figure 4.7 shows how the amplitude and width of both the compressive and rarefactive solitary waves vary with the Mach number M. It shows that as the Mach number increases the amplitude of both the compressive and rarefactive solitary waves increases, whereas their width decreases.

In order to study the dynamics of small amplitude dust-acoustic solitary waves, as before we can derive the Korteweg-de Vries (KdV) equation from Eqs. (4.1) – (4.3) and Eq. (4.22) by employing the reductive perturbation technique and the stretched coordinates $\zeta = \epsilon^{1/2}(x - v_0 t)$ and $\tau = \epsilon^{3/2} t$, where ϵ is a smallness parameter measuring the weakness of the amplitude or dispersion and v_0 is the unknown solitary wave velocity (normalised to C_d), to be determined later. We can then expand the variables n_d, u_d and φ about the unperturbed states in power series of ϵ and develop equations in various powers of ϵ, as has been done in our earlier section. To lowest order in ϵ, Eqs. (4.1) - (4.3) and Eq. (4.22) give $n_d^{(1)} = -\varphi^{(1)}/v_0^2$, $u_d^{(1)} = -\varphi^{(1)}/v_0$ and $v_0 = 1/\sqrt{1-\beta}$. To next higher order in ϵ, we have a set of equations which read

$$\frac{\partial n_d^{(1)}}{\partial \tau} - \frac{1}{\sqrt{1-\beta}} \frac{\partial n_d^{(2)}}{\partial \zeta} + \frac{\partial u_d^{(2)}}{\partial \zeta} + \frac{\partial}{\partial \zeta}(n_d^{(1)} u_d^{(1)}) = 0, \tag{4.26}$$

$$\frac{\partial u_d^{(1)}}{\partial \tau} - \frac{1}{\sqrt{1-\beta}} \frac{\partial u_d^{(2)}}{\partial \zeta} - \frac{\partial \varphi^{(2)}}{\partial \zeta} + u_d^{(1)} \frac{\partial u_d^{(1)}}{\partial \zeta} = 0, \tag{4.27}$$

$$\frac{\partial^2 \varphi^{(1)}}{\partial \zeta^2} - (1-\beta)\varphi^{(2)} - n_d^{(2)} + \frac{1}{2}[\varphi^{(1)}]^2 = 0. \tag{4.28}$$

Now, using these last three equations one can readily obtain

$$\frac{\partial \varphi^{(1)}}{\partial \tau} + a\varphi^{(1)}\frac{\partial \varphi^{(1)}}{\partial \zeta} + b\frac{\partial^3 \varphi^{(1)}}{\partial \zeta^3} = 0, \tag{4.29}$$

which is the KdV equation with coefficients a and b as

$$\left.\begin{aligned} a &= b[1-3(1-\beta)^2], \\ b &= \tfrac{1}{2(1-\beta)^{3/2}}. \end{aligned}\right\} \tag{4.30}$$

The stationary localised solution of this KdV equation, the derivation of which is quite straight forward[2], is directly given by

$$\varphi = \varphi_m \operatorname{sech}^2[(\zeta - u_0 t)\mu], \tag{4.31}$$

where $\varphi_m = 3u_0/a$ is the amplitude of the solitary waves and $\mu = \sqrt{u_0/4b}$ is the inverse of the width of the solitary waves. As $u_0 > 0$ and $b > 0$, this solution with Eqs. (4.22) and (4.30) clearly indicates that (i) small amplitude positive solitary waves exist if $a > 0$, i.e. $\alpha > (\sqrt{3}-1)/(3+\sqrt{3})$, and (ii) small amplitude negative solitary waves exist if $a < 0$, i.e. $\alpha < (\sqrt{3}-1)/(3+\sqrt{3})$. It is found that as u_0 increases, the amplitude of both the positive and negative solitary waves increases while their width decreases.

4.3.3 Solitary Waves for Trapped Ion Distribution

Recent numerical simulation studies [95] on linear and nonlinear dust-acoustic waves exhibit significant amount of ion trapping in the wave potential. Clearly, there is a departure from the Boltzmann ion distribution and one can encounter vortex-like ion distribution in phase space. To find the ion density n_i in this plasma system, we take the ion distribution function, which solves the ion Vlasov equation, to be of the form [38]

$$\left.\begin{aligned} f_{if} &= \tfrac{1}{\sqrt{2\pi}} e^{-\frac{1}{2}(v^2+2\varphi)}, \quad |v| > \sqrt{-2\varphi} \\ f_{it} &= \tfrac{1}{\sqrt{2\pi}} e^{-\frac{1}{2}\alpha(v^2+2\varphi)}, \quad |v| \le \sqrt{-2\varphi} \end{aligned}\right\} \tag{4.32}$$

[2]The derivation is given in **Appendix A.2**

where the subscript $f(t)$ represents the free (trapped) ion contribution. We note that ion distribution function, as presented above, is continuous in velocity space and satisfied the regularity requirements for an admissible BGK solution [115]. The electric potential is assumed to be negative, restricted by $\psi \leq \varphi \leq 0$, where ψ plays the role of amplitude. Furthermore, v is normalised to the ion thermal velocity v_{ti}, $\alpha = T_{if}/T_{it}$ is a parameter which determines the number of trapped ions. A plateau in the resonant ion region is given by $\alpha = 0$ and $\alpha < 0$ corresponds to a vortex-like excavated trapped ion distribution which is of our present interest. We assume here that the velocity of solitary waves is small compared to the ion thermal velocity. Integrating these ion distribution functions over velocity we can write the ion density as[3]

$$\left.\begin{aligned} n_i &= I(-\varphi) + \tfrac{e^{-\alpha\varphi}}{\sqrt{\alpha}}\mathrm{erf}(\sqrt{-\alpha\varphi}), \quad \alpha < 0 \\ n_i &= I(-\varphi) + \tfrac{2}{\sqrt{\pi|\alpha|}}W(\sqrt{\alpha\varphi}), \quad \alpha > 0 \end{aligned}\right\} \tag{4.33}$$

where

$$\left.\begin{aligned} I(-\varphi) &= [1 - \mathrm{erf}(\sqrt{-\varphi})]e^{-\varphi}, \\ \mathrm{erf}(\sqrt{\varphi}) &= \tfrac{2}{\sqrt{\pi}}\textstyle\int_0^{\sqrt{\varphi}} e^{-y^2}dy, \\ W(\sqrt{\alpha\varphi}) &= e^{-\alpha\varphi}\textstyle\int_0^{\sqrt{\alpha\varphi}} e^{y^2}dy. \end{aligned}\right\} \tag{4.34}$$

If we expand this n_i for small amplitude limit and keep the terms up to φ^2, it is found that n_i is same for both $\alpha > 0$ and $\alpha < 0$ and is finally given by[3]

$$n_i = 1 - \varphi - \frac{4}{3}a(-\varphi)^{3/2} + \frac{1}{2}\varphi^2, \tag{4.35}$$

where $a = (1-\alpha)/\sqrt{\pi}$. In order to derive the nonlinear dynamical equation for the dust-acoustic waves from Eqs. (4.1) – (4.3) and Eq. (4.35), one must find an appropriate coordinate frame where the wave can be described smoothly. To find this frame we need to know the thickness Δ and nonlinear velocity v_0 of the wave which can be taken from an equilibrium theory using flat-topped ion distributions [38,39,115,116]. We find

$$\Delta \propto \epsilon^{-1/4}, \quad (v_0 - 1) \propto \epsilon^{1/2}.$$

[3]The derivation is given in **Appendix A.3**

This leads immediately to the following stretched coordinates

$$\left.\begin{aligned} \xi &= \epsilon^{1/4}(x-t), \\ \tau &= \epsilon^{3/4}t, \end{aligned}\right\} \tag{4.36}$$

where ϵ is a smallness parameter measuring the weakness of the nonlinearity. We now employ the perturbation technique so that we can expand the perturbed quantities n_d, u_d and φ about the equilibrium values in powers of ϵ. That means, we let

$$\left.\begin{aligned} n_d &= 1 + \epsilon n_d^{(1)} + \epsilon^{3/2} n_d^{(2)} + \cdots, \\ u_d &= 0 + \epsilon u_d^{(1)} + \epsilon^{3/2} u_d^{(2)} + \cdots, \\ \varphi &= 0 + \epsilon \varphi^{(1)} + \epsilon^{3/2} \varphi^{(2)} + \cdots. \end{aligned}\right\} \tag{4.37}$$

Next, using Eqs. (4.35) – (4.37) in Eqs. (4.1) – (4.3) one can obtain a set of equations which can be solved to yield $n_d^{(1)} = u_d^{(1)} = -\varphi^{(1)}$. To next higher order in ϵ, we have a set of equations which read

$$\frac{\partial n_d^{(1)}}{\partial \tau} - \frac{\partial n_d^{(2)}}{\partial \xi} + \frac{\partial u_d^{(2)}}{\partial \xi} = 0, \tag{4.38}$$

$$\frac{\partial u_d^{(1)}}{\partial \tau} - \frac{\partial u_d^{(2)}}{\partial \xi} - \frac{\partial \varphi^{(2)}}{\partial \xi} = 0, \tag{4.39}$$

$$\frac{\partial^2 \varphi^{(1)}}{\partial \xi^2} - \varphi^{(2)} - n_d^{(2)} - \frac{4}{3} a[-\varphi^{(1)}]^{3/2} = 0. \tag{4.40}$$

Now, one can easily eliminate $\frac{\partial n_d^{(2)}}{\partial \xi}$, $\frac{\partial u_d^{(2)}}{\partial \xi}$ and $\frac{\partial \varphi^{(2)}}{\partial \xi}$ from these last three equations and obtain

$$\frac{\partial \varphi^{(1)}}{\partial \tau} + a\sqrt{-\varphi^{(1)}}\frac{\partial \varphi^{(1)}}{\partial \xi} + b\frac{\partial^3 \varphi^{(1)}}{\partial \xi^3} = 0, \tag{4.41}$$

where $a = (1-\alpha)/\sqrt{\pi} > 0$ and $b = 1/2$. This is the modified Korteweg-de Vries (mKdV) equation which contains a nonlinear term which is proportional to the three half power of the wave potential, in contrast to the usual KdV equation [17] governing the dynamics of nonlinear ion-acoustic waves in an electron-ion plasma without the dust component.

A stationary solitary wave solution of Eq. (4.41) can be obtained by introducing the transformation of the independent variables ξ and τ to $\zeta = \xi - u_0\tau$ and $\tau = \tau$,

where u_0 is a constant solitary wave velocity normalised to the dust-acoustic speed C_d, and imposing the boundary conditions for localised disturbances, viz. $\varphi \to 0$, $\frac{d\varphi}{d\zeta} \to 0$, and $\frac{d^2\varphi}{d\zeta^2} \to 0$ at $\zeta \to \pm\infty$. We have[4]

$$\varphi^{(1)} = -\psi \, \mathrm{sech}^4[(\xi - u_0 t)\mu], \tag{4.42}$$

where $\psi = (\frac{15u_0}{8a})^2$ is the amplitude and $\mu = \sqrt{\frac{u_0}{8}}$ is the inverse of the width of the solitary waves. This solution also stands for $n_d^{(1)}$ or $u_d^{(1)}$ if we replace ψ by $-\psi$. As $u_0 > 0$, this solution clearly indicates that there exist only rarefactive solitary waves of smaller width and larger velocity. It is found that as u_0 increases, the amplitude increases while the width decreases.

4.4 Time Dependent Solitary Structures

In this section, we investigate the propagation of an initial perturbation by integrating numerically the original fluid equations which can be written from our basic system of equations as

$$\frac{\partial n_d}{\partial t} + \frac{\partial (n_d u_d)}{\partial x} = 0, \tag{4.43}$$

$$\frac{\partial u_d}{\partial t} + \frac{\partial}{\partial x}(\frac{1}{2}u_d^2 - \varphi) = 0, \tag{4.44}$$

$$\frac{\partial^2 \varphi}{\partial x^2} + (1 + \beta\varphi + \beta\varphi^2)e^{-\varphi} - n_d = 0. \tag{4.45}$$

It should be mentioned here that in our simulation we have taken $n_i(\varphi)$ as $(1 + \beta\varphi + \beta\varphi^2)e^{-\varphi}$ so that we can consider both the cases of Maxwellian ($\beta = 0$) and non-Maxwellian ($\beta \neq 0$) ion distributions. The propagation of a singe pulse of two different forms is simulated by numerically solving these equations using the Lax-Wendroff difference scheme. The time difference Δt and space difference Δx are 0.05 and 0.1, respectively. The two different initial pulses, which are used in this

[4]The derivation is given in **Appendix A.4**

numerical simulation, are of the form

$$\varphi(x,0) = \begin{cases} 0.025\ \mathrm{sech}^2(x-20), \\ 0.025\exp[-(\frac{x}{2}-10)^2]. \end{cases} \tag{4.46}$$

Though these initial pulses are not stationary solutions, we use the following stationary solutions for the other initial quantities:

$$u_d(x,0) = V_0[1-\sqrt{1+2\varphi/V_0^2}], \tag{4.47}$$

$$n_d(x,0) = (1+2\varphi/V_0^2)^{-1/2}, \tag{4.48}$$

where V_0 is the velocity of the initial pulse. The value of this V_0 is chosen to be 0.773 for $\alpha = 0$ (which is nearly equal to the velocity of the solitary wave of amplitude 0.025 for $\alpha = 0$) and 0.975 for $\alpha = 0.2$ (which is close to the velocity of the solitary wave of amplitude 0.025 for $\alpha = 0.2$). We now study the time evolution of the solitary structures by numerically solving the original equations, Eqs. (4.43) – (4.45), with two different initial pulses given by Eqs. (4.46), for Maxwellian ($\alpha = 0$) and non-Maxwellian ($\alpha = 0.2$) distribution of ions. The numerical results are displayed in the adjoining plots (figures 4.8 – 4.13). The numerical simulation in figures 4.8 and 4.9 considers the Maxwellian ion distribution ($\alpha = 0$) and shows how two different types of initial perturbation, viz. $-0.025\ \mathrm{sech}^2(x-10)$ and $-0.025\exp[-(\frac{x}{2}-10)^2]$, evolve with time, whereas the numerical analyses in figures 4.10 – 4.13 assume the non-thermal ion distribution ($\alpha = 0.2$) and explain how these two types of initial pulse, with their positive and negative forms, evolve with time. The behaviour in figures 4.11 and 4.13 seems typical of the positive solitary waves. The initial disturbance breaks up into a series of solitary waves with the largest in front. The behaviour of the negative solitary waves, shown in figures 4.8 – 4.10 and 4.12, is quite different. These waves appear to be unstable and to produce positive solitary waves at a later time.

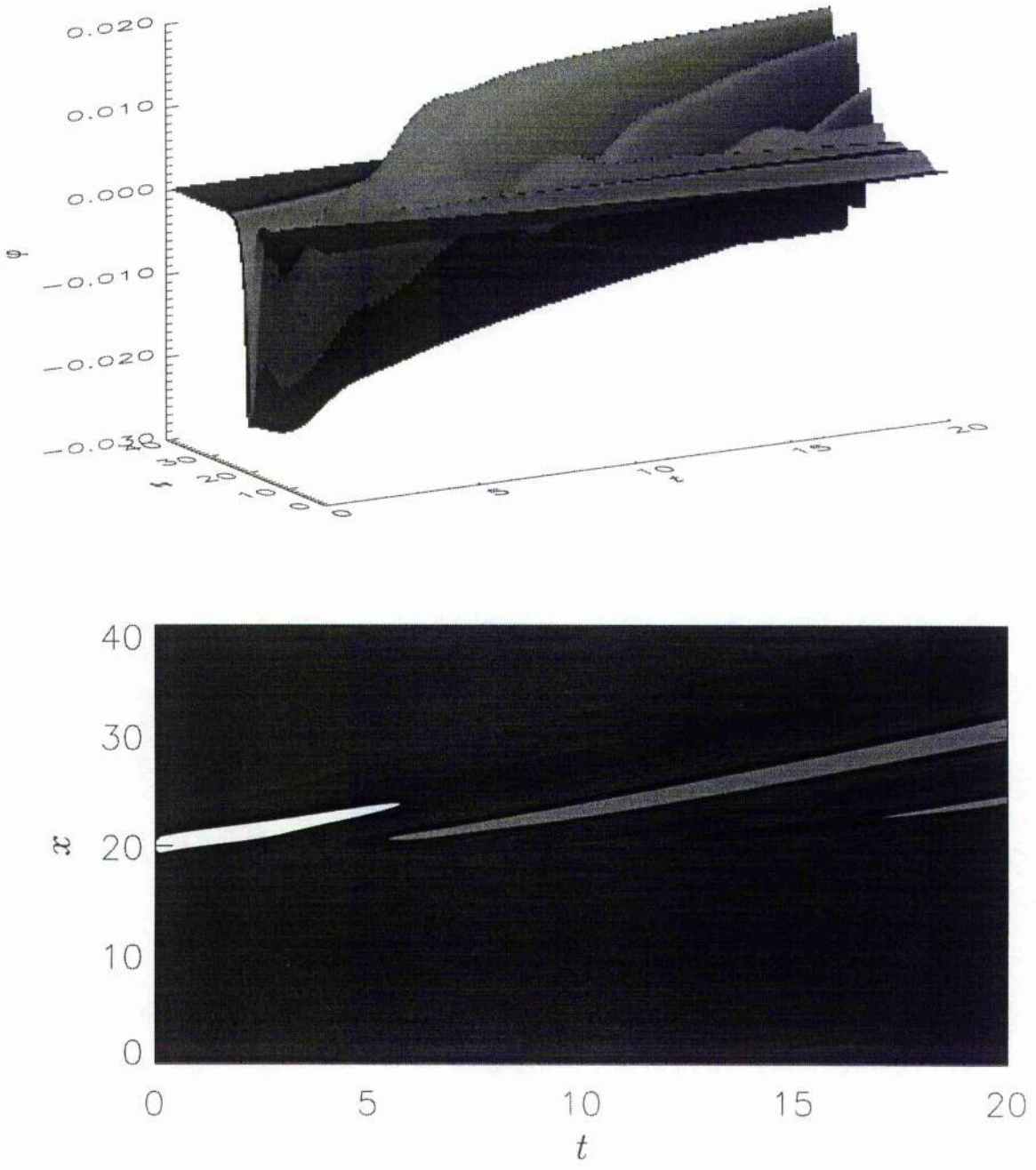

Figure 4.8: Time evolution of the initial perturbation, $-0.025\ \mathrm{sech}^2(x-20)$, for $\alpha = 0$ and $V_0 = 0.773$. The lower view is the contour map of the upper plot.

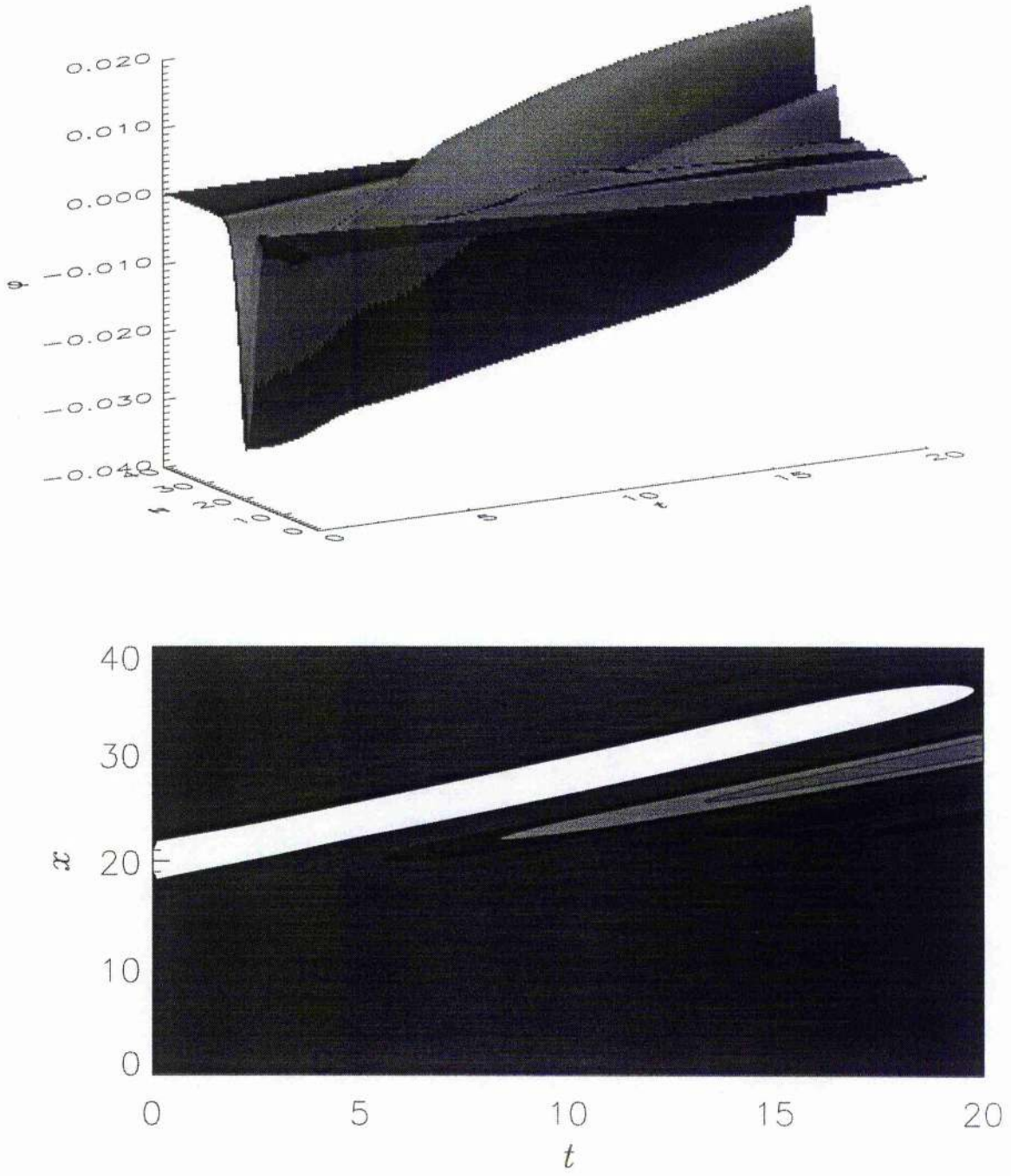

Figure 4.9: Time evolution of the initial perturbation, $-0.025\exp[-(\frac{x}{2}-10)^2]$, for $\alpha = 0$ and $V_0 = 0.773$. The lower view is the contour map of the upper plot.

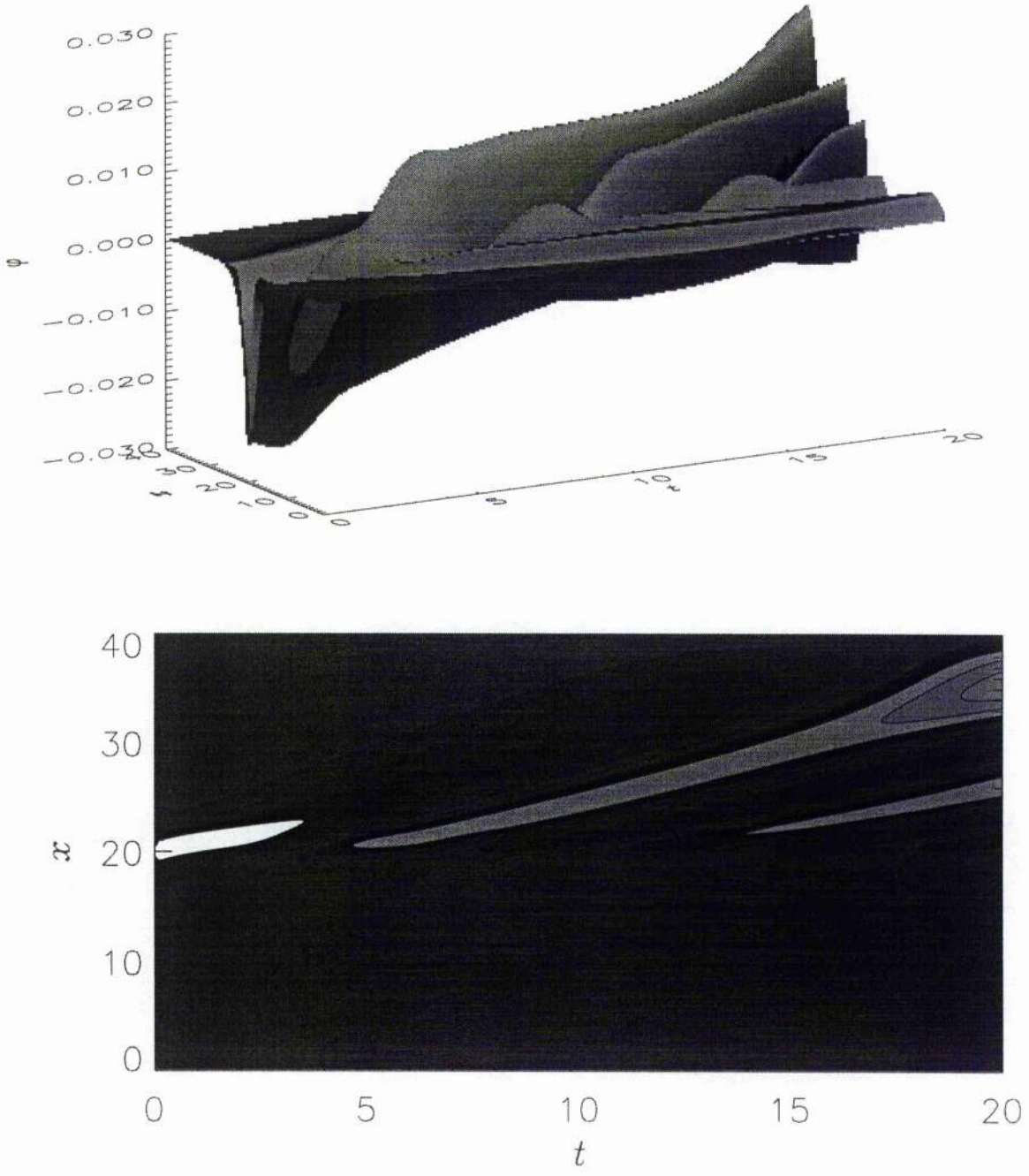

Figure 4.10: Time evolution of the initial perturbation, $-0.025\ \mathrm{sech}^2(x-20)$, for $\alpha = 0.2$ and $V_0 = 0.975$. The lower view is the contour map of the upper plot.

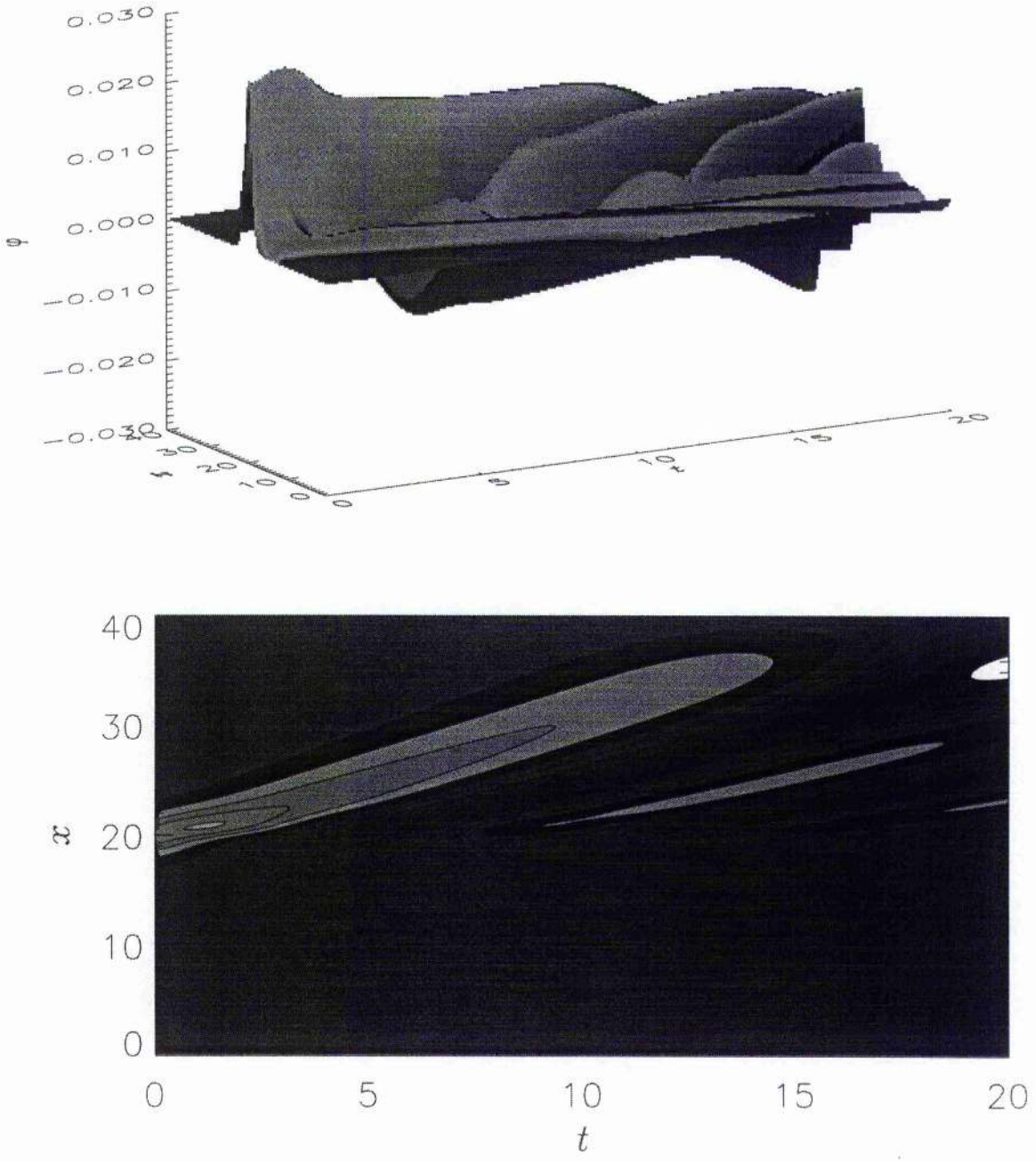

Figure 4.11: Time evolution of the initial perturbation, 0.025 $\mathrm{sech}^2(x-20)$, for $\alpha = 0$ and $V_0 = 0.975$. The lower view is the contour map of the upper plot.

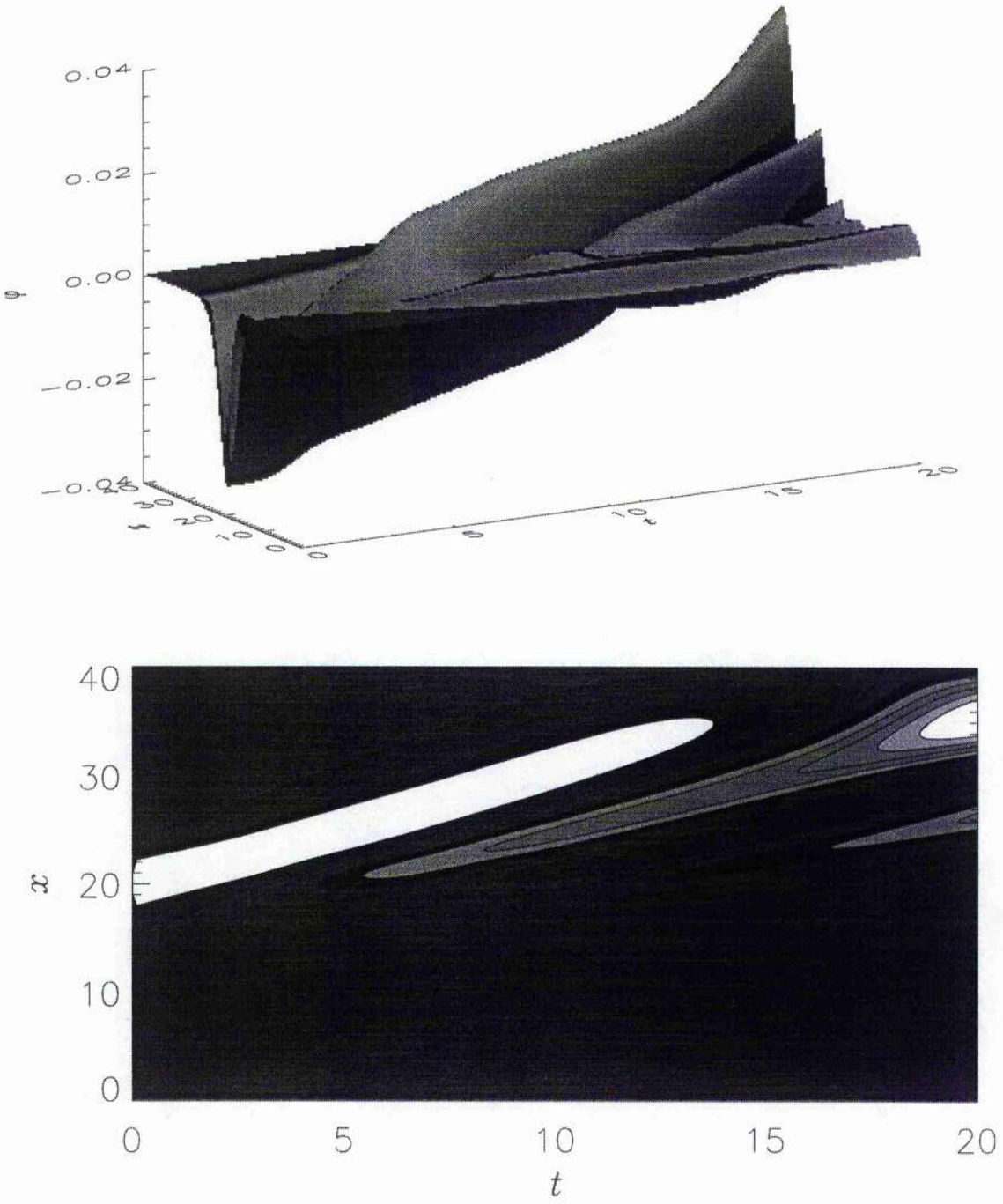

Figure 4.12: Time evolution of the initial perturbation, $-0.025\exp[-(\frac{1}{2}x-10)^2]$, for $\alpha = 0.2$ and $V_0 = 0.975$. The lower view is the contour map of the upper plot.

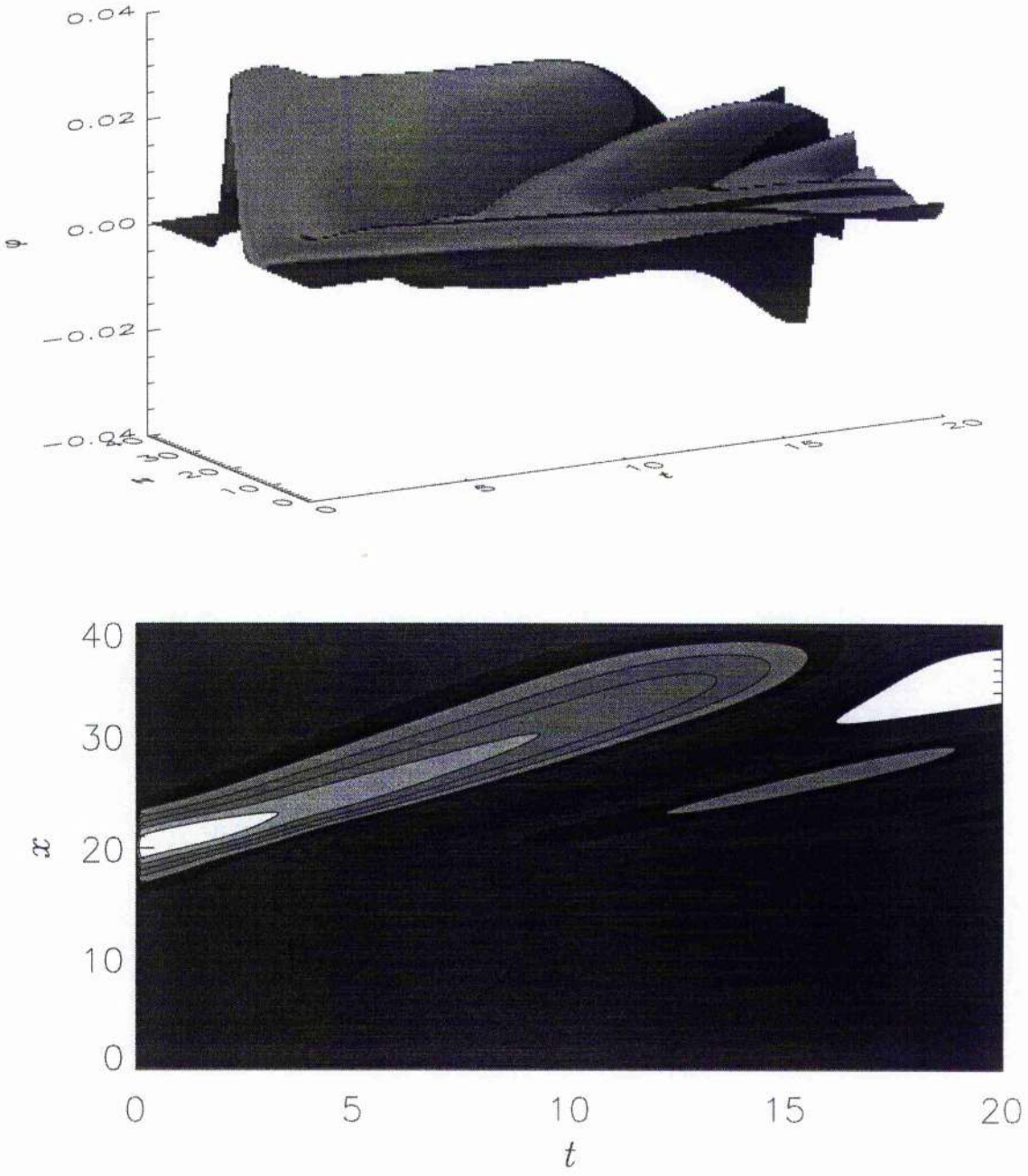

Figure 4.13: Time evolution of the initial perturbation, $0.025\exp[(\frac{x}{2}-10)^2]$, for $\alpha = 0.2$ and $V_0 = 0.975$. The lower view is the contour map of the upper plot.

4.5 Discussion

We have studied the nonlinear properties of dust-acoustic waves in a dusty plasma whose constituents are cold dust particulates and Boltzmann distributed ions. We have also investigated the properties of these dust-acoustic solitary waves by incorporating the effects of non-isothermal ion distributions which have been taken to be either a non-thermal ion distribution or a vortex-like ion distribution. Our results can be summarised as follows.

i) We have first investigated the nonlinear properties of dust-acoustic waves in a dusty plasma whose constituents are cold dust particulates and thermal ions having the Boltzmann distribution. This plasma model is appropriate when the electron number density is sufficiently depleted so that $Z_d n_d >> n_e$. Our results show that in such a plasma we can have only negative potential structures associated with the nonlinear dust-acoustic waves. The latter travel at a speed larger than the dust-acoustic speed C_d. Furthermore, it is found that the dynamics of weakly nonlinear and weakly dispersive dust-acoustic waves is governed by the standard KdV equation, in which the coefficients of the nonlinear and the wave dispersion terms are opposite to each other. The stationary solution of the KdV equation can be represented in the form of an inverted secant hyperbolic squared profile. Thus, the potential polarity of the dust-acoustic solitons in our dusty plasma is different from the usual ion-acoustic solitons in an electron-ion plasma without the dust component [28]. However, the ion density and dust density profiles associated with nonlinear dust-acoustic waves are compressive.

ii) The dusty plasma, which consists of cold dust particulates and non-thermally distributed ions, can support the coexistence of compressive and rarefactive potential structures associated with the nonlinear dust-acoustic waves. Moreover, the dynamics of weakly nonlinear and weakly dispersive dust-acoustic waves is governed by the standard KdV equation, the stationary solution of which can be represented in the form of the secant hyperbolic squared profile if $\alpha > 0.155$ as well as in the form of an inverted secant hyperbolic squared profile if $\alpha < 0.155$. Thus, the poten-

tial polarity of the dust-acoustic solitary waves in our dusty plasma is different from the ion-acoustic solitary waves in an electron-ion plasma without the non-thermal ion and dust components [17,28].

iii) The dusty plasma, whose constituents are cold dust particulates as well as free and trapped ions of different constant temperatures, are found to support only negative spiky solitary waves associated with the nonlinear dust-acoustic waves. Furthermore, in the presence of the vortex-like ion distribution, the dynamics of weakly dispersive nonlinear dust-acoustic waves is governed by the modified KdV equation, the stationary solution of which is represented in the form of an inverted secant hyperbolic fourth profile. Thus, the potential polarity of the dust-acoustic solitary waves in our dusty plasma is different from the usual ion-acoustic solitary waves in an electron-ion plasma without the dust component and trapped ions [17], or only without the dust component [115]. It is found that non-isothermal ions are responsible for dust-acoustic solitary waves, which have smaller width and larger velocity, and that they can be represented in the form $\mathrm{sech}^4(\zeta\mu)$, instead of $\mathrm{sech}^2(\zeta\mu)$ which is the stationary solution of the standard KdV equation [117]. It is also clear that, for a vortex-like excavated trapped ion distribution (i.e. for $\alpha < 0$), as $|\alpha|$ increases, the amplitude of the rarefactive solitary waves decreases very rapidly.

iv) In our dusty plasma model, we have assumed a complete depletion of the background plasma electrons, owing to the attachment of the latter to the surface of the dust grains during the charging process. This is justified, provided that $Z_d n_{d0} >> n_{e0}$ and the wave potential, involved in the Boltzmann electron distribution $n_{e0}\exp(e\varphi/T_e)$, is much smaller than $(T/e)\ln(n_{i0}/n_{e0})$, where $T = T_e T_i/(T_e+T_i)$ and n_{e0} (T_e), is unperturbed electron number density (electron temperature). Inclusion of the electron dynamics in our analysis would alter the overall quasi-neutrality condition as $n_{i0} = n_{e0} + Z_d n_{d0}$, and further it would lead to the modification of the dust-acoustic speed as $(T_i/m_d)^{1/2} Z_d (n_{d0}/n_{i0})^{1/2}(1 + n_{e0}T_i/n_{i0}T_e)^{-1/2}$, as well as include an additional nonlinear term $n_{e0}(e\phi/T_e)^2$ in the small amplitude theory of dust-acoustic solitary waves. It is expected that the nonlinear term, which is propor-

tional to the squared wave potential, will have no influence on the result of sections 4.3.1 and 4.3.2, whereas the results of section 4.3.3 should qualitatively hold for both the large and small amplitude solitary waves.

v) A numerical study has also been made of the time evolution of the solitary waves found to exist in our non-thermal dusty plasma model. We use two different types of initial perturbation and see how they evolve with time in the cases of Boltzmann ($\alpha = 0$) and non-thermal ($\alpha = 0.2$) ion distributions. These results are shown in figures 4.8 – 4.13. Figures 4.11 and 4.13 represent the usual temporal behaviour of the positive solitary waves. The initial disturbance breaks up into a series of solitary waves at the rear of the largest one. Figures 4.8 – 4.10 and 4.12 show the time evolution of negative solitary waves. The behaviour of these negative solitary waves is quite different. It seems that negative solitary waves go unstable and give rise to positive solitary waves at later time.

In conclusion, we stress that the results of the present investigation should be useful in understanding the nonlinear features of localised electrostatic disturbances in both laboratory and space plasmas, in which negatively charged dust particulates and thermally or non-thermally distributed ions are the major plasma species.

Chapter 5

Summary and Future Studies

5.1 Summary of the Thesis

A detailed study of the nonlinear properties of large amplitude solitary waves, which should be useful in understanding the nonlinear features of localised electrostatic disturbances in many laboratory and space plasma phenomena, is incorporated in the last three self-consistent chapters which are the core of this thesis. We will now re-capsulate our findings in the following two subsections.

5.1.1 Solitary Waves in Non-thermal Plasmas

Motivated by the observations of solitary structures with density depletions made by the Freja satellite [73], we have shown in chapter two (which is based on our recent works [104,105]) that the presence of a population of energetic electrons changes the properties of ion sound solitary waves. If a simple fluid response of the ions is taken, so we do not allow trapped ion distributions, then in a thermal plasma only compressive solitary waves are found to exist. However, with a suitable non-thermal electron distribution, we have shown that both the compressive and rarefactive solitary waves can exist. We have found that the minimum value of α (the parameter determining the amount of non-thermal electrons present in our plasma system), for which compressive and rarefactive solitary waves can coexist, is 0.155 and the

critical Mach number (the minimum value of the Mach number above which compressive and rarefactive density perturbations can coexist) is $\sqrt{2}$ for $\alpha = 0.20$ (a value which we have used in our study). We have also compared this non-thermal plasma model with another popular model, namely the two-electron-temperature (two Maxwellian) plasma model [35], and shown that a similar result can be obtained for this two-electron-temperature plasma model.

It is found, in our study of ion temperature effects on solitary waves in non-thermal plasmas, that as we increase ion temperature, we need more non-thermal electrons in order to make rarefactive solitary waves exist. It is also shown that as the ion temperature rises, the amplitude of both the compressive and rarefactive solitary waves decreases, whereas the width of these solitary waves increases.

In a magnetic field, the one dimensional structures would have to propagate along the magnetic field. However, we have also demonstrated that three dimensional structures can exist and these, of course, are the type of structures which may be relevant to the observations made by the Freja and Viking satellites [71,73].

A numerical study has also been made of time evolution of the solitary waves found to exist in our non-thermal plasma model. We use two different types of initial perturbation and see how they evolve with time in the cases of the Maxwellian ($\alpha = 0$) and non-Maxwellian ($\alpha = 0.2$) distribution of electrons. These results are shown in figures 2.17 – 2.22. The behaviour in figures 2.17 – 2.19 and 2.21 seems typical of the compressive solitary waves. The initial disturbance breaks up into a series of solitons with the largest in front. The behaviour of the rarefactive solitary waves shown in figures 2.20 and 2.22 is quite different. These waves appear to be unstable and to produce compressive waves at a later time. This behaviour, of course, rather casts doubt on our suggestion that such waves are observed, though it is possible that three dimensional structures could be more stable. This is a question which we have not examined.

We have then extended our study of solitary waves to a magnetised non-thermal plasma and analysed the stability of large and finite amplitude solitary waves, inves-

tigated the effects of the external magnetic field and obliqueness (angle between the directions of the magnetic field and the propagation of solitary waves) on arbitrary amplitude solitary waves and applied our method to study arbitrary amplitude solitary waves in a two electron temperature plasma model. These all are incorporated in chapter three (which is based on our recent works [118,119]). The results, which have been found in chapter three, can be briefly pointed out as follows.

It is found, in our study of small but finite amplitude solitary waves, that depending on the value of α the solitary waves may change from compressive to rarefactive and that there exist compressive solitary waves when $\alpha < 0.155$ and rarefactive solitary waves when $\alpha > 0.155$. It is also found, in both the small and large amplitude limits, that as the angle (δ) that the propagation direction of solitary waves makes with the magnetic field increases, the amplitude of both the compressive and rarefactive solitary waves increases. It is observed, with the analytical analysis in the small amplitude limit, that the width of the solitary waves increases with δ for its lower range, i.e. from 0° to $\sim 45^\circ$, but decreases for its higher range, i.e. from $\sim 45^\circ$ to 90°. When $\delta \to 90^\circ$, the width tends to 0 and the amplitude tends to ∞. It is likely that for large angles the assumption that the waves are electrostatic is no longer a valid one, and we should look for fully electromagnetic structures. The magnitude of the magnetic field ($\mathbf{B}_0$) has no direct effect on the amplitude of the solitary waves (in both the small and large amplitude limits) and the critical Mach number. However, it does have a direct effect on the width of these solitary waves (in both the small and large amplitude limits) and it is found that as its magnitude increases, the width of both the compressive and rarefactive solitary waves decreases, i.e. magnetic field makes the solitary structures more spiky. It is also important to note, from the analysis in the large amplitude limit, that as the obliqueness increases, the critical Mach number decreases.

To compare the results obtained from the analysis in the small amplitude limit with those in the arbitrary amplitude limit, it is important to note that in the small amplitude limit either compressive or rarefactive solitary waves are found to

exist, whereas in the more complete theory they may exist together. In the small amplitude limit, both of these analyses give the same results.

It is shown, in stability analysis of these solitary waves, that the α-value has no effect on whether the solitary waves will be stable or unstable. But stability depends strongly on the external magnetic field and the propagation directions of both the nonlinear wave and its perturbation mode. It is found that, for obliquely propagating perturbation mode with constant direction cosines, the solitary waves become unstable for a lower value of δ and for a higher value of the magnetic field and that as δ increases, the magnetic field, for which the solitary waves become unstable, increases. It is also found that as the magnitude of the magnetic field increases, the growth rate γ of the unstable perturbation mode decreases for the lower range of δ (from 0° to $\sim 10^\circ$) and increases for higher δ.

We have found almost the same results, in our study of arbitrary amplitude solitary waves in the two-electron-temperature plasma model, i.e. (i) as the angle that the propagation direction of solitary waves makes with the magnetic field increases, the amplitude of both the compressive and rarefactive solitary waves increases, but their width decreases and (ii) the magnitude of the magnetic field has no direct effect on the amplitude of the solitary waves and the critical Mach number, but it does have a direct effect on the width of these solitary waves and it is found that as its magnitude increases, the width of both the compressive and rarefactive solitary waves decreases. It may be added, in our study of solitary waves in a two-electron-temperature plasma, that our present results are valid for solitary waves of arbitrary amplitude and agree with the existing published results [35] for parallel propagation and [35,36] for small amplitude limit. In the small amplitude limit [35,36] the solitary waves may change from compressive to rarefactive, while our study of fully nonlinear equations may allow rarefactive and compressive solitary waves to coexist.

5.1.2 Solitary Waves in Dusty Plasmas

We have then arrived at chapter four (which is based on our most recent work [120,121]) with similar types of study (study of dust-acoustic solitary waves) but for a different plasma model, namely a dusty plasma whose constituents are cold dust particulates and Boltzmann distributed ions. In the same chapter we have also investigated the properties of these dust-acoustic solitary waves by incorporating the effects of non-isothermal ion distributions which have been taken to be either a non-thermal ion distribution or a vortex-like ion distribution. Our findings in this chapter can be outlined as follows:

The results of our study of dust-acoustic waves, in a dusty plasma whose constituents are cold dust particulates and thermal ions having the Boltzmann distribution, show that we can have only negative potential structures associated with the nonlinear dust-acoustic waves. The latter travel at a speed larger than the dust-acoustic speed C_d. It is found that the dynamics of weakly nonlinear and weakly dispersive dust-acoustic waves is governed by the standard KdV equation in which the coefficient of the nonlinear and wave dispersion terms are opposite to each other. The stationary solution of the KdV equation can be represented in the form of an inverted secant hyperbolic squared profile. Thus, the potential polarity of the dust-acoustic solitary waves in our dusty plasma is different from the usual ion-acoustic solitary waves in an electron-ion plasma without the dust component [28]. However, the ion density and dust density profiles associated with nonlinear dust-acoustic waves are compressive.

We have then considered a non-thermal ion distribution (instead of Boltzmann ion distribution) and shown that the effect of non-thermal ion distribution changes the properties of dust-acoustic solitary waves and can support the coexistence of compressive and rarefactive potential structures associated with the nonlinear dust-acoustic waves. Moreover, the dynamics of weakly nonlinear and weakly dispersive dust-acoustic waves is governed by the standard KdV equation, the stationary solution of which can be represented in the form of the secant hyperbolic squared profile

if $\alpha > 0.155$ as well as in the form of an inverted secant hyperbolic squared profile if $\alpha < 0.155$. Thus, the potential polarity of the dust-acoustic solitary waves in our dusty plasma is different from the ion-acoustic solitary waves in an electron-ion plasma without the non-thermal ion and dust components [17,28].

We have also considered the trapped ion distribution and found its effect on these dust-acoustic solitary waves. It is shown that a dusty plasma, whose constituents are cold dust particulates as well as free and trapped ions of different constant temperatures, is found to support only negative spiky solitary waves associated with these nonlinear dust-acoustic waves. It is also found that, in the presence of the vortex-like ion distribution, the dynamics of weakly dispersive nonlinear dust-acoustic waves is governed by the modified KdV equation, the stationary solution of which is represented in the form of an inverted secant hyperbolic fourth profile. Thus, the potential polarity of the dust-acoustic solitary waves in our dusty plasma is different from the usual ion-acoustic solitary waves in an electron-ion plasma without the dust component and trapped ions [17], or only without the dust component [116]. It is found that non-isothermal ions are responsible for the dust-acoustic solitary waves which have smaller width and larger velocity and that they can be represented in the form of $\text{sech}^4(\zeta\mu)$, instead of $\text{sech}^2(\zeta\mu)$ which is the stationary solution of the standard KdV equation [117]. It is also clear that, for a vortex-like excavated trapped ion distribution (i.e. for $\alpha < 0$), as $|\alpha|$ increases, the amplitude of the negative solitary waves decreases very rapidly.

Finally, a numerical study has been made of time evolution of the solitary waves found to exist in our dusty plasma model. We use two different types of initial perturbation and see how they evolve with time in the cases of the Maxwellian ($\alpha = 0$) and non-Maxwellian ($\alpha = 0.2$) distribution of ions. The numerical results are displayed in figures 4.8 – 4.13. The numerical simulation in figures 4.8 and 4.9 considers the Maxwellian ion distribution ($\alpha = 0$) and shows how the two different types of initial perturbation, viz. $-0.025\ \text{sech}^2(x-10)$ and $-0.025\exp[-(\frac{x}{2}-10)^2]$, evolve with time, whereas the numerical analyses in figures 4.10 – 4.13 assume the

non-thermal ion distribution ($\alpha = 0.2$) and explain how these two types of initial pulse, with their positive and negative forms, evolve with time. The behaviour in figures 4.11 and 4.13 seems typical of the positive solitary waves. The initial disturbance breaks up into a series of solitary waves at the rear of the largest one. The behaviour of the negative solitary waves, shown in figures 4.8 – 4.10 and 4.12, is quite different. These waves appear to be unstable and to produce positive solitary waves at a later time.

In our dusty plasma model, we have assumed complete depletion of the background plasma electrons, owing to the attachment of the latter on the surface of the dust grains during the charging process. This is justified, provided that the number of free electrons is negligible in comparison with number of electrons residing in the dust grains. It is briefly shown that inclusion of the electron dynamics in our analysis would alter the overall quasi-neutrality condition and lead to the modification of the dust-acoustic speed as well as include an additional nonlinear term in the small amplitude theory of dust-acoustic solitary waves. It is expected that the nonlinear term, which is proportional to the squared wave potential, will have no influence on the results of the study of dust-acoustic waves in dusty plasmas with Boltzmann or non-thermal ion distributions, whereas the results for consideration of the vortex-like ion distribution should qualitatively hold for both the large and small amplitude solitary waves.

5.2 Proposal for Future Studies

We have studied electrostatic solitary waves in two different plasma models, namely the non-thermal plasma model, which may be of more relevance to ionospheric or magnetospheric plasmas [71,73], and the dusty plasma model which is relevant to recent laboratory experiment [96] and also the Saturn's F ring. In our study of these electrostatic solitary waves in both the non-thermal and dusty plasma models, there are some limitations and simplifications, leaving scope for further studies. A few extensions to our study of electrostatic solitary waves in our non-thermal and dusty

plasma models, some of which might need a simple modification and some might need further studies, can be proposed as follows.

5.2.1 Further Studies in Non-thermal Plasmas

In our study of time evolution of solitary waves in non-thermal plasmas, we have considered the cold ion limit, i.e. we have neglected ion pressure. Also this study has been done in unmagnetised plasma. A further study on this time dependent solitary structures in warm (non-zero ion temperature) magnetised non-thermal plasma can be made.

To study obliquely propagating solitary waves in magnetised non-thermal plasmas, we neglected ion pressure. In the small amplitude limit, one can easily include the ion pressure term and can see the effect of ion temperature on these solitary structures. However, addition of this ion pressure term, in our numerical study of the full set of equations, adds more complexity. A further attempt could be made to develop our numerical analysis for the study of arbitrary amplitude obliquely propagating ion-acoustic solitary waves in warm magnetised non-thermal plasmas.

In our stability analysis of solitary waves, we have used reductive perturbation and small k-expansion which are only valid for small but finite amplitude solitary waves and long wavelength perturbation modes. Since in many astrophysical situations there exist extremely large amplitude solitary waves and short-wavelength perturbation modes, we propose to develop a more exact theory for the stability analysis of arbitrary amplitude solitary waves and arbitrary wavelength perturbation modes.

We have shown that when the angle that the solitary wave propagation direction makes with the magnetic field tends to 90°, the width tends to 0 and the amplitude tends to ∞. It is likely that for large angles the assumption that the waves are electrostatic is no longer a valid one, and we should look for fully electromagnetic structures that will be discussed in the last section of this chapter.

5.2.2 Further Studies in Dusty Plasmas

In our dusty plasma model, we have assumed complete depletion of the background plasma electrons, owing to the attachment of the latter to the surface of the dust grains during the charging process. This is justified, provided that the number of free electrons (n_{e0}) is negligible in comparison with the number of electrons residing on the dust grains ($Z_d n_d$), i.e. $Z_d n_{d0} >> n_{e0}$, and the wave phase velocity is much smaller than the ion thermal velocity. However, in our analyses one can easily include the effect of electron dynamics, which will alter the overall quasi-neutrality condition as $n_{i0} = n_{e0} + Z_d n_{d0}$, by rewriting our basic equations, Eqs. (4.1) –(4.3), for the Boltzmann distributed ions and electrons, in the form

$$\frac{\partial n_d}{\partial t} + \frac{\partial}{\partial x}(n_d u_d) = 0, \tag{5.1}$$

$$\frac{\partial u_d}{\partial t} + u_d \frac{\partial u_d}{\partial x} = \frac{\partial \varphi}{\partial x}, \tag{5.2}$$

$$\frac{\partial^2 \varphi}{\partial x^2} = n_d + \mu_0 e^{\alpha\varphi} - \mu_1 e^{-\varphi}, \tag{5.3}$$

where $\mu_0 = \beta/(1-\beta)$, $\mu_1 = 1 + \mu_0$, $\beta = n_{e0}/n_{i0}$, $\alpha = T_i/T_e$, and T_i (T_e) is the ion (electron) temperature in units of the Boltzmann constant (K_B). Now, following the same procedure as discussed in chapter 4, one can easily study the solitary waves and see the effect of Boltzmann distributed electrons on the dust-acoustic solitary structures, in our dusty plasma model, studied in chapter 4.

We have studied dust-acoustic solitary waves by considering the unmagnetised dusty plasma model. However, one can extend this study to a magnetised dusty plasma and study obliquely propagating dust-acoustic solitary waves following the same method as discussed in chapter 3. Also, we can further extend these studies in the same way as discussed in the previous subsection (Sec. 5.2.1).

Finally, we propose to extend our studies to a new discipline of cylindrical and spherical solitary waves [122-124]. This extension can be made in both of our non-thermal and dusty plasma models.

5.2.3 Electromagnetic Solitary Structures

We have confined ourselves only to the study of electrostatic solitary structures in non-thermal plasma and dusty plasma models. We can extend our study to electromagnetic solitary structures which might also be very useful for understanding many laboratory and space plasma phenomena. In the following we will explain briefly how one can exploit our method (discussed in Sec. 3.4.2) to study the electromagnetic solitary structures in our non-thermal plasma model.

The nonlinear behaviour of electromagnetic waves, in the plasma system considered in chapter 3, may be described by the following set of equations:

$$\frac{\partial n}{\partial t} + \nabla \cdot (n\mathbf{u}) = 0, \tag{5.4}$$

$$\frac{\partial \mathbf{u}}{\partial t} + (\mathbf{u} \cdot \nabla)\mathbf{u} = -\nabla\varphi + \omega_c(\mathbf{u} \times \hat{z}) - \frac{1}{c}\frac{\partial \mathbf{A}}{\partial t} + \frac{1}{c}\mathbf{u} \times (\nabla \times \mathbf{A}), \tag{5.5}$$

$$\nabla^2\varphi - \frac{1}{c^2}\frac{\partial^2\varphi}{\partial t^2} = n_e - n, \tag{5.6}$$

$$\nabla^2\mathbf{A} - \frac{1}{c^2}\frac{\partial^2\mathbf{A}}{\partial t^2} = (n_e - n)\mathbf{u}, \tag{5.7}$$

where c is the speed of light normalised to C_s, $\mathbf{A}$ is the vector field normalised to $K_B T_e/e$ and all other variables are as before (in chapters 2 and 3). As before, if we make all dependent variables depend on a single independent variable defined by $\xi = \hat{l} \cdot \mathbf{u} - Mt$, with M again being the Mach number and $\hat{l}$ being the unit vector in the propagation direction of the solitary waves, and eliminate n and u_z, using the appropriate boundary conditions, namely $\varphi \to 0$, $u_{x,y,z} \to 0$, $A_{x,y,z} \to 0$ and $n \to 1$ at $\xi \to \pm\infty$, we can reduce our basic equations to the form

$$\frac{du_x}{d\xi} = \frac{1}{U}(l_x\frac{d\varphi}{d\xi} - \omega_c u_y) - \frac{1}{c}(1 + \frac{u_x l_x}{U})\frac{dA_x}{d\xi}$$
$$-\frac{u_y l_x}{Uc}\frac{dA_y}{d\xi} + \frac{1}{c}\frac{l_x}{l_z}(1 + \frac{u_x l_x}{U} - \frac{M}{U})\frac{dA_z}{d\xi}, \tag{5.8}$$

$$\frac{du_y}{d\xi} = \frac{1}{U}\omega_c u_x - \frac{1}{c}\frac{dA_y}{d\xi}, \tag{5.9}$$

$$\frac{d^2\varphi}{d\xi^2} = F, \tag{5.10}$$

$$\frac{d^2A_x}{d\xi^2} = Fu_x, \tag{5.11}$$

$$\frac{d^2A_y}{d\xi^2} = Fu_y, \tag{5.12}$$

$$\frac{d^2A_z}{d\xi^2} = Fu_z, \tag{5.13}$$

where

$$U = M\sqrt{1 - \frac{l_z^2}{M^2}(u_x^2 + u_y^2 + 2\varphi + 2\frac{l_z}{M}A_z)} - l_x u_x, \tag{5.14}$$

$$F = \frac{1}{1 + M^2/c^2}[(1 - \beta\varphi + \beta\varphi^2)e^{\varphi} - \frac{M}{U}]. \tag{5.15}$$

We assume here that the solitary waves propagate in the (x, z) plane, i.e. $\hat{l} = \hat{x}l_x + \hat{z}l_z$. It may be noted that as $A_{x,y,z} \to 0$ and $c \to \infty$, these equations reduce to the set of equations, Eqs. (3.64) – (3.67), which have already been solved numerically in section 3.4.2. Therefore, following the same procedures as discussed in section 3.4.2, one can try to solve numerically this full set of equations, Eqs. (5.8) – (5.13), to study the fully electromagnetic solitary structures in our non-thermal plasma model. It is important to note here that one can also use this technique to study electromagnetic solitary structures in our magnetised dusty plasma model.

APPENDIX

A.1 To Introduce Stretched Coordinates

The energy law, Eq. (2.26), can be written as

$$\frac{1}{2}(\frac{d\varphi}{d\xi})^2 + V(\varphi) = 0, \tag{A.1}$$

where the Sagdeev potential $V(\varphi)$ for cold ion limit, Eq. (2.33), is

$$\begin{aligned} V(\varphi) = & - [1 + 3\beta(1-\varphi) + \beta\varphi^2]e^{\varphi} \\ & - M^2\sqrt{1 - 2\varphi/M^2} + 1 + 3\beta + M^2, \end{aligned} \tag{A.2}$$

Now, expanding the Sagdeev potential $V(\varphi)$ around the origin we obtain

$$V(\varphi) = -\frac{1}{2}(1 - \beta - \frac{1}{M^2})\varphi^2 - \frac{1}{2}(\frac{1}{3} - \frac{1}{M^4})\varphi^3. \tag{A.3}$$

The critical Mach number is that which corresponds to the vanishing of the quadratic term. At the same time, if the cubic term is negative, there is a potential well on the negative side and if the cubic term is positive, there is a potential well on the positive side. Therefore, using this equation, the critical Mach number, at which the second derivative changes sign, can be found as $M_c = 1/\sqrt{1-\beta}$. We now consider that M is close to M_c, i.e. $\Delta = M - M_c << M_c$. This consideration allows us to write Eq. (A.3) as

$$\begin{aligned} V(\varphi, \Delta) = & - \frac{1}{2}[\frac{1}{M_c^2} - \frac{1}{(M_c + \Delta)^2}]\varphi^2 \\ & - \frac{1}{2}[\frac{1}{3} - \frac{1}{(M_c + \Delta)^4}]\varphi^3. \end{aligned} \tag{A.4}$$

If we consider $\frac{\Delta}{M_c} << 1$, we can simplify this equation to

$$V(\varphi, \Delta) = -\frac{\Delta}{M_c^3}\varphi^2 + (C - 2\frac{\Delta}{M_c^5})\varphi^3, \tag{A.5}$$

where $C = -\frac{1}{6} + \frac{1}{2M_c^4}$. Substituting Eq. (A.5) into Eq. (A.1) we obtain

$$\begin{aligned} & \frac{d\varphi}{d\xi} = \varphi\sqrt{\frac{2\Delta}{M_c^3}}\sqrt{1 - (C\frac{M_c^3}{\Delta} - \frac{2}{M_c^2})\varphi}, \\ \Rightarrow \quad & d\xi = -(\sqrt{\frac{M_c^3}{2\Delta}})\frac{2dY}{1-Y^2}, \\ \Rightarrow \quad & d\xi = -(\sqrt{\frac{M_c^3}{2\Delta}})(\frac{1}{1-Y} + \frac{1}{1+Y})dY, \end{aligned} \tag{A.6}$$

where $Y = \sqrt{1 - (C\frac{M_c^3}{\Delta} - \frac{2}{M_c^2})\varphi}$. On integration of this equation we obtain

$$\begin{aligned} & \xi = (\sqrt{\frac{M_c^3}{2\Delta}})[\ln(1-Y) - \ln(1+Y)], \\ \Rightarrow \quad & \frac{1-Y}{1+Y} = \exp(\xi\sqrt{2\Delta/M_c^3}), \\ \Rightarrow \quad & Y = \frac{1 - \exp(\xi\sqrt{2\Delta/M_c^3})}{1 + \exp(\xi\sqrt{2\Delta/M_c^3})}. \end{aligned} \tag{A.7}$$

Therefore, substituting Y and $\xi = x - Mt$ into Eq. (A.7) , we can express φ as

$$\varphi = \frac{\Delta M_c^2}{CM_c^5 - 2\Delta}\mathrm{sech}^2[\sqrt{\frac{\Delta}{2M_c^3}}(x - Mt)]. \tag{A.8}$$

Now, introducing $\epsilon = \Delta << M_c$, which is the measure of the pulse amplitude, the argument of sech^2 can be written as

$$\frac{1}{\sqrt{2M_c^3}}[\epsilon^{1/2}(x - M_c t) - \epsilon^{3/2}t]. \tag{A.9}$$

This gives the appropriate scaling (in a frame moving with $M_c = v_0$) of space and time variables that is required to construct a weakly nonlinear theory of ion-acoustic waves which describes the evolution of small but finite amplitude localised perturbations. Thus, one can introduce the following stretched coordinates

$$\left.\begin{aligned} \xi &= \epsilon^{1/2}(x - v_0 t), \\ \tau &= \epsilon^{3/2}t. \end{aligned}\right\} \tag{A.10}$$

A.2 Stationary Solution of KdV Equation

The Korteweg-de Vries (KdV) equation, discussed in **sections 3.3.2, 4.3.1** and **4.3.2**, can be written in the form

$$\frac{\partial y}{\partial t} + ay\frac{\partial y}{\partial x} + b\frac{\partial^3 y}{\partial x^3} = 0, \tag{A.11}$$

where a and b are two different constants. To obtain a stationary localised solution of this nonlinear equation, we first transform the independent variables to

$$\left.\begin{aligned} \xi &= x - u_0\tau, \\ \tau &= t. \end{aligned}\right\} \tag{A.12}$$

This transformation, with the steady state condition ($\frac{\partial}{\partial \tau} \to 0$), reduces the KdV equation to the form

$$\begin{aligned} & -u_0\frac{dy}{d\xi} + ay\frac{dy}{d\xi} + b\frac{d^3y}{d\xi^3} = 0, \\ \Rightarrow \quad & \frac{d}{d\xi}\left(\frac{d^2y}{d\xi^2}\right) = \frac{1}{b}\frac{d}{d\xi}\left(u_0y - \frac{1}{2}ay^2\right). \end{aligned} \tag{A.13}$$

Now, under the appropriate boundary conditions, viz. $y \to 0$ and $d^2y/d\xi^2 \to 0$ at $\xi \to \pm\infty$, this equation can be integrated to give

$$\frac{d^2y}{d\xi^2} = \frac{1}{b}\left(u_0y - \frac{1}{2}ay^2\right). \tag{A.14}$$

Multiplying both sides of this equation by $dy/d\xi$ one can write

$$\frac{d}{d\xi}\left[\left(\frac{dy}{d\xi}\right)^2\right] = \frac{1}{b}\frac{d}{d\xi}\left(u_0y^2 - \frac{1}{3}ay^3\right). \tag{A.15}$$

Now, we can easily integrate this equation and, under the same boundary conditions, $y \to 0$ and $dy/d\xi \to 0$ at $\xi \to \pm\infty$, one can write

$$\begin{aligned} & \frac{dy}{d\xi} = y\sqrt{\frac{u_0}{b}}\sqrt{1 - \frac{a}{3u_0}y}, \\ \Rightarrow \quad & d\xi = -\left(\sqrt{\frac{4b}{u_0}}\right)\frac{dY}{1 - Y^2}, \\ \Rightarrow \quad & d\xi = -\left(\sqrt{\frac{b}{u_0}}\right)\left(\frac{1}{1 - Y} + \frac{1}{1 + Y}\right)dY, \end{aligned} \tag{A.16}$$

where $Y = \sqrt{1 - \frac{a}{3u_0}y}$. On integration of this equation we obtain

$$\begin{aligned} & \xi = (\sqrt{\frac{b}{u_0}})[\ln(1-Y) - \ln(1+Y)], \\ \Rightarrow \quad & \frac{1-Y}{1+Y} = \exp(\xi\sqrt{u_0/b}), \\ \Rightarrow \quad & Y = \frac{1-\exp(\xi\sqrt{u_0/b})}{1+\exp(\xi\sqrt{u_0/b})}. \end{aligned} \tag{A.17}$$

Now, substituting Y into this equation one can easily obtain

$$\begin{aligned} & y = (\frac{3u_0}{a})[\frac{2\exp(\xi\sqrt{u_0/4b})}{1+\exp(\xi\sqrt{u_0/b})}]^2, \\ \Rightarrow \quad & y = (\frac{3u_0}{a})[\frac{2}{\exp(-\xi\sqrt{u_0/4b}) + \exp(\xi\sqrt{u_0/4b})}]^2, \\ \Rightarrow \quad & y = (\frac{3u_0}{a})\mathrm{sech}^2(\xi\sqrt{u_0/4b}). \end{aligned} \tag{A.18}$$

Therefore, the stationary solution of the KdV equation is finally written as

$$y = y_m \mathrm{sech}^2[(x - u_0 t)\mu], \tag{A.19}$$

where y_m and μ are the amplitude and the inverse of the width of the solitary waves, respectively, and are given by

$$\left.\begin{aligned} y_m &= \tfrac{3u_0}{a} \\ \mu &= \sqrt{\tfrac{u_0}{4b}}. \end{aligned}\right\} \tag{A.20}$$

A.3 Derivation of Trapped Ion Density

To find the ion density n_i in a dusty plasma model, described in **Sec. 4.3.3**, we take the free and trapped ion distribution functions to be of the form

$$\left.\begin{aligned} f_{if} &= \tfrac{1}{\sqrt{2\pi}} e^{-\frac{1}{2}(v^2+2\varphi)}, \quad |v| > \sqrt{-2\varphi} \\ f_{it} &= \tfrac{1}{\sqrt{2\pi}} e^{-\frac{1}{2}\alpha(v^2+2\varphi)}, \quad |v| \leq \sqrt{-2\varphi} \end{aligned}\right\} \tag{A.21}$$

The free ion density n_{if} is given by

$$\begin{aligned} n_{if} &= \frac{1}{\sqrt{2\pi}}\Big[\int_{-\infty}^{-\sqrt{-2\varphi}} e^{-\frac{1}{2}(v^2+2\varphi)}dv + \int_{\sqrt{-2\varphi}}^{\infty} e^{-\frac{1}{2}(v^2+2\varphi)}dv\Big] \\ &= \frac{1}{\sqrt{2\pi}}\Big[\int_{-\infty}^{0} e^{-\frac{1}{2}(v^2+2\varphi)}dv + \int_{0}^{-\sqrt{-2\varphi}} e^{-\frac{1}{2}(v^2+2\varphi)}dv \\ &\qquad + \int_{\sqrt{-2\varphi}}^{0} e^{-\frac{1}{2}(v^2+2\varphi)}dv + \int_{0}^{\infty} e^{-\frac{1}{2}(v^2+2\varphi)}dv\Big] \\ &= \frac{e^{-\varphi}}{\sqrt{2\pi}}\Big[2\int_{0}^{\infty} e^{-\frac{1}{2}v^2}dv - 2\int_{0}^{\sqrt{-2\varphi}} e^{-\frac{1}{2}v^2}dv\Big] \\ &= \frac{2e^{-\varphi}}{\sqrt{2\pi}}\Big[\frac{\sqrt{2\pi}}{2} - \sqrt{2}\int_{0}^{\sqrt{-\varphi}} e^{-x^2}dx\Big] \\ &= e^{-\varphi}\Big[1 - \frac{2}{\sqrt{\pi}}\int_{0}^{\sqrt{-\varphi}} e^{-x^2}dx\Big] \\ &= e^{-\varphi}[1 - \mathrm{erf}(\sqrt{-\varphi})] \\ &= I(-\varphi), \end{aligned} \tag{A.22}$$

where $\mathrm{erf}(x)$ and $I(x)$ are defined as

$$\left.\begin{aligned} \mathrm{erf}(x) &= \tfrac{2}{\sqrt{\pi}}\textstyle\int_0^x e^{-t^2}dt, \\ I(x) &= e^x[1 - \mathrm{erf}(\sqrt{x})]. \end{aligned}\right\} \tag{A.23}$$

The trapped ion density n_{it} is given by

$$\begin{aligned} n_{it} &= \frac{1}{\sqrt{2\pi}}\int_{-\sqrt{-2\varphi}}^{\sqrt{-2\varphi}} e^{-\frac{\alpha}{2}(v^2+2\varphi)}dv \\ &= \frac{2e^{-\alpha\varphi}}{\sqrt{2\pi}}\int_{0}^{\sqrt{-2\varphi}} e^{-\frac{\alpha}{2}v^2}dv. \end{aligned} \tag{A.24}$$

Now, we will consider two special cases, namely i) $\alpha > 0$ and ii) $\alpha < 0$.

i) $\alpha > 0$: The expression for n_{it} with $\alpha > 0$ can be written as

$$\begin{aligned} n_{it} &= \frac{2e^{-\alpha\varphi}}{\sqrt{2\pi}} \int_0^{\sqrt{-2\varphi}} e^{-\frac{\alpha}{2}v^2} dv \\ &= \frac{e^{-\alpha\varphi}}{\sqrt{\alpha}} \frac{2}{\sqrt{\pi}} \int_0^{\sqrt{-\alpha\varphi}} e^{-x^2} dx \\ &= \frac{e^{-\alpha\varphi}}{\sqrt{\alpha}} \mathrm{erf}(\sqrt{-\alpha\varphi}). \end{aligned} \tag{A.25}$$

ii) $\alpha < 0$: The expression for n_{it} with $\alpha < 0$ is given by

$$\begin{aligned} n_{it} &= \frac{2e^{-\alpha\varphi}}{\sqrt{2\pi}} \int_0^{\sqrt{-2\varphi}} e^{-\frac{\alpha}{2}v^2} dv \\ &= \frac{2}{\sqrt{|\alpha|\pi}} e^{-\alpha\varphi} \int_0^{\sqrt{\alpha\varphi}} e^{x^2} dx \\ &= \frac{2}{\sqrt{|\alpha|\pi}} W(\sqrt{\alpha\varphi}), \end{aligned} \tag{A.26}$$

where $W(x)$ is known as the Dawson integral and is defined by

$$W(x) = e^{-x^2} \int_0^x e^{t^2} dt. \tag{A.27}$$

Therefore, the ion density, $n_i = n_{if} + n_{it}$, is finally given by

$$\left.\begin{aligned} n_i &= I(-\varphi) + \tfrac{e^{-\alpha\varphi}}{\sqrt{\alpha}} \mathrm{erf}(\sqrt{-\alpha\varphi}), \quad \alpha < 0 \\ n_i &= I(-\varphi) + \tfrac{2}{\sqrt{|\alpha|\pi}} W(\sqrt{\alpha\varphi}), \quad \alpha > 0 \end{aligned}\right\} \tag{A.28}$$

Small Amplitude Expansion of n_i:

The expansion of n_{if}, up to the term containing φ^2, gives

$$n_{if} = 1 - \frac{2}{\sqrt{\pi}}(-\varphi)^{1/2} - \varphi - \frac{4}{3\sqrt{\pi}}(-\varphi)^{3/2} + \frac{1}{2}\varphi^2. \tag{A.29}$$

It is found that for both the cases, $\alpha > 0$ and $\alpha < 0$, the expansion of n_{it}, up to term containing φ^2, gives the same expression which is given by

$$n_{it} = \frac{2}{\sqrt{\pi}}(-\varphi)^{1/2} + \frac{4\alpha}{3\sqrt{\pi}}(-\varphi)^{3/2}. \tag{A.30}$$

Therefore, for small amplitude expansion, i.e. expansion up to the term containing φ^2, the ion density, $n_i = n_{if} + n_{it}$, can finally be written as

$$n_i = 1 - \varphi - \frac{4}{3\sqrt{\pi}}(1-\alpha)(-\varphi)^{3/2} + \frac{1}{2}\varphi^2. \tag{A.31}$$

A.4 Stationary Solution of mKdV Equation

The modified Korteweg-de Vries (mKdV) equation, discussed in **section 4.3.3**, can be written in the form

$$\frac{\partial y}{\partial t} + a\sqrt{-y}\frac{\partial y}{\partial x} + b\frac{\partial^3 y}{\partial x^3} = 0, \tag{A.32}$$

where a and b are two different constants. To obtain a stationary localised solution of this nonlinear equation, we first transform the independent variables to

$$\left.\begin{aligned} \xi &= x - u_0\tau, \\ \tau &= t. \end{aligned}\right\} \tag{A.33}$$

This transformation, with the steady state condition ($\frac{\partial}{\partial \tau} \to 0$), reduces the mKdV equation to the form

$$\begin{aligned} & -u_0\frac{dy}{d\xi} + a\sqrt{-y}\frac{dy}{d\xi} + b\frac{d^3y}{d\xi^3} = 0, \\ \Rightarrow \quad & \frac{d}{d\xi}\left(\frac{d^2y}{d\xi^2}\right) = \frac{1}{b}\frac{d}{d\xi}[u_0 y + \frac{2}{3}a(-y)^{3/2}]. \end{aligned} \tag{A.34}$$

Now, under the appropriate boundary conditions, viz. $y \to 0$ and $d^2y/d\xi^2 \to 0$ at $\xi \to \pm\infty$, this equation can be integrated to give

$$\frac{d^2y}{d\xi^2} = \frac{1}{b}[u_0 y + \frac{2}{3}a(-y)^{3/2}]. \tag{A.35}$$

Multiplying both sides of this equation by $dy/d\xi$ one can write

$$\frac{d}{d\xi}[(\frac{dy}{d\xi})^2] = \frac{1}{b}\frac{d}{d\xi}[u_0 y^2 - \frac{8}{15}a(-y)^{5/2}]. \tag{A.36}$$

We can easily integrate this and, under the same boundary conditions, $y \to 0$ and $dy/d\xi \to 0$ at $\xi \to \pm\infty$, one can obtain

$$\begin{aligned} & \frac{dy}{d\xi} = y(\sqrt{\frac{u_0}{b}})\sqrt{1 - \frac{8a}{15u_0}\sqrt{-y}}, \\ \Rightarrow \quad & d\xi = -(\sqrt{\frac{16b}{u_0}})\frac{dY}{1-Y^2}, \\ \Rightarrow \quad & d\xi = -2(\sqrt{\frac{b}{u_0}})(\frac{1}{1-Y} + \frac{1}{1+Y})dY, \end{aligned} \tag{A.37}$$

where $Y = \sqrt{1 - \frac{8a}{15u_0}\sqrt{-y}}$. On integration of this equation we obtain

$$\begin{aligned} & \xi = (\sqrt{\frac{4b}{u_0}})[\ln(1-Y) - \ln(1+Y)], \\ \Rightarrow \quad & \frac{1-Y}{1+Y} = \exp(\xi\sqrt{u_0/4b}), \\ \Rightarrow \quad & Y = \frac{1-\exp(\xi\sqrt{u_0/4b})}{1+\exp(\xi\sqrt{u_0/4b})}. \end{aligned} \tag{A.38}$$

Now, substituting Y into this equation one can obtain

$$\begin{aligned} \Rightarrow \quad & y = -(\frac{15u_0}{8a})^2[\frac{4\exp(\xi\sqrt{u_0/4b})}{\{1+\exp(\xi\sqrt{u_0/4b})\}^2}]^2, \\ \Rightarrow \quad & y = -(\frac{15u_0}{8a})^2[\frac{2\exp(\xi\sqrt{u_0/16b})}{1+\exp(\xi\sqrt{u_0/4b})}]^4, \\ \Rightarrow \quad & y = -(\frac{15u_0}{a})^2[\frac{2}{\exp(-\xi\sqrt{u_0/16b}) + \exp(\xi\sqrt{u_0/16b})}]^4, \\ \Rightarrow \quad & y = -(\frac{15u_0}{8a})^2 \operatorname{sech}^4(\xi\sqrt{u_0/16b}). \end{aligned} \tag{A.39}$$

Therefore, the stationary solution of the mKdV equation is finally written as

$$y = -y_m \operatorname{sech}^4[(x - u_0 t)\mu], \tag{A.40}$$

where y_m and μ are the amplitude and the inverse of the width of the solitary waves, respectively, and are given by

$$\left.\begin{aligned} y_m &= (\tfrac{15u_0}{8a})^2, \\ \mu &= \sqrt{\tfrac{u_0}{16b}}. \end{aligned}\right\} \tag{A.41}$$

A.5 List of Publications

1. Electrostatic solitary structures in non-thermal Plasmas.
   R. A. Cairns, A. A. Mamun, R. Bingham, R. Boström, R. O. Dendy, C. M. C. Nairn and P. K. Shukla, *Geophys. Res. Lett.* **22**, 2709 (1995).

2. Ion Sound solitary waves in density depressions.
   R. A. Cairns, R. Bingham, R. O. Dendy, C. M. C. Nairn, P. K. Shukla and A. A. Mamun, *J. de Physique IV* **5**, C6-43 (1995).

3. Ion-acoustic solitons in a magnetised plasma with non-thermal electrons.
   R. A. Cairns, A. A. Mamun, R. Bingham and P. K. Shukla, *Physica Scripta* **T63**, 80 (1996).

4. Stability of solitary waves in a magnetised non-thermal Plasma.
   A. A. Mamun and R. A. Cairns, *J. Plasma Physics* **56**, 175 (1996).

5. Solitary potential in dusty plasmas.
   A. A. Mamun, R. A. Cairns and P. K. Shukla, *Phys. Plasmas* **3**, 702 (1996).

6. Effects of vortex-like and non-thermal ion distributions on nonlinear dust-acoustic waves.
   A. A. Mamun, R. A. Cairns and P. K. Shukla, *Phys. Plasmas* **3**, 2610 (1996).

Bibliography

[1] J. S. Russell: *Report on Waves*, British Association Reports (1844).

[2] D. J. Korteweg and G. de Vries: *Phil. Mag. Ser. 5* **39** 422 (1895).

[3] A. C. Scott, F. Y. Chu and D. W. McLaughlin: *Proc. IEEE* **61**, 1443 (1973).

[4] G. B. Whitham: *Linear and Nonlinear Waves* (Wiley-Interscience, New York, 1974).

[5] M. Toda: *Phys. Rep.* **18**, 1 (1975).

[6] R. M. Miura (edt.): *Bäcklund Transformations* (Springer, New York, 1976).

[7] K. E. Lonngren and A. C. Scott (edts.): *Solitons in Action* (Academic Press, New York, 1978).

[8] G. L. Lamb: *Elements of Soliton Theory* (Wiley-Interscience, New York, 1980).

[9] M. J. Ablowitz and H. Segur: *Solitons and the Inverse Scattering Transform* (SIAM, Philadelphia, 1981).

[10] R. Dodd, J. C. Eilbeck, J. Gibbon and H. Morris: *Solitons and Nonlinear Wave Equations* (Academic Press, New York, 1982).

[11] P. G. Drazin: *Solitons* (Cambirdge University Press, 1983).

[12] E. Infeld and G. Rowlands: *Nonlinear Waves, Solitons and Chaos* (Cambridge University Press, 1990).

[13] V. Petviashvili and O. Pokhotelov: *Solitary Waves in Plasmas and in the Atmosphere* (Gordon and Breach, 1992).

[14] H. Washimi and T. Taniuti: *Phys. Rev. Lett.* **17**, 996 (1966).

[15] H. Ikezi and R. J. Taylor: *Phys. Fluids* **13**, 2348 (1970).

[16] V. I. Karpman and B. B. Kadomtsev: *Soviet Phys. Usp.* **14**, 40 (1971).

[17] T. Taniuti and H. Washimi: *Phys. Rev. Lett.* **21**, 209 (1968).

[18] V. I. Karpman and E. M. Krushkal: *Soviet Phys. JETP* **28**, 277 (1968).

[19] A. Hasegawa: *Phys. Rev. A* **1**, 1746 (1970).

[20] V. E. Zakharov: *Soviet Phys. JETP* **35**, 908 (1972).

[21] A. Hasegawa: *Rev. Geophys. Space Phys.* **12**, 273 (1974).

[22] V. G. Makhankov: *Phys. Rep.* **35C**, 1 (1978).

[23] H. Ikezi, P. J. Barrett, R. B. White and A. Y. Wong: *Phys. Fluids* **14**, 1997 (1971).

[24] A. N. Kaufman and L. Stenflo: *Phys. Scripta* **11**, 269 (1975).

[25] K. Mio, T. Ogino, K. Minami and S. Takeda: *J. Phys. Soc. Japan* **41**, 265 (1976).

[26] P. K. Shukla and M. Y. Yu: *Phys. Lett.* **57A**, 151 (1976).

[27] H. Sanuki and Y. H. Ichikawa: *J. Phys. Soc. Japan* **41**, 654 (1976).

[28] R. Z. Sagdeev: *Reviews of Plasma Physics* (Consultants Bureau, New York, 1966), Vol. 4, p. 23.

[29] K. E. Lonngren: *Plasma Phys.* **25**, 943 (1983).

[30] Y. Nakamura, J. L. Ferreira and G. O. Ludwig: *J. Plasma Phys.* **33**, 237 (1985).

[31] Y. Nakamura, T. Ito and K. Koga: *J. Plasma Phys.* **49**, 331 (1993).

[32] E. Witt and W. Lotko: *Phys. Fluids* **26**, 2176 (1983).

[33] S. Qian, W. Lotko and M. K. Hudson: *Phys. Fluids* **31**, 2190 (1988).

[34] V. A. Marchenko and M. K. Hudson: *J. Geophys. Res.* **100**, 19791 (1995).

[35] K. Nishihara and M. Tajiri: *J. Phys. Soc. Japan* **50**, 4047 (1981).

[36] R. Bharuthram and P. K. Shukla: *Phys. Scripta* **34**, 732 (1985).

[37] L. L. Yadav and S. R. Sharma: *Phys. Lett.* **150A**, 397 (1990).

[38] S. Bujarbarua and H. Schamel: *J. Plasma Phys.* **25**, 515 (1981).

[39] H. Schamel: *Phys. Rep.* **140**, 161 (1986).

[40] K. P. Das and F. Verheest: *J. Plasma Phys.* **41**, 139 (1989).

[41] M. K. Mishra, R. S. Chhabra and S. R. Sharma: *J. Plasma Phys.* **52**, 409 (1994).

[42] H. H. Kuehl and C. Y. Zhang: *Phys. Fluids B* **3**, 555 (1991).

[43] P. Chatterjee and R. Roychoudhury: *Phys. Plasmas* **1**, 2148 (1994).

[44] Y. Nakamura and K. Ohtani: *J. Plasma Phys.* **53**, 235 (1995).

[45] Y. Nejoh and H. Sanuki: *Phys. Plasmas* **2**, 4122 (1995).

[46] R. J. Taylor, K. R. MacKenzie and H. Ikezi: *Rev. Scient. Instrum.* **43**, 1675 (1972).

[47] R. Limpaecher and K. R. MacKenzie: *Rev. Scient. Instrum.* **44**, 726 (1973).

[48] R. W. Motley: *Q Machines* (Academic Press, New york, 1975).

[49] H. Ikezi and R. J. Taylor: *J. Appl. Phys.* **41**, 738 (1970).

[50] H. Ikezi: *Phys. Fluids* **16**, 1668 (1973).

[51] H. Ikezi, R. P. H. Chang and R. A. Stern: *Phys. Rev. Lett.* **36**, 1047 (1976).

[52] S. V. Antipov, M. V. Nezlin, E. N. Shezhkin and A. S. Trubnikov: *Soviet Phys. JETP Lett.* **23**, 562 (1976).

[53] V. D. Fedorchenko, J. P. Mazalov, A. S. Bakai, A. V. Pashenko and B. N. Rutkevich: *Pisma Zh. éksp teor. Fiz.* **70**, 1768 (1976).

[54] V. I. Karpman, J. P. Lynov, P. Michelsen, H. L. Pécseli, J. J. Rasmussen and V. A. Turikov: *Phys. Rev. Lett.* **43**, 210 (1979).

[55] M. Y. Ivanov: *Soviet Phys. Plasma Phys.* **8**, 218 (1982).

[56] T. Pierre, G. Bonhomme, J. R. Cussenot and G. Leclert: *Phys. Lett.* **95A**, 159 (1983).

[57] J. L. Cooney, D. W. Aossey, J. E. Williams and K. E. Lonngren: *Phys. Rev. E* **47**, 564 (1993).

[58] K. Nishikawa, H. Hojo, K. Mima and H. Ikezi: *Phys. Rev.Lett.* **33**, 148 (1974).

[59] S. V. Antipov, M. V. Nezlin and A. S. Trubnikov: *Soviet Phys. JETP Lett.* **31**, 24 (1980).

[60] S. V. Antipov, M. V. Nezlin and A. S. Trubnikov: *Pisma Zh. éksp teor. Fiz.* **78**, 1473 (1980).

[61] S. V. Antipov, M. V. Nezlin and A. S. Trubnikov: *Physica* **3D**, 311 (1981).

[62] V. Formisano: *Nuovo Cim.* **2C**, 789 (1979).

[63] D. A. Gurnett, J. E. Maggs, D. H. Gallagher, W. S. Kurth and F. L. Scarf: *J. Geophys. Rev.* **86A**, 8833 (1981).

[64] P. G. Mamradze, G. Z. Machabeli and G. I. Melikidze: *Soviet Phys. Plasma Phys.* **6**, 707(1980).

[65] V. I. Karpman, J. P. Lynov, P. Michelsen, H. L. Pécseli, J. J. Rasmussen and V. A. Turikov: *Phys. Fluids* **23**, 1782 (1980).

[66] J. P. Lynov, P. Michelsen, H. L. Pécseli and J. J. Rasmussen: *Phys. Lett.* **80A**, 23 (1980).

[67] K. Saeki, P. Michelsen, H. L. Pécseli and J. J. Rasmussen: *Phys. Rev. Lett.* **42**, 501 (1979).

[68] M. Temerin, K. Cerny, W. Lotko and F. S. Mozer: *Phys. Rev. Lett.* **48**, 1175 (1982).

[69] R. Boström, G. Gustafsson, B. Holback, G. Holmgren, H. J. Koskinen and P. Kintner: *Phys. Rev. Lett.* **61**, 82 (1988).

[70] H. J. Koskinen, R. Lundin and B. Holback: *J. Geophys. Res.* **95**, 5921 (1990).

[71] R. Boström: *IEE. Trans. Plasma Sci.* **20**, 756 (1992).

[72] A. Mälkki, A. I. Eriksson, P. O. Dovner, R. Boström, B. Holback, G. Holmgren, and H. J. Koskinen: *J. Geophys. Res.* **98**, 15521 (1993).

[73] P. O. Dovner, A. I. Eriksson, R. Boström and B. Holback: *Geophys. Res. Lett.* **21**, 1827 (1994).

[74] V. N. Tsytovich, G. E. Morfill, R. Bingham and U. de Angelis: *Comments Plasma Phys. Controlled Fusion* **13**, 153 (1989).

[75] U. de Angelis and R. Bingham and V. N. Tsytovich: *J. Plasma Phys.* **42**, 445 (1989).

[76] V. N. Tsytovich, U. de Angelis and R. Bingham: *J. Plasma Phys.* **42**, 429 (1989).

[77] U. de Angelis, V. Formisano and M. Giordano: *J. Plasma Phys.* **40**, 399 (1988).

[78] O. Havnes, U. de Angelis, R. Bingham, C. Goertz, G. Morfill and V. N. Tsytovich: *J. Atoms. Terr. Phys.* **52**, 637 (1990).

[79] P. K. Shukla, U. de Angelis and L. Stenflo: *Phys. Scripta* **45**, 465 (1992).

[80] U. de Angelis, A. Forlani, R. Bingham , P. K. Shukla, A. Ponomarev and V. N. Tsytovich: *Phys. Plasmas* **1**, 236 (1994).

[81] A. Forlani, U. de Angelis and V. N. Tsytovich: *Phys. Scripta* **45**, 509 (1992).

[82] P. K. Shukla and V. P. Silin: *Phys. Scripta* **45**, 504 (1992).

[83] R. Bingham, U. de Angelis, V. N. Tsytovich and O. Havnes: *Phys. Fluids B* **3**, 811 (1991).

[84] R. Bingham, U. de Angelis, V. N. Tsytovich and O. Havnes: *Phys. Fluids B* **4**, 283 (1992).

[85] M. Salimullah and A. Sen: *Phys. Fluids B* **4**, 1441 (1992).

[86] M. R. Jana, A. Sen and P. K. Kaw: *Phys. Rev. E* **48**, 3930 (1993).

[87] S. V. Vladimirov: *Phys. Plasmas* **1**, 2762 (1994).

[88] P. K. Shukla and S. V. Vladimirov: *J. Geophys. Res.* **99**, 4023 (1994).

[89] P. K. Shukla and S. V. Vladimirov: *Phys. Plasmas* **2**, 3179 (1995).

[90] N. N. Rao, P. K. Shukla and M. Y.Yu: *Planet. Space Sci.* **38**, 543 (1990).

[91] N. D. Angelo: *Planet. Space Sci.* **38**, 1143 (1990).

[92] R. K. Varma, P. K. Shukla and V. Krishan: *Phys. Rev. E* **47**, 3612 (1993).

[93] M. Rosenberg: *Planet. Space Sci.* **41**, 229 (1993).

[94] O. Havnes: *Planet. Space Sci.* **41**, 321 (1993).

[95] D. Winske, S. P. Gary, M. E. Jones, M. Rosenberg, V. W. Chow and D. A. Mendis: *Geophys. Res. Lett.* **22**, 2069 (1995).

[96] A. Barkan, R. L. Merlino and N. D'Angelo: *Phys. Plasmas* **2**, 3563 (1995).

[97] A. I. Eriksson, B. Holback, P. O. Dovner, R. Boström, G. Holmgren, M. André, L. Eliasson and P. M. Kintner: *Geophys. Res. Lett.* **21**, 1843 (1994).

[98] J. L. Vago, P. M. Kintner, S. W Chesney, R. L. Arnoldy, K. A. Lynch, T. E. Moore and C. J. Pollock: *J. Geophys. Res.* **97**, 16935 (1992).

[99] V. D. Shapiro, V. I. Shevchenko, G. I. Soloview, V. P. Kalinin, R. Bingham, R. Z. Sagdeev, M. Ashour-Abdalla, J. M. Dawson and J. J. Su: *Phys. Fluids B* **5**, 3148 (1993).

[100] V. D. Shapiro, G. I. Soloviev, J. M. Dawson and R. Bingham: *Phys. Plaasmas* **2**, 516 (1995).

[101] A. Mälkki, H. Koshkinen, R. Boström and B. Holback: *Phys. Scripta* **39**, 787 (1989).

[102] V. I. Masov: *Sov. J. Plasma Phys.* **16**, 441 (1990).

[103] P. K. Shukla, R. Bingham, R. Dendy, H. Pécseli and L. Stenflo: *J. de Physique IV* **5**, C6-19 (1995).

[104] R. A. Cairns, A. A. Mamun, R. Bingham, R. Boström, R. O. Dendy, C. M. C. Nairn and P. K. Shukla: *Geophys. Res. Lett.* **22**, 2709 (1995).

[105] R. A. Cairns, R. Bingham, R. O. Dendy, C. M. C. Nairn, P. K. Shukla and A. A. Mamun: *J. de Physique IV* **5**, C6-43 (1995).

[106] P. K. Shukla and M. Y. Yu: *J. Math. Phys.* **19**, 2506 (1978).

[107] L. C. Lee and J. R. Kan: *Phys. Fluids* **24**, 430 (1981).

[108] E. Infeld: *J. Plasma Phys.* **33**, 171 (1985).

[109] E. Infeld: *J. Plasma Phys.* **8**, 105 (1972).

[110] E. Infeld and G. Rowlands: *J. Plasma Phys.* **10**, 293 (1973).

[111] G. Rowlands: *J. Plasma Phys.* **3**, 567 (1969).

[112] K. Estabrook and W. L. Kruer: *Phys. Rev. Lett.* **40**, 42 (1978).

[113] Y. Nishida and T. Nagasawa: *Phys. Fluids* **29**, 345 (1986).

[114] N. Sato, R. Hatakeyama, S. Iizuka, T. Meino, K. Saeki, J. J. Rasmussen, P. Michelsen and R. Schrittwieser: *J. Phys. Soc. Japan* **52**, 875 (1983).

[115] H. Schamel: *J. Plasma Phys.* **13**, 139 (1975).

[116] H. Schamel: *Plasma Phys.* **14**, 905 (1972).

[117] O. M. Gradov and L. Stenflo: *Phys. Fluids* **26**, 604 (1983).

[118] R. A. Cairns, A. A. Mamun, R. Bingham and P. K. Shukla: *Phys. Scripa* **T63**, 80 (1996).

[119] A. A. Mamun and R. A. Cairns: *J. Plasma Phys.* **56**, 175 (1996).

[120] A. A. Mamun, R. A. Cairns and P. K. Shukla: *Phys. Plasmas* **3**, 2610 (1996).

[121] A. A. Mamun, R. A. Cairns and P. K. Shukla: *Phys. Plasmas* **3**, 000 (1996).

[122] S. Maxon and J. Viecelli: *Phys. Fluids* **17**, 1614 (1974).

[123] S. Maxon and J. Viecelli: *Phys. Rev. Lett.* **32**, 4 (1974).

[124] S. Maxon: *Phys. Fluids* **19**, 266 (1976).